# Preparation and Characterization of Fouling Resistant Ultrafiltration Membranes




*Manish Kumar Sinha*

# Preparation and Characterization of Fouling Resistant Ultrafiltration Membranes

*Thesis submitted in partial fulfillment of the requirements*

*for the degree of*

**DOCTOR OF PHILOSOPHY**

**by**

*Manish Kumar Sinha*

*Roll No: 11610712*


**Department of Chemical Engineering**

**Indian Institute of Technology Guwahati**

**Guwahati-781039, India**

*Dedicated to my Parents for whom I have become what I am today*

**Department of Chemical Engineering**

**Indian Institute of Technology Guwahati**

**Guwahati 781039, India**

# CERTIFICATE

It is certified that the work contained in the thesis entitled "**Preparation and Characterization of Fouling Resistant Ultrafiltration Membranes**", by **Manish Kumar Sinha**, has been carried out under my supervision. The work documented in this thesis has not been submitted to any other University or Institute for the award of any degree or diploma.

**Dr. Mihir Kumar Purkait**

Associate Professor

Department of Chemical Engineering

Indian Institute of Technology Guwahati

Guwahati 781039, India

Date:

# Acknowledgements

I owe a debt of gratitude to many people who have helped me in completing this research work directly and indirectly. I would like to acknowledge them all. To begin with, I wish to express my deepest acknowledgement to my supervisor, **Dr. Mihir Kumar Purkait** for providing me inspiring guidance throughout the entire course of this work. I am indebted to him for his useful suggestions and constant encouragement throughout the entire period. I am grateful to him for his great support, encouragement, and endurance, which helped me to finish this work within time. I always admire his advises, energy and hard work for all his students. Besides this, I feel very fortunate that I got a chance to work with such experienced and enthusiastic supervisor, whom I will admire throughout my career.

I would like to thank my doctoral committee members, **Dr. G. Pugazhenthi**, **Dr. Amit Kumar** (Department of Chemical Engineering), and **Dr. P. K. Ghosh** (Department of Civil Engineering) for their valuable suggestions and constructive criticism during the project evolutions, which helped me to make necessary improvements in various stages of my research work. I would specially like to thank **Dr. G. Pugazhenthi** for the rigorous and remarkable questions that he raised during the seminar presentations which had helped me a lot in understanding many facts related to my work.

I am also thankful to all the faculty members of the Chemical Engineering Department for their encouragement and help at various stages during my stay in this Department. In this regard, I would specially like to mention the name of **Dr. Chandan Das.**

I must thank to all the technical staffs of my Department specially, **Mr. Lukumoni Borah**, **Mr. Dipak Kumar Barman, Mr. Prasun Bhattacharjee**, **Mr. Kaustavmoni Deka**, **Mr. Debajit Borah**, and the Scientific Officers, **Mrs. Ritumoni Kalita** and **Mr. Harsaraj Biswanath.** The experimental works presented in this thesis would never have been possible without the help of these proficient technicians. I am also very thankful to **Mr. Bijoy Kumar**

**Choudhury** (Senior Technician, Department of Mechanical Engineering), who helped me in installing my experimental setup.

I am fortunate enough to have my friend around me, **Ms. Snigdha Khuntia,** whose presence and cooperation comforted me in many ways. I could never have achieved my goal without her moral support. She always helped and encouraged me to be strong enough to surpass all my difficulties, frustrations and worries. Her support, suggestions and concern made my stay cheerful at IITG.

I am thankful to all my Departmental friends, seniors and juniors for their supports and good wishes. Thanks to all those lab-mates in the Department including the present and past M.Tech students for their help in different forms.

I have no word to thank **Maa Kamakhya Devi and Baba Baidyanath** who are my strength and wisdom.

Last but not the least, I would like to thank my father **Mr. Rajkumar Prasad Sinha**, My mother, **Mrs. Kanti Sinha**, my elder brothers, **Mr. Manoj Kumar Sinha**, **Mr. Mukesh Kumar Sinha** and **Mr. Mithilesh Kumar Sinha** for supporting me to do my Ph.D. Their love, affection, blessings and sacrifices made me stronger to overcome my huddles and achieve my target. Also, I would like to give my love to my nephews **Mayank**, **Mrinal**, **Arnav**, **Aditya** and my sweet niece **Akshda**.

*Manish Kumar Sinha*

# Abstract

The main objective of this work is to prepare asymmetric polymeric membranes with fouling resistance property. It is well known that fouling resistant membranes can be prepared by three methods; first by increasing the hydrophilicity of membrane surface, second by electrostatic repulsion and third by steric repulsion. Based on these three methods, polymeric membranes were modified by using different type of additives. All the additives used this thesis, increased the hydrophilicity of modified membranes compared to plain membranes. Apart from this, synthesized additives poly (VCL-co-AA) and poly (AA-co-PEGMA) provide the electrostatic repulsive property to the modified membranes. Further, synthesized amphiphilic PU macromolecules and PSF-co-PVCL copolymers provide the fouling resistant property by inducing steric repulsion to the membrane surface.

First of all flat sheet asymmetric polymeric membranes were prepared from homogeneous solution of Poly(vinylidene fluoride-co-hexafluoropropylene) (PVDF-HFP) by phase inversion method using N-methyl-2-pyrrolidone (NMP) as solvent and PEG 6000 as pore forming agent. The effects of addition of different alcohols viz. methanol, ethanol, n-propanol, n-butanol and various quantity of methanol in the casting solution on membrane properties were investigated. The morphology and structure of resulting membranes were observed by field emission scanning electron microscope (FESEM). The permeation performances of the membranes were evaluated in terms of pure water flux (PWF), hydraulic permeability and solute rejection capacity. Extent of membrane hydrophilicity was evaluated in terms of porosity, equilibrium water content (EWC) and water contact angle. Solution of bovine serum albumin (BSA) of molecular weight 68,000 Da was used to study the permeation performance of prepared membranes using a batch cell of 350 mL capacity. Membranes with 5 wt % of methanol showed highest PWF and smallest water contact angle, while membranes containing different alcohols have almost same PWF.

**Abstract**

Keeping hydrophilicity as key factor for anti-fouling property for polymeric membrane, flat sheet asymmetric polymeric membranes were prepared from homogeneous solution of polysulfone (PSF) and polyethylene glycol methyl ether (PEGME) of three different molecular weights (550 Da, 2000 Da and 5000 Da) as the polymeric additives. The morphology and structure of the resulting membranes were observed by field emission scanning electron microscope (FESEM). The pore number, pore permeability and their distribution and average pore size of the membranes were determined by the liquid-liquid displacement porosimetry (LLDP) method. Results showed that with increase in molecular weight of PEGME, the pore number as well as pore area in membranes increased. Membranes with PEGME of higher molecular weights have higher PWF and higher hydraulic permeability due to high porosity. With increase in molecular weight of PEGME from 550 to 5000, the PWF increased from 17.5 to 227.8 $Lm^{-2}h^{-1}$. Similarly, EWC increased from 59.7% for PEGME 550 to 70.8% for PEGME 5000 membranes. Contact angle was also decreased from 71 for PEGME 550 to 47 for PEGME 5000.

Further, novel polysulfone (PSF) ultrafiltration membranes with pH and thermo sensitivity were prepared using the copolymer poly (N-vinylcaprolactam-co-acrylic acid) (poly (VCL-co-AA)) as an additive. The copolymer was synthesized by free radical solution polymerization, and directly blended in membrane casting solution to prepare the asymmetric membranes by phase inversion method. The membranes were characterized in terms of pure water flux (PWF), hydraulic permeability and hydrophilicity. PWF increased from 1 to 18.8 $L/m^2h$, when wt % of copolymer increases from 0 to 2.5. Similarly, water contact angle decreased from 76˚ to 58˚. The blended membranes showed evident of pH and thermo sensitivity. The stimuli responsive behaviour of membranes was also investigated in terms of pH and temperature. A significant increase in BSA flux and decrease in membrane fouling was observed.

To provide both hydrophilicity and electrostatic repulsive property, novel cross linked pegylated functional copolymer poly (acrylic acid-co-polyethylene glycol methyl ether methacrylate) was prepared from AA and PEGMA, via precipitation polymerization using toluene as solvent. The copolymer was directly blended with PSF using NMP as solvent to prepare flat sheet polymeric membrane by the phase inversion method. Cross sectional morphology of the membranes was changed significantly with higher wt% of the copolymer. Contact angle and hydraulic permeability of modified membrane with 7 wt% of copolymer was 48.7˚ and 0.794 L/$m^2$ h kPa compared to 63.2˚ and 0.353 L/$m^2$ h kPa respectively for unmodified membrane. The blended membranes also showed evidence of pH sensitivity compared to unmodified membrane. For membrane modified with 7 wt% of the copolymer, hydraulic permeability was increased from 0.355 to 0.794 L/$m^2$ h kPa when pH was changed from 11 to 2. Effect of pH for BSA rejection on different membrane was also studied at pH 2, pH 7 and pH 11. It was found that modified membranes had almost same rejection at pH 7 and pH 11, but rejection is much lower at pH 2.

Amphiphilic PU macromolecules were also synthesized with end capping of citric acid, malic acid, lactic acid and 4-hydroxy benzoic acid, for the anti fouling modification of polymeric membrane. Chemical structure of the macromolecules was confirmed by NMR and FTIR spectroscopy. PSF was directly blended with these additives and membranes were fabricated by phase separation method. Hydration capacity, PWF, BSA adsorption and WCA for modified membrane with 6 wt % of PU-CA were 225 mg/$cm^3$, 138.2 L/$m^2$h, 0.019 mg/$cm^3$ and 49.5$^o$ compared to 130 mg/$cm^3$, 102.4 L/$m^2$h, 0.14 mg/$cm^3$ and 63.5$^o$ respectively, for plain membrane. Anti fouling behaviour of membranes was also studied with BSA ultra filtration. Flux recovery ratio for all the modified membranes was higher than plain membranes with the highest value of more than 91 %.

Thereafter, amphiphilic thermo responsive cross linked polyvinylcaprolactam-co-polysulfone (PVCL-co-PSF) copolymer was synthesized via solution polymerization of vinylcaprolactam (VCL) in PSF solution by use of three different initial ratio of PSF to VCL monomer. After the synthesis of copolymer, required amount of PSF was dissolved in PVCL-co-PSF copolymer solution. Blended membranes showed enhanced pure water flux, hydrophilicity and evident of thermo sensitivity. Reversible volume phase transition of PVCL around the lower critical solution temperature (LCST) was used as an environmental-friendly approach for membrane cleaning. Temperature change water elution hydraulic cleaning for modified membranes around the LCST of the PVCL-co-PSF copolymer brushes was proposed (as shown in Figure 8.11). Following the alternate temperature-change (40 ˚C/25 ˚C) cleaning, a flux recovery of about 92% was obtained for the modified PSF membrane (the flux recovery of the plain membrane was only about 39%).

Finally, cross linked chitosan–polyacrylic acid (CS-PAA) nanoparticle were synthesized for modification of polymeric membrane. Modified membranes showed superior pore size, pure water flux, hydraulic permeability and fouling resistance. Top and cross sectional morphology of the modified membranes was changed noticeably with higher quantity of nanoparticle. Water contact angle and BSA adsorption of modified membrane with maximum quantity of nanoparticle was 54˚ and 0.05 mg/cm$^2$ compared to 72˚ and 0.21 mg/cm$^2$ respectively for unmodified membrane. Hydraulic permeability was improved from 0.146 L/m$^2$h kPa to 0.265 L/m$^2$h kPa for modified membrane compared to unmodified membrane. Fouling resistance behaviour of modified membrane was also studied with 1000 PPM BSA solution. BSA flux was also increased from 8.3 to 24.3 L/m$^2$h for modified membranes. Modified membrane reached a maximum flux recovery ratio of 88 % after BSA UF experiment compared to 42 % flux recovery ratio of plain membrane.

# Research Publications

**Published**

- **M K Sinha**, M K Purkait, Preparation of fouling resistant PSF flat sheet UF membrane using amphiphilic polyurethane macromolecules**,** Desalination 355 (2015) 155-168.
- **M K Sinha**, M K Purkait, Preparation and characterization of stimuli-responsive hydrophilic polysulfone membrane modified with poly (N-vinylcaprolactam-co-acrylic acid), Desalination 348 (2014) 16-25.
- **M K Sinha**, M K Purkait, Preparation and characterization of novel pegylated hydrophilic pH responsive polysulfone ultrafiltration membrane, J. Membr. Sci. 464 (2014) 20-32.
- **M K Sinha**, M K Purkait, Enhancement of hydrophilicity of poly(vinylidene fluoride-co-hexafluoropylene) (PVDF-HFP) membrane using various alcohols as nonsolvent additives, Desalination 338 (2014) 106-114.
- **M K Sinha**, M K Purkait, Increase in hydrophilicity of polysulfone membrane using polyethylene glycol methyl ether, J. Membr. Sci. 437 (2013) 7-16.

**Submitted**

- **M K Sinha**, M K Purkait, Use of CS-PAA polymeric nanoparticle in fouling resistant polysulfone ultrafiltration membrane preparation, J. Membr. Sci.
- **M K Sinha**, M K Purkait, Preparation of novel thermo responsive PSF membrane, with cross linked PVCL-co-PSF copolymer for protein separation and easy cleaning, RSC Adv.

**Conference/Presentations**

- **Manish Kumar Sinha**, Mihir Kumar Purkait, "Stimuli responsive Polysulfone Membrane responding to Temperature and pH", International Conference on Membranes and Applications (ICMA-2013), CSIR-CGCRI, Kolkata, India, 22nd - 23rd November, 2013.
- **Manish Kumar Sinha**, Mihir Kumar Purkait, "Novel PEGylated pH responsive Polysulfone Ultrafiltration Membrane" International Conference on Frontiers in Chemical Engineering (ICFCE-2013), NIT Rourkela, Odisha, India, pp 345-350, ISBN 978-93-80813-24-0, 9th -11th December, 2013.

# CONTENTS

**CONTENTS**

**CONTENTS**

# LIST OF FIGURES

## LIST OF FIGURES

## LIST OF FIGURES

# LIST OF TABLES

## LIST OF TABLES

# Nomenclature

## Notations

| | |
|---|---|
| $A$ | effective membrane area |
| $A_t$ | total area |
| $C_f$ | concentration in the feed |
| $C_p$ | concentration in permeate |
| $F_{ir}$ | irreversible fouling |
| $F_r$ | reversible fouling |
| $F_t$ | total fouling |
| $h$ | hour |
| $J_p$ | BSA solution flux |
| $J_w$ | pure water flux |
| $J_{w1}$ | initial water flux |
| $J_{w2}$ | water flux in second run |
| $L$ | length of pore in equations |
| $P$ | pressure |
| $P_m$ | hydraulic permeability |
| $\Delta P$ | transmembrane pressure in equations |
| $Q$ | volume of water permeated |
| $r$ | radius of pores |
| $r_m$ | mean pore radius |
| $T_g$ | glass transition temperature |
| $V$ | volume of membrane in wet state |
| $W_d$ | weight of dry membrane |
| $W_w$ | weight of wet membrane |

| | |
|---|---|
| η | viscosity |
| ε | porosity |
| σ | interfacial surface tension |

## Abbreviations

| | |
|---|---|
| ATR | attenuated total reflectance |
| BSA | bovine serum albumin |
| CA | cellulose acetate |
| CF | compaction factor |
| Da | Dalton |
| DMAc | dimethylacetamide |
| DMSO | dimethyl sulfoxide |
| EWC | equilibrium water content |
| FESEM | field emission scanning electron microscope |
| FTIR | Fourier transform infrared |
| HD | 1, 6-hexanediol |
| IEP | isoelectric point |
| IEC | ion exchange capacity |
| LCST | lower critical solution temperature |
| LLDP | liquid-liquid displacement porosimetry |
| LA | lactic acid |
| MA | malic acid |
| MBI | 4,4'- methylenebis(phenyl isocyanet) |
| MBAAm | N,N′-methylenebisacrylamide |
| NMP | N-methyl-2-pyrrolidone |

| | |
|---|---|
| NMR | nuclear magnetic resonance |
| PAA | poly-acrylic acid |
| PP | polypropylene |
| PEG | polyethylene glycol |
| PEGMA | polyethylene glycol methyl ether methacrylate |
| PEGME | polyethylene glycol methyl ether |
| PES | polyethersulfone |
| PVCL | poly-vinylcaprolactam |
| PVDF | polyvinylidene fluoride |
| PVDF-HFP | Poly(vinylidene fluoride-*co*-hexafluoropropylene) |
| PVP | polyvinylpyrrolidone |
| PWF | pure water flux |
| PU | polyurethane |
| RO | reverse osmosis |
| THF | tetrahydrofuran |
| TMP | transmembrane pressure |
| UF | ultrafiltration |
| WCA | water contact angle |

# Chapter 1

## Introduction

# Chapter 1
# Introduction

*This chapter discusses a brief summary of the basic fundamentals, involved in membrane technology. It also summarizes the state-of-the art in polymeric membranes, their applications and the background of the problem undertaken in this work i.e. the problem associated with the fouling of the polymeric membrane. It also discusses the features of different techniques of membrane preparation. The chapter subsequently presents detailed literature review that includes the basis of two major problems of polymeric membranes in applications, i.e., membrane fouling and membrane wetting. The hydrophilic and antifouling modification methods are comprehensively reviewed as well as the objectives of the present work are also highlighted in this chapter.*

## 1.1. Background

Membranes are defined as semi-permeable barriers that prevent intimate contact between two homogeneous phases, but allow preferential passage of certain species across their structures. In recent years, membranes and membrane separation processes have grown from a simple laboratory tool to an industrial process with considerable technical and commercial impact.

The roles of membranes are to change the composition of a solution on the basis of relative permeation rates (membrane separation processes), to physically or chemically modify the permeating species (ion-exchange membranes and bio-functional membranes), to conduct electric current, to prevent permeation (packaging or coating) or to regulate the rate of permeation (controlled release).

Membrane processes are currently gaining a lot of interest in separation technology. Separation operation, in fact, occupies a key position in process industries that include foods, pharmaceuticals and other industries. The rapid growth in membrane technology has made it

a serious competitor for other conventional separation technologies like crystallization, distillation, etc. particularly for small scale operations. The membrane separation processes offer following advantages over other means of separation:

- Separation can be carried out continuously;
- Low energy utilization as no phase change or temperature change is involved;
- Low maintenance as the systems are easy to operate and maintain;
- Constituents in the concentrated stream remain chemically unaltered due to non-requirement of any chemical addition which facilitated their subsequent utilization;
- Capability of generating permeates of acceptable quality which can be reused as make-up water for emulsification and discharged directly into a receiving water body.

However, membrane separation processes suffer from the following drawbacks due to membrane fouling and concentration polarization:

- Low membrane life time;
- Low selectivity or flux.

Measures are explored to reduce membrane fouling and concentration polarization so as to overcome these limitations. Nowadays, membrane technology is seen to be applied in various industrial areas such as food and beverages, metallurgy, pulp and paper, textile, pharmaceutical, automotive, dairy, biotechnology, chemical industries, etc. [1].

### 1.1.1. Classification of membrane

In the most general sense, a synthetic membrane is a barrier which separates two phases and restricts the transport of various chemical species in a rather specific manner. Membranes can be solid or liquid. They may be either neutral or may carry negative or positive charges or both. They can be homogeneous (i.e. completely uniform in composition and structure) or

heterogeneous (i.e. containing pores of finite dimensions or consisting of some form of layered structure). Membranes can be further classified by (i) nature, (ii) structure and (iii) mechanism of action [1 - 3]. By nature, membranes can be classified as biological and synthetic membranes. These two types of membranes differ completely in structure and functionality. Biological membranes can be subdivided into living and non-living membranes. Synthetic membranes can be subdivided into organic (polymeric, liquid) and inorganic (ceramic, metal) membranes. This study emphasizes only on the polymeric membranes.

According to morphology or structure, solid membranes can be divided into two main classes: symmetric (or isotropic) and asymmetric (or anisotropic). The symmetric membranes can be subdivided further into porous, nonporous or dense and electrically charged membranes. Symmetric porous membranes have a rigid, highly voided structure with randomly distributed, interconnected pores. In general, only molecules that differ considerably in size can be separated effectively by such membranes, e.g. ultrafiltration and micro filtration. On the other hand, nonporous, dense membranes consist of a dense film through which permeates are transported by diffusion under the driving force of a pressure, concentration, or electrical potential gradient. The separation of various components of a mixture is related directly to their relative transport rate within the membrane, which is determined by their diffusivity and solubility in the membrane material e.g. pervaporation and reverse osmosis. Electrically charged membranes (or ion-exchanged membranes) can be dense or porous, but are most commonly very finely microporous, with the pore walls carrying fixed positively or negatively charged ions. The separation is affected by the charge and concentration of the ions in solution e.g. electro dialysis.

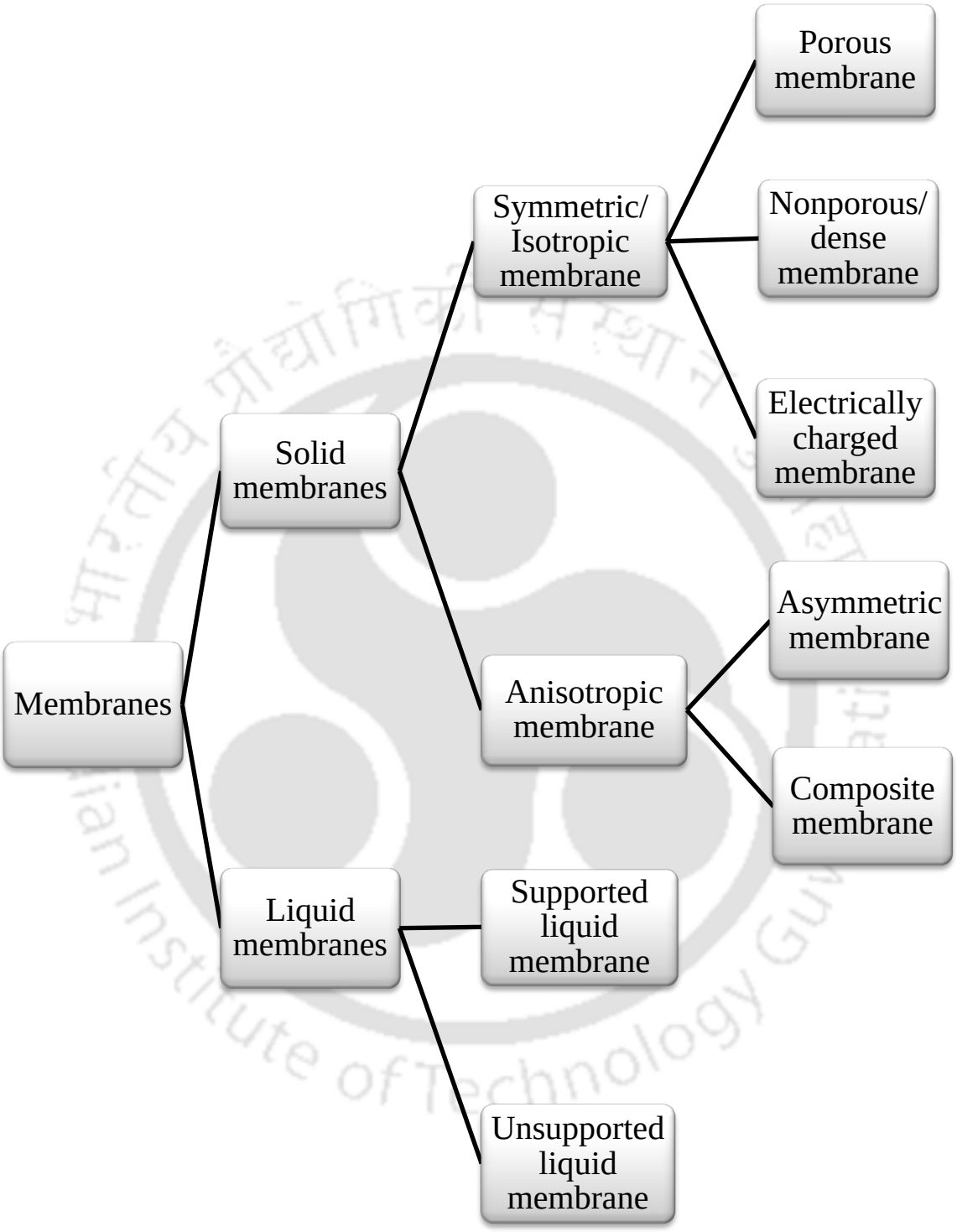


**Figure 1.1: Membrane classifications according to the morphology.**

Asymmetric membranes consist of a very dense top layer or skin of thickness 0.1 – 0.5 $\mu m$ supported by a porous sub-layer with a thickness of about 50 -150 $\mu m$. The top layer and its substructure may be formed in a single operation or separately. In composite membranes, the layers are usually made from different polymers; each layer of which can be optimized independently. The separation properties and permeation rates of the membrane are determined exclusively by the top layer; the sub-layer functions as a mechanical support. The advantages of the higher fluxes provided by such membranes are so great that almost all commercial processes use such membranes.

There are two types of liquid membranes; supported liquid membranes and unsupported liquid membranes. Supported liquid membranes have a microporous structure which is filled with the liquid membrane phase; the microporous structure provides the mechanical strength and the liquid-filled pores the selective separation barrier. The microporous substructure should have a high porosity and a pore size small enough to support the liquid membrane phase sufficiently under hydrostatic pressure. Unsupported liquid membranes are composed of thin films of liquid stabilized by a surfactant in an emulsion type mixture. Figure 1.1 shows membrane classes according to their morphology. On the basis of mechanism of action, membranes are classified as adsorptive or diffusive, ion-exchange, osmotic or nonselective (inert) membranes [1].

### 1.1.2. Classification of membrane separation processes

The wide variety of membrane separation processes differ from one another in the type and configuration of the membrane, the mechanism of trans-membrane transport for various feed components, the nature of the process driving force and other features. Some processes which are well proven in full scale industrial applications, have been widely used for separation,

purification and concentration of water-soluble solutes or water dispersible materials in industries such as pharmaceutical, chemical processing, food processing, oil industries, wastewater treatment plant, etc. Other processes, which are still in experimental stage, are yet to get into industrial use.

Membrane separation processes may be classified and categorized by a number of criteria. It is a filtration technique in which a membrane acts as a selective barrier between two phases [1]. As a result of a driving force across the membrane, components are transported towards the membrane surface, where some components pass the membrane and others are retained at the membrane surface. Membrane processes are available for numerous applications, each with its own driving force and separation characteristics. Table 1.1 provides further information on these processes, such as membrane type, method of separation and range of applications [3, 4].

Pressure driven membrane separation processes differ mainly in the pore size of their membranes, which makes a particular membrane effective for the removal of a specific range of impurities. Reverse osmosis has the smallest membrane pore size and therefore is used to remove all ionic species. Nanofiltration is sometimes referred to as 'loose reverse osmosis' as it can remove divalent ions and low molecular weight contaminants while allowing monovalent ions to pass through. Ultrafiltration is used for removal of macromolecules such as proteins and small colloids, but not ionic species. Microfiltration is used to remove particulates, bacteria, and other larger colloids only. Table 1.2 reports a summary of the main characteristics of the pressure driven processes in terms of pressure, pore size and removable components.

In pressure driven membrane systems the pressure of the feed solution permits passage of the major portion of the solution through a semi-permeable membrane. The portion of the feed solution that passes through the membrane is called permeate, or filtrate.

The portion of the feed solution that does not pass through the membrane is called concentrate or retentate. A simple schematic representation of a membrane process is shown in Figure 1.2.

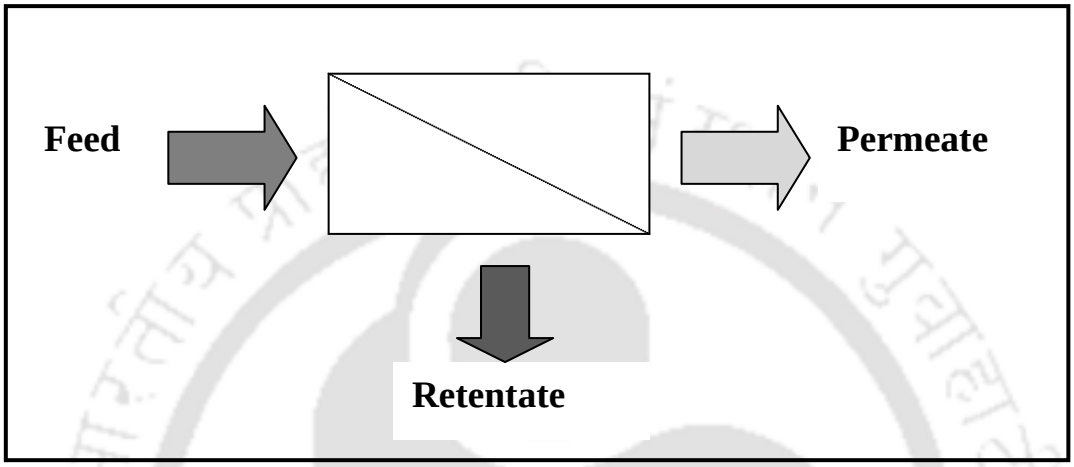


**Figure 1.2: Schematic representation of a membrane process.**

**Table 1.1: Typical membrane separation processes: Operating principles, driving force and applications [3, 4].**

| Separation process | Membrane type | Driving force | Separation mechanism | Range of application | Size range (nm) |
|---|---|---|---|---|---|
| **Micro filtration** | Symmetric and asymmetric microporous membrane | Pressure difference (ΔP) | Sieving mechanism as a function of pore size and adsorption | Sterile filtration clarification | 100-10000 |
| **Ultra filtration** | Asymmetric microporous membrane | Pressure difference (ΔP) | Sieving mechanism | Separation of macromolecular solutions | 10-100 |
| **Nano filtration** | Asymmetric 'skin type' membrane | Pressure difference (ΔP) | Solution diffusion mechanism | Separation of divalent ions from solutions | 0.5-5 |

| | | | | | |
|---|---|---|---|---|---|
| **Reverse osmosis** | Asymmetric 'skin type' membrane | Pressure difference (ΔP) | Solution diffusion mechanism | Separation of salts and micro solutes from solutions | <1 |
| **Dialysis** | Symmetric microporous | Concentration difference (ΔC) | Diffusion | Separation of salts and micro solutes from macro moleculr solutions | <1 |
| **Electro dialysis** | Cation and anion exchange membrane | Electric potential difference (ΔE) | Selective transport of ions or molecules according to electric charge | Desalting of ionic solutions | <1 |
| **Supported liquid membrane** | Microporous membranes supporting adsorbed organic liquid | Concentration difference (ΔC) | Solution diffusion via carrier | Separation and concentration of metal ions and biological species | <1 |
| **Membrane distillation** | Microporous membrane | Temperature difference (ΔT) | Vapour transport into hydrophobic membrane | Ultra pure water concentration of solutions | 1-10 |
| **Pervaporation** | Asymmetric membrane | Concentration difference (ΔC) | Solution diffusion mechanism | Separation of organics | <1 |

The UF membrane is considerably more porous i.e. its nominal pore size is larger compared to the reverse osmosis (RO) membrane. As a result, most soluble species including inorganic salts pass through the membrane with the water; but colloids, suspended solids and high molecular weight organic molecules (e.g. BSA) do not pass through the membrane with the water. They are rejected and remain in the concentrate (retentate)

stream. The porous nature of the UF membrane allows the process to be operated with high fluxes at relatively low pressures (e.g. 1 – 10 bars). This is possible because the osmotic pressure of colloids and high molecular weight organics is extremely low. The degree and quantity of the separation are a result of the pore size of the membrane and the molecular structure, size, shape and flexibility of the colloids and organic molecules. Pore sizes ranging from 0.001–0.01 $\mu m$ allow separation from solution of molecules with a molecular weight between 500 and 3,00,000.

**Table 1.2: Characteristics of the pressure driven membrane processes [1]**

| Membrane processes | Transmembrane pressure (bar) | Pore size (nm) | Removable components |
|---|---|---|---|
| Microfiltration | 1 - 2 | 100 - 1000 | Suspended solids, bacteria |
| Ultrafiltration | 2 - 10 | 1 - 100 | Macromolecules, viruses, proteins |
| Nanofiltration | 10 - 30 | 0.5 - 5 | Micropollutants, bivalent ions |
| Reverse osmosis | 35 - 100 | < 1 | Monovalent ions, hardness |

## 1.2. Materials for ultrafiltration membranes

The most important class of material for ultrafiltration membranes includes the polymers. The choice of the polymeric material for a particular membrane is based on its chemical and physical properties originating from structural factors such as molecular weight, chain flexibility and chain interaction. Those factors also determine the membrane permeability [1]. Chemical properties describe how the material chemical structure changes under certain

circumstances such as change in pH, temperature, etc. Physical properties include density, melting point, glass transition temperature, compressibility, etc [5].

The process of making the UF and MF membranes has to control both the surface characteristics, and the supporting sub-structure. Polymers should have good mechanical properties to produce membranes, with a reasonable degree of flexibility. Also, they need to have good chemical resistance, tolerance limit of a wide pH range, and high chlorine concentrations, enabling rigorous cleaning to be conducted if necessary. In addition, thermal resistance should be good, so that moderate elevated temperatures can be used without affecting the membrane properties or life [6].

Commercial thermoplastics and cellulose were primarily used as membrane materials for large scale production. Basically all polymers can be used as membrane material but the chemical and physical properties differ so much that only a limited number is used in practice. Since the initial development of the first asymmetric cellulose acetate membrane, significant progress has been made in the field of non-cellulosic membrane materials that are more durable, less susceptible to biodegradation, and perform well within broad pH and temperature ranges. The materials most commonly used for the production of UF membranes by phase inversion method are:

- Cellulose acetate (CA)
- Aromatic Polyamide (PA)
- Polysulfone (PSF) and Polyethersulfone (PES)
- Polyvinylidene fluoride (PVDF)
- Polyacrylonitrile (PAN)
- Polypropylene (PP)
- Polyethylene (PE)

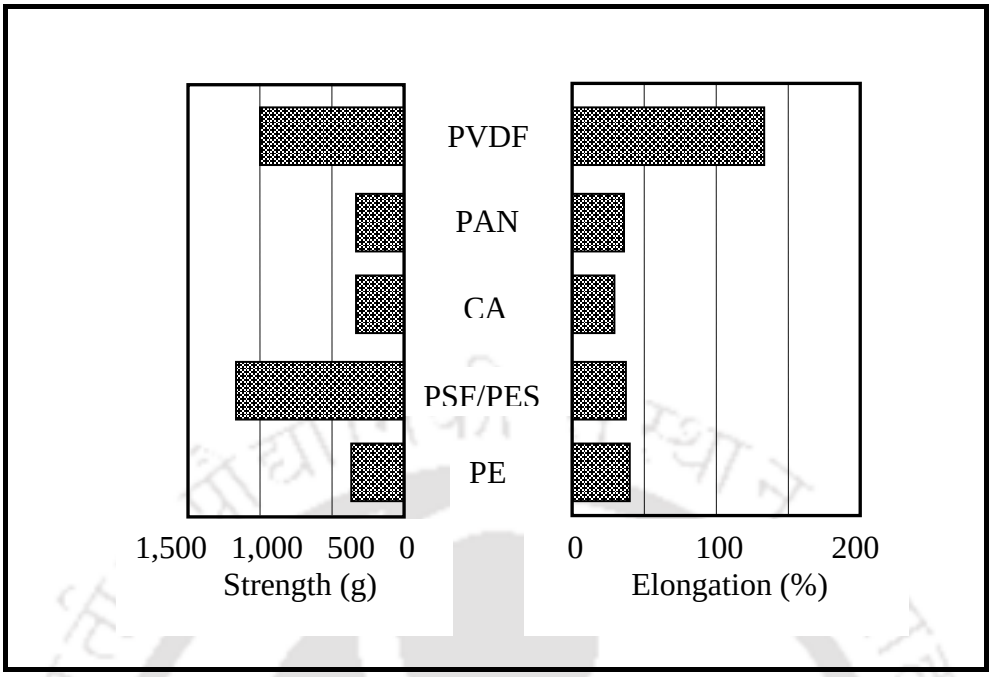


**Figure 1.3: Comparison of physical stability of different membrane materials.**

Figure 1.3 compares the common polymers in terms of strength and flexibility [7]. PES has similar mechanical properties to those of PSF. It shows that PSF and PVDF are the strongest polymers, whilst PVDF is more flexible. Of the polymers discussed above, the PSF/PES family has the widest chemical resistance, and can tolerate a pH range from 1.5 to 13, as well as moderate chlorine levels. PVDF tolerates acids, but is limited to pH 11 with caustic. However, its major advantage is a very high tolerance to chlorine, which makes it ideal for membrane reactors. Chlorine cleaning is preferred for PVDF membranes while PSF/PES may choose for caustic cleaning. PAN has similar pH tolerance to PVDF, combined with a moderate chlorine tolerance (almost similar to PSF/PES). CA is much more limited in its chemical resistance, since its natural hydrophilicity makes it susceptible to hydrolysis in the presence of acids below pH 4 and alkalis above pH 8. It tolerates chlorine, but is biodegradable which makes it sensitive to bacterial attack. The polyolefin family, PP and PE, has good tolerance to acid and caustic, but low tolerance to chlorine, particularly in the case

of PP. The lack of chlorine tolerance is a major limitation in the water industry, and this has limited the prospects for these membranes. Apart from this, solubility of PSF and PVDF makes them ideal candidate for polymer blend membranes since other polymer can be co-dissolved. PSF and PVDF has following advantages over other organic membrane materials [2]:

- High chemical resistance.
- Usability in a wide pH range.
- Soluble in solvents like DMAc and NMP, making it easily applicable for the conventional phase inversion processes.
- High thermal stability.
- Good mechanical strength and permeability.
- Ability to modify properties through blending with other polymers.

However, PSF and PVDF membrane exhibits drawback mainly due to their hydrophobic nature which causes the adsorption and deposition of foulants (colloids, proteins and particles) on the surface of the membrane and inside the membrane pores. This leads to lower permeation flux and deterioration in performance [8, 9].

That's why various methods are adopted to make them hydrophilic and less prone to fouling. The methods include surface coating by adsorption, free radical or radiation grafting of hydrophilic polymers, plasma treatment, chemical conversion of polymer side chains to hydrophilic groups, blending with hydrophilic polymers, etc [2].

## 1.3. Fouling and its mechanism

During UF, some constituents of the feed deposit on the membrane surface and/or in the membrane matrix resulting in gradual decrease in permeate flux. This process is often

referred to as fouling of the membrane. The common definition of membrane fouling is provided by the International Union for Pure and Applied Chemistry (IUPAC), which defined fouling as: '*Fouling is the process resulting in loss of performance of a membrane due to the deposition of suspended or dissolved substances on its external surfaces, at its pore openings, or within its pores*' [10].

Mulder (1997) gave a second definition of fouling as: '*The (ir)reversible deposition of retained particles, colloids, emulsions, suspensions, macromolecules, salts etc. on or in the membrane*' [1].

Wiesner and Aptel (1996) defined fouling as an irreversible flux reduction: '*A reduction in permeate flux that cannot be reversed*' [11].

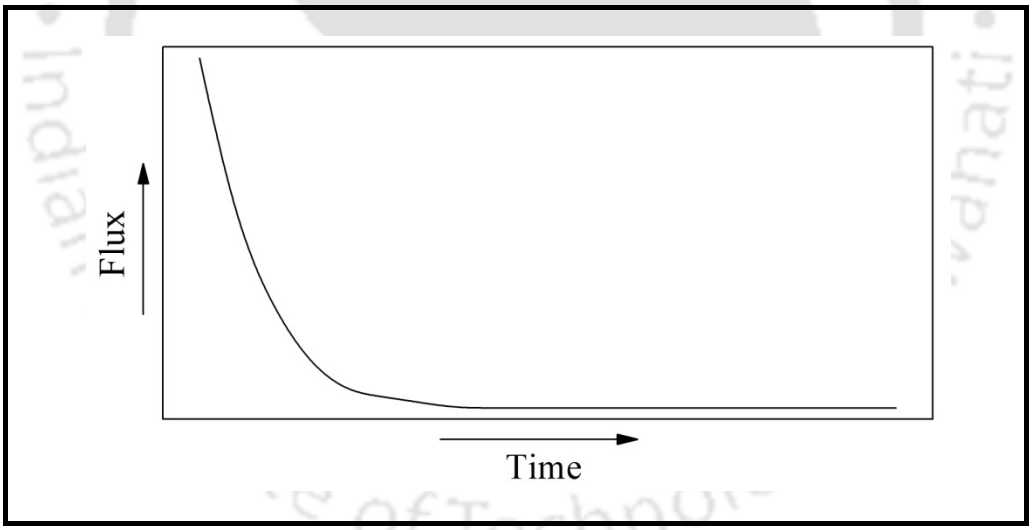


**Figure 1.4: Flux declination with time at a constant TMP.**

The easily removable part of the retained material is called the reversible part of the fouling layer, the remaining part is called the irreversible fouling layer. The feed constituents that are retained on or in the membrane surface are called foulants. The retention of feed constituents causes an increase of the total resistance over the membrane, resulting in a

decreased flux at a constant TMP. The decrease in flux that is found during membrane filtration is schematically shown in Figure 1.4.

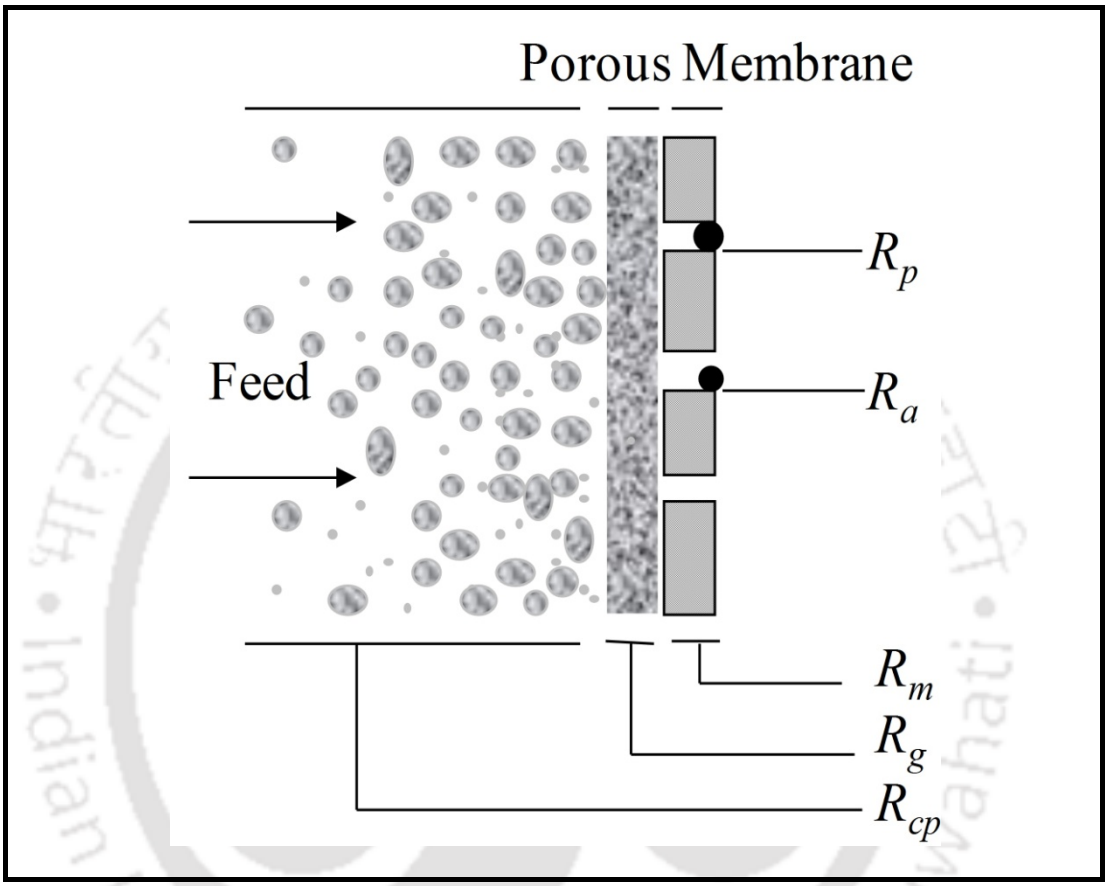


**Figure 1.5: Overview of various resistances of a fouled membrane in pressure driven process; $R_a$ = adsorption, $R_p$ = pore blocking, $R_m$ = membrane resistance, $R_g$ = gel layer resistance, $R_{cp}$ = concentration polarization.**

Flux decline can be caused by several factors, such as plugging of the membrane pores, adsorption inside the membrane pores, concentration polarization and gel layer formation. All these factors induce additional resistances on the feed side to the transport across the membrane. Essentially, four 'fouling mechanisms' can be distinguished which are schematically shown in Figure 1.5. During membrane filtration, these mechanisms may occur simultaneously. The membrane resistance ($R_m$), is mainly involved in the initial period of

filtration. After some time, accumulation of retained solutes near the membrane surface results in a highly concentrated layer which exerts a resistance towards mass transfer; this is the concentration polarization resistance ($R_{cp}$). When the concentration of the accumulated solute molecules is sufficiently high, a gel layer is formed which exerts gel layer resistance ($R_g$). With porous membranes it is possible that some smaller solute molecules penetrate into the membrane pores and block them, leading to the pore-blocking resistance ($R_p$). Another resistance ($R_a$) may likely to arise due to adsorption of solute molecules upon the membrane surface as well as within the pores. Among these four resistances $R_{cp}$ and $R_g$ are responsible for reversible fouling ($F_r$), where as $R_p$ and $R_a$ are responsible for irreversible fouling ($F_{ir}$). $F_r$ is caused by reversible solute deposition on the membrane surface, which can be removed by hydraulic cleaning of the membrane. $F_{ir}$ is caused by irreversible solute adsorption and it cannot be keep away from hydraulic cleaning.

## 1.4. Antifouling mechanism

It is generally accepted that an increase in hydrophilicity offers better fouling resistance because many foulants such as protein are hydrophobic in nature [12]. A pure water layer is easily formed on highly hydrophilic surface, which can prevent the adsorption and deposition of hydrophobic foulants onto membrane surface, thus reducing fouling (Figure 1.6a). In fact, numerous studies have been conducted to enhance surface hydrophilicity of membranes aiming at the improvement of antifouling performance. Similarly, the surface charge is also an important factor influencing membrane fouling. It is easy for us to understand that the electrostatic repulsive force but not the attraction force between the charged membrane surface and foulant in feeding solution is advantageous to reducing membrane fouling (Figure 1.6b). In other words, the antifouling membranes should be developed according to the

electrostatic character of foulants in practical situation. The surface-bound long-chain hydrophilic molecules (e.g. polyethylene glycol, PEG) were very effective in preventing adsorption of macromolecules such as protein onto membrane surface due to the steric repulsion mechanism [13]. When hydrophilic polymer chains are grafted or created on membrane surface, this diffused hydrophilic layer will exert steric repulsion to hydrophobic proteins that reach the surface (Figure 1.6c). Steric repulsion is due to the loss of configurational entropy resulting from volume restriction and/or osmotic repulsion between the overlapping polymer layers [13, 14].

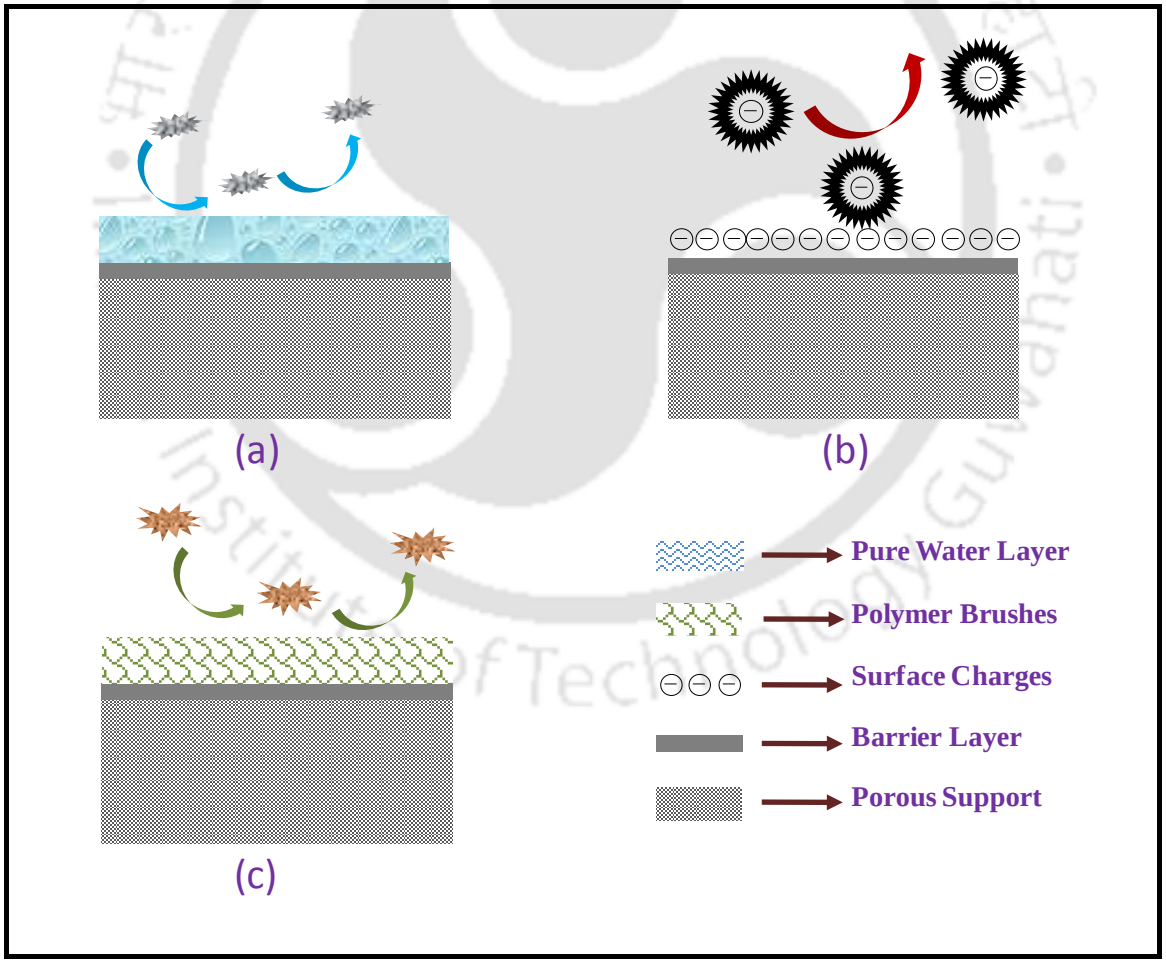


**Figure 1.6: Schematic diagrams of antifouling mechanism: (a) pure water layer (b) electrostatic charges (c) steric repulsion.**

# 1.5. Anti fouling modification methods for polymeric membranes

## 1.5.1. Improvement of membrane preparation process

The anti fouling modification of polymeric membranes can be achieved during preparation process, e.g., the introduction of hydrophilic or anti fouling modifiers by blending. The anti fouling modifiers can be mainly classified into two categories: polymer material and inorganic nanoparticle.

### 1.5.1.1. Introduction of organic materials

The blending of organic material is a simple way to enhance the hydrophilicity of polymeric membranes. In this method, the additives are usually dissolved into membrane separation process. Water soluble polymers [14–18], charged polymer [19], surfactants [20], organic acids [21] and other hydrophilic polymer [9, 22, 23] have been used to prepare hydrophilic UF membrane through homogeneous blending. Apart from these materials different type of copolymers has also been used consisting stimuli responsive property or amphiphilic property. Copolymers of acrylic acid or methacrylic acid are used as pH responsive modifier like poly-(acrylonitrile-co-acrylic acid) [24], poly(acrylonitrile-acrylic acid-vinyl pyrrolidnone) [25], poly(N-isopropylacrylamide-co-methacrylic acid-co-methyl methacrylate) [26] etc. Amphiphilic modifier like β-cyclodextrin polyurethane [27], polystyrene-b-poly (ethylene glycol) methacrylate [28] etc.

### 1.5.1.2. Introduction of inorganic nanoparticles

Besides organic materials, the inorganic nanoparticle is another type of important modifier. Polymer-nanoinorganic particles composite membranes present an interesting approach for improving the separation, physicochemical, as well as anti- fouling properties of polymer

membranes [29]. The introduction of nanoparticles into polymeric membranes to enhance hydrophilicity has been proven to be an effective way and attracted much attention. The nanoparticles mixed into the polymeric membrane casting solution mainly include $TiO_2$ [30], $SiO_2$ [31], $Mg(OH)_2$ [32], ZnO [33], carbon naotubes [34], boehmite nanoparticles [35]. There are two ways of introducing nanoparticles into PVDF membranes during the preparation process: blending them in coagulation bath or in polymer solution.

## 1.5.2. Surface modification of existing polymeric membranes

The surface modification of existing polymeric membranes is another effective and frequently used method to enhance hydrophilicity. In general, the aim is to form a hydrophilic layer on the existing polymeric membrane surface which can prevent the contact between membrane and pollutants, thus reducing membrane fouling. The surface modification can be mainly classified into two categories according to the interaction between modifiers and membranes: physical modification and chemical modification.

### 1.5.2.1. Physical modification

Here, the physical modification means that the hydrophilic modifiers exist on polymeric membrane surface via physical interaction but not covalent bonding. In other words, the chemical composition of polymeric membrane is unchanged. However, the chemical reaction may be required during the modification. The physical modification of PVDF membranes can be achieved by two ways: (1) The hydrophilic polymers is directly coated or deposited on membrane surface (further treatment is conducted sometimes). (2) The polymeric membrane is firstly immersed in or coated by a solution of chemically active monomers. Then, the monomers are immobilized onto membrane surface by cross linking or polymerization

reaction without the chemical participation of base membrane. The hydrophilic polymers for surface modification of polymeric membranes can be selected from commercial materials such as poly vinyl alcohol [36],chitosan [37], polyether block amide (PEBAX) [38],etc.

#### 1.5.2.2. Chemical modification

In chemical treatment, the polymeric membrane surface is modified through covalent bonding interaction. Generally, base polymer chains are firstly activated by chemical reaction or high-energy radiation, followed by the grafting of hydrophilic modifiers. The membrane surface properties can be improved while the membrane bulk is not significantly affected. Moreover, the covalent attachment of modifiers on membrane surface offers a long-term chemical stability, in contrast with physical surface coating. So far, the chemical modification of polymeric membranes is mostly focused on the pegylaytion [39], sulfonation [40, 41], O3/O2 pre activation [42, 43], electron beam radiation [44], plasma treatment [45] etc.

## 1.6. State of the art

With a brief overview of the contemporary research, this section outlines the research outcome of various literatures so as to identify few promising areas of research that needs to be addressed in this thesis. The state of the art has been presented for anti fouling modification of polymeric ultrafiltration membranes.

### 1.6.1. Modification of polymeric membrane by using nonsolvent additives

**Literature survey**

Uses of asymmetric membranes in various fields like reverse osmosis, ultrafiltration, nanofiltration and gas separation processes are increased day by day due to their high

selectivity, permeability and mechanical strength in high pressure applications [46]. The most common method for fabrication of flat sheet asymmetric membrane is wet phase inversion method. The key parameters for this technique are polymers-solvent-additives, their compositions and coagulant bath conditions (temperature and composition) [47].

Some studies illustrated that the addition of organic non-solvents in casting solution could improve the performance and structure of the asymmetric membranes. Ghaemi et al. [21] investigated the effect of different concentration of organic acids (Ascorbic acid, citric acid and malic acid) on the morphology and performance of PSF membrane for xenobiotics removal. They found that PWF increased with increase in concentration of organic acid. Addition of citric acid increases the efficiency of solute retention compared to other two acids. The effect of several organic non-solvents in PSF/solvent and poly ether sulfone (PES)/solvent systems was investigated and reported in detail [48-53]. Organic non-solvents used were methanol, ethanol, propanol, butanol, pentanol, ethylene glycol, diethylene glycol as well as acetic acid, propionic acid and water. Various literatures related to non-solvent addition is reported in Table 1.3.

**Table 1.3: Literatures related to non-solvent additive.**

| Polymer | Solvent | Non-solvent additive | Reference |
|---|---|---|---|
| PSF | NMP | Organic acids | [21] |
| PSF | NMP | Ethanol, Glycerol | [54] |
| Polycarbonate | Dichloromethane | Ethanol, Propanol, Butanol | [55] |
| PVDF-HFP | NMP | LiCl, glycerol | [56] |
| PSF | NMP | Ethanol, Propanol, Butanol, chloroform | [57] |
| PSF + poly (vinyl-4) pyridine | NMP | Diethylene glycol | [58] |

| | | | |
|---|---|---|---|
| PSF | THF+DMAc | Ethanol | [59] |
| Cardo polyamide | DMAc | LiCl | [60] |
| Polyimide | NMP | Ethanol | [48] |
| PSF | NMP | Water, Ethanol | [49] |
| PSF | THF+DMAc | Ethanol | [61] |
| PSF, PES, PEI, CAB | NMP, DMAc | Water, Ethanol | [50] |
| PES | NMP | Water | [51] |
| PSF | DMAc+THF | Water | [62] |
| PPO | Chloroform | Branched and linear alcohol | [63] |
| PES | NMP | Methanol, Ethanol, Propanol, Butanol, pentanol, ethylene glycol, diethylene glycol | [52] |
| PSF, PES | NMP, DMAc | Methanol, diethylene glycol, deionized water | [53] |

**Possible scope for further research**

From the above literatures it may be envisaged that although several authors have reported addition of various non solvent to PSF/PES membranes, but the effect of alcohols additives on PVDF membranes is scant. Moreover, variation in membrane hydrophilicity in presence of alcohols as additives has not been investigated yet. Therefore, in the present work, the effect of various alcohols (like methanol, ethanol, n-propanol and n-butanol) on the morphology, permeation characteristic and on the hydrophilicity of PVDF membrane was investigated. Membrane casting solution contains poly(vinylidene fluoride-co-hexafluoropropylene) (PVDF-HFP) as base polymer, N-Methyl-2-pyrrolidone (NMP) as

solvent, poly ethylene glycol of mol wt 6000 Da (PEG 6000) as pore forming agent and various alcohols as non solvent additives.

## 1.6.2. Modification of polymeric membrane by blending water soluble polymer

### Literature survey

Blending of polymers is an important alternate to obtain various polymeric materials with desired properties and the process is less complicated and inexpensive. Water soluble polymers [14-18], charged polymer [19], surfactants [20] and other hydrophilic polymer [9, 22, 23] have been used to prepare hydrophilic UF membrane through homogeneous blending. Chakrabarty et al. [15, 17] prepared PSF membrane by using PVP and PEG of different molecular wt. as additive, in the case of PEG pure water flux (PWF) was increased with increase in molecular weight of PEG, but BSA rejection was not increased in same trend, it was highest for PEG 6000. For PVP they found that as the molecular weight of PVP was increased, membranes had more compact structure and consequently less PWF. Malek et al. [16] investigated the effect of PVP concentration on poly ether sulfone (PES) membrane and they found that addition of PVP to the casting solution strongly enhances the permeability of membrane to a specific point, after which higher concentration of PVP causes denser top layer and which lead to lower PWF. Sikder et al. [22] and Sivakumar et al. [23] et al. reported the effect of different concentrations of CA in PSF membrane. They found that, as the CA concentration increased in the membrane casting solution, largest pore diameter of membranes significantly decreased and microfiltration performance get enhanced. Ghaemi et al. [21] investigated the effect of different concentration of organic acids (Ascorbic acid, citric acid and malic acid) on the morphology and performance of PSF membrane for

xenobiotics removal. They found that hydrophilicity and PWF increased with increase in concentration of organic acid and citric acid presented highest efficiency in retention of the solutes compared to other two acids.

**Possible scope for further research**

From the review of above literatures it may be concluded that although several authors have reported various additives to increase the hydrophilicity of PSF membrane, but the role of different molecular weights of polyethylene glycol methyl ether (PEGME) in PSF membrane has not been accounted yet. Therefore, in the present work, the effect of addition of PEGME of mol. wt. 550, 2000 and 5000 Da at constant concentration of 5 wt % in casting solution on PSF membrane have been investigated. Effects of mol. wt. of PEGME additive on morphology, permeation characteristic and on the hydrophilicity of membrane was reported and explained well. Morphology of each membrane was analyzed by field emission scanning electron microscope (FESEM). The performances of the membranes were investigated by water permeation and bovine serum albumin (BSA) rejection at different pH (4.8, 7.2 and 10).

## 1.6.3. Use of functional copolymers for the modification of polymeric membranes

**Literature survey**

Use of polymeric membrane in water purification [64], protein separation [65], biotechnology for gene and tissue engineering [66], food industry [67] for separation of fermentation and food products with high purity and yield is increasing day by day. Among these materials, PES and PSF are favourable for membrane casting, because of good physicochemical

constancy, resistance to chlorine and oxidation [68]. Solubility of PSF makes it more suitable for polymer blend membranes as others polymers can be simultaneously dissolved, this permit different properties (like hydrophilic, hydrophobic, thermo responsive, pH responsive, antifouling properties) of the finished membrane to be customized. To proceed for the aforesaid applications, many studies have been done to investigate the modification of polymeric membranes [9, 17-20, 23, 66]. The modification of membranes with stimuli-responsive polymers, which can exhibit relatively large and abrupt property variations in reply to small change in external stimulus (like change in temperature, pH, ionic strength, electric field and concentration of specific chemical species), added a variety of new abilities to the membranes and broadened the application fields of membrane [70-71].

Much interest has been shown in the study of functional copolymers for the modification of polymeric membrane. Various functional copolymers have been mixed in casting solution of polymeric membrane to induce required property like hydrophilicity and pH sensitivity. Qian et al. [72] have prepared PES membrane by blending a copolymer of acrylonitrile and acrylic acid. The membrane showed good pH sensitivity and pH effect was observed at the pH between 4.5−11. Wang and co-workers [25, 73-75] have prepared different types of pH responsive copolymers for the modification of PES membrane. In some other works, graft polymerizations of a functional monomer with commercial polymer was done, which improved the physicochemical properties of the parent polymer [76]. Shi et al. [77] have modified the PES membrane by grafting methacrylic acid with PES and studied its effect on flux behaviour between 2 to 10 pH. In another study [78], pH sensitive membrane was prepared by grafting poly (N-isopropylacrylamide)-block-poly (methacrylic acid) in commercial porous nylon 6 membrane, which worked between pH 3 and 8. Similarly, Himstedt et al. [79] have modified the commercially available NF 270 membranes by

growing PAA nanobrushes on the surface of membrane and studied the flux behaviour at pH around 3 and 7.

**Possible scope for further research**

Among different stimuli responsive materials, pH and thermo responsive materials have been widely used for drug delivery systems and various advance separation processes. So, keeping the main objective of preparation of fouling resistant membrane, this part of thesis focussed on the preparation and characterization of the dual responsive membrane using pH and thermo responsive copolymer with hydrophilicity. Although, various studies have done on the addition of functional copolymer, but study of fouling resistant behaviour is fewer. Apart from that, in the best of our knowledge nobody has study the effect of dual responsive double hydrophilic poly (N-vinylcaprolactam-co-acrylic acid) (poly (VCL-co-AA)) copolymer on polymeric membranes. Thus, poly (VCL-co-AA) was synthesized by radical copolymerization of VCL with AA in the presence of AIBN as initiator. The PSF membrane was modified by blending poly (VCL-co-AA) in casting solution. In this copolymer, PAA is a typical polymer which can respond to the change in pH on the other hand PVCL have lower critical solution temperature (LCST) of ~ 35˚C, which provides thermo responsive property to the copolymer [70]. Apart from giving pH and thermo sensitivity to the membrane, this copolymer also increases the hydrophilicity of the membrane, as PAA contains carboxylic group and PVCL contains large number of hydrophilic cyclic amide group in side chain. Due to hydrophilic in nature, it can improve the antifouling property of the membrane.

## 1.6.4. Preparation of polymeric membrane with cross-linked hydrophilic pH responsive copolymers

### Literature survey

Among different type of polymers PEG and PVP is most favourable additive for membrane preparation due to their protein resistant character. This protein resistant character of these polymers is accredited to their highly hydrophilic, non-ionic and supple character [80, 81]. Although blending PEG and PVP into the casting solution may increase the surface hydrophilicity of PES membranes only for the short term, they will ultimately leach out from the surface as they are water soluble [82]. Therefore, in order to increase hydrophilicity, Pezesk et al. [83] modified the UF membrane by blending PEG based hydrophilic polyurethane macromolecule. Modified membranes had a lower water contact angle compared to unmodified membranes with a high of 6.5 times more flux. In another study Wang et al. [9] modified PSF membrane by pluronic F 127 (tri block copolymer of PEG) with PEG as a pore forming agent. They got a maximum of 90% flux recovery for modified membrane compared to unmodified membrane which had flux recovery of only 40%.

In recent studies functional polymers had been mixed in the casting solution of polymeric membrane to persuade necessary properties like hydrophilicity and pH sensitivity. Poly-acrylic acid (PAA) and poly-methyl methacrylate (PMMA) are most commonly used polymers to obtain pH sensitivity. Their shrinking-swelling behaviour is caused by deionization (–COOH) and ionization ($–COO^-$) around their $pK_a$ value. In this regard, Wei et al. [84] prepared poly ether sulfone (PES) membrane by blending PAA gel. The blended PES membranes showed the pH-valve effect at pH between 3 and 8. In another work, M'Bareck et al. [85] prepared pH responsive membrane with the help of PAA. To obtain the membranes, they dissolved PSF and PAA separately in dimethyl formamide (DMF), and then the two

solutions were mixed in desired proportions. Although, when PAA or PMAA were blended directly with PSF as mentioned in the literature [85], the leaching of these polymers was unavoidable like other water soluble polymer. This problem can be avoided by cross linking of polymer. Wei et al. [84] had prepared cross linked PAA gel and directly blend it with membrane casting solution. Cross linking resist the elusion of copolymer into the water. Instead of getting dissolved in water, cross linked copolymer of PAA gets swell and shrink according to change in pH [86].

**Possible scope for further research**

Most of the literatures have modified the polymeric membranes with either PEG or PAA for hydrophilicity or pH sensitivity, respectively. Therefore, in this part of thesis novel cross linked pegylated copolymers of PAA were synthesized and used in PSF membrane preparation in order to increase dual properties of membrane simultaneously i.e. pH sensitivity as well as hydrophilicity of the membrane. This study focused on the preparation and characterization of hydrophilic PSF membrane with pH sensitivity. Pegylated pH sensitive cross linked copolymer poly (acrylic acid-co-polyethylene glycol methyl ether methacrylate) (poly (AA-co-PEGMA)) was synthesized in presence of cross linker N,N′-methylenebisacrylamide (MBAA) in toluene as a solvent by precipitation polymerization. PEGMA segment provides the hydrophilicity to the membrane, while PAA segment provides the pH sensitivity to the modified membranes and MBAA keep them together and avoid their elusion in water. Different types of copolymer were synthesized by varying the ratio of AA and PEGMA.

## 1.6.5. Fabrication of polymeric ultrafiltration membrane using amphiphilic additives

### Literature survey

Ultrafiltration is a pressure driven separation process with pore size in the range of 1 nm to 100 nm and can separate macromolecules like protein and colloids. PSF is largely used as membrane material for fabrication of membrane by phase inversion method.Generally two types of hydrophilic modifiers are used for modification of PSF membranes, inorganic nanoparticle and polymer material. Various types of metal oxide nanoparticles like ZnO, $Al_2O_3$, $TiO_2$ and $SiO_2$ have been mixed in membrane casting solution. It is accounted that inclusion of NPs in membrane matrix improves the antifouling property, hydrophilicity and water permeation [30, 87-88]. Leo et al. [87] found that contact angle reduced from $85^o$ to $63^o$ and permeability increased from 2.14 to 25.45 m $s^{-1}Pa^{-1}$, when 2 wt % of ZnO nanoparticle was added to PSF membrane. But, main problem with nanoparticles is their uniform dispersion due to agglomeration and high viscosity of the membrane casting solution. Razmjou et al. [30] used modified $TiO_2$ nanoparticle and reported that when wt % of nanoparticle increased from 2 % to 6 %, flux recovery ratio reduced from 84 % to 61 %. In same study, water flux for membrane with 6 wt % of nanoparticle decreased from 350 to 170 L $/m^2$ h compared to plain PSF membrane. Reason for water flux reduction was agglomeration of nanoparticle, which resulted in pore blockage. From the literature, it may be deduced that use of nanoparticle for the increase of hydrophilicity is not encouraging for higher membrane permeability. So, blending of polymer material with desire property is an important alternate.

But, blending of these polymers in casting solution may increase the surface hydrophilicity of the modified membranes, but after some time these polymers will

eventually leach out from the surface as they are water soluble [83]. To overcome these deficiencies, amphiphilic copolymers were introduced in membrane casting solution. These copolymers have two segments viz; hydrophobic and hydrophilic. Hydrophobic segment has the affinity for the host hydrophobic polymer and it ensured the copolymers to be firmly anchored in the host polymer matrix. On the other side, hydrophilic segment in copolymer endowed the membrane surface with improved hydrophilicity [89]. Loh et al. [90] reported the effect of different pluronic block copolymer. With highest wt % of 10 for pluronic F127, they got highest water permeability of 113.8 $L/m^2$ h bar and lowest MWCO of 9 kDa. Zhao et al. [89] used different wt % of pluronic F127 in PES membranes and got higher lysozyme rejection and flux recovery ratio compared to plain membrane. In another study, UF membrane was modified with PEG-200 and PEG-600 based PU macromolecule. Modified membranes had highest PWF (6.5 times) compared to controlled membrane and membrane modified with PEG-200 based PU macromolecule had higher rejection of 100 kDa PEO. Table 1.4 shows the literature of some synthesized PU macrmolecules.

**Table1.4: Literatures related to polyurethane additive.**

| Materials | End cap | Application | Reference |
|---|---|---|---|
| –PES as base polymer<br>–NMP as solvent | PEG | Ultrafiltration | [91] |
| –PES as base polymer<br>–NMP as solvent | PEG 200, PEG 400, PEG 600, PEG 1000 and PPG 425 | Ultrafiltration | [82] |
| –SPEEK as base polymer<br>–NMP as solvent | Hydroxybenzene sulfonate | Direct methanol fuel cell | [92] |
| –PES as base polymer<br>–NMP as solvent | Oligomeric fluoro alcohol and hydroxybenzene sulfonate | Ultrafiltration | [12, 93] |

| | | | |
|---|---|---|---|
| –PVDF as base polymer<br>–DMAc and acetone in a ratio of 2:3 as a solvent | PEG 400, PEG 600, PEG 1000 | Ultrafiltration | [94] |
| –PVDF as base polymer<br>–NMP as solvent | PEG200, PEG600 | Ultrafiltration | [83] |

**Possible scope for further research**

From the above discussed literature it can be infers that finding of novel amphiphilic additives having hydrophilic end group will be a novel work in fouling free PSF membrane preparation. Also, blending of amphiphilic additives in membrane casting solution is a most facile and cost effective method driven by hydrophobic interaction between base membrane polymer and hydrophobic segment of additive molecules, as it helps the copolymer additive by strong hydrophobic anchorage group. Therefore, in this section of thesis, different end capped amphiphilic PU macromolecules were synthesized and used for the modification of PSF membrane to increase the hydrophilicity and anti fouling property of the fabricated membrane. This work focused on fabrication and characterization of fouling resistance hydrophilic flat sheet PSF membrane by phase inversion method. Amphiphilic PU macromolecules were synthesized by two step solution polymerization and end capped with four different compounds containing carboxylic group i.e., citric acid, malic acid, lactic acid and 4-hydroxy benzoic acid.

## 1.6.6. Fabrication of polymeric membrane with thermo sensitivity for easy cleaning

### Literature survey

Usually two types of additives are used, inorganic materials and organic materials. Inorganic material includes various kinds of metal oxide nanoparticles like $TiO_2$, $Al_2O_3$, $SiO_2$, ZnO etc. Blending of organic material like water soluble polymer (PVP, PEG) hydrophilic polymers (pluronic, cellulose acetate), surfactants and copolymer have been mix together with membrane casting solution [9, 14-23, 30, 87, 88]. Problem with conventional additives is that once the foulants get deposited on membrane surface, the modified surface no longer remains efficient in checking the fouling. As due to the formation of fouling layer, the membrane surface and solute particle interaction did not remain the same. And due to the changed property, it cannot prevent the further deposition of foulants [95]. In conventional fouling resistance membranes, the fouling resistant additives or layer on the membrane surface remain stagnant and foulants get deposited on these additives, after some time of use. And due to stagnant property of these additives, it is difficult to remove the foulants from those deposited areas. So, to remove these foulants from deposited areas chemical cleaning is applied. Chemical cleaning of membranes reduces the effectiveness and selectivity as well as life time of membranes. Thus, to overcome these issues stimuli responsive materials are used to blend with casting solution of membranes. These stimuli responsive materials are responsive to change in temperature, pH, ion concentration etc. The swelling and shrinking properties of the stimuli responsive materials, helps in membrane cleaning by simple hydraulic cleaning. As, due to shrink and swell behaviour, the deposited foulants layer get damaged and can be removed by hydraulic cleaning. Previously we have prepared a pH responsive membrane by adding pegylated functional copolymer poly (acrylic acid-co-

polyethylene glycol methyl ether methacrylate) [96]. This additive had provided excellent anti fouling resistance behaviour.

**Possible scope for further research**

In this part of thesis, we want to capitalize the thermo responsive behaviour of PVCL by applying a novel and modified hydraulic cleaning method for fouled membranes. In this modified method, membranes were hydraulically cleaned by rinsing and keeping the membrane at two temperatures i .e. at 25˚C and 40˚C alternately. So, to provide fouling resistant property to polymeric membrane, cross-linked polyvinylcaprolactam-co-polysulfone (PVCL-co-PSF) amphiphilic copolymer was synthesized. In this copolymer PVCL is a thermo responsive polymer, with lower critical solution temperature (LCST) around (≈35 ℃). So, above this temperature it remains in swollen state and below this temperature it rejects absorbed water and comes to shrunken state. PSF segment of the copolymer has the natural affinity for base membrane polymer due to hydrophobic nature and kept the copolymers to be securely attached to membrane surface. Also, due to amphiphilic behaviour of the copolymer it is expected that in the membrane casting solution the hydrophilic segment of copolymer located at the upper interface, will be oriented toward the liquid, which provides a more hydrophilic environment. Hydrophobic segment should be in the contact with air, but after the immersion of casting solution in coagulation bath, once phase inversion has been prompted, copolymer molecules are rearranged up-side down. Certainly, the polymer system becomes more hydrophobic due to the outflow of solvent. At the end, hydrophobic segment interact with PSF while hydrophilic segments should be oriented toward the top surface. Apart from that, copolymer molecules initially present in the bulk solution phase may migrate toward the top surface of membrane during phase inversion [90].

## 1.6.7. Modification of polymeric membrane by nanoparticles

**Literature survey**

Besides blending different type of polymer materials, recently a lot of attention has been given to the blending of nanoparticles. The nanoparticles mixed into the polymeric membrane casting solution mainly include $TiO_2$, $SiO_2$, $Mg(OH)_2$, $Al_2O_3$, ZnO, carbon naotubes, boehmite nanoparticles. Razmjou et al. [30] used modified and unmodified $TiO_2$ nanoparticle for the modification of PES membrane by blending it in PES membrane casting solution. They found that modified $TiO_2$ could produce membrane with higher hydrophilicity and better permeation performance. Although, the maximum flux and flux recovery ratio was obtained when 2 wt. % of modified $TiO_2$ nanoparticle was used. Unmodified $TiO_2$ nanoparticle produced poor performance then plain PES membrane. In another study, Ahmad et al. [97] prepared PSF membrane with $SiO_2$ and found that the modified membrane had bigger pore size with consistent surface pores. Permeation for the modified membrane was 16 times higher then plain membrane. Fouling of PSF membrane with humic acid was also studied and $TiO_2$ nanoparticles were used to modify the membrane [98]. They found that modified membranes had better resistance towards fouling specially those due to concentration polarization, cake layer formation and adsorption. ZnO nanoparticles were used as alternate to $TiO_2$ [35, 87]. It was used as hydrophilic modifier to polymeric membrane as well as pore forming agent. Various literatures associated to nanoparticle addition for modification of polymeric membranes are reported in Table 1.5.

**Table 1.5: Literatures related to nanoparticle additive.**

| Nano Particle | Modified/Unmodified | Base polymer | Application | Reference |
|---|---|---|---|---|
| **$TiO_2$** | Modified | PSF | UF (BSA solution) | [30] |
| **$TiO_2$** | Unmodified | PSF | UF (humic acid) | [97] |
| **$TiO_2$** | Unmodified (synthesized) | PVDF | UF (BSA solution) | [98] |
| **ZnO** | Unmodified | PSF | UF (oleic acid) | [87] |
| **Boehmite** | Unmodified | PES | UF (whey solution) | [35] |
| **$SiO_2$** | Unmodified | PSF | UF (oil on water emulsion) | [31] |
| **ZnO** | Unmodified | PES | Dye removal | [33] |
| **Carbon nanotube** | Amine functionalized | PES | UF (BSA solution) | [34] |
| **$SiO_2$** | Polymer grafted | PSF | UF (PEG solution) | [99] |
| **$CaCO_3$** | Unmodified (synthesized) | PSF | UF (BSA solution) | [100] |
| **Silver** | Unmodified | PSF | UF (protein and carbohydrate) | [101] |
| **Silver** | Unmodified | PSF | UF (BSA solution) | [102] |
| **$Al_2O_3$** | Unmodified | PES | UF (PEG solution) | [103] |
| **Carbon nanotube** | Unmodified (synthesized) | PSF | UF (PEG, PVP and BSA solution) | [104] |
| **$Fe_3O_4$** | Modified | PES | UF (Powder milk solution) | [105] |
| **$Mg(OH)_2$** | Unmodified | PVDF | Bacterial solution | [32] |

**Possible scope for further research**

A critical insight into the above literatures concludes that even though a number of authors have reported the addition of various nanoparticles to polymeric membrane, but the effect of polymeric nanoparticle as additives on polymeric membranes is scant and nobody studied the effect of chitosan-polyacrylic acid (CS-PAA) nanoparticle on polymeric membrane. Therefore, in this study cross-linked CS-PAA nanoparticles were synthesized and blended in PSF membrane casting solution in order to increase the hydrophilicity and fouling resistant behaviour of PSF membrane. As both component of CS-PAA nanoparticle contain large number of hydrophilic group of –OH, –COOH and $–NH_2$ in their structure. Also, CS-PAA nanoparticles are non-poisonous as they are generally used as carrier for drug delivery [106].

## 1.7. Objectives and scope of work

Based on the above state of the art, the present PhD thesis incorporates the following main objectives

- Modification and study the effect of non solvent additives on PVDF membranes.
- Preparation and characterization of polysulfone (PSF) UF membranes by blending water soluble polymer (polyethylene glycol methyl ether).
- Synthesis and characterization of double hydrophilic functional copolymer, poly (N-vinylcaprolactam-co-acrylic acid) (poly (VCL-co-AA)) by using N-vinylcaprolactam (VCL) and acrylic acid (AA) and its application for the modification of PSF membranes.
- Synthesis and characterization of novel pegylated pH sensitive cross linked copolymer poly (acrylic acid-co-polyethylene glycol methyl ether methacrylate) (poly (AA-co-PEGMA)) for the modification of PSF UF membranes.

- Synthesis and characterization of novel custom made amphiphilic polyurethane macromolecules with different end capping and their effect on fouling resistant behaviour of PSF UF membranes.
- Fabrication of novel temperature responsive PSF membrane, with cross linked PSF/polyvinylcaprolactam copolymer for protein separation and easy cleaning.
- Modification of PSF membrane by chitosan (CS)–poly (acrylic acid) (PAA) complex nanoparticles.

## 1.8. Organization of the thesis

**Chapter 1** discusses the background of the problem undertaken in this work i.e. the problem associated with the fouling tendency of polymeric UF membranes. The objectives of the present work are also highlighted in this chapter. **Chapter 2** gives a complete description of the experimentation involved in the fabrication and characterization of polymeric membranes by phase inversion method. **Chapter 3** describes the modification and characterization of PVDF membrane by non solvent additive. Effect of different alcohols i.e. methanol, ethanol, propanol and butanol were studied as non solvent additive; apart from that effect of different wt. % of methanol was also studied. **Chapter 4** presents results obtained from the addition of different molecular wt. of polyethylene glycol methyl ether in the polysulfone membrane casting solution and their effects on membrane morphology, water permeation as well as on fouling behavior. **Chapter 5** discusses the synthesis and characterization of poly (N-vinylcaprolactam-co-acrylic acid) and its application for the modification of PSF membrane by phase inversion method. **Chapter 6** converses the synthesis and characterization of novel cross linked pegylated functional copolymer poly (acrylic acid-co-polyethylene glycol methyl ether methacrylate). Effect of these copolymers and their amount on membrane morphology,

BSA transport and fouling behavior were discussed in detail. **Chapter 7** focused on fabrication and characterization of fouling resistance hydrophilic flat sheet PSF membrane by phase inversion method. Amphiphilic PU macromolecules were synthesized by two step solution polymerization and end capped with four different compounds containing carboxylic group i.e. citric acid, malic acid, lactic acid and 4-hydroxy benzoic acid. Synthesized PU macromolecules were blended directly in membrane casting solution. Water flux, hydraulic permeability, UF performance and anti fouling property were studied. **Chapter 8** deals the synthesis of cross linked PSF/polyvinylcaprolactam (PVCL) copolymer by solution polymerization and its direct application for the modification of PSF membrane. PVCL with lower critical solution temperature (LCST) at around 32˚C, is a temperature sensitive polymer. Below the LCST, the PVCL polymer chains adopt an extended random coil conformation. As the temperature increases above the LCST, the PVCL polymer chains dehydrate to form a compact structure. Based on the reversible volume phase transition of PVCL at temperatures close to the LCST, a simple temperature-change cleaning method for modified PSF UF membrane had been used, which had been fouled by BSA. **Chapter 9** discusses the modification of PSF membrane by blending polymeric nanoparticle. Chitosan-polyacrylic acid (CS-PAA) complex nanoparticle was synthesizes and mixed with PSF membrane blending solution for the hydrophilic modification of PSF membrane. Water flux, hydraulic permeability, UF performance, BSA adsorption and hydrophilicity of the modified membranes were studied **Chapter 10** summarized the inferences drawn from this work and provided some suggestions towards future research.

# Chapter 2

## Membrane preparation and characterization

# Chapter 2
# Membrane preparation and characterization

*This chapter gives a complete description of the experimentation involved in the preparation and characterization of polymeric membranes. The chapter also provides information regarding the materials used for the preparation of polysulfone membranes along with their sources from where they are obtained. It presents the detail of instruments used for characterization of synthesized polymeric material and modified membranes like FTIR, ATR-FTIR, NMR, SEM, FESEM, AFM, DSC, UV-VIS spectrophotometer and Rheometer. It further elaborates the characterizations of the prepared membranes through measurement of pure water flux (PWF), compaction factor (CF), equilibrium water content (EWC), hydraulic permeability ($P_m$), ion exchange capacity, pH sensitivity, thermo sensitivity, water contact angle, hydration capacity, BSA adsorption, BSA flux and rejection through prepared membranes. Specific details of membrane preparation described in section 1.6 and conditions for different experiments are reported in subsequent chapters.*

## 2.1. Materials

Base polymer used for the membrane preparation was PSF in all the cases except chapter 3, where PVDF was used as base polymer. NMP was used as solvent for the preparation of membrane casting solution throughout the experiments. In the present study various kind of additives were used for the modification of polymeric membranes. Some additives were used directly like PEGME and different alcohols; where as other additives were synthesized for specific membrane properties like amphiphilic, pH responsive, thermo responsive and hydrophilic. Details of the chemicals used for membrane preparation and modification are tabulated in Table 2.1. All the chemicals were used without further purification. Deionized

water purified by Millipore system (Millipore, France) was used as non- solvent in coagulation bath as well as for all other purposes.

**Table 2.1: Chemicals used in this work.**

| Sr. No. | Chemicals (specification) | Brand |
|---|---|---|
| **1.** | Polysulfone (average molecular weight 35000 Da) | Sigma-Aldrich Co. USA |
| **2.** | N- methylpyrrolidone (reagent grade) | LOBA Chemie, India |
| **3.** | Polyethylene glycol methyl ether(average molecular weight 550 Da, 2000 Da and 5000 Da) | Sigma-Aldrich Co. USA |
| **4.** | Bovine serum albumin (68,000 Da) | Otto Chemie, India |
| **5.** | Poly(vinylidene fluoride-*co*-hexafluoropropylene) (average molecular weight 400000 Da) | Sigma-Aldrich Co. USA |
| **6.** | Polyethylene glycol 6000 (synthesis grade) | Merck, India |
| **7.** | Methanol (synthesis grade) | Merck, India |
| **8.** | Ethanol (synthesis grade) | Merck, India |
| **9.** | Propanol (synthesis grade) | Merck, India |
| **10.** | Butanol (synthesis grade) | Merck, India |
| **11.** | Potassium bromide (FTIR grade) | LOBA Chemie, India |
| **12.** | N- vinylcaprolactam | Sigma-Aldrich Co. USA |
| **13.** | Acrylic acid (synthesis grade) | Merck, India |
| **14.** | Azobisisobutyronitrile | Otto Chemie, India |
| **15.** | Polyethylene glycol methyl ether methacrylate | Sigma-Aldrich Co. USA |
| **16.** | N,N′-methylenebisacrylamide (average molecular weight 500 Da) | Sigma-Aldrich Co. USA |
| **17.** | 4-hydroxybenzoic acid | Sigma-Aldrich Co. USA |

| | | |
|---|---|---|
| **18.** | 4,4'- methylenebis(phenyl isocyanet) | Sigma-Aldrich Co. USA |
| **19.** | Dimethyl acetamide (synthesis grade) | Merck, India |
| **20.** | Polyethylene glycol 4000 (synthesis grade) | Merck, India |
| **21.** | Citric acid | Otto Chemie, India |
| **22.** | Malic acid | Otto Chemie, India |
| **23.** | Lactic acid | Otto Chemie, India |
| **24.** | Stannous octoate | Otto Chemie, India |
| **25.** | 1, 6-Hexanediol | Otto Chemie, India |
| **26.** | Dimethyl sulfoxide-d6 | Sigma-Aldrich Co. USA |
| **27.** | Potassium persulphate | Merck, India |
| **28.** | Glutaraldehyde | Merck, India |
| **29.** | Chitosan (medium molecular weight) | Sigma-Aldrich Co. USA |

## 2.2. Membrane preparation

The casting solution was stirred with the help of magnetic stirrer for 12-24 h at required temperature and further degassed for 6-12 h at required temperature. The solution was then cast on a clean glass plate with a casting knife maintaining a uniform thickness of 200 – 250 µm, in ambient atmosphere. The glass plate was immediately immersed into the water bath at room temperature. The casted films immediately changed to white colour after the immersion in the water bath and separated out from the glass plate. The fabricated membrane was immersed in fresh deionized water for overnight to remove any residual solvent. Membrane sheets were finally air dried at room temperature thereafter [69, 96,]. Membrane preparation steps are shown in Figure 2.1.

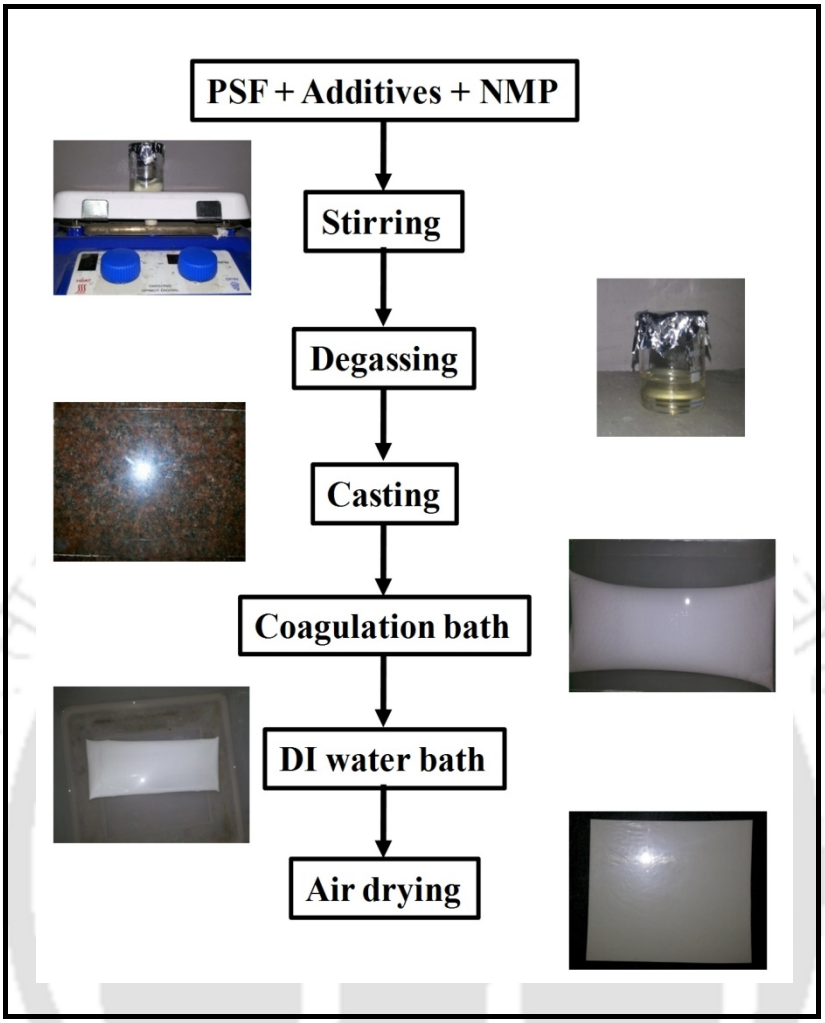


**Figure 2.1: Membrane preparation steps by phase inversion method.**

## 2.3. Membrane characterization

The porosity and pore size distribution are important parameters deciding the membrane performance [107]. The prepared membranes were characterized by morphological analysis and permeation experiments. The morphology of the prepared membranes was studied by microscopic observations and liquid-liquid displacement porosimetry (LLDP) method. The performance of each membrane was evaluated in terms of water contact angle, equilibrium water content, compaction factor, hydraulic resistance, porosity, pure water flux, permeate

flux, BSA adsorption. Detail methods are elaborated in subsequent sections of the current chapter.

### 2.3.1. Microscopic observation

Microscopic observation was done by field emission scanning electron microscope (FESEM, Make: Zeiss LSM 510 Meta) and scanning electron microscope (SEM, Make: LEO 1430VP, UK) after the samples were coated with thin gold layer. The pore size on the membrane surface as well as skin layer thickness was measured with the help of image J software. These images directly provide the top layer visual information as well as cross sectional information of the membranes. A number of FESEM images were taken at different magnification for both top surface and cross section of the prepared membranes. Computerized analysis of FESEM [108] image was extensively performed for this study. Cross section images were taken by SEM with an acceleration voltage of 10 kV after the samples were coated with thin gold layer.

### 2.3.2. Liquid-liquid displacement (LLDP) porosimetry method

The average pore size, number of pores and pore area distribution of the prepared membranes were determined by LLDP [1]. In this method, membrane was wetted with an appropriate penetrating liquid and then an immiscible liquid that does not wet the membrane was pressurized to pass through the pores displacing the previous liquid which was already occupying the pores. Water - isobutanol - methanol (25:15:7, v/v) was taken with surface tension of 0.35 mN/m and dynamic viscosity of 3.4 mPa s. The mixture was prepared by pouring proper amount of ultra pure water and mentioned alcohols in a separating funnel and shaking it vigorously. After that this mixture was allowed to stand overnight. The separated

water reach phase was used to wet the membrane and alcohol reach phase was used as displacing liquid. The pore size distribution was obtained from the data of variation of flow with pressure [109]. The radius (r) was calculated by well known Cantor's equation:

$$r = \frac{2\sigma}{P} \tag{2.1}$$

Where, $P$ is the transmembrane pressure and $\sigma$ is the interfacial tension between the two liquids. The total hydraulic permeability coefficient ($L_n$) was obtained by:

$$L_n = \sum L_{i,k} = \sum \frac{J_{i,k}}{P_{i,k}} \tag{2.2}$$

Where $J_{i,k}$ is flux at pressure $P_{i,k}$ and $L_{i,k}$ is partial permeability coefficient of the pores with radius $r_i$ and $r_k$ evaluated at $P_{i,k}$, which corresponds to a mean radius $r_{i,k}$.

$$r_{i,k} = \frac{r_i + r_k}{2} \tag{2.3}$$

Combining equations (1) and (2), flux versus pressure data gives the permeability versus pore radius curve. Again, the pore number versus pore radius and pore area versus pore radius curves can be obtained using the following equations [110, 111]:

$$N_{i,k} = \frac{d\eta}{2\pi\sigma^4} P_{i,k}^3 J_{i,k} \tag{2.4}$$

$$A_{i,k} = \pi r_{i,k}^2 N_{i,k} \tag{2.5}$$

Where $N_{i,k}$ is the pore density, i.e. the number of pore having radius between $r_i$ and $r_k$ per unit area of the membrane surface, d is the length of the pore which is approximately

equivalent to thickness of the skin layer and $\eta$ is the viscosity of the alcohol rich mixture. $A_{i,k}$ is the area of the pores having radii between $r_i$ and $r_k$. Both the equations are derived from the Hagen-Poiseuille's permeation equations assuming cylindrical pores and laminar flow. An average value of the thickness of the skin layer equal to 0.1 µm was considered in the present work even though it was likely to vary along the surface of the membrane. The total area $A_t$ and the total number of pores per unit area of the membrane $N_t$ was calculated as follows:

$$A_t = \sum A_{i,k} \tag{2.6}$$

$$N_t = \sum N_{i,k} \tag{2.7}$$

The mean pore radius $r_m$ was calculated as [109]:

$$r_m = \frac{\sum N_{i,k} r_{i,k}}{\sum N_{i,k}} \tag{2.8}$$

The limitation of this methods is that the absolute values of the $A_t$, $N_t$ and their distribution are likely to be associated with an error because of the deviation from the assumption of cylindrical pores and non-uniform thickness of membranes skin layer. However, the information may be useful in comparing the different membranes.

### 2.3.3. Permeation experiments

The unstirred batch experiment was conducted in a 350 ml permeation cell made of stainless still. Inside the cell, a flat circular membrane was placed over a base support. The membrane

diameter was $3 \times 10^{-2}$ m and the effective area of the membrane was $7.065 \times 10^{-4}$ $m^2$. The permeating solution was collected from the bottom of the cell. The cell was pressurized using a nitrogen cylinder. The schematic of batch experimental setup is shown in Figure 2.2 [69].

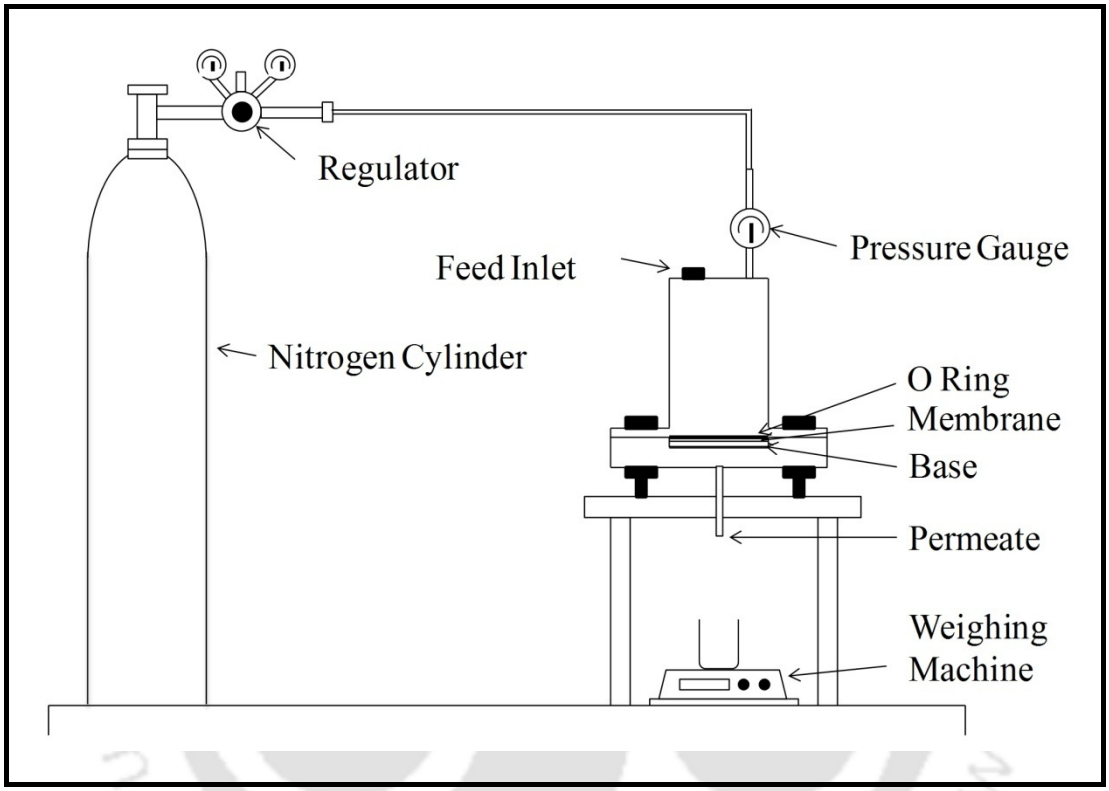


**Figure 2.2: Schematic of experimental setup [69].**

### 2.3.3.1. Compaction of membranes at constant pressure

Prepared membrane was compacted with deionized water for 2-4 h at a transmembrane pressure of 240-400 kPa which was higher than the maximum operating pressure in this study. The water permeation flux was at regular time interval after attaining flow stabilization through the membrane. The compaction factor (CF) was calculated as the ratio of initial pure water flux ($PWF_{initial}$) to steady state pure water flux ($PWF_{steady\ states}$).

### 2.3.3.2. Pure water flux (PWF) and hydraulic permeability ($P_m$)

Membrane hydraulic permeability has got significance particularly for membranes used in pressure driven separation processes. Pure water flux (PWF) was determined by allowing deionized water to pass through the compacted membrane. Flux values of pure water at different transmembrane pressures were measured under steady state condition using following equation:

$$J_w = \frac{Q}{A\,\Delta t} \tag{2.9}$$

Where, $J_w$ is pure water flux ($L/m^2$ h), Q is volume of water permeated (L), A is effective membrane area ($m^2$) and t is permeation time (h). $P_m$ ($L/m^2h$ kPa) is evaluated from the slope of the plot of $J_w$ vs P. Hydraulic permeability was calculated as

$$P_m = \frac{J_w}{\Delta P} \tag{2.10}$$

### 2.3.3.3. Average pore size by hydraulic permeability

Average pore sizes of the membranes have been calculated by hydraulic permeability using following equation [112]:

$$r_m = \frac{8\mu l P_m}{\varepsilon} \tag{2.11}$$

Where $r_m$ is average pore radius, μ is viscosity of water at room temperature, l is length of pore, $P_m$ is hydraulic permeability of membrane and ε is porosity of membrane.

### 2.3.4. Equilibrium water content (EWC), porosity and hydrophilicity

EWC is directly related to the porosity of membrane. It also indicates the hydrophilicity or hydrophobicity of the membranes. EWC at room temperature was calculated as:

$$EWC\ (\%) = \frac{W_w - W_d}{W_w} \times 100 \tag{2.12}$$

The membrane porosity was determined as [15]:

$$Porosity = \frac{W_w - W_d}{\rho_w \times V} \tag{2.13}$$

Where, $W_w$ and $W_d$ is the weight of membrane in wet and dry state, respectively. $\rho_w$ is the density of water and $V$ is volume of the membrane. Membranes were weighed in electronic balance in wet state after mopping the surface water with a clean tissue paper. The wet membranes were dried by putting in a vacuum oven for 24 h at a temperature of 50-60˚ C and again they were weighed in dry state. For calculation of volume of membrane, thickness of membranes was measured by FESEM image at different place and the average was taken. The error was found within 2-3 %. The hydrophilic property of the membrane was evaluated by measuring the static contact angle between the de-ionized water and membrane films at ambient condition at room temperature using a digital camera (canon power shot) and a goniometer was used to determine the contact angle. Farbod et al. [113] had also used the same technique to measure contact angle. For measuring the contact angle, membrane coupons of about 3 cm × 1.5 cm areas were prepared by cutting the membrane sheet and then these samples were fixed at glass palates with the help of tape. Then, a drop DI water (20 µl) was placed on the surface using a micropipette.

Mean pore radius of membrane was calculated by Guerout–Elford–Ferry equation (equation (2)) [97]. This equation is based on porosity and pure water flux data.

$$r_m = \sqrt{\frac{(2.9 - 1.7\varepsilon) \times 8\eta l Q}{\varepsilon \times A \times \Delta P}} \tag{2.14}$$

Here, $A$ is area of membrane, $l$ thickness of membrane and $d_w$ is the density of water (0.998 g/cm$^3$). Thickness of the membranes were measured by a digimatic measuring unit (model: Litematic, VL 50, Mitutoyo, Japan) at 10 different places and average was taken. Also, η is the water viscosity (8.9×10−4 Pa s), Q is the volume of the permeated water per unit time (m$^3$/s), and ΔP is the operation pressure.

### 2.3.5. BSA adsorption on membranes surface

The adsorption of BSA on membrane surface was performed. At first, membranes were placed in 5 ml vials and were soaked in 4 ml of phosphate buffer for 1 h at 25 $^o$C. After that, buffer was removed and membranes were incubated with 4 ml of 1000 ppm BSA solution for 12 h at 25 $^o$C. The absorbed amount of BSA was measured by UV-VIS spectrophotometer at wavelength of 280 nm. Three duplicate tests were performed for each membrane. Thickness of the membranes for calculation of membrane volume were measured by a digimatic measuring unit (model: Litematic, VL 50, Mitutoyo, Japan) at 10 different places and average was taken.

### 2.3.6. Ion exchange capacity (IEC) of membranes

The ion exchange capacity (IEC) of membranes was determined by using standard titration method [114]. First, modified membranes were kept in 2M NaCl solution for 24 h at 30˚C in

orbital shaker for the complete substitution of $H^+$ by $Na^+$. Then, the remaining solution was titrated with 0.01M NaOH solution using phenolphthalein indicator. Finally, the IEC value was calculated using the following equation:

$$IEC\ (mmol/g) = \left(\frac{0.01 \times 1000 \times V_{NaOH}}{W_d}\right) \quad (2.15)$$

Where $V_{NaOH}$ is the volume of NaOH solution (L) consumed for titration and $W_d$ is the weight of dry membrane sample.

### 2.3.7. ATR-FTIR of modified membranes

Fourier transform infrared (FTIR) analyses of the polymers were measured with FTIR spectrometer (IRAffinity-1, Shimadzu, Japan) with the help of a attachment called ATR-8200 HA (Shimadzu, Japan). For doing analysis, film samples were clamped firmly on the surface of attenuated total reflectance (ATR) crystal.

### 2.3.8. Ultrafiltration experiment and fouling studies

Ultrafiltration experiments were conducted in the batch cell explained in the preceding section to study the influence of molecular weight of PEGME on solute separation and permeate flux behaviour of the prepared membranes. The protein, Bovine Serum Albumin (BSA), was dissolved in deionized water and the concentration was kept constant at 1000 $mgL^{-1}$ for all the experiments. After the membrane was fixed in the membrane cell, the cell was filled deionized water. Each membrane was initially pressurized for 30 to 60 min at pressure higher then operating pressure, then the pressure was reduced to the operating pressure and the water flux ($J_{w1}$) was measured. After that cell was emptied and refilled with

1.0 mg/mL BSA solution; the flux was recorded ($J_p$). The BSA rejection ratio was calculated by the following equation:

$$R\ (\%) = \left(1 - \frac{C_p}{C_f}\right) \times 100 \tag{2.16}$$

Where, $C_p$ and $C_f$ are the concentration in permeate and the feed in mg/mL, respectively. After ultrafiltration, the membrane was cleaned with deionized water and water flux was measured ($J_{w2}$). BSA concentration in permeate was determined spectrophotometrically using a UV-VIS spectrophotometer (Perkin-Elmer Precisel, Lamda-35) at wavelength of 280 nm. The concentration values were plotted against corresponding values of absorbance. The relation between absorbance versus concentration was found to be a linear one with $R^2$ = 0.9995. This relation was used for measuring concentration of unknown sample i.e. permeate. The calibration curve so formed is shown in Figure 2.3.

Membrane fouling causes flux loss ($J_{w1}$-$J_p$). To study the antifouling property, Wang et al. [9] defined some ratios to describe the fouling process. The first ratio is $F_t$, which is the degree of total flux loss caused by total fouling. $R_t$ was calculated by following equation:

$$F_t = 1 - \frac{J_p}{J_{w1}} \tag{2.17}$$

$F_r$ and $F_{ir}$ are other two ratios. Where, $F_r$ is reversible fouling and $F_{ir}$ is irreversible fouling. $F_r$ and $F_{ir}$ were calculated by the following equations:

$$F_r = (J_{w2} - J_p)/J_{w1} \tag{2.18}$$

$$F_{ir} = (J_{w1} - J_{w2})/J_{w1} \tag{2.19}$$

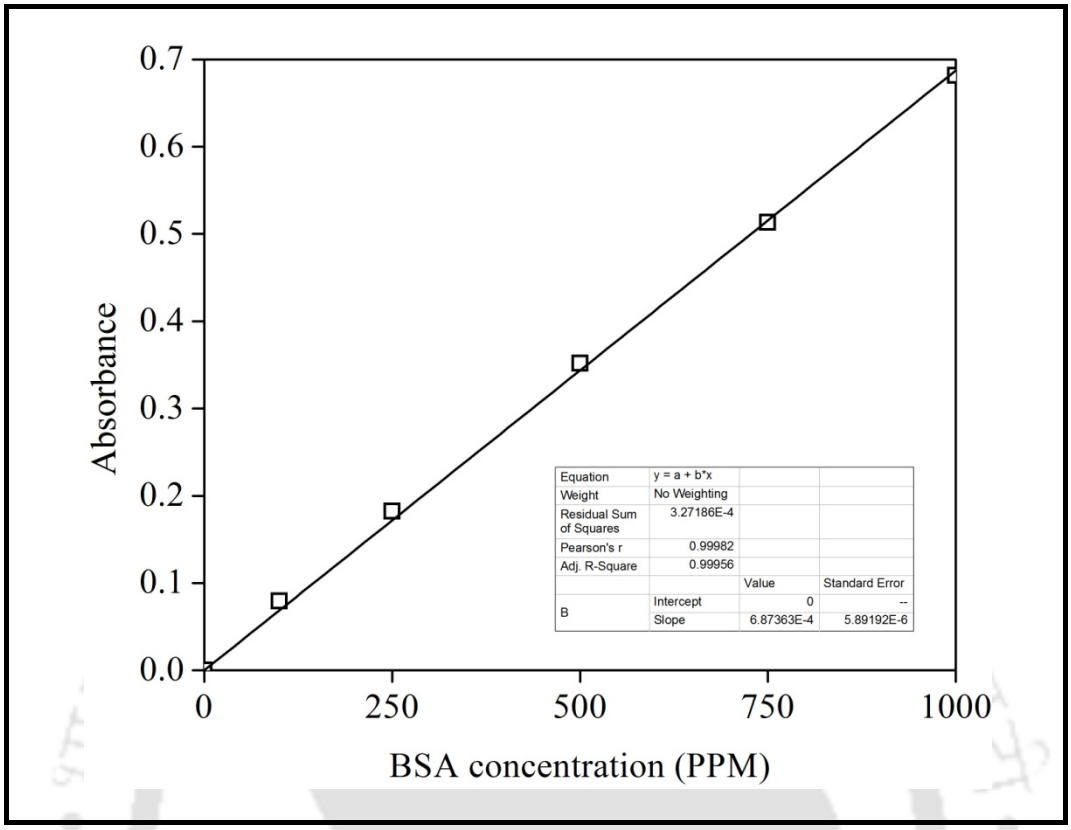


**Figure 2.3: Calibration plot of BSA solution.**

The reversible BSA adsorption on the membrane surface causes reversible fouling, which can be eliminated by hydraulic cleaning. Irreversible fouling caused by irreversible BSA adsorption, cannot be avoided by hydraulic washing. Thus $F_t$ is sum of $F_r$ and $F_{ir}$.

$$F_t = F_r + F_{ir} \tag{2.20}$$

With the help of $J_{w1}$ and $J_{w2}$, flux recovery ratio ($Flux_{RR}$) was measured using the following equation:

$$Flux_{RR}(\%) = \frac{J_{w2}}{J_{w1}} \times 100 \tag{2.21}$$

## 2.4. Characterization of synthesized additives

To prepare fouling resistant polymeric membranes, various additives had been synthesized and blended with membrane casting solution. These additives are (a) dual responsive double hydrophilic poly (N-vinylcaprolactam-co-acrylic acid) copolymer (b) pegylated pH sensitive cross linked copolymer poly (acrylic acid-co-polyethylene glycol methyl ether methacrylate) (c) Amphiphilic PU macromolecules end capped with four different compounds containing carboxylic group i.e., citric acid, malic acid, lactic acid and 4-hydroxy benzoic acid (d) cross-linked polyvinylcaprolactam-co-polysulfone amphiphilic copolymer with temperature sensitivity and (e) cross-linked chitosan-polyacrylic acid nanoparticle. These additives were characterized by various techniques, which are discussed below and the results of these characterization are reported in the respective chapters.

### 2.4.1. Proton nuclear magnetic resonance ($^1$H NMR) spectroscopy

Structure of the synthesized molecule was confirmed by NMR spectroscopy. $^1$H NMR (600 MHz) spectra were recorded with Bruker Ascend 600 (Bruker Co., Japan) using DMSO-d6 as solvent. To prepare NMR sample, the copolymer was first dissolved in DMSO d6 and filled in NMR tubes.

### 2.4.2. Fourier transform infrared spectroscopy

Fourier transform infrared (FTIR) analyses of the polymers were measured with FTIR spectrometer (IRAffinity-1, Shimadzu, Japan). To prepare FTIR sample, the copolymer was first dissolved in DMAc and cast on a KBr palette. The casted polymer solution was dried to remove the DMAc. FTIR analysis was done with 30 numbers of scans and apparatus resolution was set at 4.

### 2.4.3. Photon correlation spectroscopy (PCS)

The hydrodynamic size distribution and zeta potential of the CS-PAA nanoparticles was done by PCS (Delsanano, Bckman Coulter, Switzerland). For the zeta potential analysis each sample was adjusted to a concentration of 0.1 % (w/w) in 10 mmol/L sodium chloride solution.

### 2.4.4. Differential scanning calorimetry (DSC)

Differential scanning calorimetry (DSC 1, Mettler Toledo, Switzerland) measurement was used to measure the glass transition temperature (Tg). The solid samples were sealed onto a DSC pan and scanned in the temperature ranging of - 25 °C to 200 °C at a heating rate of 5 °C/min under nitrogen gas.

# Chapter 3

## Enhancement of hydrophilicity of poly (vinylidene fluoride-co-hexafluoropropylene) (PVDF-HFP) membrane using various alcohols as nonsolvent additives

# Chapter 3
# Enhancement of hydrophilicity of poly (vinylidene fluoride-co-hexafluoropropylene) (PVDF-HFP) membrane using various alcohols as nonsolvent additives

*In the present chapter flat sheet asymmetric polymeric membranes were prepared from homogeneous solution of Poly(vinylidene fluoride-co-hexafluoropropylene) (PVDF-HFP) by phase inversion method using N-methyl-2-pyrrolidone (NMP) as solvent and PEG 6000 as pore forming agent. Effect of different wt % of methanol on cross sectional as well as on top surface morphology was analyzed by field emission scanning electron miscroscopy (FESEM). Addition of different quantity of methanol in casting solution and the membrane performance thereon was studied. Performance of membranes was also investigated by the water permeation and bovine serum albumin (BSA) rejection efficiency. Effect of various alcohols (methanol, ethanol, n-propanol and n-butanol)on membranes morphology as well as on the performance of modified membranes were also studied.*

## 3.1. Experimental

### 3.1.1. Materials

PVDF-HFP, NMP and PEG 6000 were used as base polymer, solvent and pore forming agent repectively, in the membrane casting solution. Methanol, ethanol, n-propanol and n-butanol were used as non-solvent additives in the casting solution. BSA was used as model foulant. Details of the entire chemical are reported in chapter 2 (Table 2.1).

---

Content of this chapter is published as below:

M.K. Sinha, M.K. Purkait, Enhancement of hydrophilicity of poly(vinylidene fluoride-co-hexafluoropropylene) (PVDF-HFP) membrane using various alcohols as nonsolvent additives, Desalination. 338 (2014) 106–114.

### 3.1.2. Membrane preparation

Flat sheet PVDF membranes were prepared by phase inversion method (Figure 2.1). Composition and nomenclature of different membranes are shown in Table 3.1. The prepared polymer solution was casted on a clean glass plate with a casting knife maintaining a uniform thickness of 250 µm, in ambient atmosphere. Detail method of membrane preparation is given in section 2.2 of chapter 2.

**Table 3.1: Composition of various membranes casting solution modified with non solvent additives.**

| Membrane | PVDF (wt.%) | PEG 6000 (wt.%) | NMP (wt.%) | Alcohol (wt.%) |
|---|---|---|---|---|
| **Me_0** | 12 | 3 | 85 | 0 |
| **Me_1** | 12 | 3 | 84 | Methanol (1) |
| **Me_2** | 12 | 3 | 83 | Methanol (2) |
| **Me_5** | 12 | 3 | 80 | Methanol (5) |
| **Me_10** | 12 | 3 | 75 | Methanol (10) |
| **Me_15** | 12 | 3 | 70 | Methanol (15) |
| **Et_10** | 12 | 3 | 75 | Ethanol (10) |
| **Pr_10** | 12 | 3 | 75 | Propanol (10) |
| **Bu_10** | 12 | 3 | 75 | Butanol (10) |

## 3.2. Membrane characterization

### 3.2.1. Morphological studies

Microscopic observation was done by field emission scanning electron microscope**.** These images directly provide the top layer visual information as well as cross sectional information of the membranes.

## 3.2.2. Characterization by permeation studies

Prepared membranes were compacted with deionized (DI) water for 4 h at transmembrane pressure of 240 kPa which was higher than the maximum operating pressure in this study. The water flux was calculated from the experimental permeate flow rate measured at 30 min interval after attaining flow stabilization. The compaction factor (CF) was calculated as the ratio of initial pure water flux ($PWF_{Initial}$) to steady state pure water flux ($PWF_{Steady\ state}$) [15, 17]. Permeation set up details is presented in section 2.3.3 of chapter 2.

### 3.2.2.1. Pure water flux (PWF) and hydraulic permeability ($P_m$)

Hydraulic permeability, $P_m$ has got significance particularly for membranes used in pressure-driven separation processes. Pure water fluxes (PWF) of different membranes were measured at different transmembrane pressures (ranging 0 – 240 kPa) using the equation 2.9. $P_m$ ($L/m^2h\ kPa$) was evaluated from the slope of the plot of $J_w$ vs $P$ by using equation 2.10. Average pore sizes of the membranes have been calculated by hydraulic permeability using equation 2.11.

### 3.2.2.2. Equilibrium water content (EWC), porosity and hydrophilicity

EWC is directly related to the porosity of membrane. It also indicates the hydrophilicity or hydrophobicity of the membranes. EWC and porosity at room temperature were calculated by equations 2.12 and 2.13, respectively. The hydrophilic property of the membrane was evaluated by measuring the static contact angle between the deionized water and membrane films at room temperature.

### 3.2.3. Ultrafiltration experiment

Ultrafiltration experiments were conducted in the batch cell mentioned in section 2.3.3 of chapter 2, the influence of different alcohols on solute separation and permeate flux of the membrane prepared. Bovine serum albumin (BSA) was dissolved in deionized water and the initial concentration was kept constant at 1000 mg/L for all the experiments. The pH of the BSA solution (molecular weight 68000 Da) was kept approximately at 7. The membrane cell was filled with deionized water after fixing the membrane. Each membrane was initially pressurized for 60 min at 150 kPa, to get the steady permeation. Thereafter the pressure was reduced to the operating pressure of 100 kPa and the water flux ($J_{w1}$) in L/m$^2$h was measured. The cell was emptied and refilled with 300 ml of 1000 mg/L BSA solution and the flux was recorded ($J_p$) in L/m$^2$.hr at 100 kPa pressure. The BSA rejection ratio was calculated by the equation 2.16. After that the membrane was removed from the cell and washed using running water. Thereafter the membrane was placed in the cell, filled with deionized water and cleaned by pressurizing at 150 kPa for 30 min. The water flux ($J_{w2}$) in L/m$^2$h of cleaned membrane was measured using equation 2.9 at 100 kPa. Membrane fouling causes flux loss ($J_{w1}$ - $J_p$). The flux loss caused by total fouling ($F_t$), reversible fouling ($F_r$) and irreversible fouling ($F_{ir}$) are calculated by equations 2.17, 2.18 and 2.19 respectively.

## 3.3. Results and discussions

### 3.3.1. Morphological studies

Qualitative information regarding surface and cross-sectional morphology of the membranes prepared was obtained through FESEM and SEM analysis, respectively. FESEM images for the top surface (air side) of different membranes (Table 3.1) prepared by addition of various alcohols and different wt % of methanol are shown in Figure 3.1 and Figure 3.2, respectively.

The formation of top surface was probably a result of spinodal demixing. The diffusion process during formation of top layer was fast enough for the polymer solution to become highly unstable and cross the spinodal curve [115, 116] which caused top surface with much better interconnected pores. The unified pores can be considered as a continuous PSF lean phase entwined by a continuous PSF rich phase which forms the membrane matrix. It may be seen from Figure 3.1 that there is not much difference in the image of top surface of the membranes containing different alcohols. Pore size and pore density seems to be same for all the membranes.

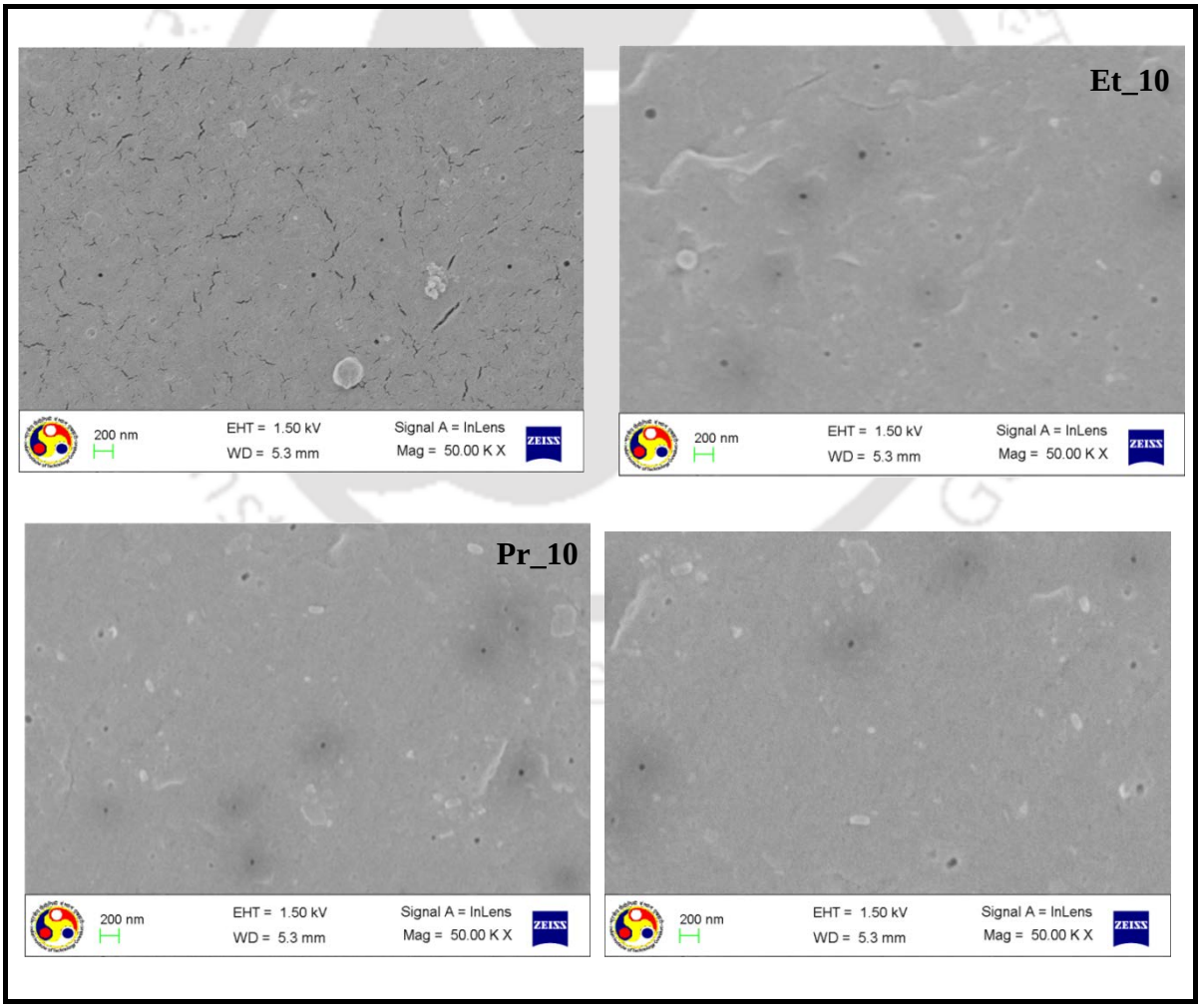


**Figure 3.1: FESEM images of top surface of membranes prepared using different alcohols.**

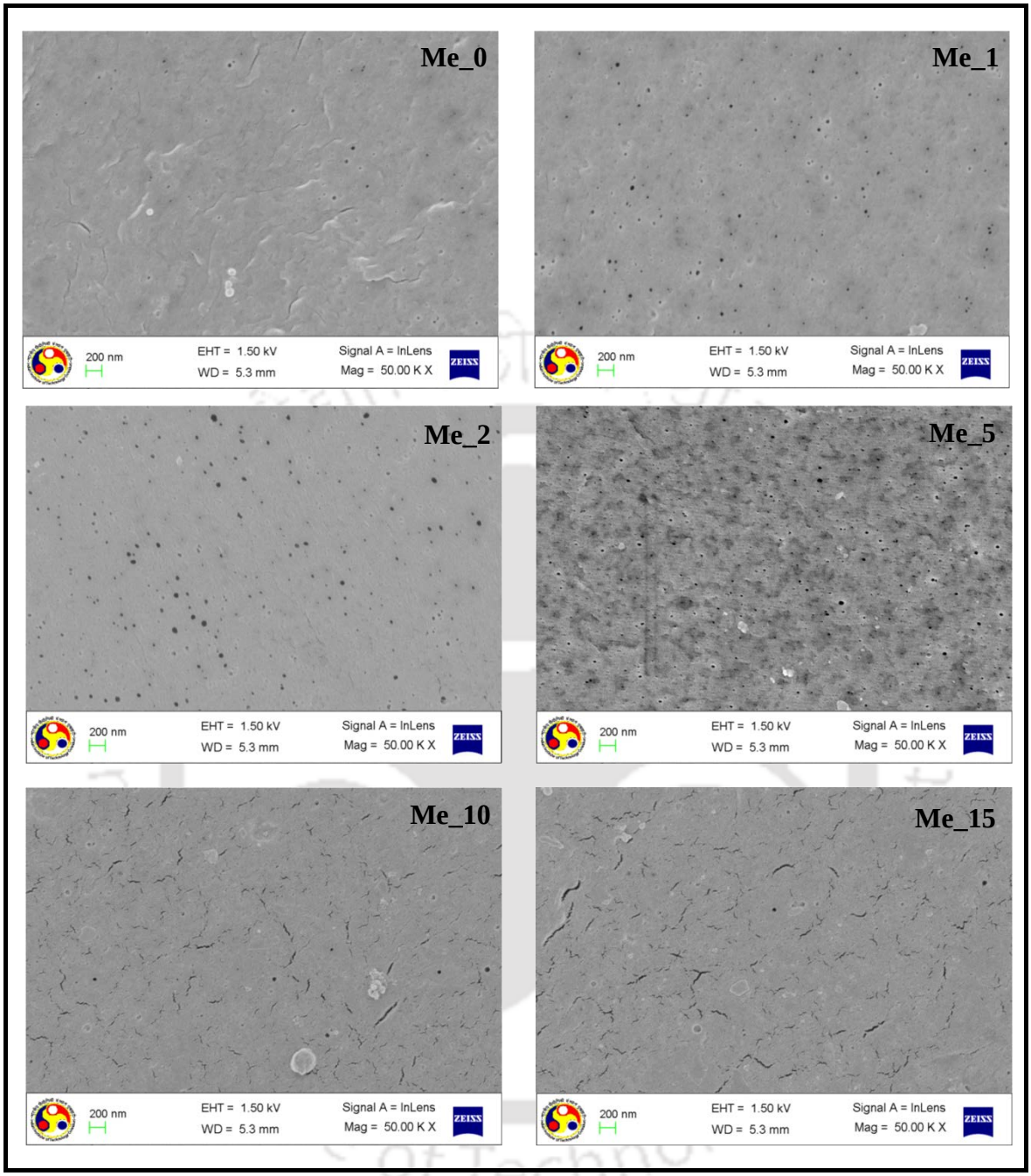


**Figure 3.2: FESEM images of top surface of membranes prepared using varying methanol concentration.**

In the case of membranes containing methanol in different wt % (Figure 3.2), it may be seen that up to certain wt % of methanol, pore density of membrane increased but after that it decreased. It may be noticed that as the wt % of methanol increased from 0 to 5%, the pore density of membrane was enhanced but beyond that the pore density was reduced

(Figure 3.2). From the figure it may also be found that membrane Me_5 has the highest pore density compared to all other membranes. So, it is clear that when alcohol is added in low quantity, it works as a pore forming agent beyond 5 wt% it simply work as a non-solvent. This reduces the fraction of solvent in casting solution and more compact membrane was formed. The same may also be evident from the cross sectional images (Figure 3.3) of the membranes containing different wt % of methanol. Similar result was also observed by Arthanareeswaran et al. [117]. They had used PEG 600 and highest permeability was found at 2.5 wt %. Lower permeability was observed at 5 wt % and much lower permeability was reported for 7.5 wt %.

From Figure 3.3, it is evident that membranes Me_0 and Me_1 have similar type of cross sectional structure but Me_2 and Me_5 have very porous cross sectional structure. After increasing the methanol quantity further from 5 wt%, membranes became more compact and the same may be seen for Me_10 and Me_15 membranes. This is also supported by the porosity of the membranes (Table 3.2) discussed in subsequent section. Pore size was determined by using Image J software from FESEM results and shown in Figure 3.4 for various membranes. Average pore sizes were calculated as 30.25 nm, 29.2 nm, 28.49 nm, 26.70 nm, 26.08 nm and 25.67 nm for Me_0, Me_1, Me_2, Me_5, Me_10 and Me_15 membranes, respectively. It may be observed that average pore size was decreased as the methanol wt% increased in the casting solution. This is because of the fact that adding a non-solvent additive into a polymer solution increases the tendency of polymer chains to approach a more tightly coiled conformation. Moreover, with the addition of non-solvent alcohols in the polymer solution, solidification of polymer may occur rapidly at the membrane surface. Therefore, membrane with a thinner skin layer and a more uniform structure was formed [54]. It may also be seen that the nature of pore size distribution for membranes containing 2 wt% to 15 wt% methanol was almost same and the maximum number of pores were in the

range of 20 nm. On the other hand the value was around 30 nm for membranes Me_0 and Me_1.

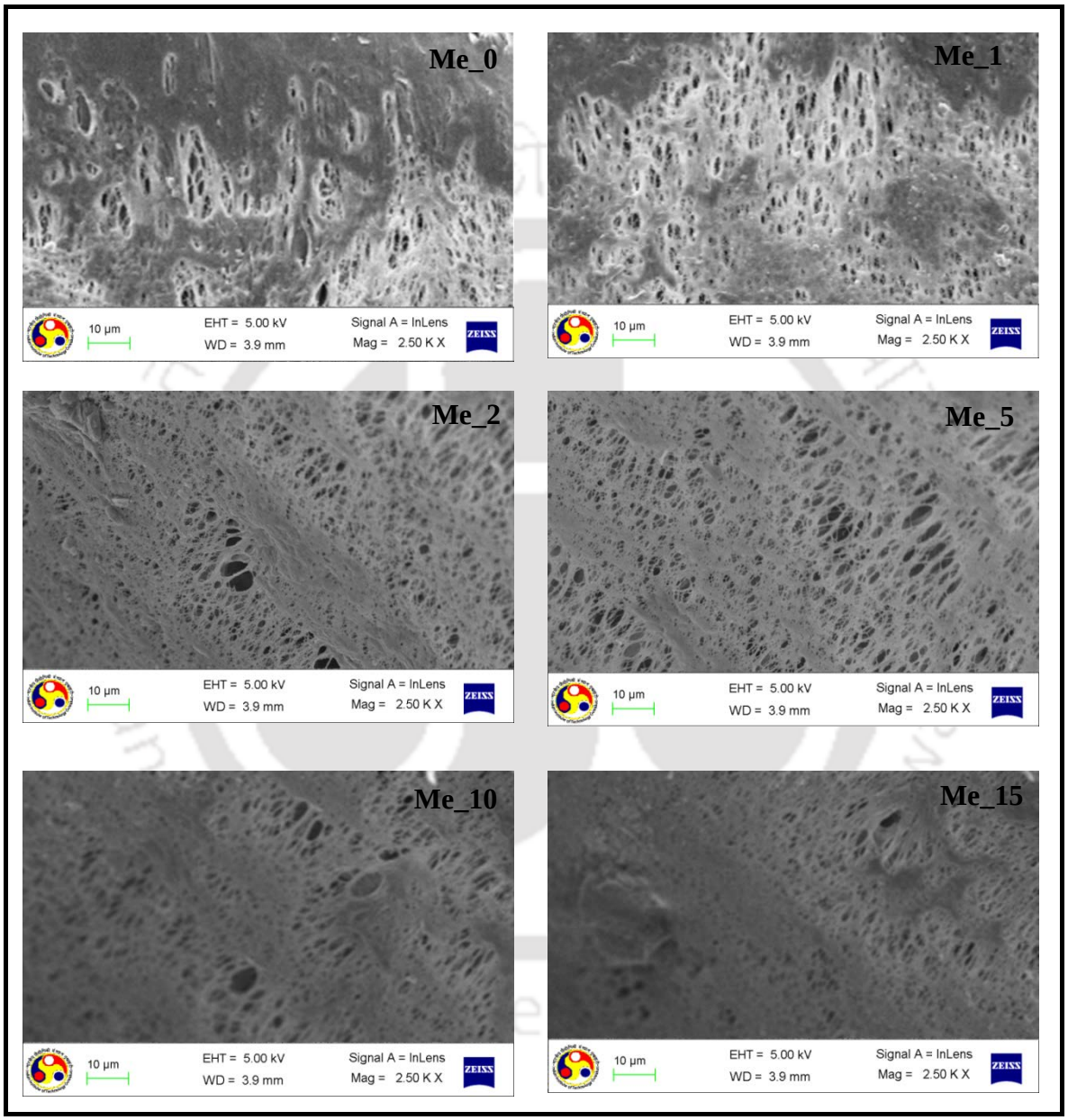


**Figure 3.3: FESEM images of cross section of membranes prepared with different % of methanol.**

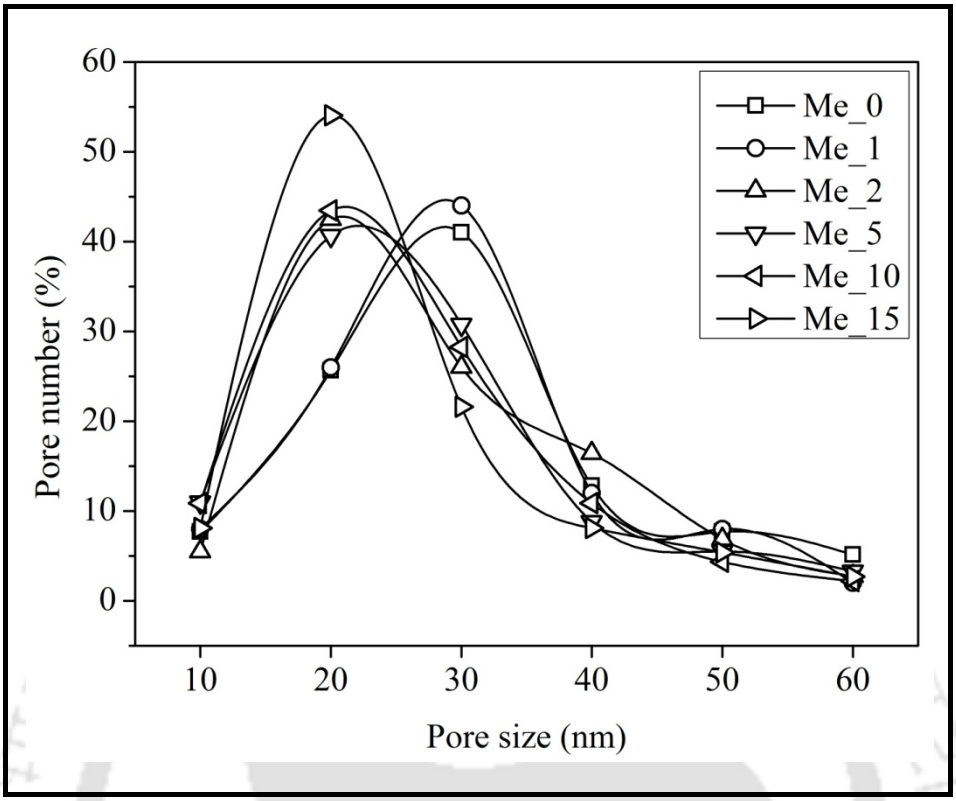


**Figure 3.4: Pore size distribution of various membranes.**

### 3.3.2. Permeation studies

All the membranes were subjected to hydraulic compaction at a constant transmembrane pressure of 240 kPa. The compaction was carried out for 4 h until a steady-state flux was attained. The water flux was calculated using equation 2.9 from the experimental permeate flow rate measured at every 30 min interval. The effect of compaction time on PWF for all the membranes is shown in Figures 3.5 and 3.6 for different alcohol and for different wt % of methanol, respectively. It may be seen from both the figures that the PWF declines sharply initially and became gradual thereafter with time due to compaction. After about 2.5 h of compaction, it reaches a steady state value. This was due to the fact that the walls of the pores become closer, denser and uniform resulting in reduction in pore size as well as the flux during compaction [1].

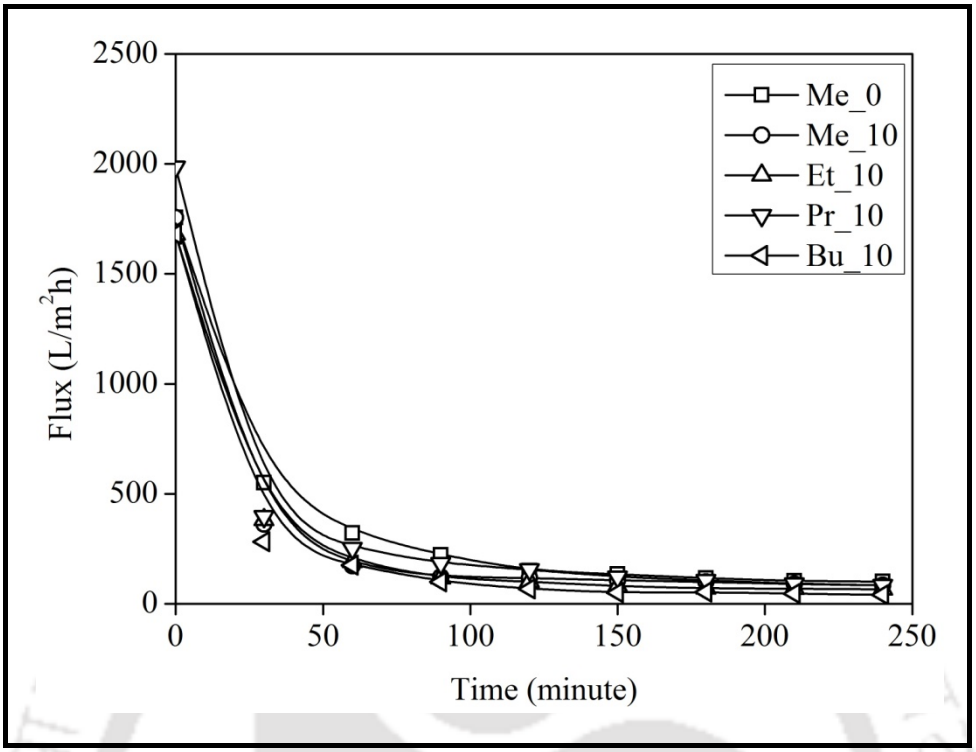


**Figure 3.5: Flux profile during compaction of membranes prepared using different alcohols.**

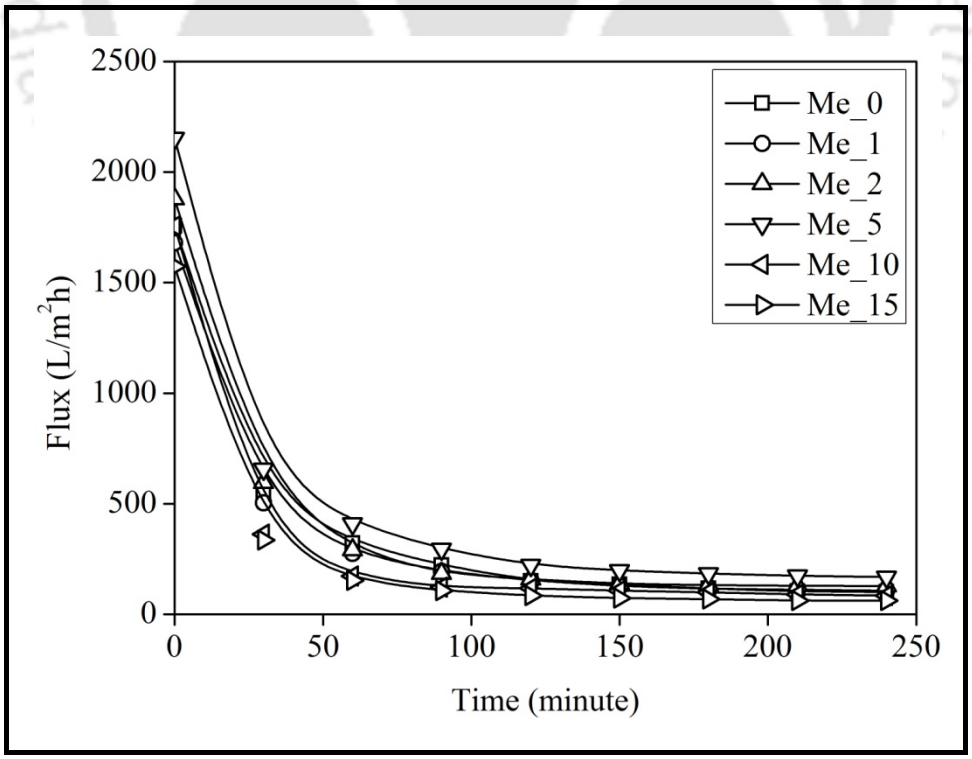


**Figure 3.6: Flux profile during compaction of membranes prepared with varying methanol concentration.**

The steady-state value of PWF for each membrane corresponding to applied pressure (240 kPa) is marginally changed for all the membranes containing same quantity of different alcohols (Figure 3.5). The steady state flux for membranes Me_10, Et_10, Pr_10 and Bu_10 are 84, 78, 82.5 and 85 L/$m^2$h, respectively. This result is corroborating with the FESEM observation discussed in the preceding section. On the other hand, steady state value of PWF for membranes containing different quantity of methanol (Figure 3.6) was increased with the increase in quantity of methanol initially but starts to decrease when methanol concentration exceeds 5 wt%. The steady state PWF value for membranes Me_0, Me_1, Me_2, Me_5, Me_10, and Me_15 were 100, 107, 128.3, 168, 84 and 61 L/$m^2$h, respectively. It may be observed that there is a significant increment in steady state PWF for membranes Me_2 and Me_5. The increase in flux was in the range of 28% and 68% for Me_2 and Me_5, respectively compared to Me_0 membrane. Moreover flux was lower for Me_10 and Me_15 than that of for Me_5 membrane. This was due to the fact that beyond 5 wt% of methanol it acts as simply non solvent and membranes became more compact. This observation is also supported by the FESEM analysis result discussed in the previous section. Compaction factor (CF) of all the membranes containing different quantity of methanol were calculated (Table 3.2). It may be seen that CF initially decreased with the methanol concentration but beyond 5 wt% it starts to increase. The variation in flux profile with methanol concentration is also supported by the trend in CF value change.

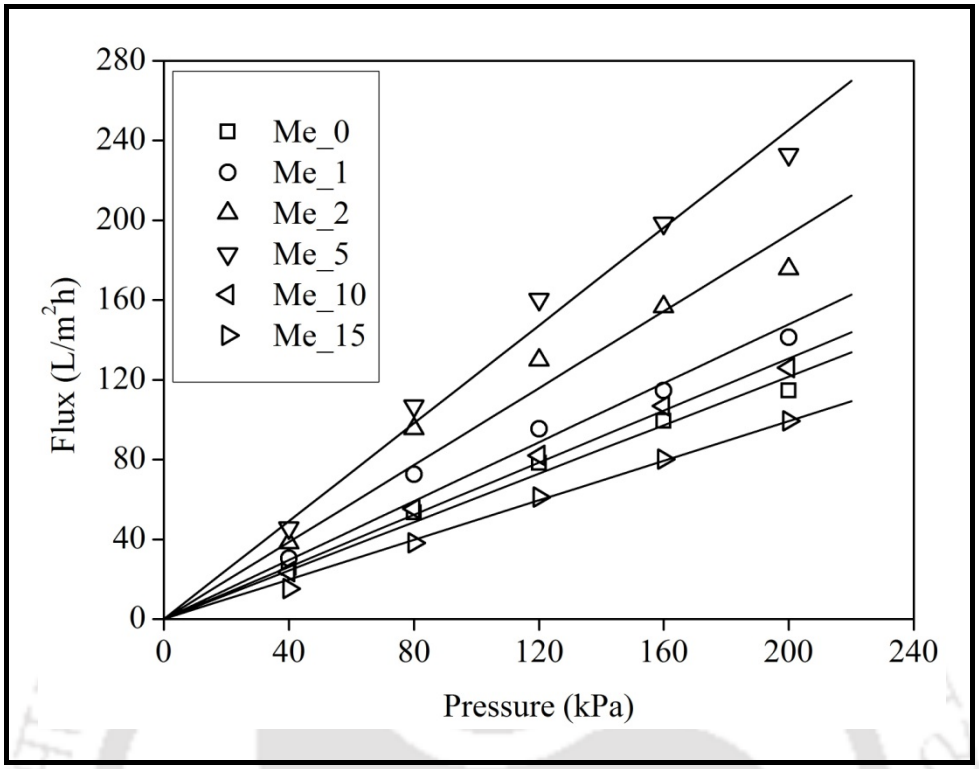


**Figure 3.7: Effect of transmembrane pressure on pure water flux.**

**Table 3.2: Values of some characterization parameters of prepared membranes with different wt % of methanol.**

| Membrane | EWC (%) | Porosity | Contact angle (degree) | C.F. | $P_m$ ($L/m^2$ h kPa) |
|---|---|---|---|---|---|
| **Me_0** | 42.72 | 0.172 | 71±1.5 | 17.44 | 0.607 |
| **Me_1** | 49.80 | 0.246 | 68.5±1 | 15.71 | 0.739 |
| **Me_2** | 58.60 | 0.350 | 66±1 | 14.64 | 0.965 |
| **Me_5** | 64.01 | 0.395 | 63.5±1.5 | 12.81 | 1.22 |
| **Me_10** | 45.47 | 0.193 | 72±0.5 | 20.90 | 0.653 |
| **Me_15** | 38.26 | 0.154 | 73±0.5 | 25.75 | 0.496 |

Hydraulic permeability ($P_m$) is another key factor for any membrane. $P_m$ was determined from the slope of the plots flux versus pressure (Figure 3.7) using Equation 2.10 and is represented in Table 3.2. The permeability value of Me_10, Et_10, Pr_10 and Bu_10 membranes are 0.653, 0.728, 0.695 and 0.73, respectively. This marginal variation is also dictated by the FESEM images of top surfaces (Figure 3.1). It may be observed from Table 3.2 that hydraulic permeability ($P_m$) increases with the wt % of methanol up to 5 wt% and beyond that that it starts to decrease. The permeability value of membrane Me_5 is almost double than that of Me_0. These results clearly indicate that addition of methanol in different quantity influences the formation of pores in the membrane. Permeability results also confirm the results obtained from morphological analysis as there was significance loss in permeability of membrane when methanol content increased from 5 wt% to 10 wt% and further more for 15 %. This is due to the fact that the increase in concentration of non solvent increases the polymer-polymer interaction which results in more compact membrane. Hydraulic permeability was also used to find the average pore size of the membranes by using Equation 2.11 and shown in Table 3.2. It also confirms that all the modified membranes have smaller average pore size than unmodified membranes. This is inline with the results obtained from FESEM image analysis.

### 3.3.3. Variation in EWC, porosity and hydrophilicity

EWC, Porosity and hydrophilicity of the membrane are important parameters in membrane preparation and separation processes. It is closely related to PWF and morphology of the membrane. The EWC of all the membranes was calculated using Equation 2.12 and presented in Table 3.2. It may be found from the Table 3.2 that with the increase in quantity of methanol, EWC of the membrane increases up to 5 wt% of methanol and decreases thereafter. The EWC for Me_5 is 64.01 %. This increasing trend confirms the presence of

increasing number of pores in the membrane with more quantity of methanol up to 5 wt% (as discussed in Section 3.2.1). The pores on the surface as well as cavities in the sub layer are responsible for accommodating water molecules in the membrane [23]. The EWC value of the membranes also coincides with PWF of different membranes as both the values increases for membrane containing up to 5 wt% of methanol.

Porosity of the membrane is another important parameter in membrane permeation and it is closely related to membrane performance. Porosity of the membrane was measured using Equation 2.13. The porosity of membranes with different quantity of methanol is shown in Table 3.2. Porosity value is maximum for membrane Me_5 (0.395) which is also corroborating with previous characterization results. Trend of porosity values supports the result of PWF experiment. PWF of the membrane increases with increase in value of the membrane porosity.

Surface hydrophilicity is often described by the contact angle [69, 118] measurement. In general, smaller the contact angle values higher the hydrophilicity. The contact angle of membranes with different % of methanol is shown in Table 3.2. It can be found from Table 3.2 that contact angle decreases and porosity increases with the increase in wt% of methanol and it is minimum for membrane containing 5 wt% methanol. The contact angle for Me_0 is 71±1.5˚ and for Me_5 is 63.5±1.5˚. So, for membrane Me_5, there is remarkable increase in hydrophilicity compared to membrane Me_0. The findings are uniform with the PWF and morphology study of membranes. In case of porous membrane, contact angle depends upon porosity of the membrane. Higher the porosity lower will be the contact angle. Similar observation was also reported by Huang et al [119] during preparation of PVDF nanofibre membranes.

### 3.3.4. Ultrafiltration of BSA

Apart from transmembrane pressure, the rejection and flux characteristics of the membranes strongly depend on the structure of the membrane as well as the properties of the feed solution. So, the prepared UF membranes were also characterized by estimating rejection and flux during permeation experiment using BSA solution. To investigate the fouling behaviour, membranes were cleaned after BSA solution ultrafiltration and the PWF of the cleaned membranes was measured. Figure 3.8 shows the time dependent flux of membranes during ultrafiltration. It may be seen that the PWF ($J_{w1}$) before UF of the BSA solution changes marginally but it decreased drastically at the initial operation of BSA ultrafiltration. It happened due to the deposition or adsorption of protein molecules on membrane surface at the initial BSA ultrafiltration operation [118-120]. After some time of operation it reaches equilibrium so that a relatively steady flux ($J_p$) was obtained in the final operation of BSA ultrafiltration.

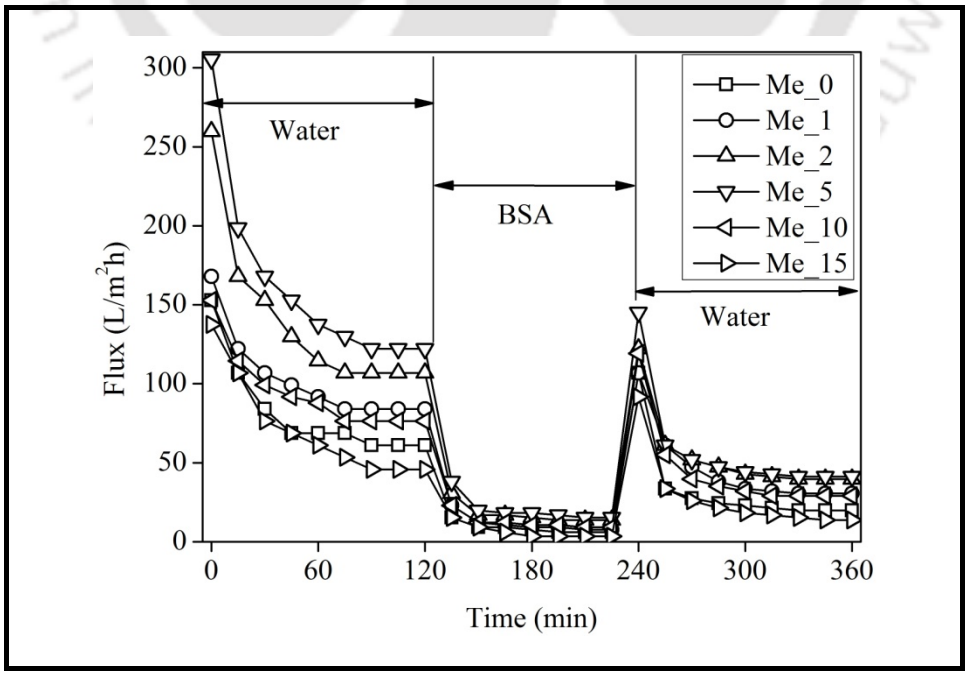


**Figure 3.8: Time dependent flux of various membranes during ultrafiltration of BSA**

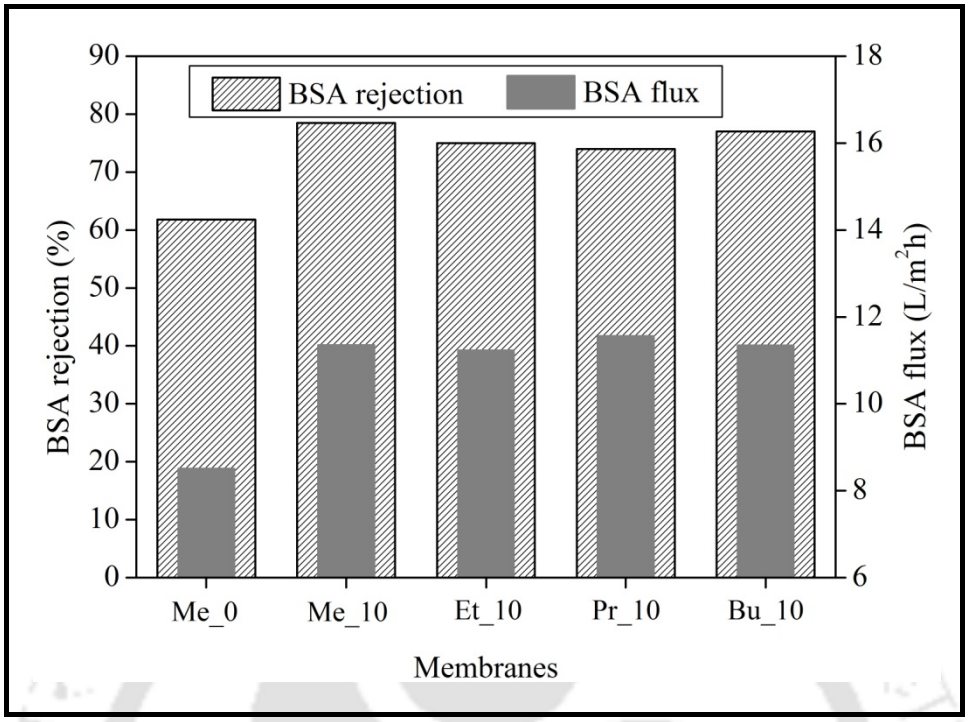


**Figure 3.9: Effect of various alcohols on flux and rejection behaviour during ultrafiltration of BSA.**

Rejection of BSA through different membranes was calculated by Equation 2.16. Variation of flux and rejection for membranes having different alcohols of same concentration is shown in Figure 3.9. It may be seen from the figure that in presence of alcohols as non solvent additives, the increase in rejection and flux was around 30% and 33%, respectively. Further, this increment was almost same for all the four alcohols considered in this work. On the other hand, rejection and flux value varies for membranes containing methanol in different composition (Figure 3.10). It may be seen from the figure that the flux was increased as the quantity of methanol increased (Me_0 to Me_5). Further increase in methanol content beyond 5 wt%, the flux was decreased (Me_10 and Me_15). This variation was also corroborating the change in permeability and hydrophilicity as discussed in Table 3.2. Figure 3.9 also dictated that the rejection was increased for membrane containing methanol up to 2 wt % and became minimum for 5 wt %. The Rejection was increased with the further increase of methanol concentration. The initial increase in rejection

was because of smaller pore size of the membranes in presence methanol. The decrease in rejection for Me_5 membrane was probably due to higher flux and having minimum fouling (more hydrophilic) compared to Me_1 and Me_2 membrane. The increase in rejection value for Me_10 and Me_15 membrane was due to the decrease in porosity (Table 3.2) value. Again, non solvent helps in pore formation but after certain concentration (5 wt % in this case) it also helps to decrease macro void formation in sub-layer [54] resulting increase in rejection efficiency.

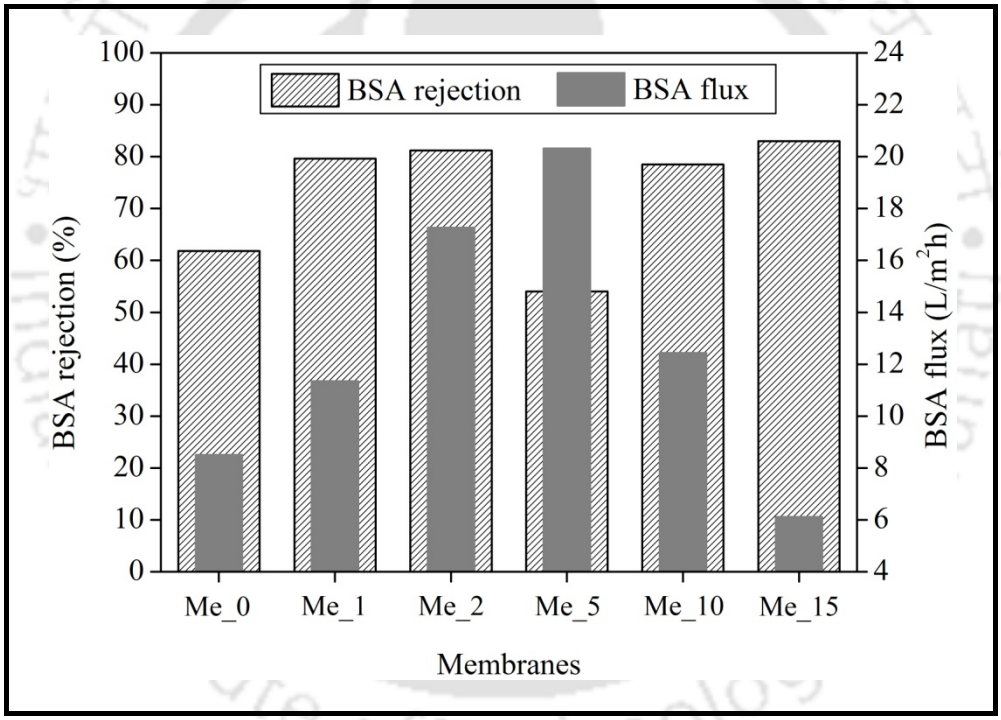


**Figure 3.10: Effect of different wt. % of methanol on flux and rejection during ultrafiltration of BSA.**

There are two types of membrane fouling, reversible and irreversible. Reversible deposition and adsorption of protein causes reversible fouling that can be removed by hydraulic cleaning. Irreversible protein adsorption causes irreversible fouling. This can only be eliminated by chemical cleaning or enzymatic degradation [120]. To find out these fouling values, ultrafiltration of BSA was performed using various membranes (Me_0 to Me_15) at

transmembrane pressure of 100 kPa and at pH of 7. The values of total fouling ($F_t$), reversible fouling ($F_r$) and irreversible fouling ($F_{ir}$) is shown in Figure 3.11 for different membranes having various wt % of methanol. It can be seen from the figure that $F_t$ decreases from 0.91 to 0.87 with increase in wt % of methanol from 0% to 5 % but it again increases to 0.92 for 15 % methanol. The lower value of $R_t$ indicates lower total flux loss resulting in less protein adsorption or deposition on the membrane surface [118, 122]. From the figure it may be seen that membrane containing 5 wt% of methanol has lower value of $F_{ir}$. Finally, it is to be noted that the fouling behaviour of membranes decreases as the hydrophilicity of membrane increases. These observations confirm the results of hydrophilicity and porosity analysis of the membranes discussed earlier.

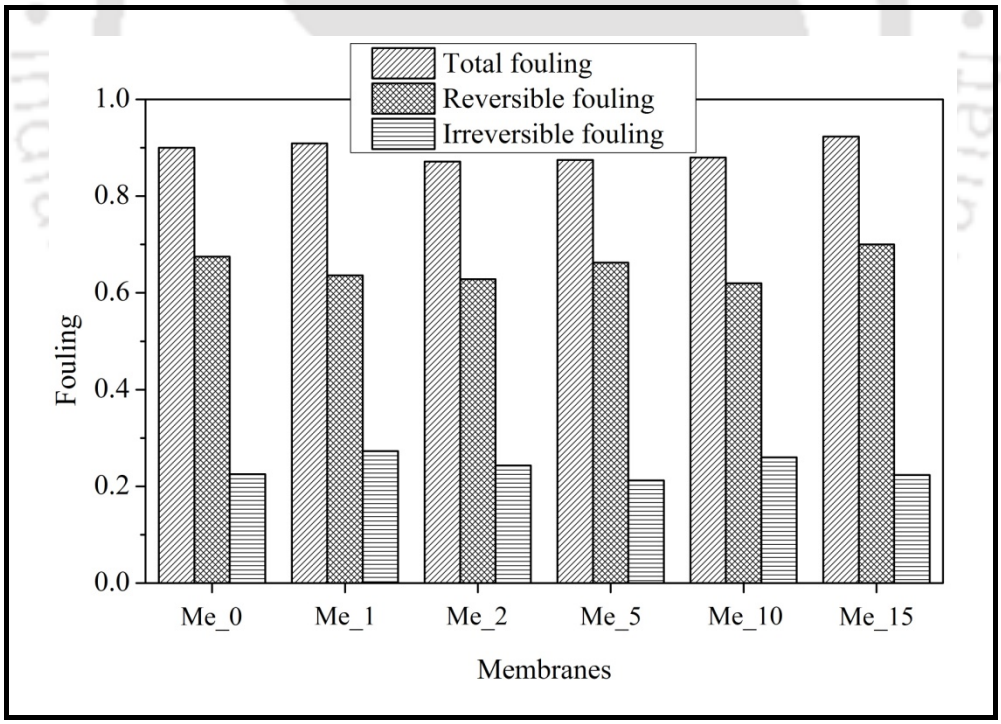


**Figure 3.11: Summary of $F_t$, $F_r$, and $F_{ir}$ of different membranes prepared by changing wt % of methanol.**

# Chapter 4

## Increase in hydrophilicity of polysulfone membrane using polyethylene glycol methyl ether

# Chapter 4
# Increase in hydrophilicity of polysulfone membrane using polyethylene glycol methyl ether

*In this chapter flat sheet asymmetric polymeric membranes were prepared from homogeneous solution of polysulfone (PSF) by phase inversion method using N-methyl-2-pyrrolidone (NMP) as solvents. Polyethylene glycol methyl ether (PEGME) of three different molecular weights (550 Da, 2000 Da and 5000 Da) was used as the polymeric additives in the casting solution. The morphology and structure of the resulting membranes were observed by field emission scanning electron microscope (FESEM). The pore number, pore permeability and their distribution and average pore size of the membranes were determined by the liquid-liquid displacement porosimetry (LLDP) method. The permeation performances of the membranes were evaluated in terms of pure water flux (PWF), hydraulic permeability, and solute rejection, while hydrophilicity was evaluated in terms of porosity, equilibrium water content (EWC) and water contact angle. Solution of bovine serum albumin (BSA) of molecular weight 68,000 Da was used to study the permeation performance of prepared membranes.*

## 4.1. Experimental

### 4.1.1. Materials

PSF and NMP were used as base polymer and solvent respectively, in the membrane casting solution. PEGME (average molecular weight 550 Da, 2000 Da and 5000 Da) were used as additives in the casting solution and BSA was used as model foulant in UF experiments. Detail of all the materials used in the present chapter is given in Table 2.1 of chapter 2.

---

Content of this chapter is published as below:

M.K. Sinha, M.K. Purkait, Increase in hydrophilicity of polysulfone membrane using polyethylene glycol methyl ether, J. Membr. Sci. 437 (2013) 7–16.

### 4.1.2. Membrane preparation

Flat sheet PSF membranes were prepared by phase inversion method as described in section 2.2 of chapter 2 with a thickness of 200 µm. Composition of different membrane casting solution and their viscosity is given in table 4.1.

**Table 4.1: Composition of membrane casting solutions containing different molecular weight of PEGME.**

| Membrane | Composition | | | Viscosity (Pa s) |
|---|---|---|---|---|
| | Base polymer | Additive | Solvent | |
| **PSF1** | PSF (12 %) | PEGME550 (5%) | NMP (83%) | 0.132 |
| **PSF2** | PSF (12 %) | PEGME2000 (5%) | NMP (83%) | 0.149 |
| **PSF3** | PSF (12 %) | PEGME5000 (5%) | NMP (83%) | 0.170 |

## 4.2. Membrane characterization

### 4.2.1. Microscopic observation

Microscopic observation was performed by field emission scanning electron microscope (FESEM). The pore size on the membrane surface as well as skin layer thickness was measured with the help of image J software. A number of FESEM images were taken at different magnification for both top surface and cross section of the prepared membranes. Computerized analysis of FESEM [108] image was extensively performed for this study. The average pore size, number of pores and pore area distribution of the prepared membranes were determined by LLDP as discussed in section 2.3.2 of chapter 2.

## 4.2.2. Permeation experiments

Permeation experiments were performed as conversed in the section 2.3.3 of chapter 2. Prepared membrane was compacted with deionized water for 4 h at a transmembrane pressure of 240 kPa which was higher than the maximum operating pressure in this chapter. The water permeation flux was at every 30 minutes interval after attaining flow stabilization through the membrane. The compaction factor (CF) was calculated as the ratio of initial pure water flux ($PWF_{initial}$) to steady state pure water flux ($PWF_{steady\ states}$).

### 4.2.2.1. Pure water flux (PWF) and hydraulic permeability ($P_m$)

Membrane hydraulic permeability has got significance particularly for membranes used in pressure driven separation processes. Pure water flux (PWF) was determined by allowing deionized water to pass through the compacted membrane. Flux values of pure water at different transmembrane pressures (upto 240 kPa) were measured under steady state condition using equation 2.9. $P_m$ (L/m$^2$h kPa) is evaluated from the slope of the plot of $J_w$ vs $P$. Hydraulic permeability was calculated by equation 2.10.

### 4.2.2.2. Equilibrium water content (EWC), porosity and hydrophilicity

EWC is directly related to the porosity of membrane. It also indicates the hydrophilicity or hydrophobicity of the membranes. EWC and porosity at room temperature was calculated by equations 2.12 and 2.13, respectively. The hydrophilic property of the membrane was evaluated by measuring the static contact angle between the de-ionized water and membrane films at ambient condition at room temperature.

### 4.2.3. Ultrafiltration experiment

Ultrafiltration experiments were conducted in the batch cell explained in the preceding chapter to study the influence of molecular weight of PEGME on solute separation and permeate flux behaviour of the prepared membranes. The pH of protein solution plays an important role in protein-membrane interaction [121, 123]. The pH of the BSA solution (molecular weight 68000) was kept approximately at three values: 4.7 (i.e. at isoelectric point), 7 (i.e. neutral condition) and 9.5 (i.e. basic condition). After the membrane was fixed in the membrane cell, the cell was filled wit deionized water. Each membrane was initially pressurized for 60 min at 150 kPa, then the pressure was reduced to the operating pressure of 100 kPa and the water flux ($J_{w1}$) was measured. After that cell was emptied and refilled with 1.0 mg/mL BSA solution; the flux was recorded ($J_p$). The BSA rejection ratio was calculated by the equation 2.16. After 2 hr of ultrafiltration, the membrane was cleaned with deionized water and water flux was measured ($J_{w2}$). Membrane fouling causes flux loss ($J_{w1}$-$J_p$). The flux loss caused by total fouling ($F_t$), reversible fouling ($F_r$) and irreversible fouling ($F_{ir}$) are calculated by equations 2.17, 2.18 and 2.19 respectively.

## 4.3. Results and discussion

### 4.3.1. Morphological study

PSF/PEGME blended membranes were prepared by phase inversion method in a wet process. The morphology of the prepared membranes of different composition was qualitatively examined by high resolution field emission scanning electron microscope. Whereas quantitative information like average pore size, pore number, pore density and pore area was determined by liquid-liquid displacement porosimetry method.

#### 4.3.1.1. SEM analysis

Figure 4.1a shows the FESEM images of cross sectional view of various PSF/PEGME blend membranes prepared in this chapter. From the image it can be seen that membranes so formed were asymmetric structure. General structure was very similar for all the membranes consisting of a top dense skin layer and a porous sub layer. The porous sub layer consists of finger like structure. Similar observation were also found by Chakrabarty et al. [15] for the system of PSF as polymer using NMP and DMAc as solvent, separately with PVP as additive. Due to high mutual affinity of NMP for water, instantaneous demixing results, leading to the formation of finger like cavities in the sub layer of the prepared membranes [1]. There was no appreciable morphological variation between the membranes with different molecular weight of PEGME in the blend membranes, as molecular weight is not that much different.

Figure 4.1b shows the FESEM images of top surface (air side) of the different membranes. The formation of top surface was probably a result of spinodal demixing. The diffusion process during formation of top layer was fast enough for the polymer solution to become highly unstable and cross the spinodal curve [115, 116]. This result in a top surface with much better interconnected pores. The interconnected pores can be considered as a continuous PSF lean (i.e. PEGME rich) phase entangled by a continuous PSF rich (i.e. PEGME lean) phase which forms the membrane matrix.

Pore size was determined using Image J software from FESEM results and shown in Figure 4.2 for various membranes. Average pore size was calculated as 29.77 nm, 28.71 nm and 27.56 nm for PSF1, PSF2 and PSF3 membrane, respectively. It may also be seen that the pore size distribution for PSF1 and PSF2 is almost same, as maximum number of pores were of 25 nm size and for PSF3 that value was 30 nm.

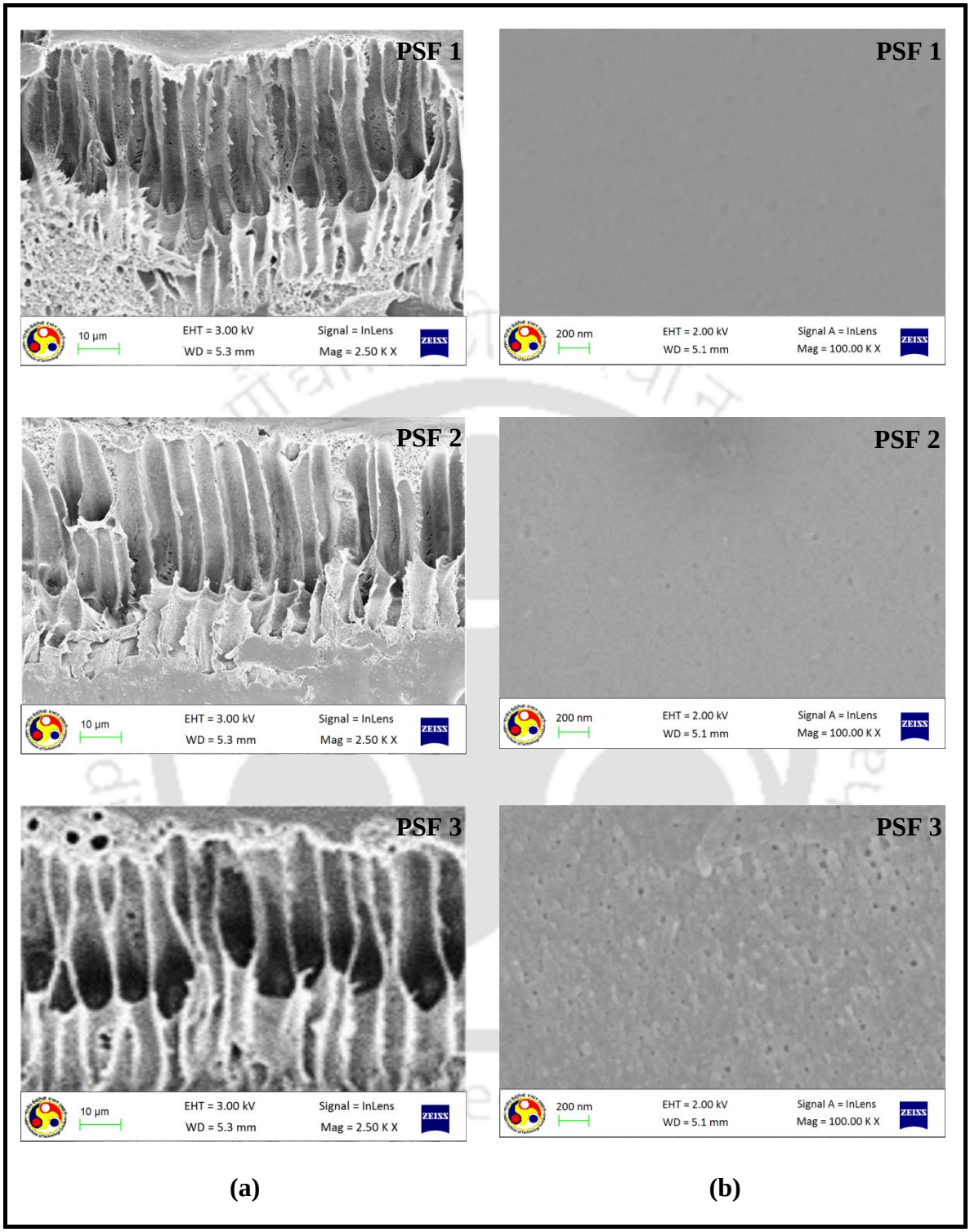


**Figure 4.1: FESEM images of membranes; a) cross section, b) top surface.**

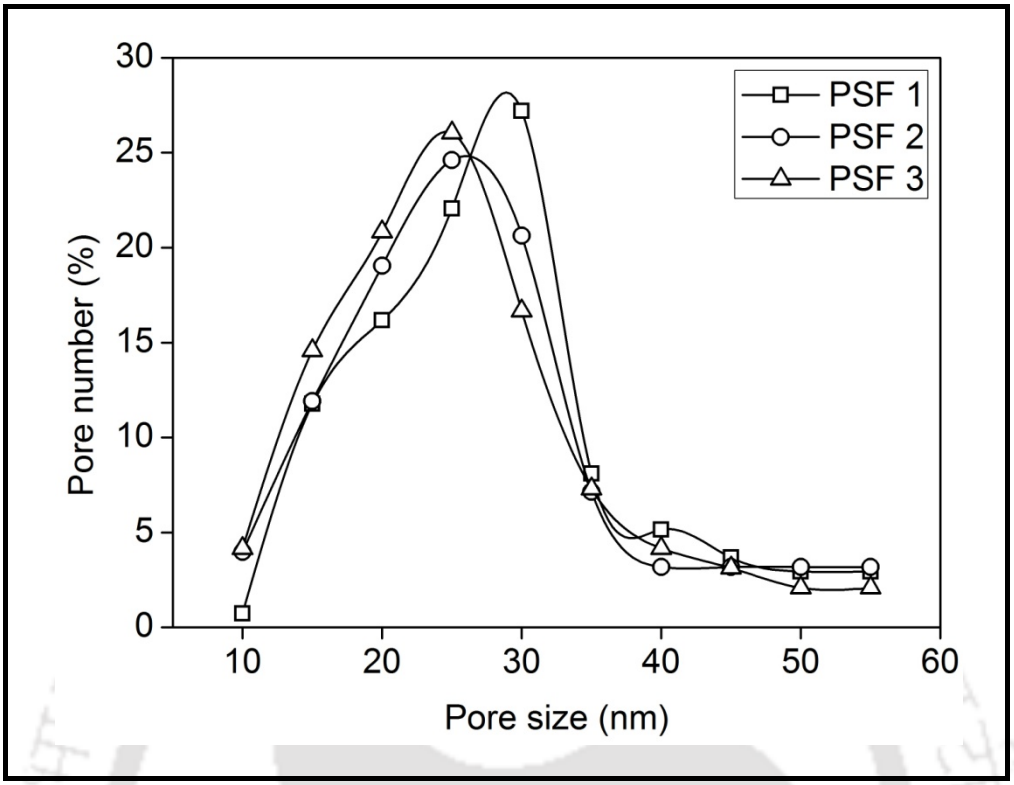


**Figure 4.2: Pore size distribution of membranes by FESEM.**

#### 4.3.1.2. Liquid-liquid displacement porosimetry studies

Figure 4.3 shows the LLDP flux profile for prepared membranes. The pore size, membrane permeability, pore number and pore area for each membrane were determined by Equations 2.1, 2.2, 2.4 and 2.5, respectively. Pore size distributions of the membranes are shown in Figure 4.4. 24 % of the pores were in the size of around 4 nm for PEGME 5000. For PEGME 550 and PEGME 2000 these numbers are 19 % and 21 %, respectively. Pore size distribution obtained from LLDP analysis was smaller than that of FESEM method. It may be due to the fact that in FESEM analysis using ImageJ software, comparatively pores bigger than 10 nm were considered on the membrane surface. So, it is possible that, this method may overestimate the pore size by considering the wider pores on the surface which may not even continue till the end of the membrane surface.

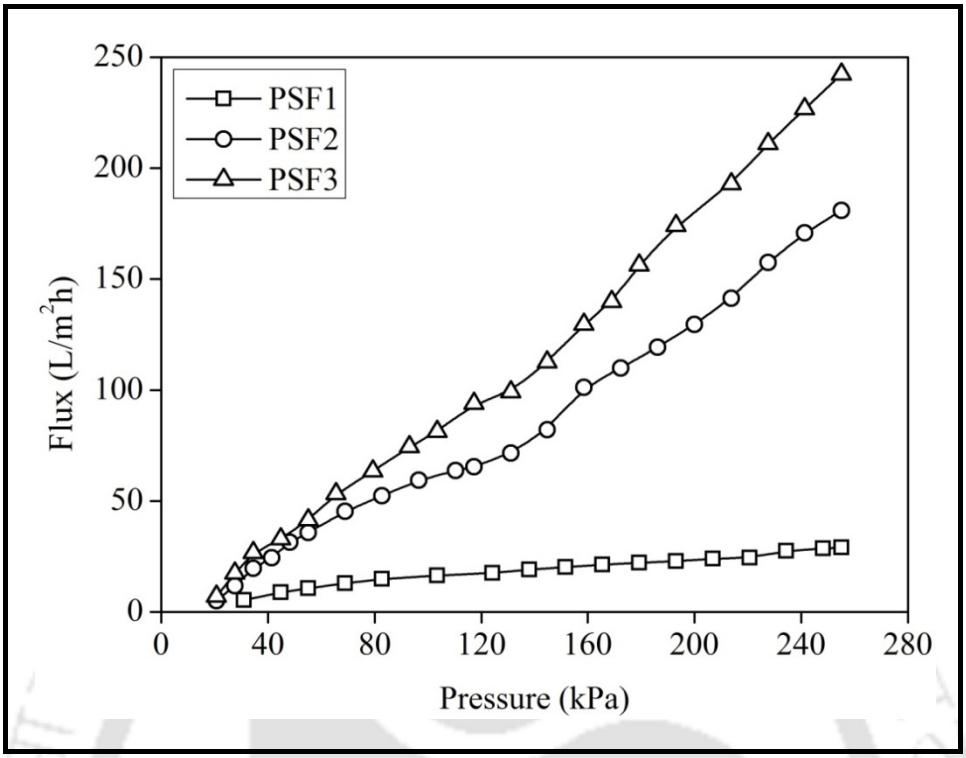


**Figure 4.3: LLDP flux profile for membranes prepared with different molecular weight of PEGME.**

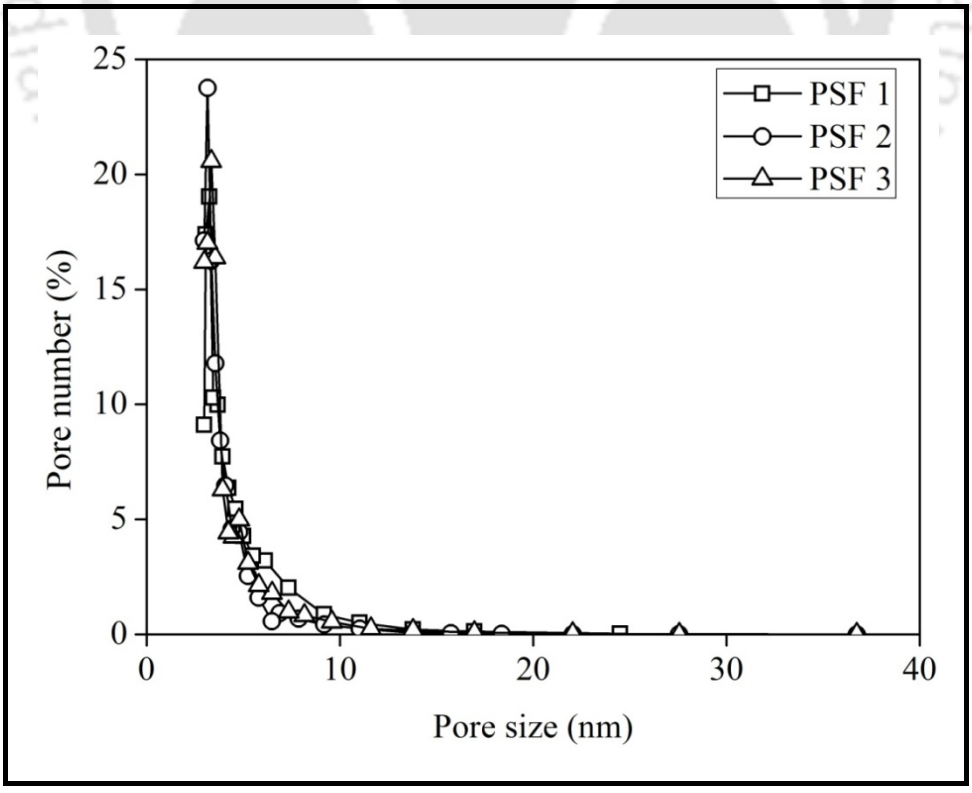


**Figure 4.4: Pore size distribution of membranes by LLDP.**

Membrane permeability and pore number were plotted against pore radius as cumulative curves and presented in Figures 4.5 and 4.6, respectively. From both the figures it may be observed that majority of the pores (approx. 90%) over three membranes are in the range of 3 – 5 nm which indicates that the prepared membranes were suitable for UF purpose. However, the exact fraction of the larger pores (>100 nm) as well as smaller pores (< 3 nm) is difficult to determined using LLDP method. For all the membranes, the majority of pores (approx. 90%) are having radii in the range of 3 - 5 nm; these pores contribute around 65% to the overall permeability. The lesser number of larger pores actually governs the overall membrane performance by increasing the permeability. The major increase in flux with the increase in pore radius can be explained from the Hagen-Poissuille equation which dictates that transport through membranes (i.e. permeability) is directly proportional to the fourth power of pore radius i.e. $L_n$ varies with $r^4$. Similar type of result was observed by Calvo et al. [124] for UF track-etched membrane. Table 4.2 reports the results of liquid displacement method. It is seen that, with increase in molecular weight of PEGME, the pore number of all the membranes increases resulting in more porous membranes. The pore number per unit area ($N_t$) is found to increase from $7.3 \times 10^8$ to $54 \times 10^8$. The mean pore size $r_m$ of the membranes for each membrane system calculated using equation 2.8 is seen to decrease marginally with increase in molecular weight of additives. The total hydraulic permeability coefficient $L_n$ was also affected by the molecular weight of PEGME. The values of $L_n$ for membranes were found to be 0.172 $ms^{-1}MPa^{-1}$, 0.752 $ms^{-1}MPa^{-1}$ and 1.057 $ms^{-1}MPa^{-1}$ for PEGME 550, PEGME2000 and PEGME 5000, respectively.

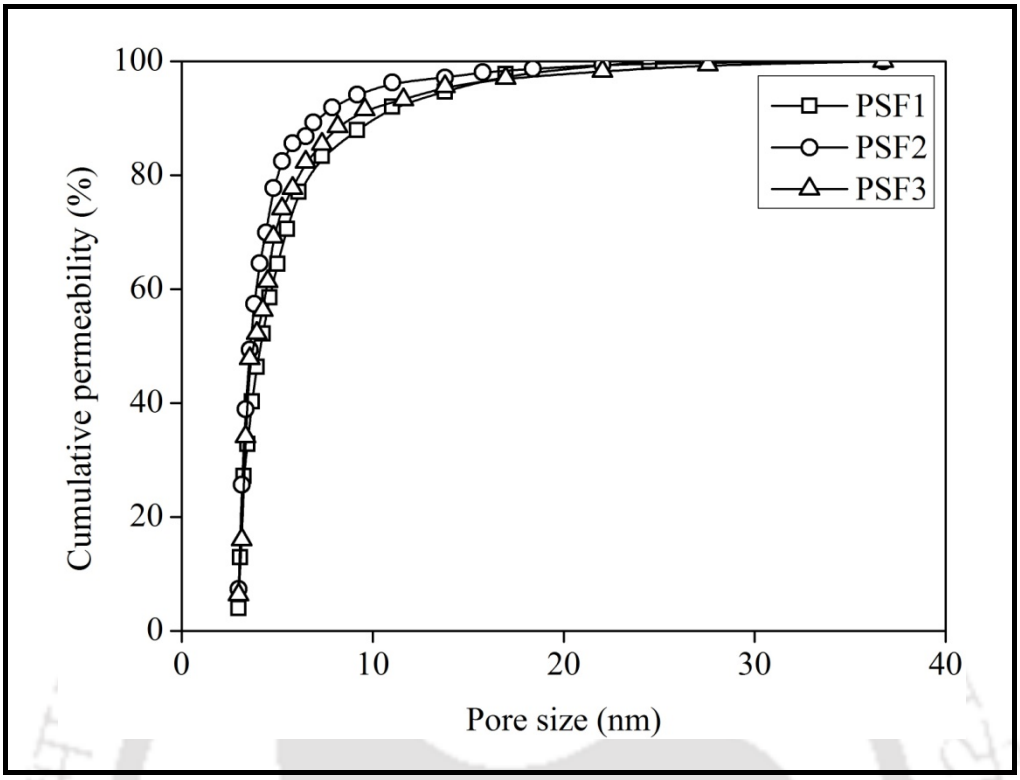


**Figure 4.5: Variation of cumulative permeability (%) with pore size for membranes prepared with different molecular weight of PEGME.**

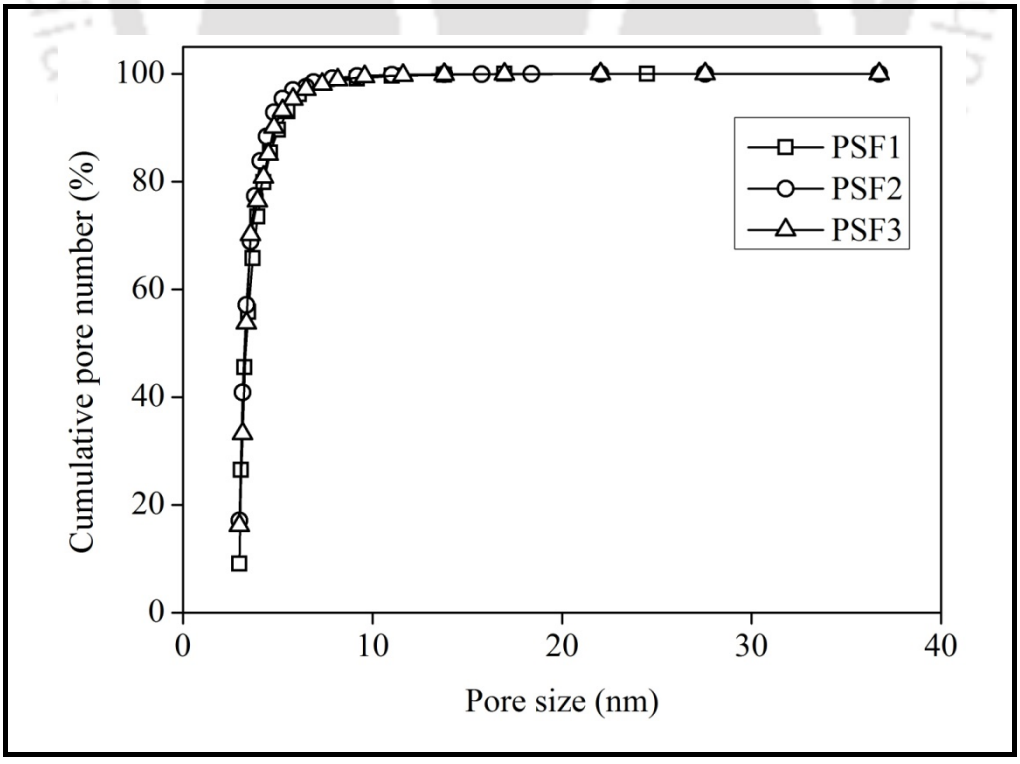


**Figure 4.6: Variation of cumulative pore number (%) with pore size for membranes prepared with different molecular weight of PEGME.**

**Table 4.2: Effect of molecular weight of PEGME on morphological parameters of prepared membranes obtained from LLDP.**

| Membrane | $L_n$(m/sMPa) | $r$(nm) | $N_t$(m$^{-2}$) × 10$^{-8}$ | $A_t$(m$^2$) × 10$^8$ |
|---|---|---|---|---|
| **PSF1** | 0.172 | 3.77 | 7.3 | 3.51 |
| **PSF2** | 0.752 | 3.58 | 45 | 19.3 |
| **PSF3** | 1.057 | 3.51 | 54 | 24.7 |

## 4.3.2. Permeation studies

PSF/PEGME blended membranes were examined through permeation behaviour to observe the effect PEGME and its different molecular weight. The membranes were characterized in terms of CF, PWF and hydraulic permeability as described in chapter 2. Finally, the membranes were subjected to study for rejection as well as permeate flux behaviour with protein (BSA) at different pH.

### 4.3.2.1. Effect of molecular weight of PEGME on compaction factor

Compaction factor (CF) relates to the structure of the membrane, especially membrane sub layer. Higher the CF, more likely the membrane compacts due to presence of large number of macrovoids in the sublayer. The effect of compaction time on PWF for all the membranes is shown in Figure 4.7. For all the membranes, PWF is seen to decline sharply with time due to compaction and finally attain a steady state after around 60 min. This was due to the fact that the walls of the pores become closer, denser and uniform resulting reduction in pore size as well as the flux during compaction [1]. From the figure it is found that the steady state PWF increases with increase in molecular weight of PEGME. For example, the steady state flux increases from 17.5 L/m$^2$h to 227.8 L/m$^2$h, when molecular weight increases from 550 to

5000. The increase in steady state flux with increase in molecular weight of PEGME is due to increase in number of pores on the surface of membrane as discussed in section 4.3.1. Figure 4.7 also depicts that the extent of increase in steady state PWF is not proportionate with the increase in molecular weight of PEGME. For example at steady state PWF increases from 17.5 L/m$^2$h to 172.8 L/m$^2$h when molecular weight of PEGME increased from 550 Da to 2000 Da. Whereas steady state PWF increased to 227.8 L/m$^2$h for PEGME 5000 Da. This shows that increase in molecular weight of 1450 Da (2000 Da – 550 Da) in the lower molecular range, PWF increases around 10 times. Whereas in the higher molecular weight range around 1.3 times of PWF increase is observed even after change in molecular weight of 3000 Da (5000 Da - 2000 Da). This disproportionate increase in PWF behaviour was due to the decrease in end group effects of PEGME with increase in molecular weight. The CF was calculated and shown in Table 4.3 for all the membranes. It is seen that the CF decreases from 32.3 to 8.8 with increase in molecular weight of PEGME from 550 Da to 5000 Da. This observation may be explained from the fact that addition of additives into the casting solution can either enlarge or suppress the macrovoids in the membrane sublayer depending upon their molecular weight [15].

**Table 4.3: Effect of molecular weight of PEGME on some characterization parameters of prepared membranes.**

| Membrane | C.F. | $P_m$ | *EWC* (%) | Porosity | Contact angle |
|---|---|---|---|---|---|
| **PSF1** | 32.3 | 0.088 | 59.7 | 0.36 | 71±1 $^o$ |
| **PSF2** | 9.7 | 0.72 | 66.4 | 0.44 | 59±2 $^o$ |
| **PSF3** | 8.8 | 0.99 | 70.8 | 0.57 | 47±1.5 $^o$ |

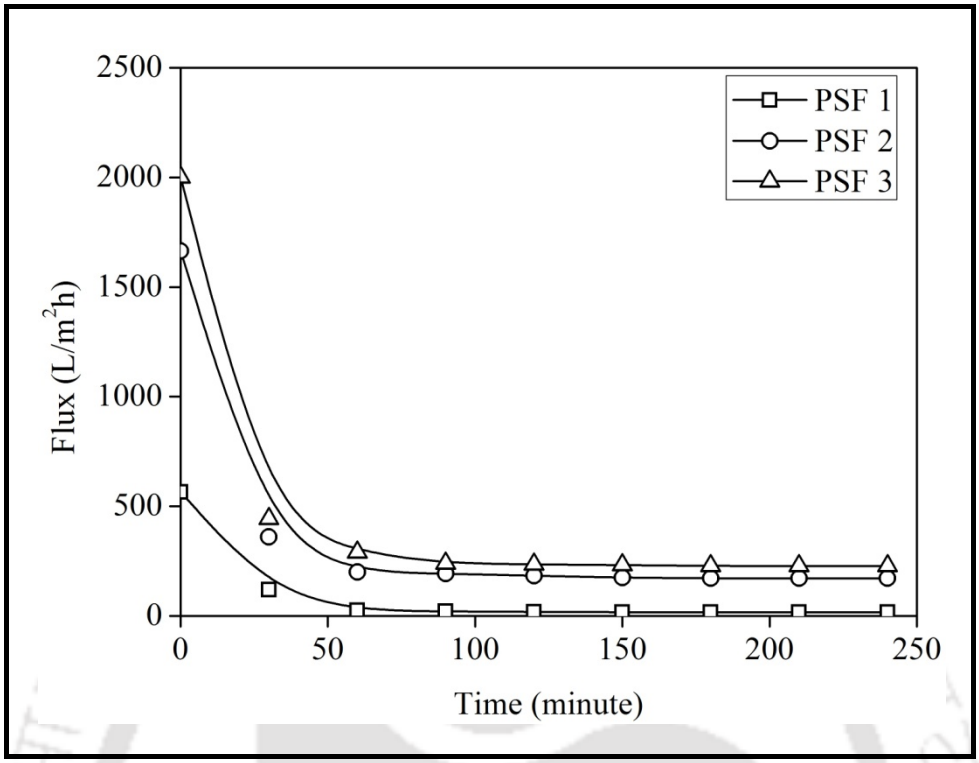


**Figure 4.7: Effect of molecular weight of PEGME on flux profile during compaction.**

#### 4.3.2.2. Effect of molecular weight of PEGME on PWF and hydraulic permeability

The effect of molecular weight of PEGME on PWF at various transmembrane pressures is shown in Figure 4.8. This experiment was carried out at various transmembrane pressures in the range of 0-240 kPa. It is seen that with increase in transmembrane pressure, PWF increases almost linearly for all the membranes. This was due to the increase in effective driving force (transmembrane pressure) required for water permeation. The PWF is also seen to increase with increase in molecular weight of PEGME, which agrees with the findings of the compaction study. For example, at 200 kPa, the PWF increases from 16.8 to 198.2 L/m$^2$h, when molecular weight of PEGME increases from 550 to 5000. Permeability was determined from the slope of the plots (Figure 4.8) using equation 2.10 and shown in Table 4.3. It is observed that hydraulic permeability ($P_m$) increases with increase in molecular weight of

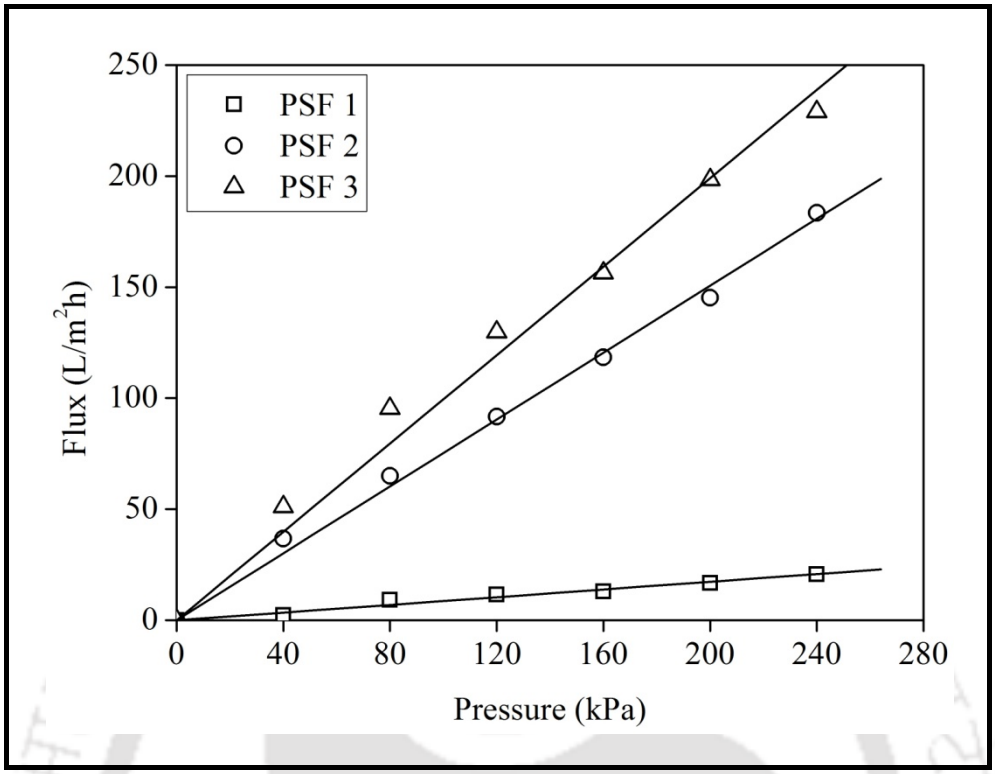


**Figure 4.8: Effect of molecular weight of PEGME on PWF at different transmembrane pressure.**

PEGME and it increases from 0.088 to 0.99 (L/m$^2$h kPa). The result clearly indicates that addition of PEGME with different molecular weight influences the formation of pores in the membranes, which affect the permeability as the latter is conceptually related to its pores for UF membranes [125]. It is to be noted from the figure that the increase in permeate flux for three membranes are not proportionate. This is due to the decrease in end group effects of PEGME as discussed in the preceding section. According to Feng et al. [126], removal of additives completely from the membrane matrix becomes more and more difficult as the molecular weight of additives goes on increasing. Therefore, the residual additives, which are hydrophilic in nature, are compelled to stay inside the matrix permanently, thus, making the membrane more hydrophilic [125, 126].

## 4.3.3. Membrane characterization by EWC, porosity and hydrophilicity

### 4.3.3.1. Effect of molecular weight of PEGME on EWC

The EWC of all the membranes was calculated using equation 3.12 and presented in Table 4.3. It is an important parameter for membrane characterization and has a close relationship with PWF. It may be found from the table that increase in molecular weight of PEGME, EWC of the membrane increases. The EWC for PEGME550, PEGME 2000 and PEGME 5000 are 59.7 %, 66.4 % and 70.8 %, respectively. This increasing trend confirms the presence of increasing number of pores in the membrane with the molecular weight of PEGME (as discussed in section 4.3.1). The pores on the surface as well as cavities in the sub layer are responsible for accommodating water molecules in the membrane [23]. The EWC value of the membranes also coincides with PWF of different membranes, as both the values increases with increase in molecular weight of additive.

### 4.3.3.2. Effect of molecular weight of PEGME on porosity and hydrophilicity

Porosity and hydrophilicity of the membrane are important parameters in membrane permeation and separation processes and it is closely related to PWF and morphology of the membrane. Surface hydrophilicity is often described by the contact angle [113] measurement. In general, smaller the contact angle values higher the hydrophilicity. Porosity of the membranes was measured using equation 2.13. The contact angle and porosity of membranes with different molecular weight of PEGME are shown in Table 4.3. It can be found from Table 4.3 that contact angle decreases and porosity increases with the increase of molecular weight of PEGME. The contact angle for PEGME550 is 71˚, for PEGME 2000 is 59˚ and for PEGME 5000 is 47˚. Similarly, Porosity for PEGME550, PEGME 2000 and PEGME 5000 is 0.36, 0.44 and 0.57, respectively. The findings are uniform with the PWF and LLDP results. The variation of porosity can be explained on the basis of thermodynamic and kinetic

consideration. Addition of an additive into the casting solution has two effects. Firstly, it causes thermodynamic enhancement of the phase separation by reducing the miscibility of the casting solution with nonsolvent; this results in the instantaneous demixing. Secondly, it causes kinetic hindrance against phase separation by increasing the viscosity of the solution; thus result in delayed demixing [1, 127]. The viscosity of casting solution was measured as 0.132 Pa.s, 0.149 Pa.s and 0.170 Pa.s for PSF1, PSF2 and PSF3 membranes, respectively. Increase in viscosity increase the ratio of nonsolvent inflow to solvent outflow which according to the theory suggested by Young et al. [128] results in a more porous membranes. Thus, the increase in membrane porosity with higher molecular weight of PEGME may be due to decrease in miscibility of the casting solution in water with addition of higher molecular weight of PEGME [129]. This in turn, can work in favour of the thermodynamic enhancement in the demixing of casting solution. The residual presence of small amount of PEGME molecules within the membrane matrix, a membrane might gains a hydrophilic behaviour. Thus, the entrapment of PEGME improves the hydrophilicity of membrane and higher molecular weight of PEGME lead to more residual of PEGME and decrease of contact angle.

### 4.3.4. Ultrafiltration of BSA

Apart from transmembrane pressure, the rejection and flux characteristics of the membranes strongly depend on the structure of the membrane as well as the properties of the feed solution. So, the prepared UF membranes were also characterized by estimating rejection and flux during permeation experiment using BSA solution. To investigate the fouling behaviour, membranes were cleaned after BSA solution ultrafiltration, and the PWF of the cleaned membranes was measured. Figure 4.9 shows the time-dependent flux of membrane during ultrafiltration. It may be seen that the PWF ($J_{w1}$) before UF of the BSA solution changes

marginally, but it decreased drastically at the initial operation of BSA solution ultrafiltration. It happened due to the deposition or adsorption of protein molecules on membrane surface at the initial BSA ultrafiltration operation [118, 120, 121]. After some time of operation it reaches equilibrium, so that a relatively steady flux ($J_p$) was obtained in the final operation of BSA ultrafiltration.

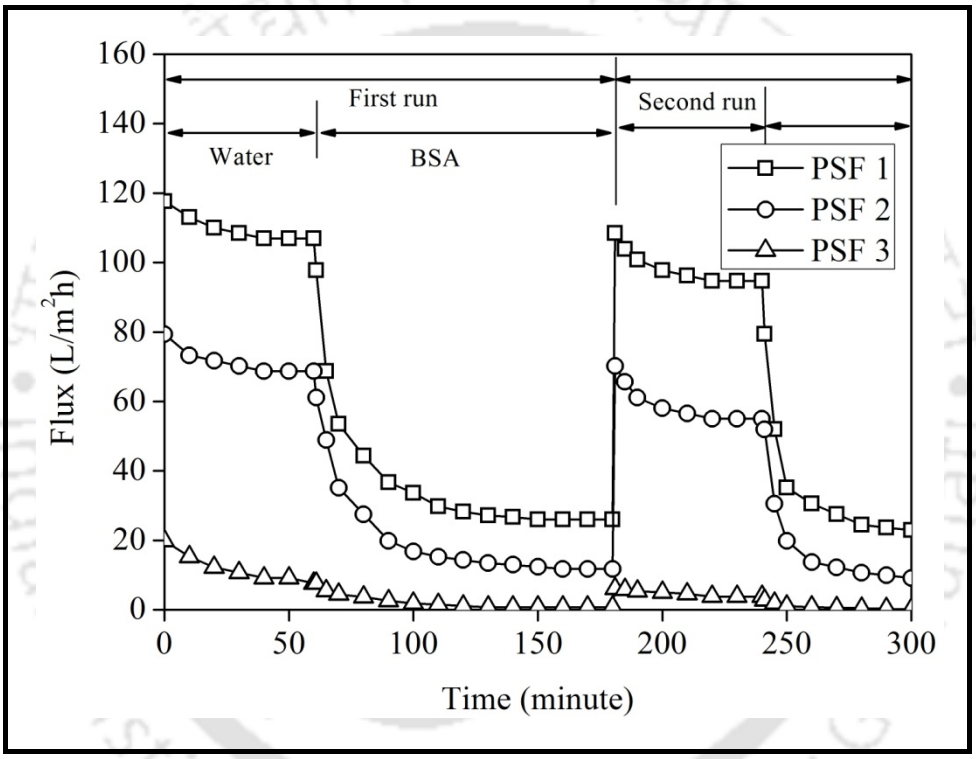


**Figure 4.9: Effect of molecular weight of PEGME on time dependent flux of membrane during ultrafiltration.**

#### 4.3.4.1. Reversible and irreversible fouling

There are two types of membrane fouling, reversible and irreversible. Reversible deposition and adsorption of protein causes reversible fouling, which can be removed by hydraulic cleaning. Whereas irreversible protein adsorption causes irreversible fouling that can only be eliminated by chemical cleaning or enzymatic degradation [116]. To find out these fouling

values, pH of 7 was used during experiments. The summarizing of total fouling ($F_t$), reversible fouling ($F_r$) and irreversible fouling ($F_{ir}$) as a function of molecular weight of PEGME is shown in Figure 4.10. It can be seen that $F_t$ decreases from 0.9 to 0.77 with increase in molecular weight of PEGME from 550 to 5000. The lower value of $F_t$ indicates lower total flux loss, resulting in less protein adsorption or deposition on the membrane surface [116, 120]. From figure it may also be seen that membrane containing higher molecular weight PEGME has lower value of $F_{ir}$. This is due to the fact that the membrane containing higher molecular weight of PEGME has lower value of persistent protein adsorption on the membrane and initial water flux could be recovered by a simple cleaning methods using deionized water.

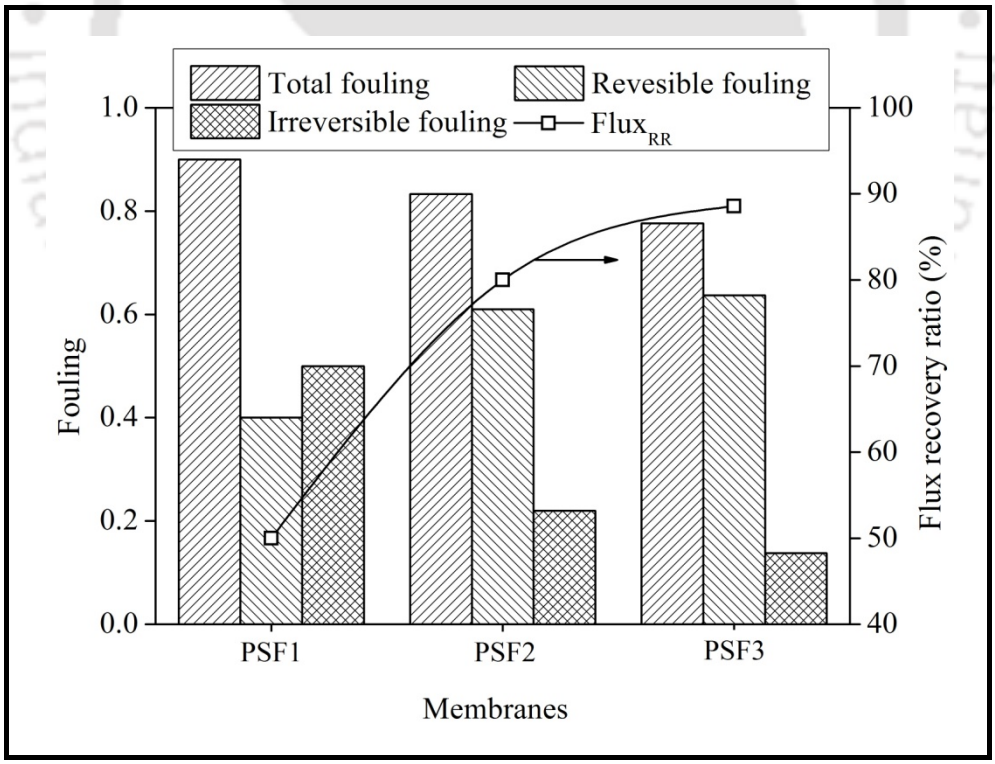


**Figure 4.10: Effect of molecular weight of PEGME on different fouling parameters.**

### 4.3.4.2. Effect of molecular weight of PEGME

Figure 4.11 shows the effect of molecular weight of PEGME in membrane casting solution on the average flux using BSA solution during 2 h ultrafiltration. The pH of the BSA solution was maintained at 4.8, 7 and 10. It is observed from the figure that with increase in molecular weight of PEGME from 550 to 5000, the flux gradually increases from 0.9 to 9.2 L/m$^2$h, 4.7 to 61.1 L/m$^2$h and 1.5 to 30.5 L/m$^2$h when pH of BSA solution is 4.8, 7 and 10, respectively. This increasing trend of flux, irrespective of the pH of BSA, may be attributing to the formation of membranes with higher pore density, which is seen in LLDP experiment. It is also clear from FESEM image (Figure 4.1) that more porous membranes are formed as the molecular weight of PEGME increases.

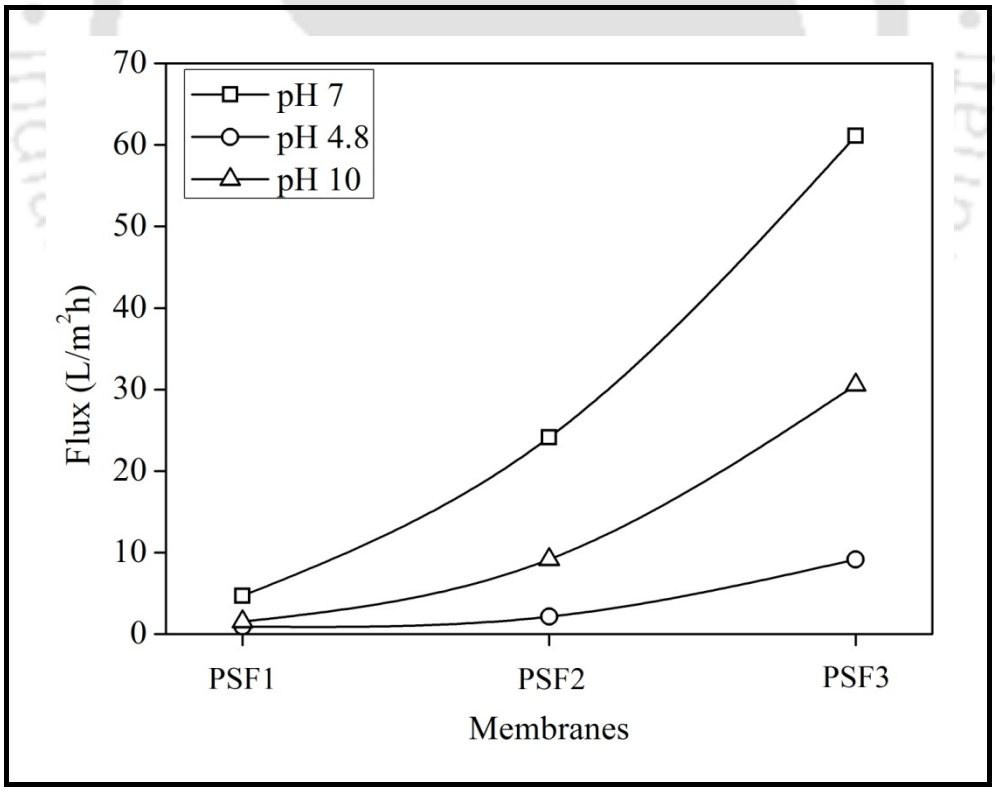


**Figure 4.11: Effect of molecular weight of PEGME on BSA flux at different pH.**

Figure 4.12 shows the effect of molecular weight of PEGME in membrane casting solution on the rejection of BSA at solution pH of 4.8, 7 and 10. It is observed from the figure that with the increase of molecular weight of PEGME from 550 to 5000, the rejection gradually increases from 29 to 85%, 5.5 to 51 % and 13 to 60 % when pH of BSA solution is 4.8, 7 and 10, respectively. The rejection of protein by ultrafiltration membranes can be explained under the concept of protein adsorption and consequent pore narrowing, as a result of both hydrophobic and electrostatic interactions between the membrane surface and the protein molecules [118, 121, 125]. The morphological structure of the membrane (which includes both top layer and sublayer) in protein transmission or rejection also play an important role. The increasing trend in percentage rejection with increase in molecular weight of PEGME may be because of the resistance offered by the dense and sponge like structure of the membranes (Figure 4.1) with higher molecular weight of PEGME.

#### 4.3.4.3. Effect of pH of BSA

The BSA rejection is very much pH dependent. Rejection is highest and flux is least at isoelectric point (IEP) of BSA solution [121, 125, 130]. BSA molecules have no charge at IEP (i.e. at pH 4.8). The BSA molecules remained in most compact size when get deposited on the membrane surface form least permeable layer [121, 125]. This compact layer is responsible for highest BSA rejection and least flux. At pH 7, BSA molecule bears net negative charge and enlarges due to electrostatic repulsion. These effects would give a more permeable deposited layer and should give a higher flux and lower rejection [121, 125]. Higher rejection and lower flux at pH 10 compare to pH 7 can be explained by Coulomb's law [118]. As BSA molecules have more negative charged at pH 10 compare to pH 7 and due to the $–CH_3$ group of retained PEGME in membrane, there is a positive inductive effect (+I effect), which causes a positive charge on $–CH_3$ group. So, positive charge on membrane

surface and negative charge on BSA, leads to more protein adsorption on membrane surface, which cause lower flux and higher rejection compare to pH 7.

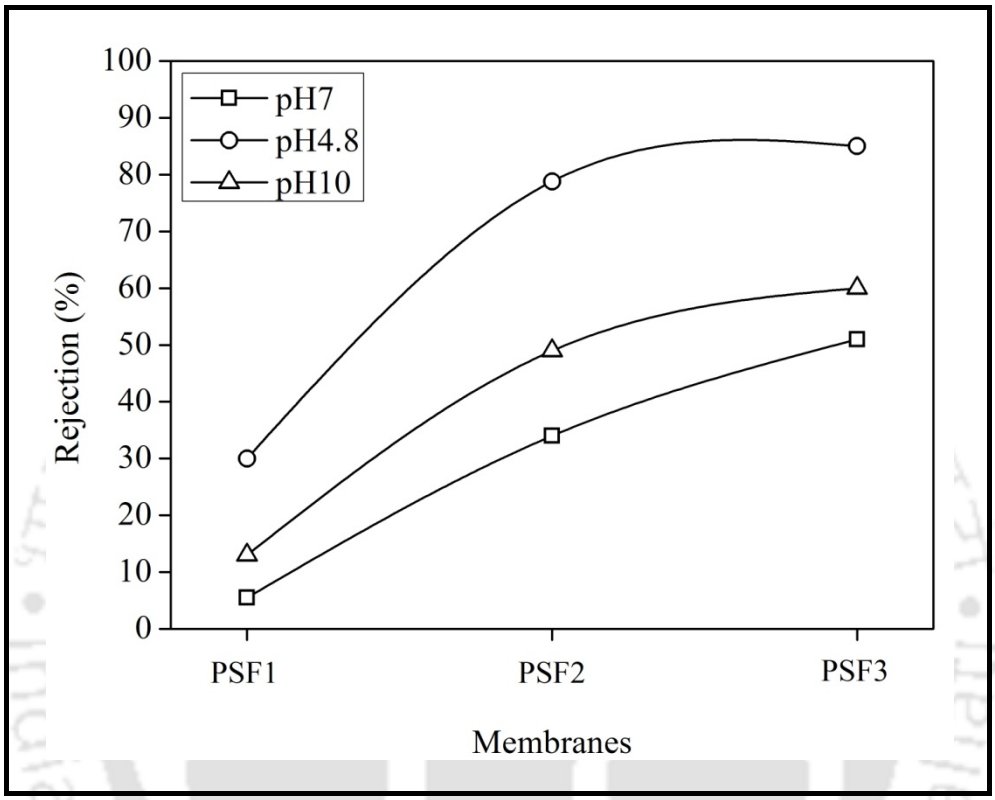


**Figure 4.12: Effect of molecular weight of PEGME on BSA rejection through prepared membranes at different pH.**

# Chapter 5

## Preparation and characterization of stimuli-responsive hydrophilic polysulfone membrane modified with poly (N-vinylcaprolactam-co-acrylic acid)

# Chapter 5
# Preparation and characterization of stimuli-responsive hydrophilic polysulfone membrane modified with poly (N-vinylcaprolactam-co-acrylic acid)

*This chapter discussed the preparation of novel polysulfone (PSF) ultrafiltration membranes with pH and thermo sensitivity using the copolymer poly (N-vinylcaprolactam-co-acrylic acid) (poly (VCL-co-AA)) as an additive. The copolymer was synthesized by free radical solution polymerization, and directly blended in membrane casting solution to prepare the asymmetric membranes by phase inversion method. The presence of copolymer in blended membranes was confirmed by comparing IR spectra of plain PSF membrane and blended PSF membrane. The morphology and structure of the resulting membranes were observed by scanning electron microscope (SEM) and field emission scanning electron microscope (FESEM). The membranes were characterized in terms of pure water flux (PWF), hydraulic permeability and hydrophilicity. The stimuli responsive behaviour of membranes was also investigated in terms of pH and temperature. In addition, solution of bovine serum albumin (BSA) was used to study the permeation and antifouling performance of prepared membranes.*

## 5.1. Experimental

### 5.1.1. Materials

PSF and NMP were used as base polymer and solvent respectively, in the membrane casting solution. N–vinylcaprolactam, acrylic acid, azobisisobutyronitrile (AIBN), potassium

Content of this chapter is published as below:

M.K. Sinha, M.K. Purkait, Preparation and characterization of stimuli-responsive hydrophilic polysulfone membrane modified with poly ( N-vinylcaprolactam-co-acrylic acid ), Desalination 348 (2014) 16–25.

bromide (KBr) and BSA were used in this chapter. All the details of used chemical are provided in Table 2.1 of chapter 2.

### 5.1.2. Synthesis and Characterization of Poly (VCL-co-AA) Copolymer

The poly (VCL-co-AA) copolymers were prepared by free radical copolymerization of VCL with AA in presence of AIBN as initiator. Monomers of VCL and AA (the mass ratio = 6:4) were dissolved in NMP with total monomer concentration of 33 wt %. The AIBN was added to the solution at 0.3 % of the total weight of the monomers. The mixture was purged with nitrogen for 30 min and allowed to react in an oil bath at 75˚C for 24 h in an air tight flask. After reaction, the product was cooled to room temperature and washed several times with millipore water to remove residual initiator and monomer. The obtained product was dried completely at 50˚ C for 4 days.

Fourier transform infrared (FTIR) analysis was carried out to confirm the chemical groups of the synthesized copolymer. Differential scanning calorimetry measurement was used to measure the glass transition temperature ($T_g$) and also to confirm that it is a copolymer rather than a mixture of polymers. The solid samples were sealed onto a DSC pan and scanned in the temperature ranging of - 25˚C to 200˚C at a heating rate of 5˚C/min under nitrogen gas. Methods and instrument details are provided in section 2.4 of chapter 2.

### 5.1.3. Preparation of Flat Sheet Membranes

Flat sheet membranes were prepared by phase inversion method using different composition of PSF, poly (VCL-co-AA) and NMP (as shown in Table 5.1). The casting solution was stirred with the help of magnetic stirrer for 18 h at 50˚C and further degassed for 12 h at room temperature. The solution was then casted on a clean glass plate with a casting knife

maintaining uniform thickness of 200 µm in ambient atmosphere. Further details are given in section 2.2 of chapter 2.

**Table 5.1: Composition of different membrane casting solution containing poly (VCL-co-AA).**

| Membranes | PSF (wt.%) | Poly (VCL-co-AA) (wt.%) | NMP (wt.%) |
|---|---|---|---|
| **M_0** | 15.0 | 0.0 | 85 |
| **M_1** | 14.5 | 0.5 | 85 |
| **M_2** | 14.0 | 1.0 | 85 |
| **M_3** | 13.5 | 1.5 | 85 |
| **M_4** | 13.0 | 2.0 | 85 |
| **M_5** | 12.5 | 2.5 | 85 |

## 5.2. Membrane characterization

### 5.2.1. Surface Characterization of Poly (VCL-co-AA) Blended Membranes

The presence of copolymer in blended membranes was confirmed by comparing IR spectra of plain PSF membrane and blended PSF membrane. Microscopic observation of plain and blended membranes was done by field emission scanning electron microscope (FESEM) and scanning electron microscope (SEM)**.** Cross section images were taken by SEM with an acceleration voltage of 10 kV after the samples were coated with thin gold layer. As top surface images required higher magnification, so these images were taken by FESEM with an acceleration voltage of 3 kV after the samples were coated with thin gold layer. Hydrophilic property of the membrane was evaluated by measuring the static contact angle between the DI water and membrane films at room temperature. Standard titration method was used to

determine the ion exchange capacity (IEC) of different membranes [131]. The IEC value was calculated using the equation 2.15. All the details of characterization techniques and instrument details are reported in section 2.3 of chapter 2.

## 5.2.2. Water Permeation Experiment

### 5.2.2.1. Membrane compaction and hydraulic permeability

For compaction study, prepared membranes were compacted with DI water for 4 h at a transmembrane pressure of 250 kPa and water permeation flux was measured at every 30 min interval through the membranes. The ratio of initial pure water flux ($PWF_{initial}$) to the steady state pure water flux ($PWF_{steady\ state}$) gives the value of compaction factor (CF). Water flux was measured by the equation 2.9. Flux values of pure water at different transmembrane pressures were measured under steady state condition. Permeability ($P_m$) (L/m$^2$h kPa) was evaluated from the slope of the plot of $J_w$ vs $P$. Hydraulic permeability was calculated by equation 2.10.

### 5.2.2.2. Stimuli-responsive permeability experiment

The variation in PWF of blended membranes with pH and temperature change was measured using the same setup as described earlier. The pH value of the permeating solution was adjusted between 2 to 11, using 0.1 M NaOH and 0.1 M HCl solution. Each membrane was initially compacted with DI water for 30 min at 250 kPa, after that membrane was pre-treated by soaking it in an aqueous solution at certain pH or temperature for 15 min. Then, 15 min flux measurement was conducted with desired pH or temperature of water under a constant transmembrane pressure of 150 kPa. Flux was measured by using equation 2.9. For pH sensitivity experiments, temperature was kept constant at 25˚C and for thermal sensitivity pH was kept at 7. After cleaning the system with DI water, membrane permeability was re-

evaluated with DI water. It was observed that the membrane permeability remained almost constant after pH and thermo sensitivity experiment.

### 5.2.3. Membrane performance characterization by BSA ultrafiltration experiment

The solute separation and permeate flux behaviour of the prepared membranes were studied by BSA ultrafiltration experiments. BSA was dissolved in DI water and the concentration was kept constant at 1000 $mgL^{-1}$ for all the experiments. The pH of the BSA solution (molecular weight 68000 Da) was kept at 2, 7 and 11. pH of the solution was adjusted by using 0.1 M NaOH and 0.1 M HCl solution. Each membrane was initially compacted for 30 min at 250 kPa, then the pressure was reduced to the working pressure of 150 kPa and the water flux ($J_{w1}$) was measured. In the second stage, membrane cell was emptied and refilled with BSA solution; the flux was recorded ($J_p$). The BSA rejection ratio was calculated by the equation 2.16.

After 1 hr of ultrafiltration, the membrane was cleaned with DI water and again water flux was measured ($J_{w2}$). With the help of $J_{w1}$ and $J_{w2}$, flux recovery ratio ($Flux_{RR}$) was measured. UV-VIS spectrophotometer (Perkin-Elmer Precisel, Lamda-35) was used to find out the BSA concentration, at wavelength of 280 nm. Membrane fouling causes flux loss ($J_{w1}$-$J_p$). The flux loss caused by total fouling ($F_t$), reversible fouling ($F_r$) and irreversible fouling ($F_{ir}$) are calculated by equations 2.17, 2.18 and 2.19 respectively.

## 5.3. Results and discussion

### 5.3.1. ATR-FTIR spectroscopy and DSC analysis

Figure 5.1a shows the FTIR spectra of poly (VCL-co-AA) copolymer. As shown in Figure 5.1a, peaks at 1658 $cm^{-1}$ and 1476 $cm^{-1}$ are characteristic peaks of VCL, due to tertiary amide group and $-CH_2$ group attached to N atom respectively. The peaks at 1739 $cm^{-1}$ and 3275 $cm^{-1}$ are characteristic peaks of −COOH group present in AA, which is the evidence of presence AA, another peak at 2947 $cm^{-1}$ is due to the C−H stretching in copolymer.

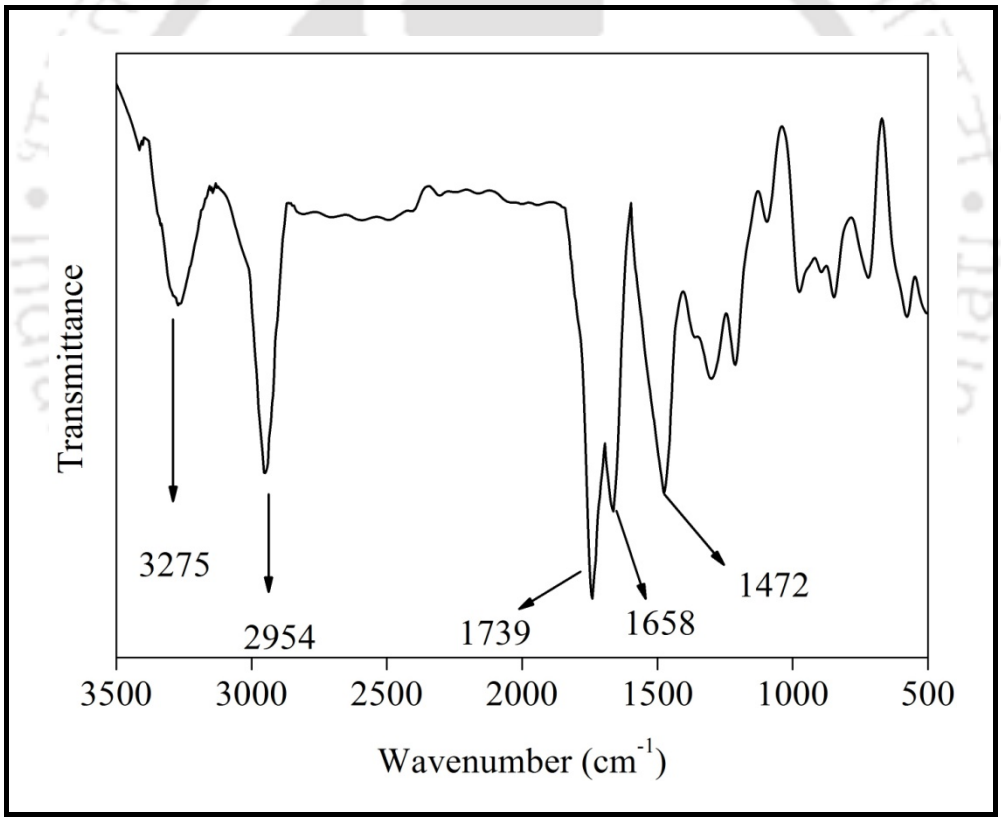


**Figure 5.1a: FTIR spectra of poly (VCL-co-AA).**

Figure 5.1b shows the DSC thermogram, which is used to measure $T_g$ of the copolymer. It was found that there is only one $T_g$ of copolymer (107˚C). Whereas, $T_g$ for homopolymers, PAA and PVCL are 85−115 $^oC$ and 100−155 $^oC$, respectively [132]. The

presence of only one $T_g$ (Figure 5.1b), depicts that it is not a blend of polymer but a copolymer. Collectively with the results of FTIR, the synthesized copolymer could be distinguished as copolymer.

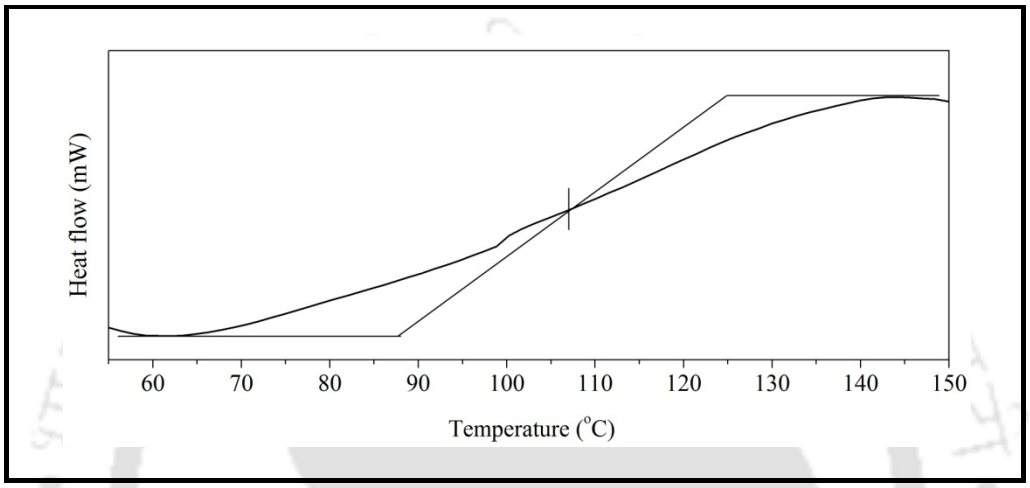


**Figure 5.1b: DSC thermogram of synthesized polymer.**

Figure 5.1c shows ATR-FTIR spectra of plain and blended PSF membranes. New peaks at around 1476 $cm^{-1}$ and 1658 $cm^{-1}$ are for amide group. Another new peak appears around 1739; confirms the presence of −COOH group. The peak around 2950 $cm^{-1}$ becomes broader due to the addition of C−H stretching, present in the copolymer. These peaks authenticate the presence of poly (VCL-co-AA) in the blended membrane. The peaks at 1155 $cm^{-1}$ and 1295 $cm^{-1}$ are due to −C−O−C− and S=O group present in polysulfone, thereby confirming the presence of polysulfone. Although, these peaks shifted little bit in blended membranes, this might be due to the changes in confrontation and interaction of molecules upon blending. Apart from that, position of the amide band depends on the degree of hydrogen bonding and physical state of the compound [133]. These results indicate that the copolymer was blended well in the PSF membrane.

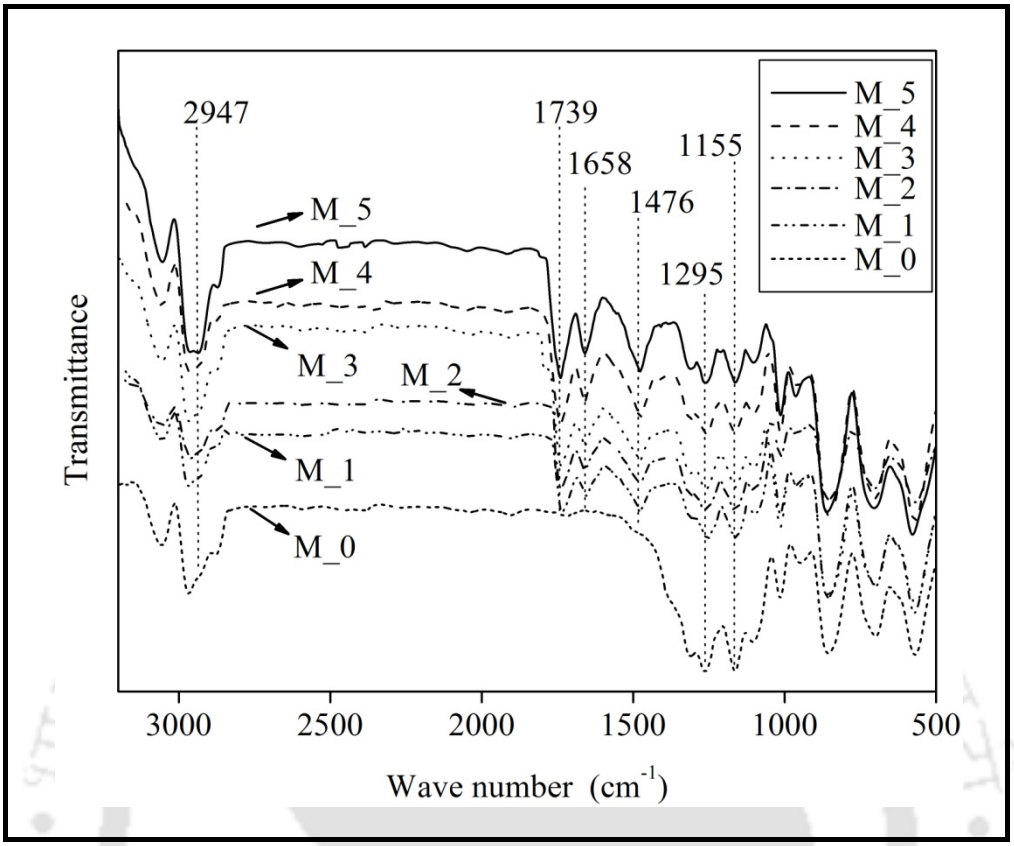


**Figure 5.1c: ATR-FTIR spectra of plain and blended PSF membranes.**

## 5.3.2. Membrane structure

FESEM images of top surface of the plain and blended PSF membranes are shown in Figure 5.2a. It was observed that, the top surface of the blended membranes have comparatively rougher surface with respect to the controlled PSF membrane. As the weight % of copolymer increased in blended membranes, their surface became more and more rough. This roughness is due to the settlement of copolymer on the membrane surface. As the amount of copolymer increased in the blended membranes, the number of these structures also increased. According to Reuvers et al [115], the formation of top surface is probably a result of spinodal demixing. Further, the diffusion process during the formation of top layer was fast enough for the polymer solution to become highly unstable and cross the spinodal curve [115, 122].

These interactions actively supported the disarticulation of the copolymer towards the growing, and then developed at the polymer–solvent interface. Result of all these activities is higher localized concentration of the copolymer at the polymer-solvent interfaces before the solidification of the macro-structures.

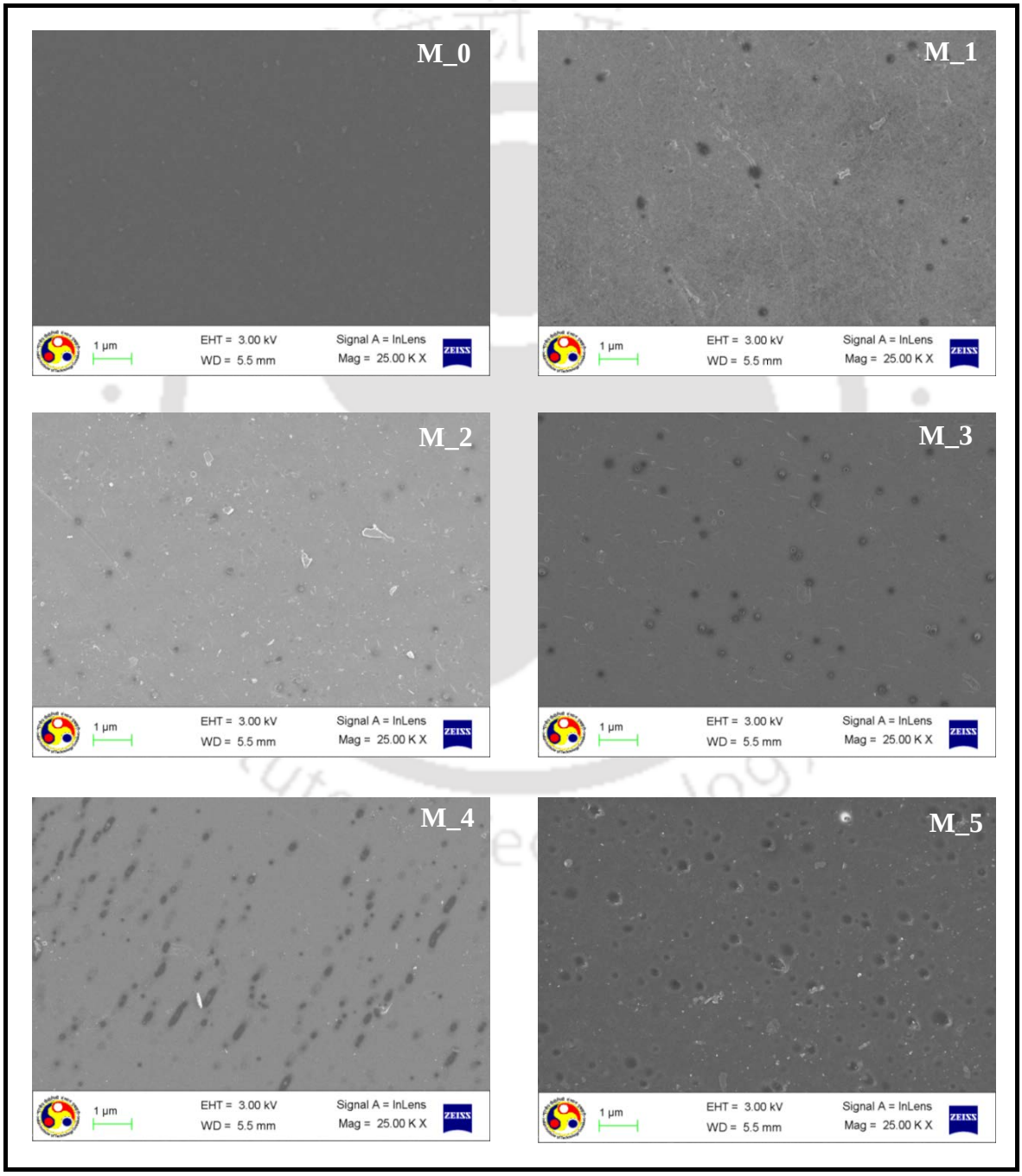


**Figure 5.2a: Effect of wt % of poly (VCL-co-AA) on top surface of membranes.**

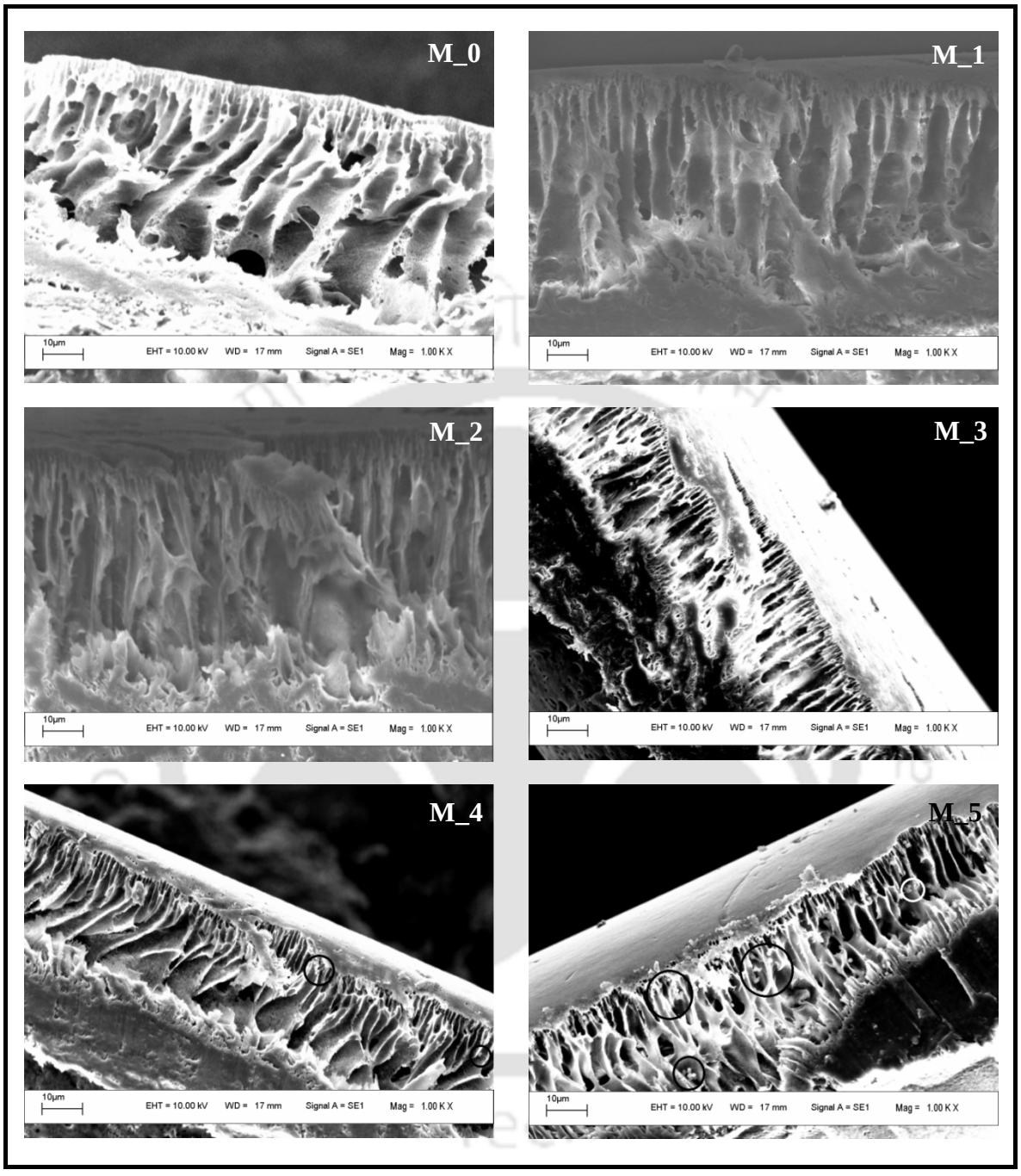


**Figure 5.2b: Effect of wt % of poly (VCL-co-AA) on cross section of membranes.**

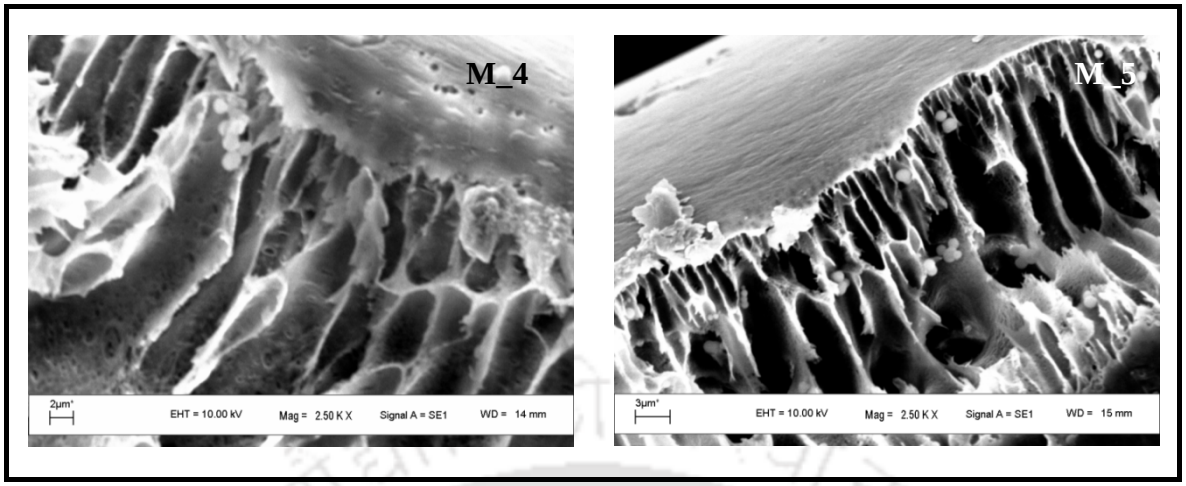


**Figure 5.2c: SEM images of cross section of membranes M_4 and M_5 showing deposition of copolymer in cross section.**

Figure 5.2b shows the SEM images of cross sectional view of the plain and blended membranes prepared in this chapter. From the images, it is clear that all the prepared membranes have asymmetric structure. General structure was very similar for all the membranes consisting of a top dense skin layer and a porous sub-layer. The porous sub-layer of all the membranes consists of finger like structure. NMP and water have mutual affinity towards each other, which results in instantaneous demixing, leading to the formation of finger like cavities in the sub-layer of the prepared membranes [1]. For M_0, M_1, M_2 and M_3 there was no significant change in morphology. However, when the copolymer content increased to 2 wt. % (M_4) as shown in Figure 5.2c, trace amounts of copolymer appeared in the finger like structure, and more particles appeared when the copolymer content increased to 2.5 wt % (M_5). The particles may be caused by the self assembly of the copolymer poly (VCL-co-AA) when the concentration of the copolymer was higher than 1.5 wt % [134].

### 5.3.3. Effect of wt % of poly (VCL-co-AA) copolymer on hydrophilicity, PWF and hydraulic permeability

Contact angle (CA) is a straightforward way to detect the relative hydrophilicity/hydrophobicity of the membrane surface. Contact angles of different membranes are shown in Table 5.2. CA decreases with increase in wt % of copolymer. This indicates that modified PSF membranes are more hydrophilic. The existence hydrophilic functional group in PAA and PVCL, which were confirmed by FTIR analysis, would increase the hydrophilicity of the membrane. Compaction factor (CF) relates to the structure of the membrane, especially membrane sub layer. Higher the CF, more likely the membrane compacts due to the presence of large number of macrovoids in the sublayer. The outcome of compaction time on PWF for all the membranes is shown in Figure 5.3. For all the membranes, PWF declined sharply with time as a result of compaction and eventually attained a steady state at around 60 min. This was due to the fact that the walls of the pores become closer, denser and uniform resulting in reduction of pore size as well as the flux during compaction [1]. From the figure 5.3 it was found that the steady state PWF increases with increase in wt % of copolymer. For example, the steady state flux increases from 0.92 $L/m^2h$ to 21.4 $L/m^2h$, for membrane M_0 and M_5 respectively. These results are in line with earlier works [73-75].

The effect of wt % of the copolymer on PWF at various transmembrane pressures is shown in Figure 5.4. This experiment was done at different transmembrane pressures in the range of 0−250 kPa. It was observed that with increasing transmembrane pressure, PWF increased almost linearly for all the membranes. This was due to the increase in effective transmembrane pressure (driving force) required for water permeation. The PWF was also found to increase with increasing wt % of the copolymer, which agrees with the results of the

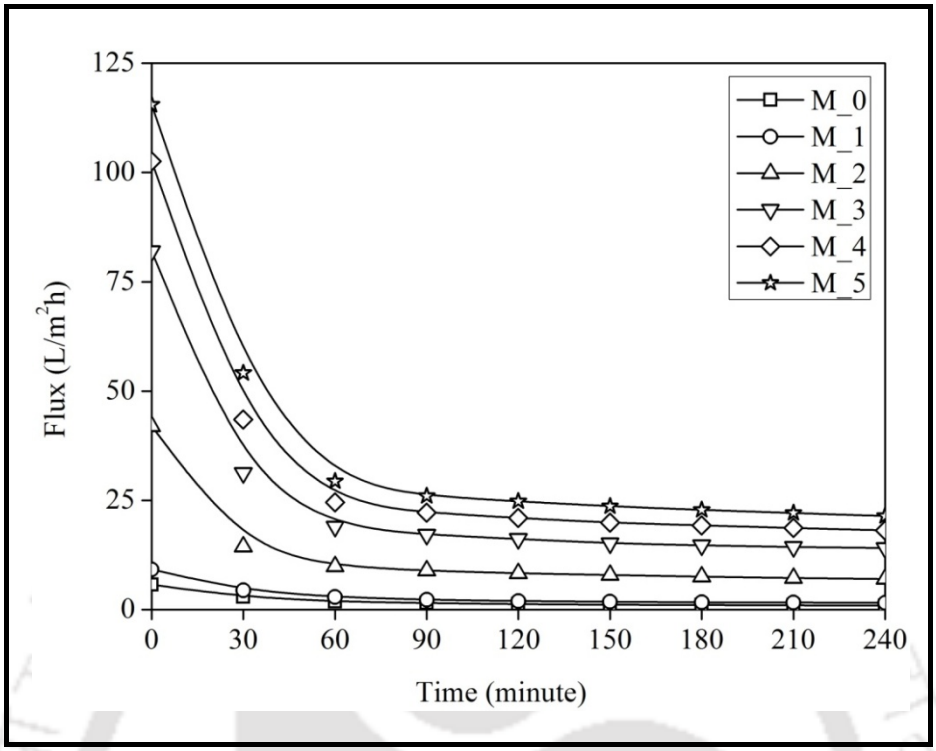


**Figure 5.3: Effect of wt. % of poly (VCL-co-AA) on flux profile during compaction.**

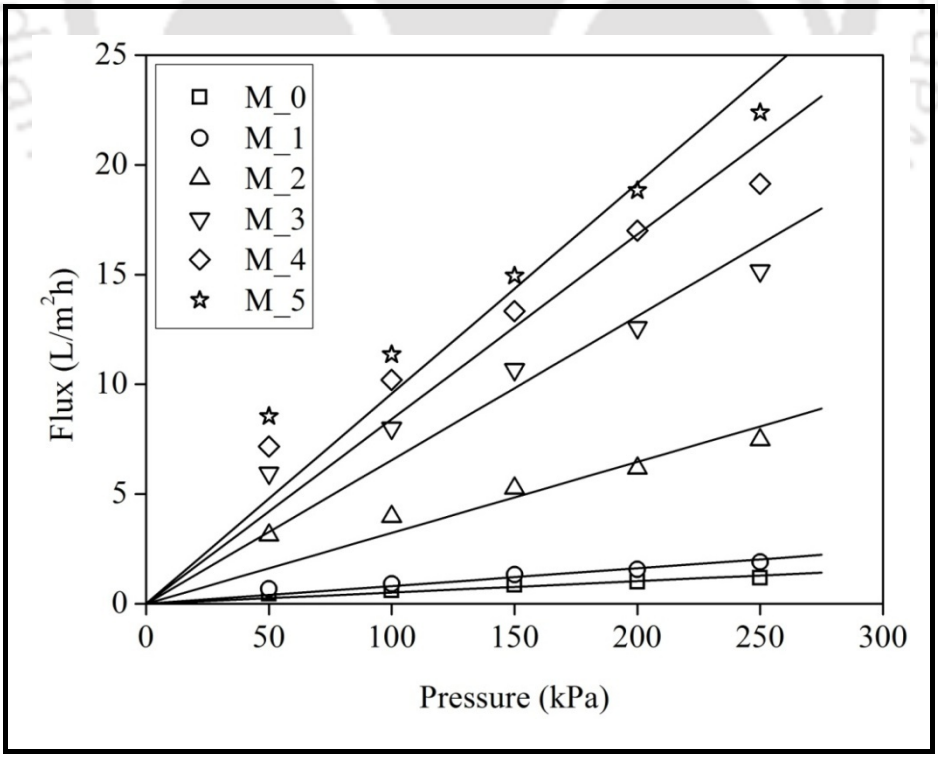


**Figure 5.4: Effect of wt. % of poly (VCL-co-AA) on flux at different transmembrane pressure.**

compaction study. For example, at 200 kPa, the PWF increases from 1 to 18.8 L/m$^2$h, when wt % of copolymer increases from 0 to 2.5. Permeability was determined from the slope of the plots (Figure 5.4) using equation 2.10 and shown in Table 5.2. It was observed that the hydraulic permeability ($P_m$) increases with increase in wt % of the copolymer and it increases from $0.37 \times 10^{-2}$ to $7 \times 10^{-2}$ (L/m$^2$h kPa). The result clearly indicates that the addition of dual hydrophilic copolymer making the membranes more hydrophilic, which leads to the increase in PWF. These finding are in line with the results of some earlier works [73, 84, 93, 135].

**Table 5.2: Values of some characterization parameters of membranes modified with poly (VCL-co-AA).**

| Membranes | Contact angle (deg) | Compaction factor | Hydraulic permeability (L/m$^2$h kPa)×10$^3$ | IEC capacity (mmol/g) |
|---|---|---|---|---|
| **M_0** | 76±1 | 6.23 | 3.72 | – |
| **M_1** | 70±1 | 6.05 | 6.12 | 0.12 |
| **M_2** | 68±2 | 5.97 | 21.8 | 0.15 |
| **M_3** | 65±2 | 5.81 | 46.1 | 0.19 |
| **M_4** | 62±1 | 5.65 | 61.5 | 0.21 |
| **M_5** | 58±2 | 5.38 | 70.3 | 0.28 |

## 5.3.4. pH and thermo responsive study

The effect of pH value on water flux was studied and results are shown in Figure 5.5. It was noted in the figure that, when pH changed from 2 to 11, the water flux for membrane M_0 was not changed, which was about 1 L/m$^2$h. But, water flux for membranes M_1, M_2, M_3,

M_4 and M_5 increased from 1.17 to 2.18, 4.12 to 11.0, 7.43 to 25.05, 7.65 to 32.82 and 7.9 L/m$^2$h to 41.4 L/m$^2$h, respectively, when pH decreased from 11 to 2. So, modified

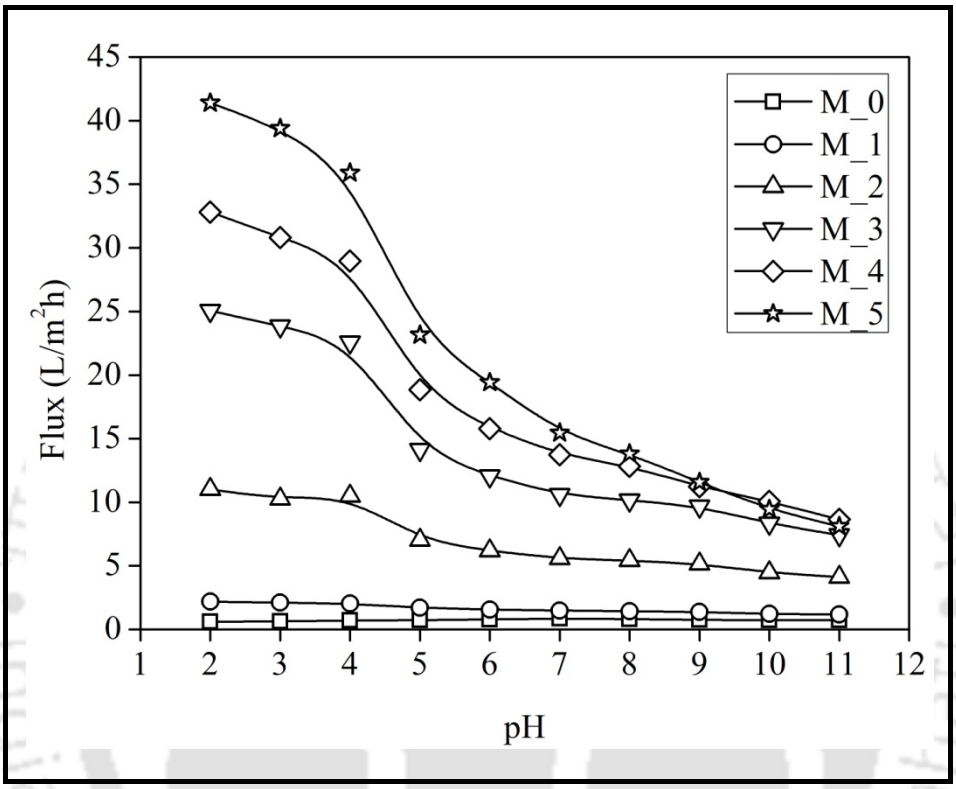


**Figure 5.5: Effect of wt. % of poly (VCL-co-AA) on flux at different pH.**

membrane prepared by mixing poly (VCL-co-AA) copolymer, showed evident pH sensitivity. From figure it was clear that flux decreases with increase in pH, but at pH between 4 and 6 there was sudden drop in flux, later then flux decreases gradually. Sudden change in flux was caused by the ionisation of PAA. The pKa value of PAA was 4.4−4.9, which was in conformity with flux change as shown in Figure 5.5 [136, 137]. This change in water flux with pH can be explained by dissociation of carboxylic acid of AA to carboxylate ions at pH around 5. These carboxylate ions provide high charge density in the copolymer, which leads to the expansion of copolymer and these expanded copolymer blocks the pores of the membrane. Again on increment of the pH beyond 8 or more, there is further loss of flux,

which is because of electroviscous effect. The electroviscous effect is defined as the physical phenomenon that takes place when an electrolyte solution is pressed through a fine capillary or pore having charged surfaces [134]. As permeating solution and membrane, both contain negative charge, so membrane repels the solution to pass through the pores. This whole phenomenon is depicted in Figure 5.6. So, as the pH increases more and more negative charge comes in solution, which feels more repulsion from the membrane and flux continues to decrease. Therefore it concludes that, in pH sensitivity of the membrane, electroviscous effect also plays a dominant role. The water flux at pH 2 and pH 11, and the flux change ratio are represented in Figure 5.7a. With the increase in the copolymer content, the flux change increased. For M_1, the flux change was about 1.9 times and for M_5, the flux change was around 5.2 times. These changes are attributed to the increasing amount of copolymer, which led to the higher electroviscous effect. It was also confirmed by IEC of the different membranes (shown in Table 5.2).

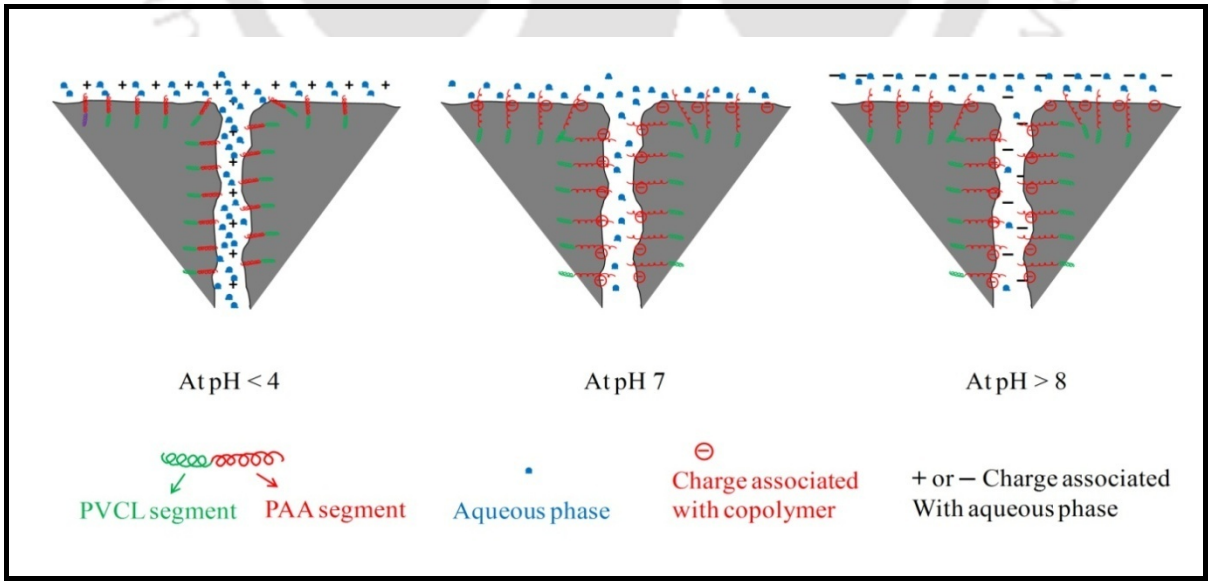


**Figure 5.6: Schematic presentation for the mechanism of pH responsive phenomenon of membranes.**

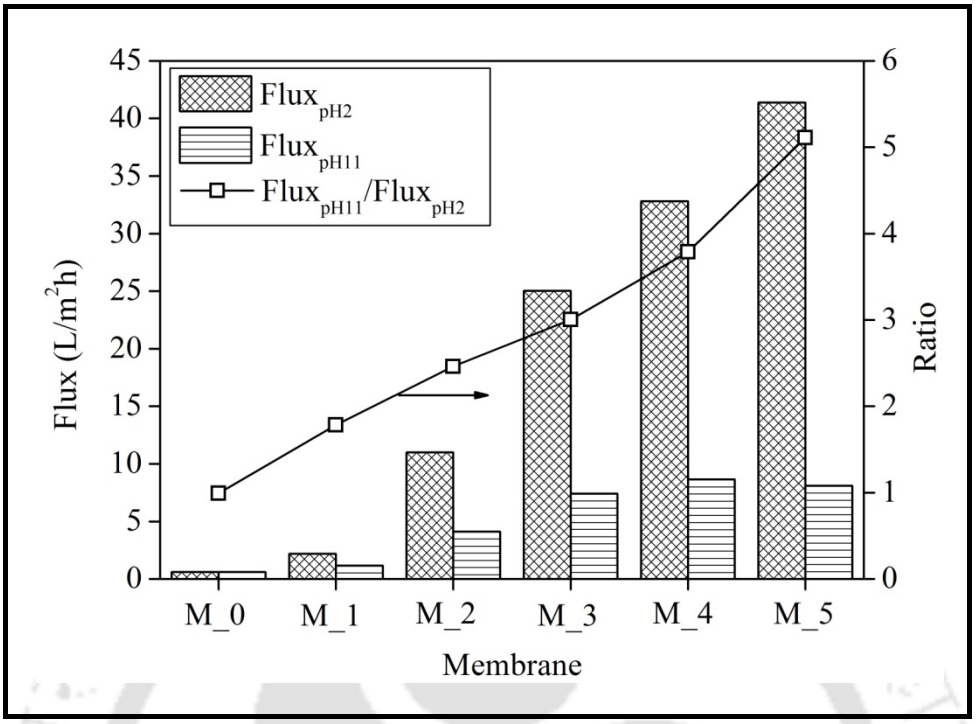


**Figure 5.7a: Effect of wt. % of poly (VCL-co-AA) on flux ratio between pH 2 and 11.**

The water flux at 25˚C and 40˚C, and the flux change ratio are represented in Figure 5.7b. The change in flux is due to the fact that, PVCL segment of copolymer has LCST around 35˚C. So, below this temperature, PVCL remains in swell state, but when temperature goes over LCST, PVCL segment shrinks [70]. Due to this swell and shrink function of PVCL, pore size of the membrane changes with change in temperature, below and above LCST. In addition to that, with the increase in copolymer content, the flux change increased. PAA segment of copolymer would change their conformation from expanded to collapsed or vice-versa as the pH of the surrounding medium decreases or increases across its pKa. Thus due to the pH responsive property of PAA segment of the copolymer, the effective membrane pore sizes for trans-membrane permeation would vary according to the change of pH value of the environmental medium. Similarly, PVCL segment of copolymer would change their conformation from coil to globule and vice-versa as the temperature of the surrounding medium decreases or increases across its LCST. Thus due to thermo responsive property of

PVCL segment of the copolymer, the effective membrane pore sizes for trans-membrane permeation would vary according to the change in the environmental temperature.

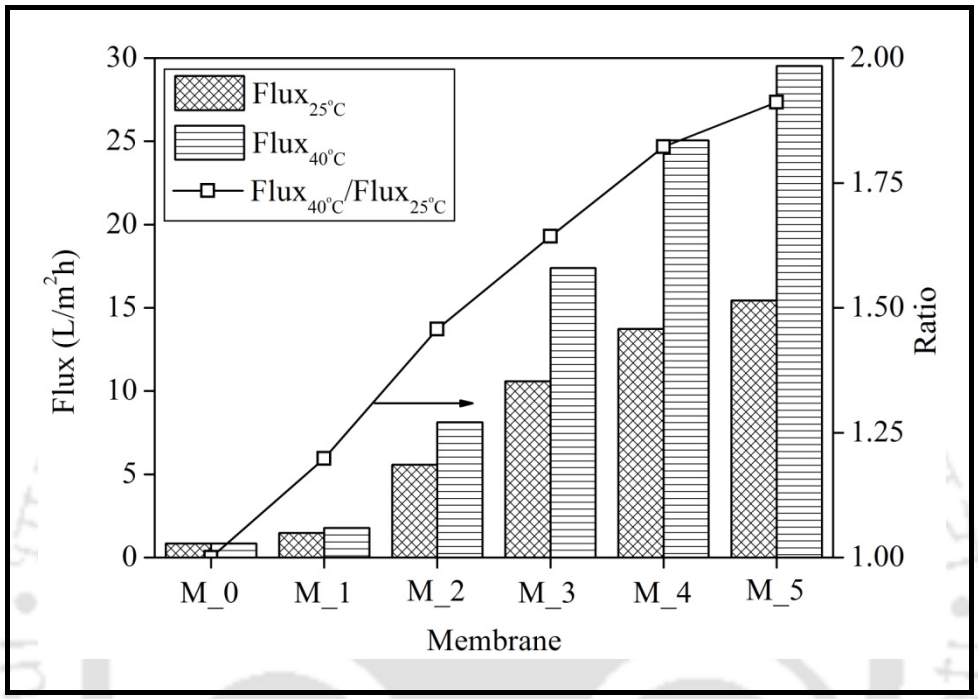


**Figure 5.7b: Effect of wt. % of poly (VCL-co-AA) on flux ratio between temperature 25˚C and 40℃.**

## 5.3.5. Performance study of the membrane

Apart from transmembrane pressure, the rejection and flux characteristics of the membranes strongly depend on the structure of the membrane as well as the properties of the feed solution like pH. So, the prepared UF membranes were also characterized by estimating the rejection and flux during permeation experiment using BSA solution. To investigate the fouling behaviour, membranes were cleaned after BSA solution ultrafiltration, and the PWF of the cleaned membranes was measured. It was noticed that the PWF ($J_{w1}$) before UF of the BSA solution changes marginally, but it decreased drastically at the initial operation of BSA

solution ultrafiltration (Figure 5.8). It happened due to the deposition or adsorption of protein molecules on membrane surface at the initial BSA ultrafiltration operation [118, 120, 121]. After some time of operation it reached equilibrium, so that a relatively steady flux ($J_p$) was obtained in the final operation of BSA ultrafiltration. After 1 hr of ultrafiltration, the membrane was cleaned with DI water and water flux was measured ($J_{w2}$). The ratio of $J_{w1}$ and $J_{w2}$ was used to find the $Flux_{RR}$, which is shown in Figure 5.9. It was found that $Flux_{RR}$ increases from 33.33 % to 93.5 %, when wt % of copolymer increased from 0 to 2.5. This increase in $Flux_{RR}$ can be defined by fouling behaviour of membranes.

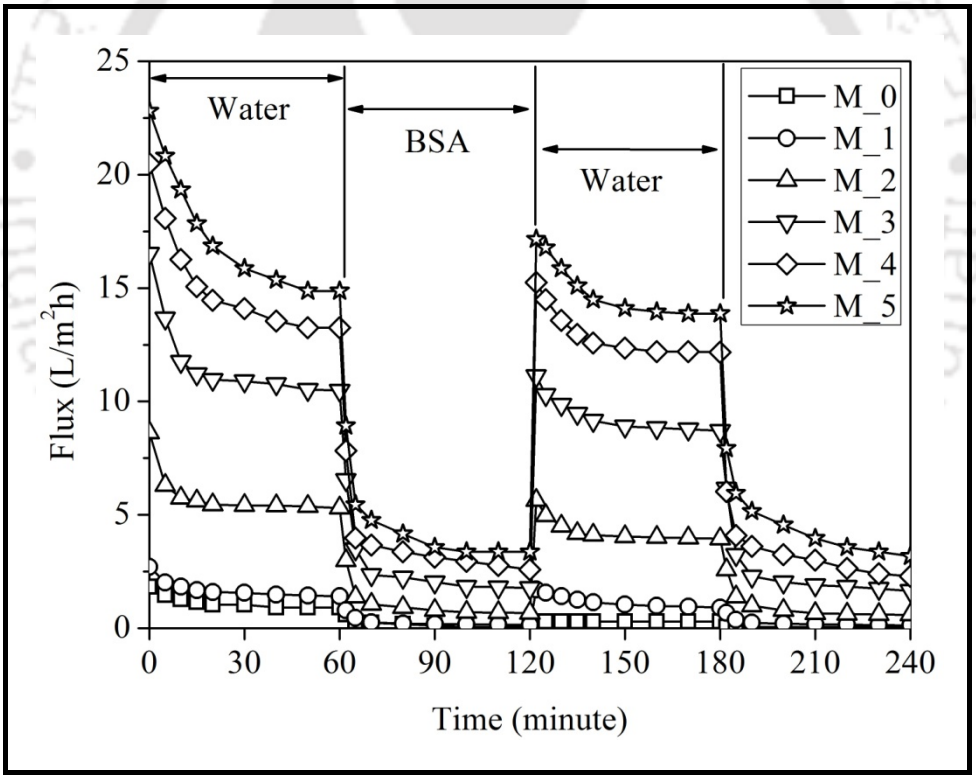


**Figure 5.8: Effect of wt. % of poly (VCL-co-AA) on time dependent flux.**

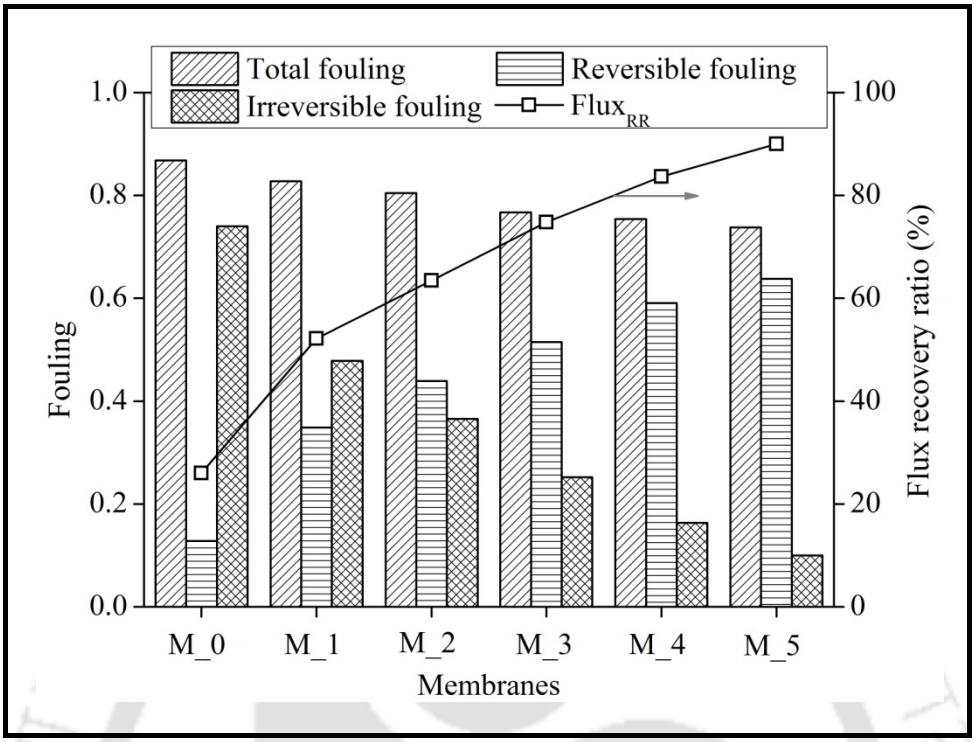


**Figure 5.9: Effect of wt. % of poly (VCL-co-AA) on different fouling parameters.**

There are two types of membrane fouling, reversible and irreversible. Reversible deposition and adsorption of protein causes reversible fouling, which can be removed by hydraulic cleaning. Whereas, irreversible protein adsorption causes irreversible fouling that can only be eliminated by chemical cleaning or enzymatic degradation [127]. To find out these fouling values, pH = 7 was used during the experiments. The summarizing of total fouling ($F_t$), reversible fouling ($F_r$) and irreversible fouling ($F_{ir}$) as a function of wt % of poly (VCL-co-AA) is shown in Figure 5.9. It was observed that $F_t$ decreases from 0.93 to 0.77 with increase in wt % from 0 to 2.5. The lower value of $F_t$ indicates lower total flux loss, resulting in less protein adsorption or deposition on the membrane surface [84, 125, 127]. From Figure 5.9 it may also be seen that the membrane containing higher wt % of copolymer has lower value of $F_{ir}$. This is due to the fact that the membrane containing higher wt % of copolymer has lower value of persistent protein adsorption on the membrane and

initial water flux could be recovered by a simple cleaning method using DI water. Another important reason is the IEC of the modified membrane (shown in Table 5.2), which is due to the presence of PAA in the membrane. BSA molecules are negatively charged at pH 7, as well as the membrane surface is negatively charged due to the presence of −COOH groups. This results in strong repulsion of BSA molecules from the membrane surface, which leads to lower protein adsorption to the membrane surfaces. These results signified that the introduction of the carboxylic acid groups capable of reducing total membrane fouling, particularly irreversible membrane fouling.

### 5.3.6. Effect of pH on transport property of BSA solution

Figure 5.10 shows the effect of wt% of poly (VCL-co-AA) copolymer on BSA flux and rejection. As the copolymer content increases, average BSA flux increases due to increase in hydrophilicity of the membrane because of hydrophilic functional group. There is slight decline of rejection also, despite the fact that BSA flux is much higher for modified membranes. Figure 5.11 shows the effect of pH on BSA rejection for different membranes. It was observed from the figure that rejection variation with change in pH of BSA solution shows a noticeable difference between the modified membranes and unmodified membrane. For unmodified membrane M_0, BSA rejection was almost same for all pH values, but for modified membranes, BSA rejection decreases with decrease in pH of BSA solution. Furthermore, with increase in wt % of poly (VCL-co-AA), drop in BSA rejection with pH also increases. For example, BSA rejection for membrane M_1 at pH 11, 7 and 2 are 90.2 %, 87.8 % and 86.9 % respectively, while those values for membrane M_5 are 91.5 %, 76.5 % and 29.5 % respectively. From Figure 5.11, it can also be observed that difference in rejection

at pH 7 and 11 is not much large for different modified membranes, but at pH 2 that difference is much larger with increase in wt % of poly (VCL-co-AA).

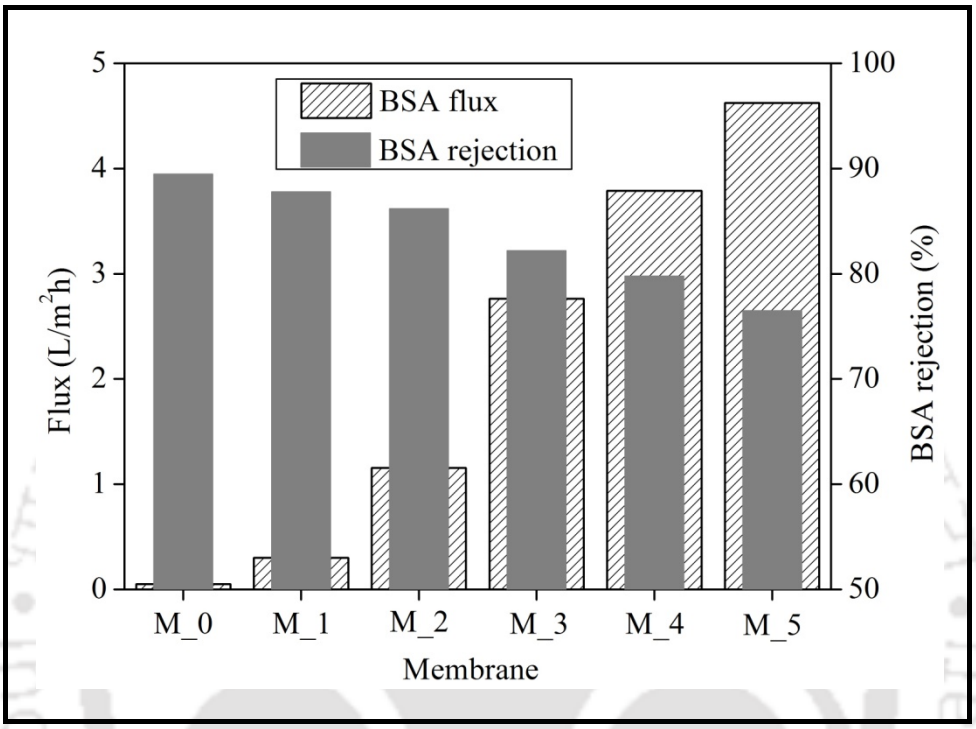


**Figure 5.10: Effect of wt. % of poly (VCL-co-AA) on BSA flux and rejection.**

Rejection performance of pH-responsive membrane is combined effort of pore size and electrostatic interaction. Change in pH can lead to conformational change of poly (VCL-co-AA) copolymer and that result in change in pore size of the membrane, as discussed earlier. Thus, due to the swelling of poly (VCL-co-AA) in skin layer of modified membranes at pH 11, pores of the modified membranes become smaller, which results in higher BSA rejection. Further, when the pH of BSA solution decreases to 2, membrane pore size become larger due to collapse of poly (VCL-co-AA) copolymer and thus results in lower rejection of BSA.

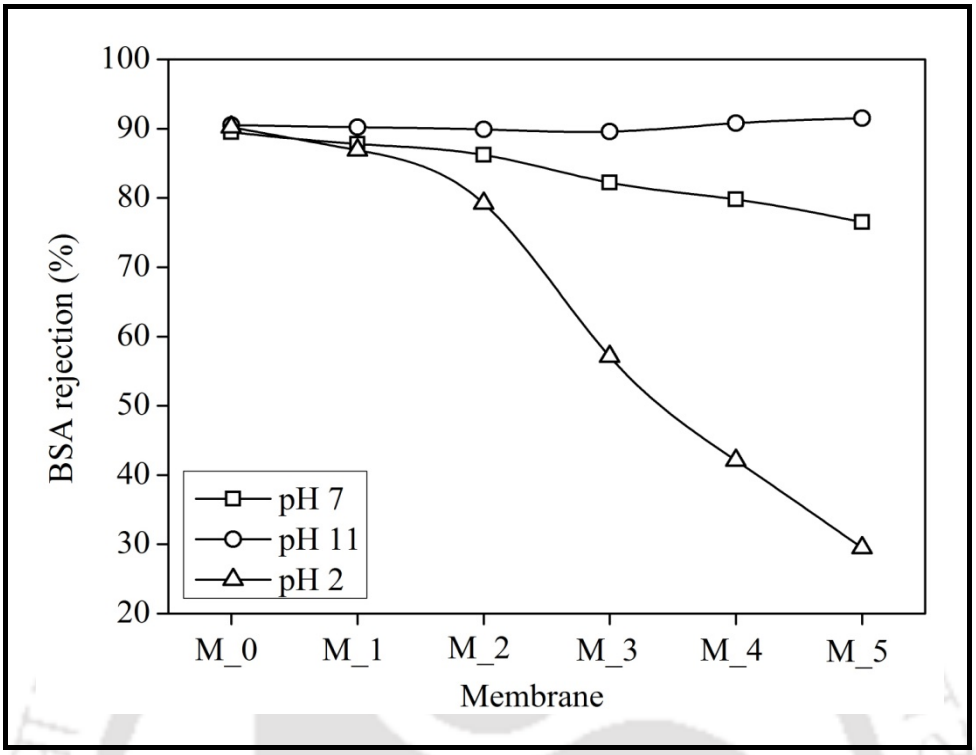


**Figure 5.11: Effect of wt. % of poly (VCL-co-AA) on pH dependent BSA rejection.**

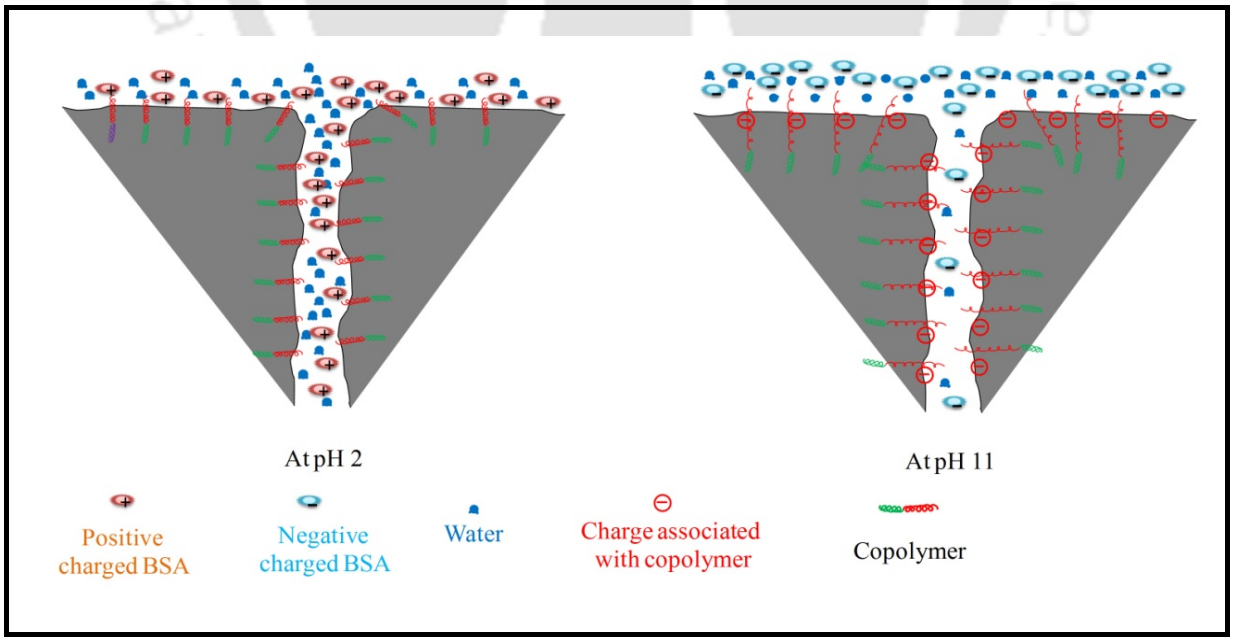


**Figure 5.12: Schematic presentation for the mechanism of pH responsive phenomenon of membranes for BSA rejection.**

The second factor that affects the rejection is the electrostatic interaction between solute molecule and poly (VCL-co-AA) copolymer present in the membrane. As we know, BSA molecules isoelectric point is around pH 4.7. At this pH, BSA molecules contain no net charge, whereas, above pH 4.7 BSA molecules have net negative charge and below pH 4.7 BSA molecules have net positive charge [69]. So, at pH 11 BSA molecules have negative charge and poly (VCL-co-AA) copolymers molecules are also negatively charged due to complete deprotonation of −COOH group. Thus, the electrostatic repulsion between negatively charged BSA molecules and deprotonated poly (VCL-co-AA) copolymer present in the membrane makes the permeation of BSA molecules very difficult, which results in higher rejection. At pH 11, all the membranes have rejection around 90 %, in fact membranes M_4 and M_5 have slightly higher rejection. At pH 7 the electrostatic repulsion is less compare to pH 11 and also pores are larger, so rejection values are lower than pH 11. Further, at pH 2 only BSA molecules have positive charge and membranes contain no net charge. Also the pores are comparatively much larger due to the collapse of PAA component of the copolymer, which results in very low rejection of BSA. This, phenomena is schematically shown in Figure 5.12.

# Chapter 6

## Preparation and characterization of novel pegylated hydrophilic pH responsive polysulfone ultrafiltration membrane

# Chapter 6
# Preparation and characterization of novel pegylated hydrophilic pH responsive polysulfone ultrafiltration membrane

*In this chapter, novel cross linked pegylated functional copolymer poly (acrylic acid-co-polyethylene glycol methyl ether methacrylate) was prepared from AA and PEGMA, via precipitation polymerization using toluene as solvent. The copolymer was directly blended with PSF using NMP as solvent. Prepared copolymers were mixed in the casting solution at various wt % and membranes were prepared by phase inversion method. Presence of copolymer in blended membrane was confirmed by FTIR-ATR spectroscopy. Blended membranes showed enhanced pore density, pure water flux and hydrophilicity. The blended membranes also showed evidence of pH sensitivity compared to unmodified membrane. Finally, fouling resistance behaviour of modified membrane was studied by bovine serum albumin protein separation study.*

## 6.1. Experimental

### 6.1.1. Materials

Polysulfone (PSF), polyethylene glycol methyl ether methacrylate (PEGMA), N,N′-methylenebisacrylamide (MBAA), N- methylpyrrolidone (NMP), poltasium bromide (KBr), Azobisisobutyronitrile (AIBN) and Bovine serum albumin (BSA) were used for this chapter. Deionized water was used throughout the experiments. Detail of all the chemicals is given in Table 2.1 of chapter 2.

---

Content of this chapter is published as below:

M.K. Sinha, M.K. Purkait, Preparation and characterization of novel pegylated hydrophilic pH responsive polysulfone ultra filtration membrane, J. Membr. Sci. 464 (2014) 20–32.

## 6.1.2. Synthesis and characterization of poly (AA-co-PEGMA)

The poly (AA-co-PEGMA) copolymer was prepared by precipitation polymerization in toluene with AIBN as initiator. AA, PEGMA and cross-linker MBAA were dissolved in toluene. AIBN was introduced to the solution at 0.3 % of the total weight of the reactants. The mixture was taken in triple neck round bottom flask with a condenser, nitrogen inlet and outlet, allowed to react in an oil bath in boiling condition. The initially homogeneous reaction mixture became opalescent and then deepened in colour as a milky white dispersion after boiling for 15 min. The reaction was carried for another 2 h. After reaction, the product was cooled down to room temperature and vacuum filtered. The obtained product was dried completely at 50˚ C for 4 days. Copolymer was prepared in three different weight ratios of AA, PEGMA and MBAAm (viz 45:45:10, 30:60:10 and 60:30:10) and named as $C_1$, $C_2$ and $C_3$ respectively (shown in Table 6.1). Fourier transform infrared (FTIR) analysis was carried out to confirm the chemical groups of the synthesized copolymer. The process and instrument details are provided in section 2.4 of chapter 1.

**Table 6.1: Composition of different poly (AA-co-PEGMA) copolymers.**

| Copolymer | PEGMA (wt %) | AA (wt %) | MBAA (wt %) |
|---|---|---|---|
| **$C_1$** | 45 | 45 | 10 |
| **$C_2$** | 60 | 30 | 10 |
| **$C_3$** | 30 | 60 | 10 |

### 6.1.3. Preparation of flat sheet blended membranes

Flat sheet membranes were prepared by phase inversion method using different composition of poly (AA-co-PEGMA) (as shown in Table 6.2). Membranes were named as $M_{XY}$, where X represents copolymer and Y represents wt % of the copolymer in casting solution. The casting solution was stirred for 24 h with the help of magnetic stirrer at 50˚C and further kept 6 h for degassing at 50˚C temperature. The solution was then cast on a clean glass plate with a casting knife maintaining a uniform thickness of 200 µm, in the ambient atmosphere. Detail membrane preparation process is provided in section 2.2 of chapter 2. Viscosities of membrane casting solutions were also measured at a constant shear rate of 50 $s^{-1}$.

**Table 6.2: Composition and viscosity of casting solution of different membranes containing poly (VCL-co-AA).**

| Membranes | PSF (wt %) | PEG 4000 (wt %) | Copolymer (wt %) | | | NMP (wt %) | Viscosity (Pa s) |
|---|---|---|---|---|---|---|---|
| | | | $C_1$ | $C_2$ | $C_3$ | | |
| $M_{10}$ | 12 | 5 | 0 | – | – | 83 | 0.05884 |
| $M_{11}$ | 12 | 5 | 1 | – | – | 82 | 0.07753 |
| $M_{13}$ | 12 | 5 | 3 | – | – | 80 | 0.13028 |
| $M_{15}$ | 12 | 5 | 5 | – | – | 78 | 0.24882 |
| $M_{17}$ | 12 | 5 | 7 | – | – | 76 | 0.41141 |
| $M_{25}$ | 12 | 5 | – | 5 | – | 78 | 0.24642 |
| $M_{35}$ | 12 | 5 | – | – | 5 | 78 | 0.25065 |

## 6.2. Characterization of blended membranes

### 6.2.1. Surface Characterization of poly (AA-co-PEGMA) Blended Membranes

The presence of the copolymer in blended membranes was confirmed by comparing IR spectra of plain PSF membrane and blended PSF membrane. Microscopic observation of plain and blended membranes was done by field emission scanning electron microscope (FESEM) and scanning electron microscope (SEM). Top surface images required higher magnification, so these images were taken by FESEM. The static contact angle between water and membrane surface is the measure of hydrophilicity or hydrophobicity of the membrane. For all the membranes, 4 angles had been measured in different places and average was taken. Details of membrane characterization techniques are listed in section 2.3 of chapter 2.

### 6.2.2. Liquid-liquid displacement porosimetry (LLDP) method

LLDP method was used to find out the number of pores, average pore size and pore size distribution of the fabricated membranes [8]. This method is based on the assumption that all the pores are cylindrical and thickness of the membrane layer is uniform. So, the absolute values of different parameter and their distribution are likely to be associated with an error. In present work average thickness of skin layer was taken equal to 0.1 μm. Further details of LLDP method is provided in section 2.3.2 of chapter 2.

### 6.2.3. Pure water permeation experiment

Prepared membranes were compacted with deionized water for 4 h at a transmembrane pressure of 250 kPa and flux was measured at every 30 minute interval. The compaction

factor (CF) was calculated as the ratio of initial pure water flux to steady state pure water flux. Pure water flux (PWF) was determined by allowing deionized water to pass through the compacted membrane. PWF was measured by the equation 2.9. Flux values of pure water at different transmembrane pressures were measured under steady state condition. Permeability ($P_m$) (L/m$^2$h kPa) was evaluated from the slope of the plot of $J_w$ vs $P$. Hydraulic permeability was calculated by equation 2.10.

### 6.2.4. Ion exchange capacity (IEC) of membranes

The ion exchange capacity (IEC) of membranes was determined by using standard titration method [114]. The IEC value was calculated using the equation 2.15.

### 6.2.5. pH-responsive permeability experiment

Hydraulic permeability of blended membranes in acidic, basic and neutral condition was measured at different transmembrane pressure as mentioned in the previous section. For acidic and basic condition pH were maintained at 2 and 11 using 0.1 M HCl and 0.1 M NaOH solution respectively. For neutral condition DI water was used. The variation in water flux of membranes with pH change was also measured. Each membrane was initially compacted with DI water for 30 min at 250 kPa, after that membrane was soaked in aqueous solution of different pH for 10 min. Then, permeated solution was collected over 10 min after 15 min equilibration by the feed flow at the given pH. The flux was measured by using equation 2.9. After cleaning the system with DI water, membrane permeability was re-evaluated with DI water.

### 6.2.6. Ultrafiltration Experiment

Ultrafiltration experiment was conducted to study the solute separation, permeate flux and fouling behaviour of the prepared membranes. BSA was dissolved in DI water and the concentration and pH were kept constant at 1000 $mgL^{-1}$ and 7 respectively for all the experiments. Each membrane was initially compacted for 30 min at 250 kPa, then the pressure was reduced to 100 kPa and the water flux ($J_{w1}$) was measured for 1 h duration. After water permeation, cell was refilled with BSA solution and flux was measured ($J_p$). The BSA rejection ratio was calculated by the equation 2.16.

After 1 h of ultrafiltration and later hydraulic cleaning of the membrane, water flux was measured ($J_{w2}$). With the help of $J_{w1}$ and $J_{w2}$, flux recovery ratio ($Flux_{RR}$) was measured. Fouling of membrane causes flux loss $(J_{w1}\text{-}J_p)$ and the flux loss caused by total fouling ($F_t$), reversible fouling ($F_r$) and irreversible fouling ($F_{ir}$) are calculated by equations 2.17, 2.18 and 2.19 respectively.

## 6.3. Results and discussion

### 6.3.1. FTIR spectroscopy analysis of poly (AA-co-PEGMA) copolymer and blended membranes

Figure 6.1a shows the FTIR spectra of different poly (AA-co-PEGMA) copolymers. As shown in Figure 6.1a, peaks at 1110 $cm^{-1}$ and 1529 $cm^{-1}$ are characteristic peaks of ether and secondary amide groups present in PEGMA and cross-linker MBAAm respectively. The peak at 1730 $cm^{-1}$ is characteristic peak of –COOH group present in AA, which is the confirmation of presence of AA. Another peak at 2900 $cm^{-1}$ is due to C–H stretching in copolymer. Furthermore, it was found that with increase in feed ratio of PEGMA and AA, intensity of

peak at 1110 $cm^{-1}$ and 1730 $cm^{-1}$ increased respectively and it is highest for $C_2$ in the case of PEGMA and $C_3$ in the case of AA.

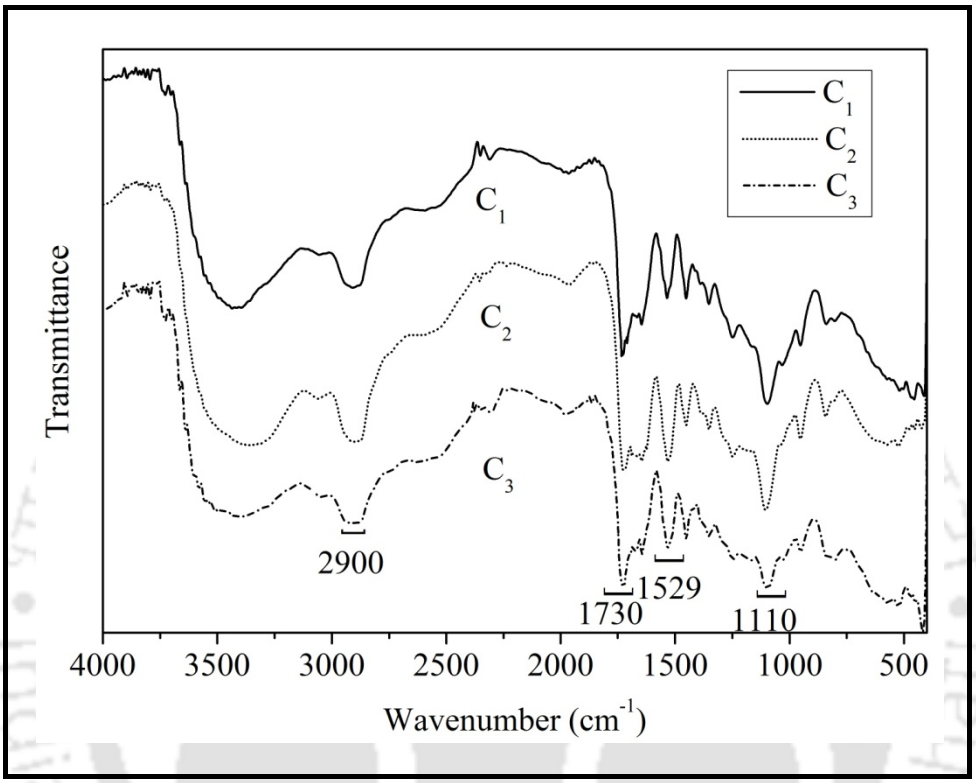


**Figure 6.1a: FTIR spectra of poly (AA-co-PEGMA) copolymers.**

Figure 6.1b shows ATR-FTIR spectra of plain and blended PSF membranes fabricated with different wt % of $C_1$ copolymer. One can see new peaks at around 1110 $cm^{-1}$ and 1529 $cm^{-1}$, which are for ether and amide group. Another new peak appears around 1730 $cm^{-1}$, confirms the presence of –COOH group. These peaks authenticate the presence of poly (AA-co-PEGMA) in the blended membrane. Also the intensity of these peaks varies with the wt % of copolymer in modified membranes. The peaks at 1155 $cm^{-1}$ and 1295 $cm^{-1}$ are due to –C–O–C– and S=O group present in polysulfone, thereby confirming the presence of polysulfone.

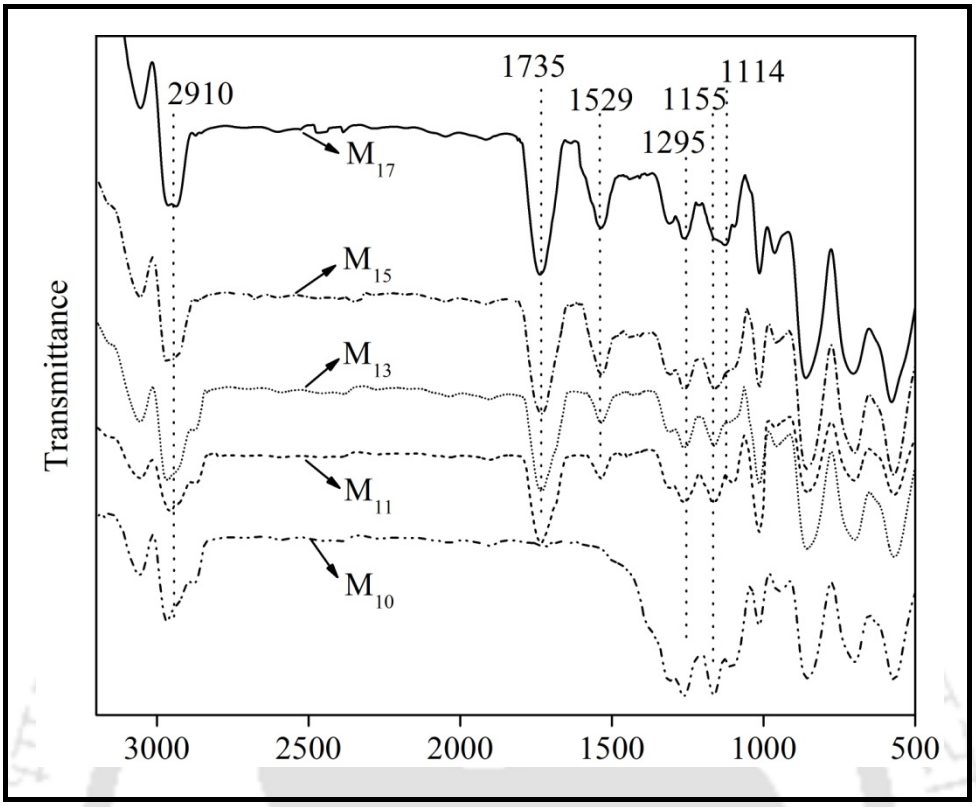


**Figure 6.1b: ATR-FTIR spectra of PSF and poly (AA-co-PEGMA) blended membranes.**

## 6.3.2. Morphological study

Figure 6.2a shows the cross sectional SEM images of various blended membranes with different wt % of $C_1$ copolymer prepared in this chapter. From the Figure it is clear that, all the membranes exhibit asymmetric structure in cross section. All the membranes have dense top skin layer, porous sub layer and sponge like bottom layer. The porous sub-layer consists of finger like structure. These structures formed due to the high mutual affinity of NMP for water, which results instantaneous demixing [1]. However, as the wt % of poly (AA-co-PEGMA) copolymer increased in membrane casting solution, those fingers like structure became shorter and larger voids formed in the sublayer, because poly (AA-co-PEGMA) increased the viscosity of membrane casting solution (shown in Table 6.1), which resulted in

more rapid demixing between polymer rich solvent phase and non-solvent phase during phase inversion [138]. Further, last SEM image of Figure 6.2a shows the cross sectional view of membrane $M_{13}$ after permeation experiment. It may be seen from the figure that permeation did not affect the cross sectional morphology of the membrane.

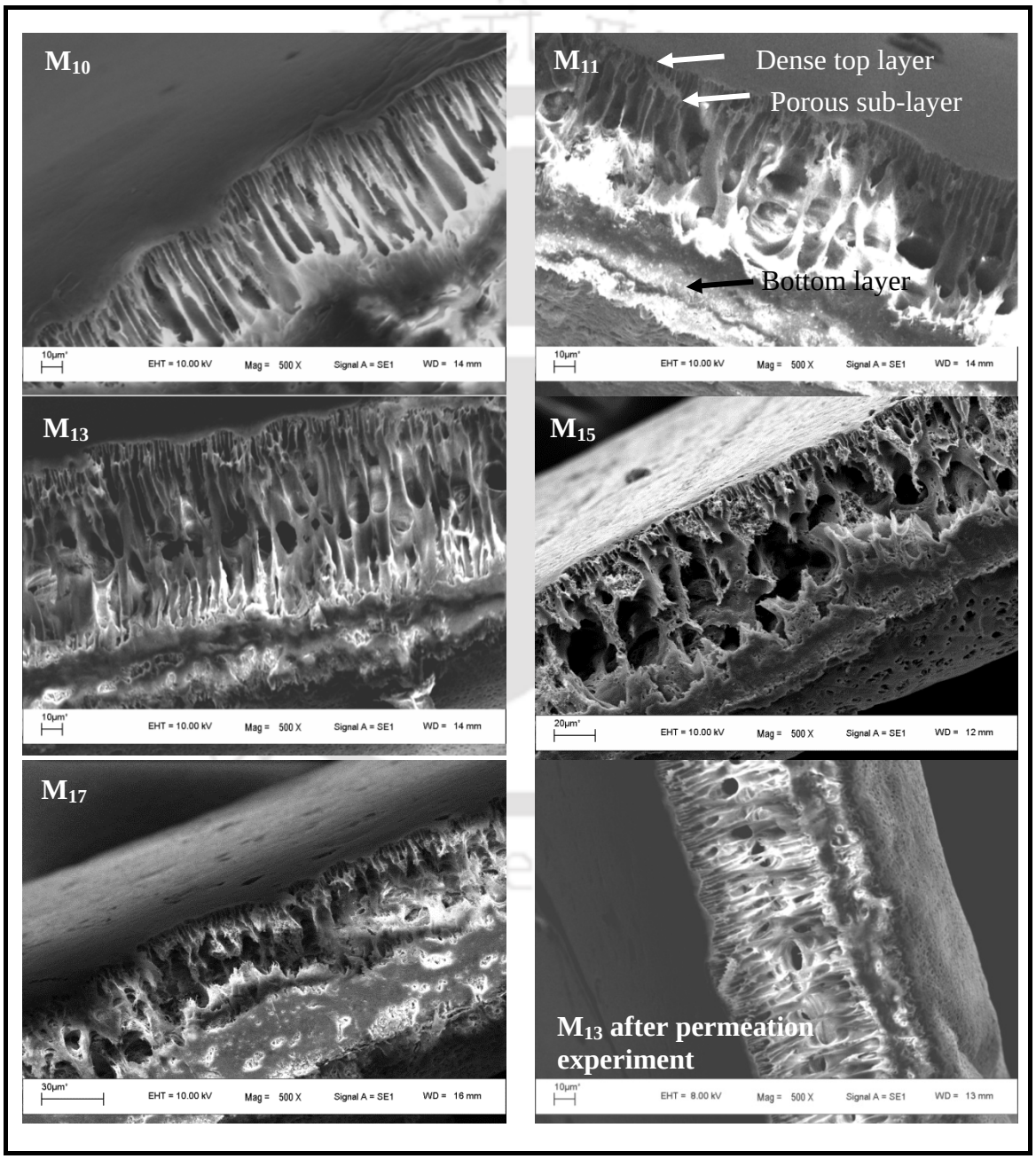


**Figure 6.2a: Effect of wt% of poly (AA-co-PEGMA) on cross section of membranes.**

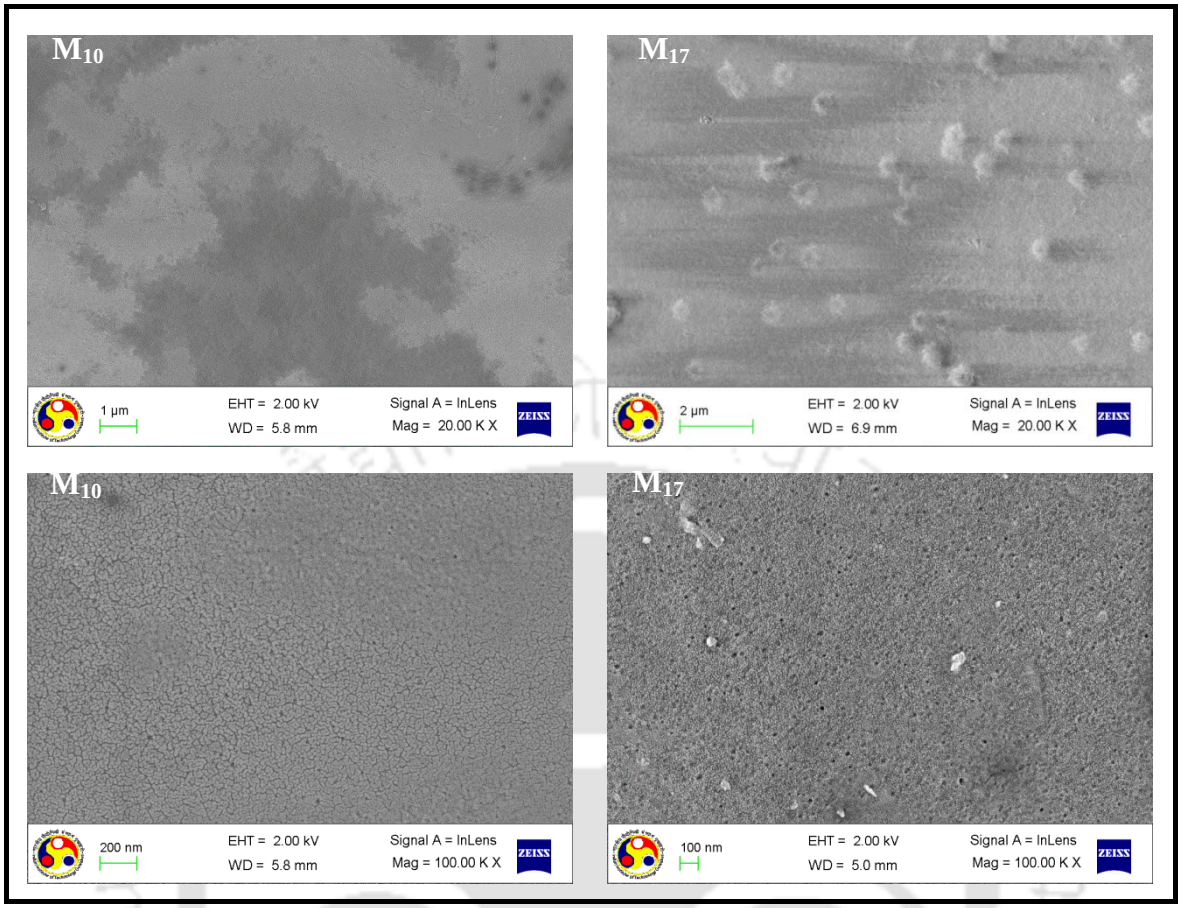


**Figure 6.2b: Effect of wt% of poly (AA-co-PEGMA) on top surface of membranes.**

Figure 6.2b shows the FESEM images of top surface of the plain and blended PSF membranes with 7 wt % of copolymer at different magnification. At lower magnification, it can be observed that top surface of the blended membrane has comparatively rougher surface with respect to plain PSF membrane. This roughness is due to the settlement of copolymer on the membrane surface. At higher magnification, it can be seen that blended membrane has higher pore density. The reason is presence of additive into casting solution increases the viscosity of blended casting solution (shown in Table 6.2) which, causes increase in the ratio of nonsolvent inflow to solvent outflow according to theory suggested by Young and Chen [128]. This in turn, increases the pore density of the modified membrane.

### 6.3.3. LLDP studies

LLDP study helps us to estimate transmembrane pore of the membranes in wet state i.e. similar to the condition of ultrafiltration operation. Pore size, pore density, total pore area per unit membrane area, total number of pores and mean pore size of all the membranes were determined by equations 2.1, 2.4, 2.6, 2.7 and 2.8 respectively. Figure 6.3a shows the LLDP flux profile of membranes prepared with different wt % of copolymer. From that data and by use of equation 2.4, pore number per unit area of membrane were calculated, which is also shown in Figure 6.3b. For all the membranes, nature of LLDP flux is almost same. To start the flow, minimum pressure is required (in this case that value is 32 kPa) and after that penetrating liquid (alcohol rich) starts to replace the wetting liquid (water rich) in biggest pores. Therefore, as the pressure is increased in the system, smaller pores start to open and once all the pores in the membrane are opened by replacing the wetting liquid in the pores, the flux increases marginally (Figure 6.3). From the Figure 6.3a it may be seen that initially flux increases slowly with increase in pressure. However, from 300 kPa to 400 kPa flux increased rapidly and thereafter flux increasingly slowed down. Similar type of trend in pore size distribution plot may also be seen in the Figure 6.3b. Number of pores greater than the size of 4 nm is almost negligible. It may also be seen that the number of pores starts to increase as size of pores decreased from 4 nm to 2 nm. Contrary to this trend, number of pores decrease when pore size decrease from 2 nm.

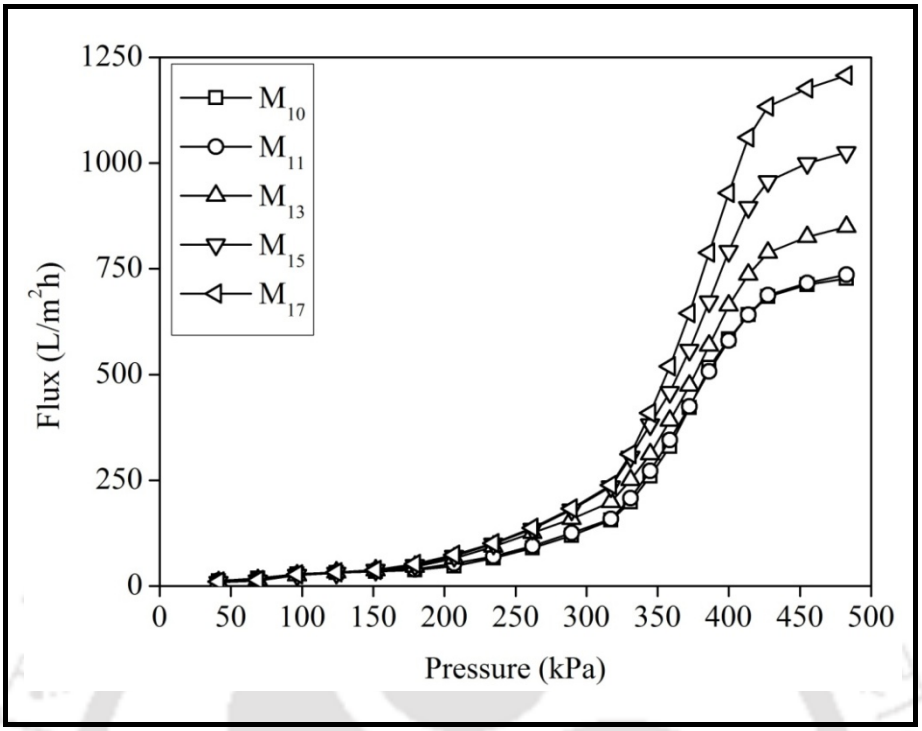


**Figure 6.3a: Effect of wt. % of poly (AA-co-PEGMA) on LLDP flux profile.**

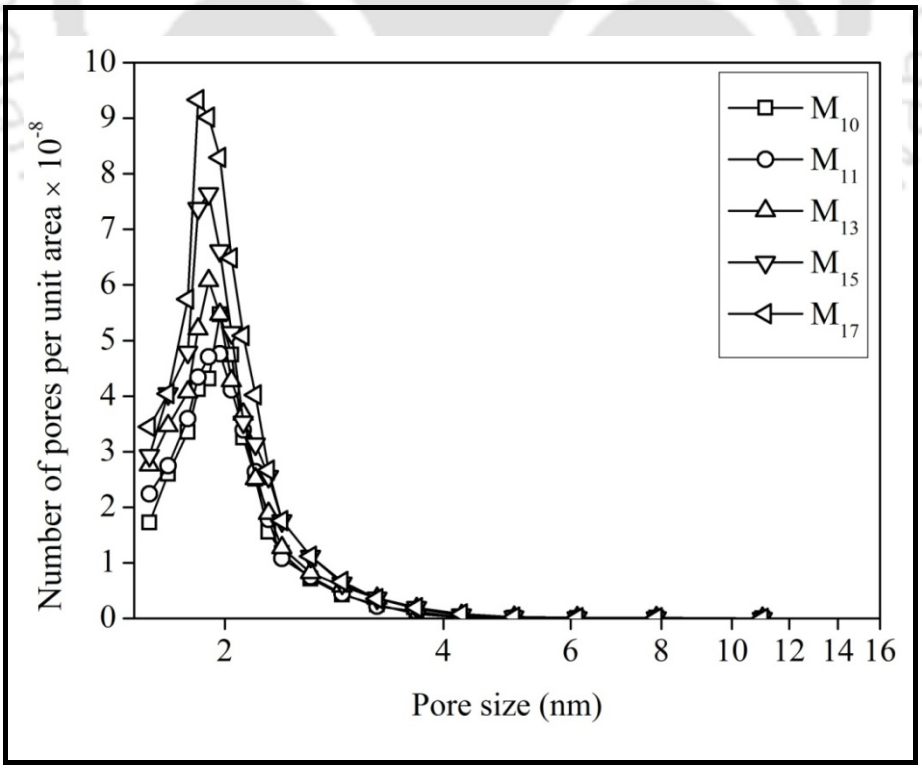


**Figure 6.3b: Effect of wt. % of poly (AA-co-PEGMA) on number of pores per unit area.**

Figure 6.4 shows the pore size distribution in percentage. It is almost same for all the membranes. In all the membranes, size of 95 % of total pores are less than 3 nm (Figure 6.4b), it means that prepared membranes are suitable for ultrafiltration purpose. Table 6.3 reports the results of LLDP study. It is seen that, with increase in wt % of copolymer, total pore number per unit area ($N_t$) also increases resulting more porous membranes. The total number of pores for modified membrane ($M_{17}$) is $6.23\times10^9$ and for unmodified membrane is $3.63\times10^9$. These results indicate that copolymer content in membrane casting solution enhances the pore forming process, which is discussed in previous section. Also, these results are in line with morphological study of the membranes.

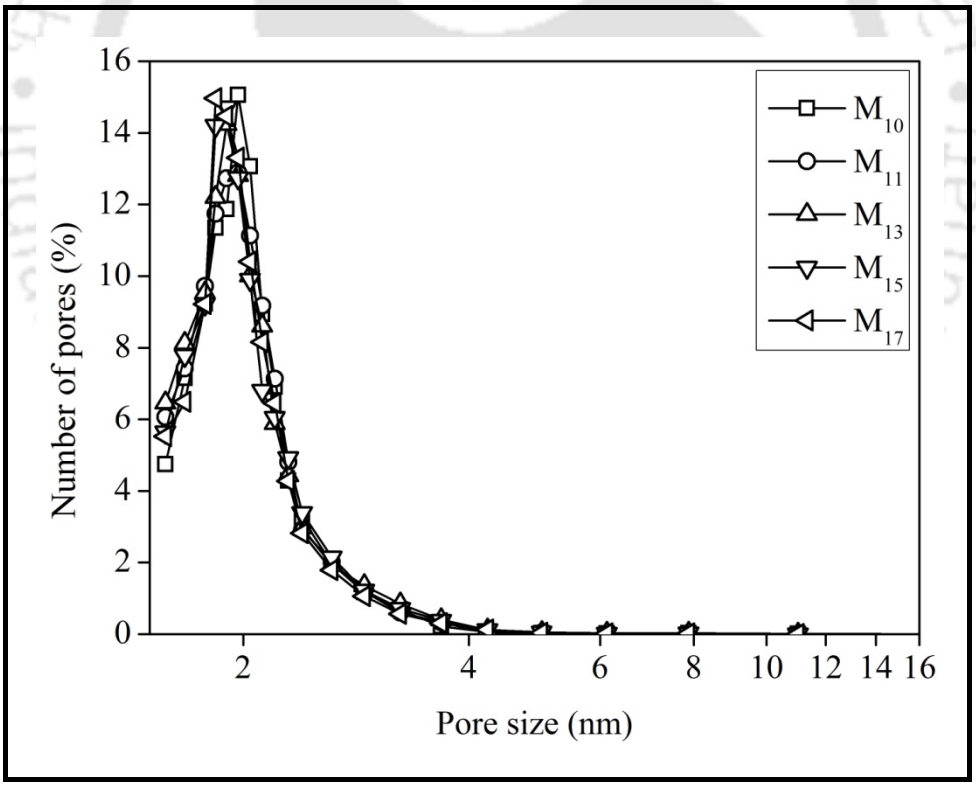


**Figure 6.4a: Effect of wt. % of poly (AA-co-PEGMA) on Pore size distribution.**

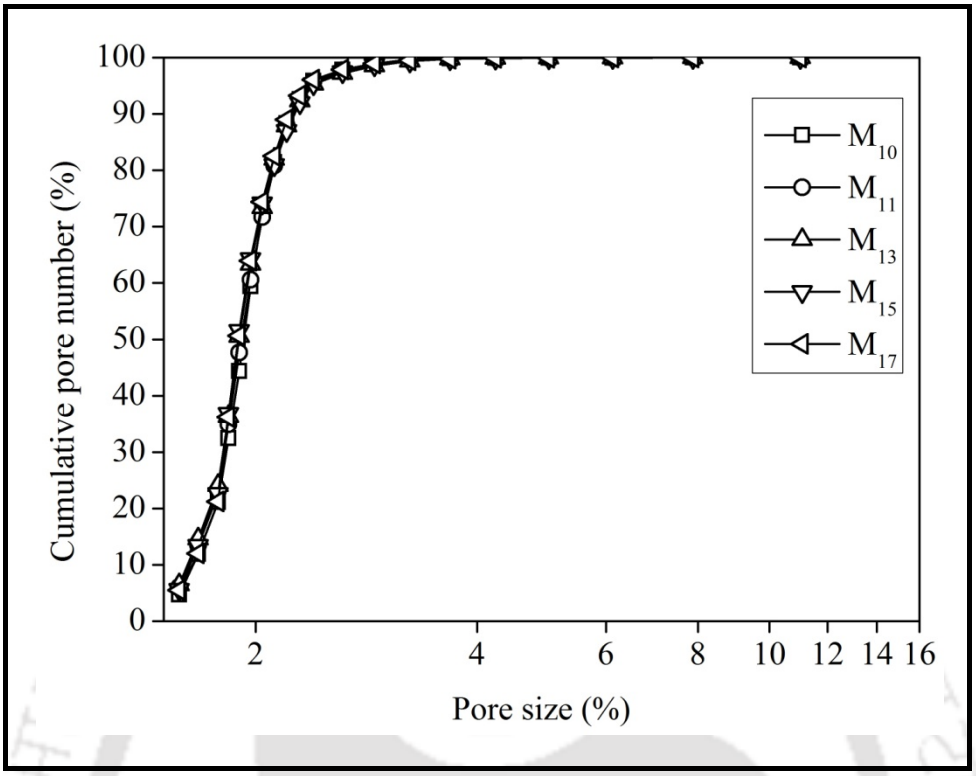


**Figure 6.4b: Effect of wt. % of poly (AA-co-PEGMA) on cumulative pore number variation.**

## 6.3.4. Hydrophilicity and pure water permeation studies

Hydrophilicity of the membranes is described by water contact angle measurement. Lower the contact angle (CA) higher will be the hydrophilicity of the membranes. It is an important parameter in membrane permeation and separation process and also related to membrane's fouling behaviour because more hydrophilic membranes are less prone towards fouling. CA for all the membranes are shown in Table 6.3, for unmodified membrane CA is 63.2˚ and for membrane ($M_{17}$) with highest copolymer content it decreased considerably to 48.7˚. These results indicate that poly (AA-co-PEGMA) enhances the hydrophilicity of the membrane. In case of different copolymer, membrane $M_{25}$ has the lowest CA of 46.5˚. It is due the highest PEGMA content in copolymer $C_2$. The increased hydrophilicity of membrane could result in higher water flux.

**Table 6.3: Value of some characterization parameters of membranes prepared with poly (VCL-co-AA).**

| Membrane | $N_t$ ($m^{-2}$) × $10^{-9}$ | $A_t$ ($m^2$) × $10^8$ | $r_m$ (nm) | WCA (°) | CF | $P_m$ ($L/m^2$ h kPa ) | IEC (mmol/g) |
|---|---|---|---|---|---|---|---|
| $M_{10}$ | 3.63 | 4.66 | 1.99 | 63.2±2 | 10.93 | 0.353 | – |
| $M_{11}$ | 3.69 | 4.72 | 1.99 | 61.5±1.5 | 10.89 | 0.357 | 0.09 |
| $M_{13}$ | 4.26 | 5.44 | 1.98 | 55.6±2 | 10.02 | 0.384 | 0.14 |
| $M_{15}$ | 5.19 | 6.62 | 1.98 | 50.4±1 | 8.75 | 0.473 | 0.18 |
| $M_{17}$ | 6.23 | 7.87 | 1.98 | 48.7±1.5 | 8.36 | 0.572 | 0.22 |
| $M_{25}$ | – | – | – | 46.5±2 | – | 0.494 | 0.15 |
| $M_{35}$ | – | – | – | 53±1 | – | 0.437 | 0.21 |

Figure 6.5 shows the compaction profile during time dependent flux of all the membranes. The initial sharp decline in flux for all the membranes can be observed due to compaction. This was due to the fact that with application of pressure wall of the pores become denser, closer and uniform resulting partial blocking of the pores and decline in the flux. However after around 1 h flux became steady for all the membranes and it remains almost constant thereafter. It is observed that with the increase in copolymer content final flux also increases and for any composition of copolymer in the membrane, the steady state flux remains higher than unmodified membrane. For unmodified membrane $M_{10}$ and modified $M_{17}$ the steady state flux values are 85.8 and 140.5 $L/m^2h$ respectively, which is much higher and due to higher pore density of the modified membranes (as shown in Figure 6.2b and 6.3b).

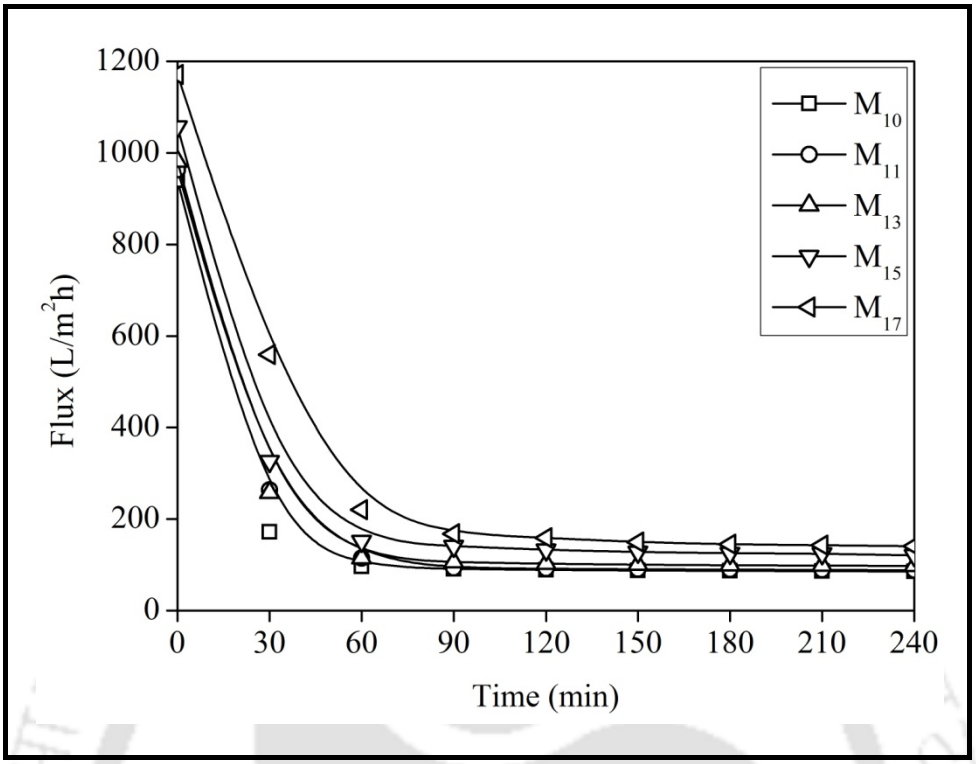


**Figure 6.5: Effect of wt. % of poly (AA-co-PEGMA) on flux profile during compaction.**

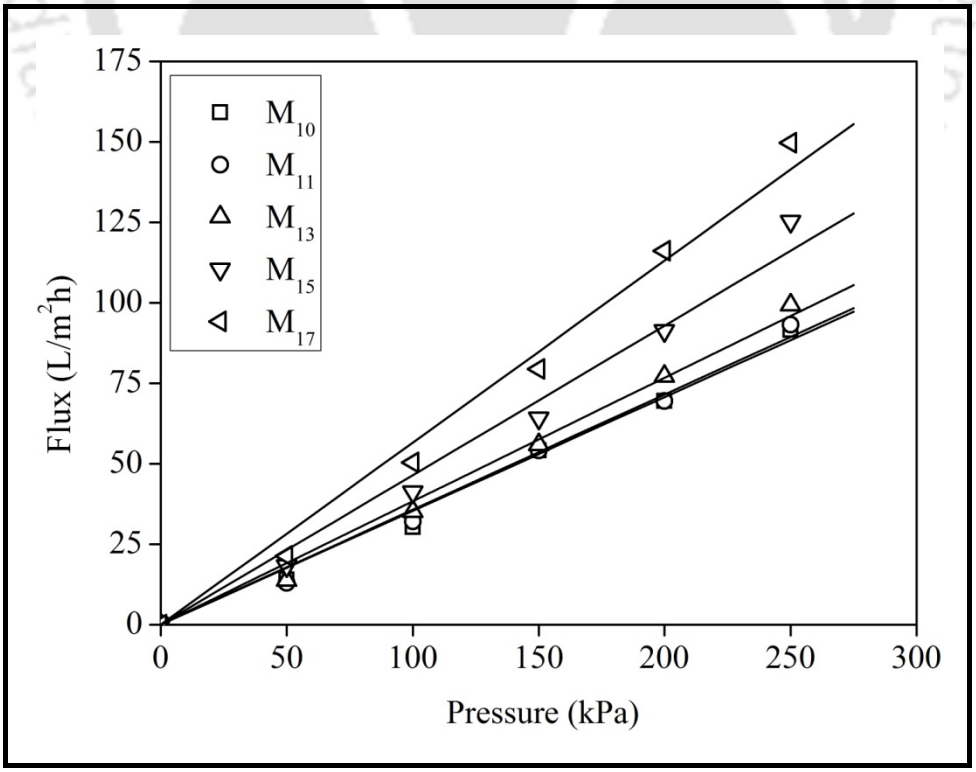


**Figure 6.6: Effect of wt. % of poly (AA-co-PEGMA) on flux at different transmembrane pressure.**

Figure 6.6 shows the effect of wt % of copolymer on PWF of the membrane at different transmembrane pressure. This experiment was done at different transmembrane pressure between 0-250 kPa at a difference of 50 kPa. For all the cases PWF increases almost linearly with increase in pressure. It is seen that with increase in wt % of copolymer PWF also increases, for example at 100 kPa PWF for membranes $M_{10}$, $M_{11}$, $M_{13}$, $M_{15}$ and $M_{17}$ are 30.3, 32.1, 35.2, 41.2 and 50.5 L/m$^2$h, respectively. These results are in agreement with the findings of compaction studies and also with the water contact angle measurements. These pressure dependent flux profiles were also used to calculate the hydraulic permeability ($P_m$) of the membranes. It was found that with the increase in copolymer content $P_m$ was also increased and it increased from 0.353 to 0.794 L/m$^2$ h kPa (Table 6.3) for unmodified membrane to modified membrane with highest copolymer content. Findings of the pure water permeability study clearly indicates that addition of copolymer poly (AA-co-PEGMA) enhances the pore forming activity in the membranes, which affect the permeability as it is conceptually related to membranes pore for ultrafiltration membranes [125]. These finding are uniform with morphological study, LLDP and hydrophilicity of the membranes.

### 6.3.5. Ion exchange and pH responsive studies

IEC gives the information about charge density in the membranes and it also affects their pH responsive behaviour and fouling behaviour by BSA protein. Table 6.3 shows the IEC of different membranes, membrane $M_{17}$ has the highest IEC value because it contained maximum amount of copolymer. Although, membranes with same amount of copolymer with different composition has different IEC. In this case membrane $M_{35}$ has the highest IEC because fraction of AA was highest during the synthesis of $C_3$ copolymer, which was later used for the modification of membrane $M_{35}$. pH dependent fluxes of different membranes are

shown in Figures 6.7a and 6.7b. Figure 6.7a shows the effect of wt % of copolymer on pH dependent flux. It may be seen from the figure that flux of unmodified membrane does not change with pH, but when copolymer was added to the membrane casting solution flux starts to increase with decrease in pH. Initially with decrease in pH, flux increases gradually however in between pH 6 and 4, there is an abrupt change in flux for all the modified membranes. So, membrane modified by poly (AA-co-PEGMA), showed visible pH sensitivity. Change in water flux was caused by the ionisation of PAA present in the copolymer, as pKa value of PAA is 4.4 – 4.9, which is in agreement with flux change reported in the literature [84, 85]. Change in water flux with pH can be explained by protonation and deprotonation capacity of PAA, as above its pKa (≈ 5) value carboxylic group of PAA deprotonated to carboxylate ions. These carboxylate ions provide high charge density in the copolymer, which results in expansion of copolymer and expansion of copolymer partially blocks the membrane pores. Again on further increment of pH, there is more loss of flux, which is due to the electro viscous effect. It is a physical phenomenon which ours when an electrolyte solution is passed through a narrow capillary or pore with charged surface [134]. In this case at pH above 7, permeating liquid and membrane both contains negative charge. So membrane repels the permeating liquid to pass through the membrane pores and as the pH increases more negative charge comes to the permeating liquid, which feel more repulsion from the membrane and results more loss of flux. It can be seen from the graph that with increase in copolymer contain in membrane, there is more change in flux with pH change for example flux of membranes $M_{11}$ and $M_{17}$ changed from 28.5 to 38.2 L/$m^2$h and from 38.5 to 75.5 L/$m^2$h respectively when pH changed from 11 to 2. These changes are attributed to the increasing amount of copolymer, which led to the higher electro viscous effect. And, it was also confirmed by IEC of the different membranes (shown in Table 6.3).

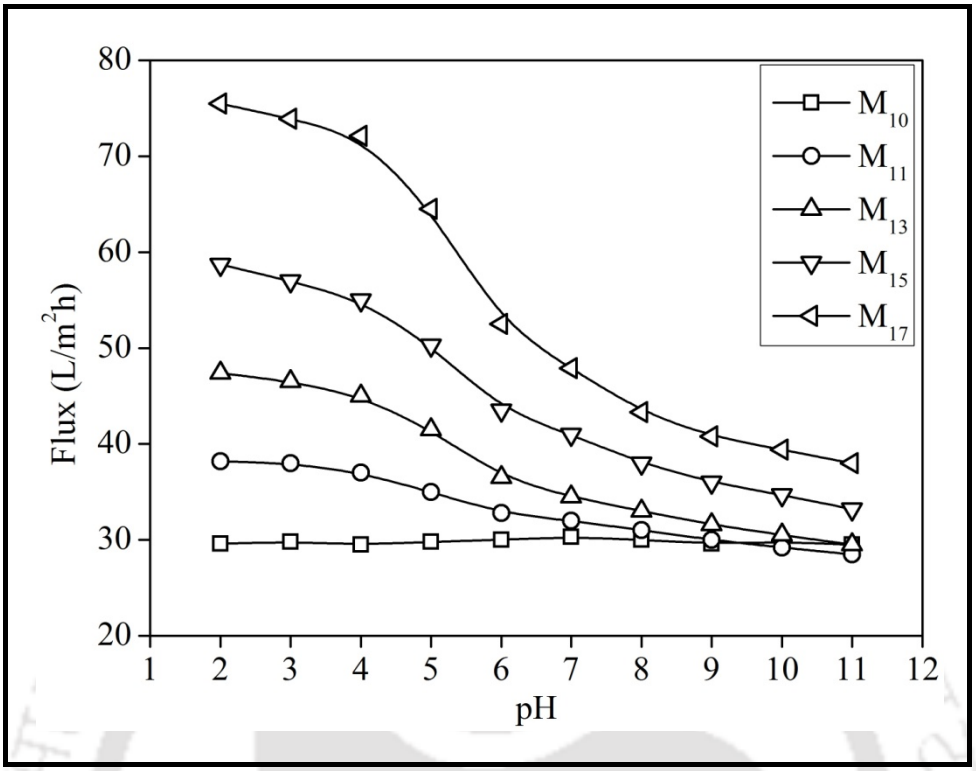


**Figure 6.7a: Effect of wt. % of poly (AA-co-PEGMA) on pH dependent flux.**

Similar observation (as that of Figure 6.7a) is also seen for membrane $M_{15}$, $M_{25}$ and $M_{35}$ (prepared with same amount of copolymer but copolymer composition is different) for pH dependent flux in Figure 6.7b. It can be seen that for membranes $M_{15}$, $M_{25}$ and $M_{35}$ flux changed from 33.2 to 58.7, 38.2 to 53.7 and 29 to 67.3 $L/m^2h$, when pH changed from 11 to 2. Membrane $M_{35}$ has the biggest change because AA fraction was highest in copolymer synthesis and membrane $M_{35}$ has also highest IEC value (21 mmol/g) among these three membranes.

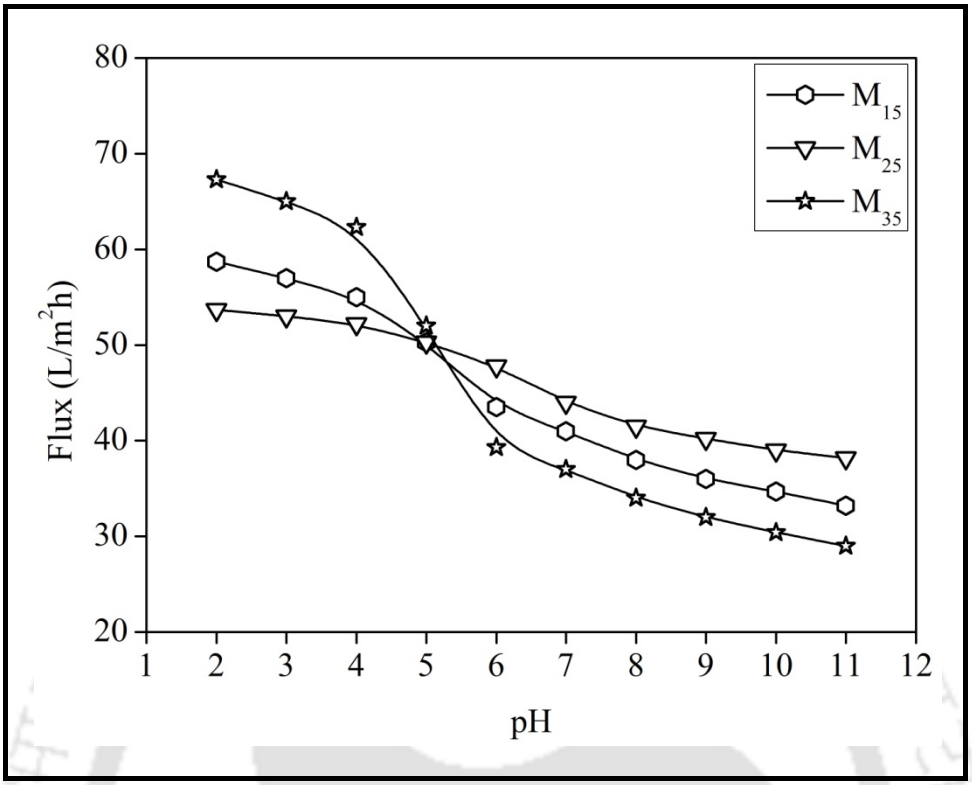


**Figure 6.7b: Effect of of poly (AA-co-PEGMA) composition on pH dependent flux.**

Figure 6.8 shows the hydraulic permeability of membranes in different pH condition i.e. acidic, basic and normal pH. As the pH decreases water flux increases. Hence, hydraulic permeability of the membrane was also highest in acidic condition for all the modified membrane. In acidic condition PAA chains are protonated and contracted. As a result, the effective pore size of membranes increases and therefore permeability through membrane also get increases. The pH responsive hydraulic permeability of membrane can be described by Hagen–Poiseuille's Law [84]. This law states that water flux through membrane is directly proportional to fourth power of pore radius. However, in basic condition PAA chains are deprotonated and expanded due to negative charge density. Therefore, the effective pore size of membranes decreases, hence permeability through membrane also decreases.

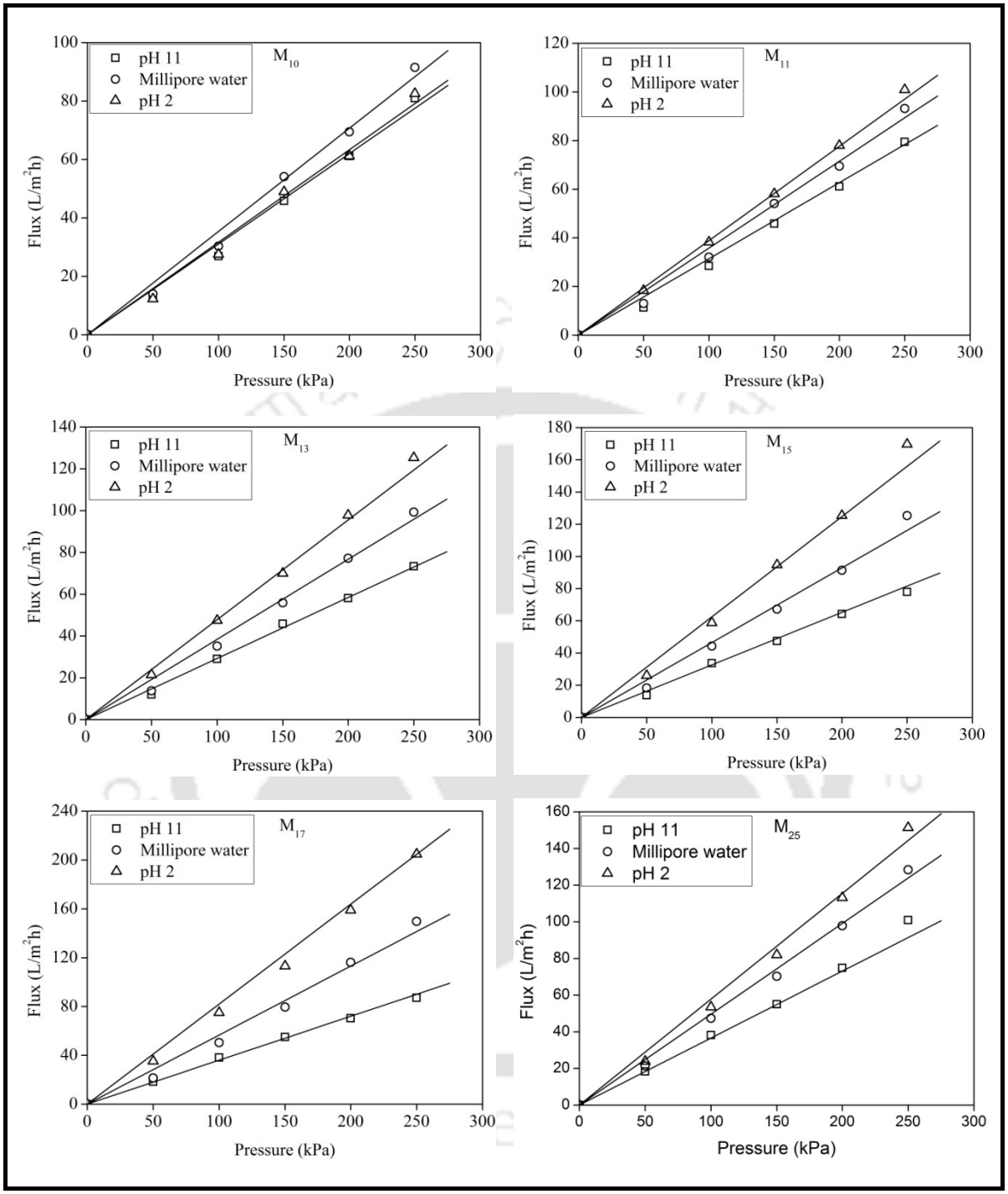


**Figure 6.8: Effect of poly (AA-co-PEGMA) on hydraulic permeability in different pH condition.**

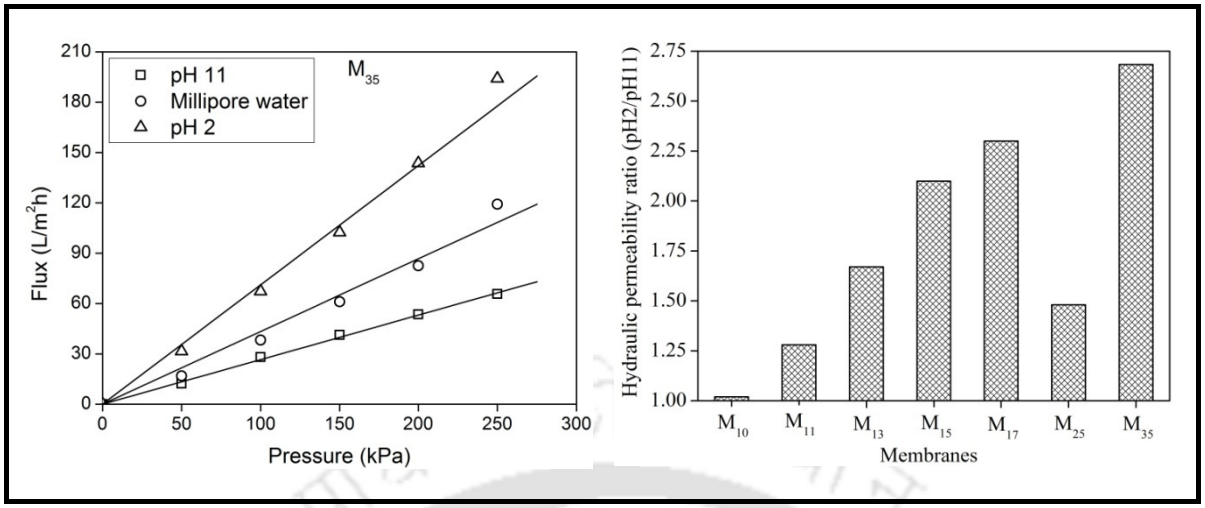


**Figure 6.8: Effect of poly (AA-co-PEGMA) on hydraulic permeability in different pH condition (continued).**

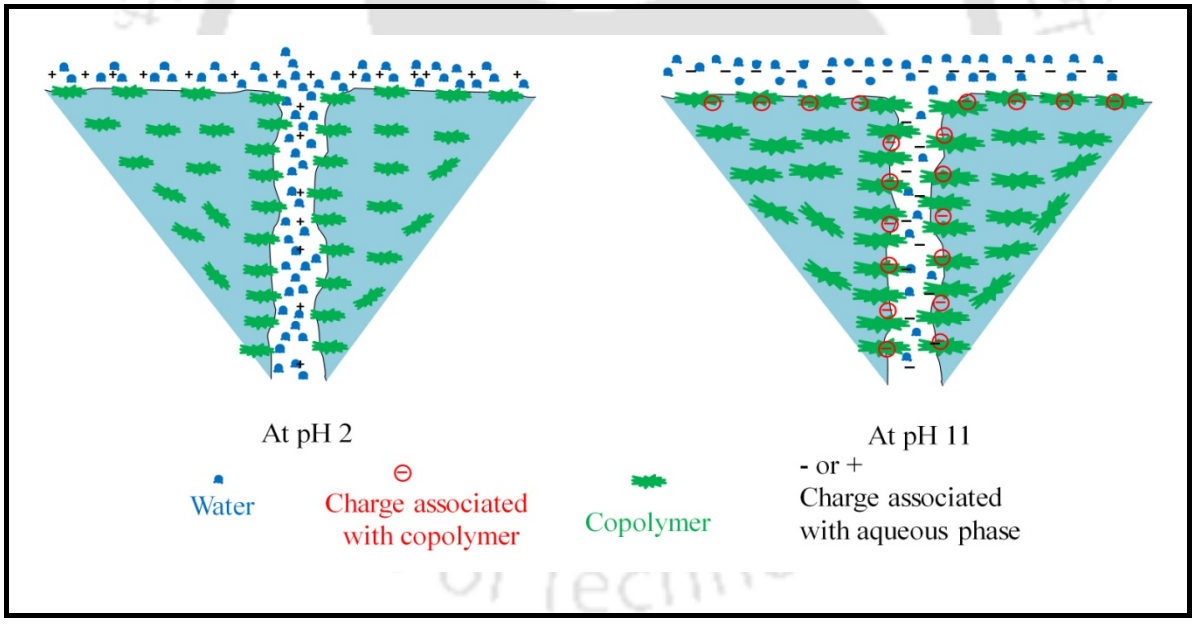


**Figure 6.9: Schematic presentation for the mechanism of pH responsive phenomenon of membranes.**

It is shown in Figure 6.8, among membranes containing different amount of copolymer, membrane $M_{17}$ has highest hydraulic permeability ratio, as it contain highest copolymer content. Membrane $M_{35}$ has highest permeability ratio between pH 2 and 7 among the 3 membranes containing different copolymer. This is because of the fact that membrane

$M_{35}$ contains more fraction of AA in its copolymer composition. pH responsive behaviour of membranes is shown schematically in Figure 6.9. It is described in preceding section that copolymer remains in compact form at pH 2 and therefore more amount of water can pass through pores. On the other hand, copolymer molecules get deprotonated at pH 11 and result in expansion of copolymer. This expansion leads to the smaller pore size, so less amount of water can pass through the pores. The result is also supported by the concept of inter ionic repulsion. Both membrane and water remains negatively charged at pH 11. Therefore, same charge repels each other causing decrease in pore size which leads to lower permeability.

### 6.3.6. Ultrafiltration and fouling studies

Figures 6.10a and 6.10b show the time dependent flux of membranes modified with different wt % of poly (AA-co-PEGMA) and with different copolymer. From 0-60 min, 120-180 min millipore water flux was measured and from 60-120, 180-240 BSA flux was measured. One can observed that during water permeation initially a slight loss of flux is observed and after that it remain constant for all the membranes, however when BSA permeation is started, a drastic loss of flux was observed during initial permeation in all membranes. In modified membranes loss is less than unmodified membrane. Initial loss of flux during BSA ultrafiltration was due to the deposition or adsorption of BSA molecule on the surface or inside the pores of membranes. So, to have fouling resistance to BSA or any other biofoulants the membrane should effectively resist the adsorption or deposition of foulants to their surface or pore as reported in literatures [118, 139].

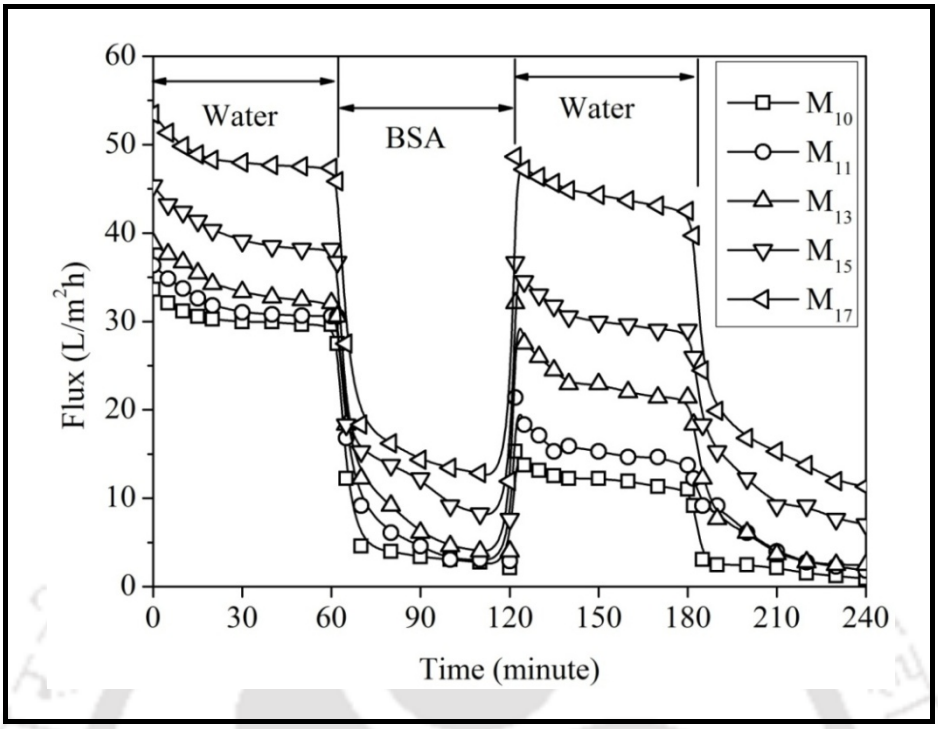


**Figure 6.10a: Effect of wt % of poly (AA-co-PEGMA) on time dependent flux; millipore water: 0-60 min and 120-180 min, BSA solution: 60-120 min and 180-240 min.**

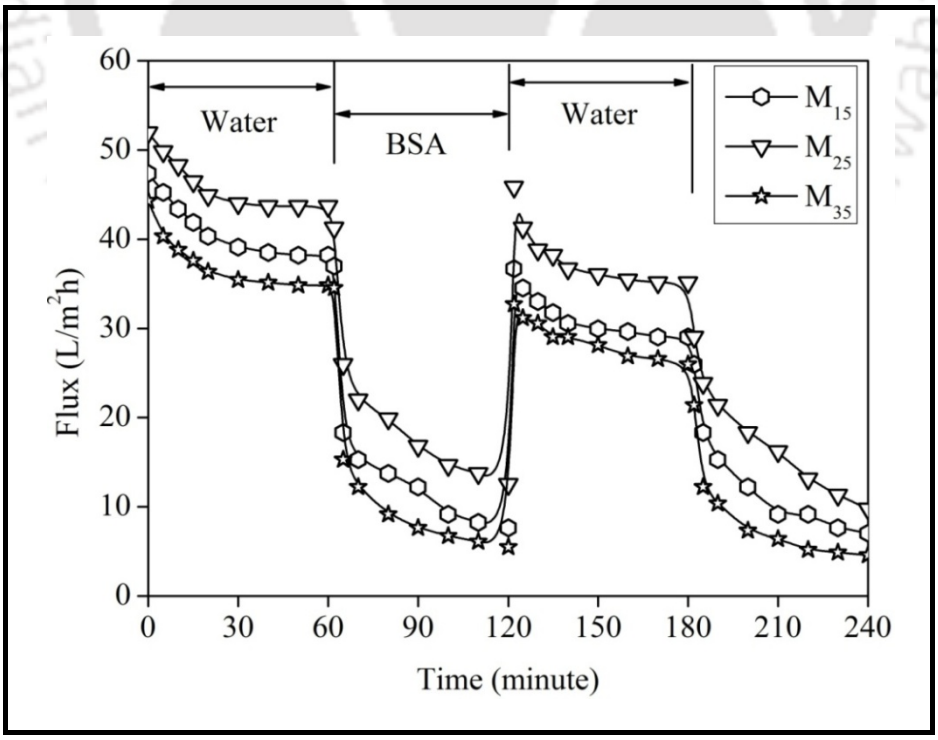


**Figure 6.10b: Effect of different poly (AA-co-PEGMA) copolymer on time dependent flux; millipore water: 0-60 min and 120-180 min, BSA solution: 60-120 min and 180-240 min.**

Membrane fouling caused by deposition or adsorption of foulants, which cannot be removed by simple hydraulic cleaning is termed as irreversible fouling ($F_{ir}$) and fouling caused by deposition or adsorption of foulants, which can be removed by simple hydraulic cleaning is termed as reversible fouling ($F_r$). Sum of $F_{ir}$ and $F_r$ is total fouling. These values were found from Figures 6.10a and 6.10b by using equations 6.17-6.19 and are shown in Figures 6.11a and 6.11b. It can be observed (Figure 6.11a) that as the copolymer content is increased in modified membranes, $F_t$ values are also get reduced, but $F_{ir}$ values are reduced remarkably with increase in copolymer content. So, the $F_r$ values are increased. $F_t$ and $F_{ir}$ values decreases from 0.93 to 0.75 and 0.63 to 0.11 respectively with increase in copolymer content from 0 to 7 wt%. Lower value of $F_{ir}$ means lower amount of irreversible adsorption or deposition of foulants on membrane surface. Here, two major factors are working in favour of modified membrane to control the fouling, first is hydrophilicity and second is charge on membrane surface. The contact angle measurements have already established that modified membranes have higher hydrophilicity and presence of PEG derivative also reduces the adsorption of BSA into the membrane pores or on the membrane surface [80]. On the other hand at pH 7 BSA molecules are negatively charged and due to deprotonation of –COOH group, membrane surface has also negative charge. Hence again, BSA molecules get strong repulsion from membrane surface. Previously from IEC study, it is known that with the increase in copolymer content in modified membranes, their IEC also get increased. So, on the whole with the increase in wt% of poly (AA-co-PEGMA) in modified membrane, their PEG and –COOH content both increases, which in result reduces the irreversible fouling of the modified membrane. Due to lower $F_{ir}$ values for modified membrane, flux recovery ratio of modified membranes also get increased, as it is directly depend on the irreversible fouling of membranes.

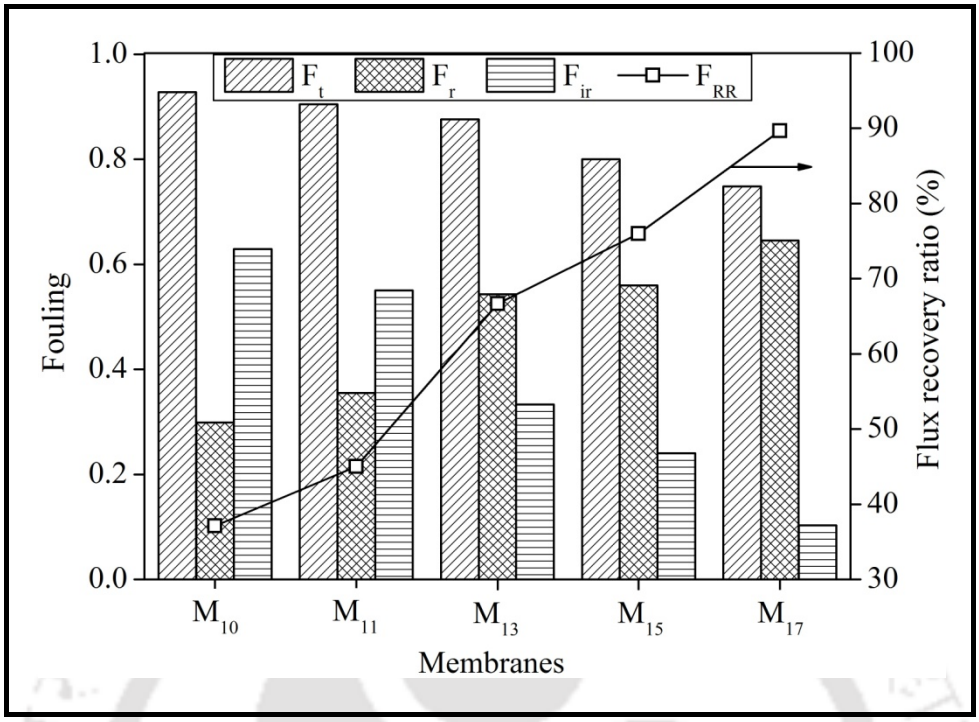


**Figure 6.11a: Effect of wt % of poly (AA-co-PEGMA) on fouling behaviour and flux recovery ratio of membranes.**

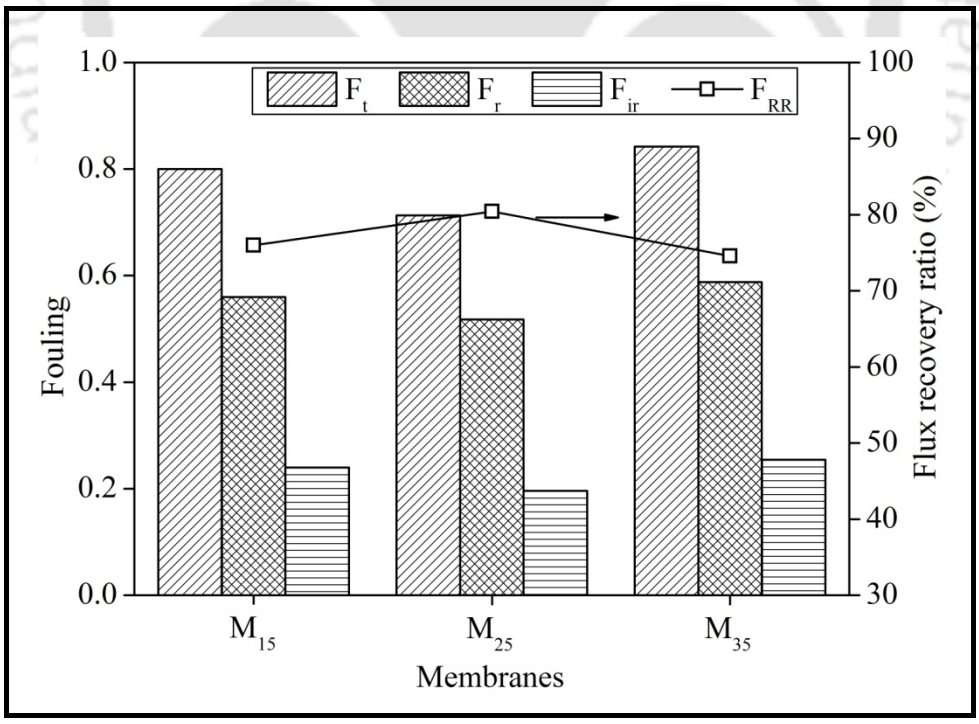


**Figure 6.11b: Effect of different poly (AA-co-PEGMA) copolymer on fouling behaviour and flux recovery ratio of membranes.**

Membrane $M_{17}$ has almost 90 % $F_{RRR}$ value because its $F_{ir}$ value is very less (0.11). In case of different copolymer (Figure 6.11b), as the PEGMA chain content increases their hydrophilicity increases, which results in comparatively less fouling and less adsorption of BSA molecule on membrane surfaces. So, membrane $M_{25}$ is slightly less affected by fouling and its $F_{RRR}$ value is also comparatively higher than other two membranes.

### 6.3.7. Transport property of BSA solution through membrane

Figure 6.12a shows the effect of wt% of poly (AA-co-PEGMA) copolymer on BSA flux and rejection. As the copolymer content increases, average BSA flux increases due to increase in hydrophilicity of the membrane because of PEG derivative. There is slight increment of rejection also, despite the fact that BSA flux is much higher for modified membrane. The –COOH group present on membrane surface or inside the membrane pores repel the BSA molecules from passing through the membranes. In case of different copolymer (Figure 6.12b), membrane $M_{35}$ has the highest BSA rejection value. The membrane $M_{35}$ contained copolymer $C_3$, which had maximum fraction of AA. The ionization of –COOH group expanded the copolymer, which resulted in reduced pore size and loss of flux through membrane $M_{35}$.

Figures 6.13a and 6.13b show the effect of pH on BSA rejection for different membranes and it is schematically represented in Figure 6.14. It can be observed from the Figures 6.13a and 6.13b that rejection variation with change in pH of BSA solution shows a clear difference between the modified membranes and unmodified membrane. For unmodified membrane $M_{10}$, BSA rejection is almost same for all pH values. For modified membranes rejection is almost same at pH 7 and 11, but at pH 2 that difference is much

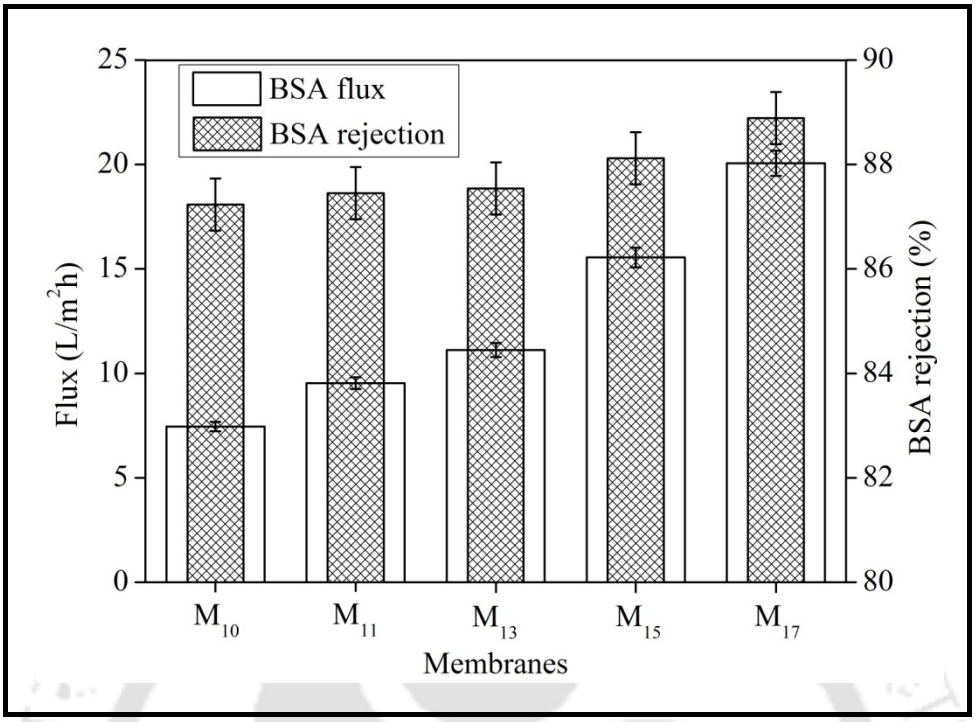


**Figure 6.12a: Effect of wt % of poly (AA-co-PEGMA) on BSA flux and rejection of membranes.**

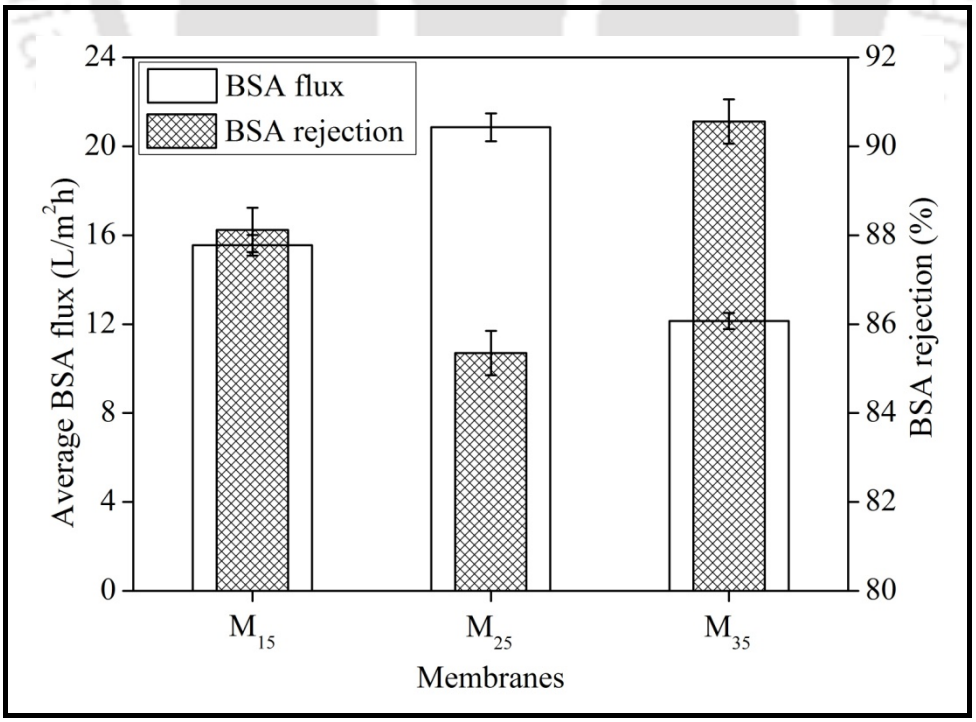


**Figure 6.12b: Effect of different poly (AA-co-PEGMA) copolymer on BSA flux and rejection of membranes.**

larger with increase in wt % of poly (AA-co-PEGMA). For example, BSA rejection for membrane $M_{10}$ at pH 11, 7 and 2 are 88.5 %, 87.2 % and 87.5 % respectively. On the other hand, those values for membrane $M_{15}$ are 93.5 %, 90.5 % and 23.2 % respectively. Again, for membranes with different copolymer, membrane $M_{35}$ has the diverse behaviour in rejection at different pH. At pH 7, 11 and 2 BSA rejection values for membrane $M_{35}$ are 90.6 %, 93.5 % and 23.2 % respectively.

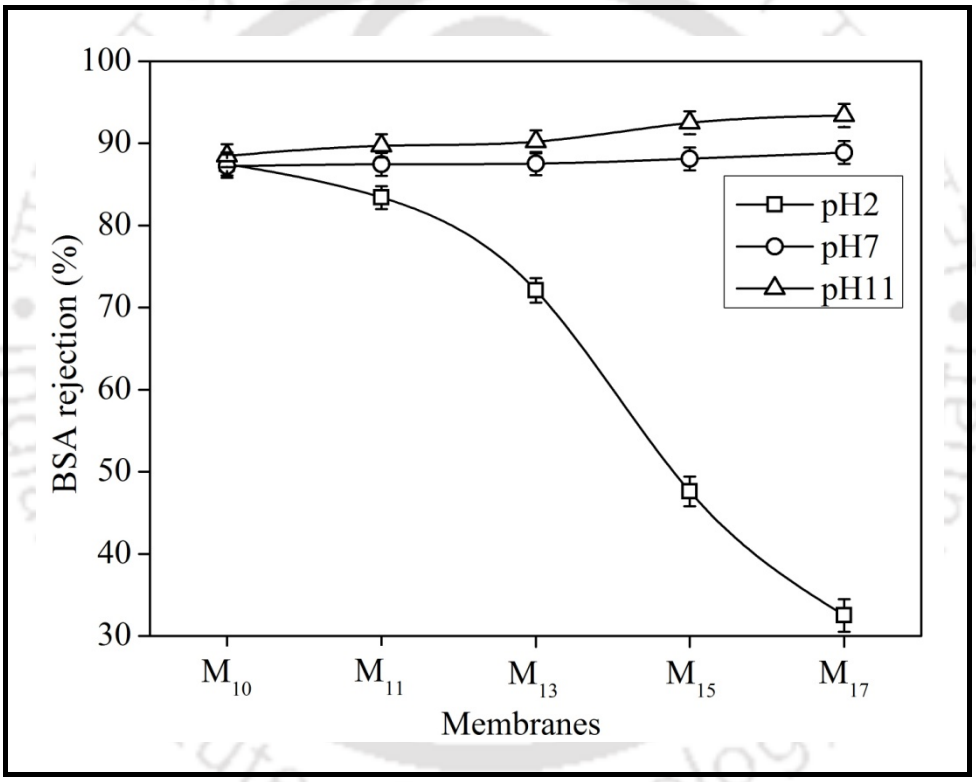


**Figure 6.13a: Effect of pH on BSA rejection behaviour of membranes containing different wt % of poly (AA-co-PEGMA).**

Rejection through pH-responsive membrane is combined effort of electrostatic interaction and pore size as discussed in the preceding section. In this case electrostatic interaction was prevailing between BSA molecule and poly (AA-co-PEGMA) copolymer present in membrane matrix. As discussed earlier, change in pH can lead to conformational

change of poly (AA-co-PEGMA) copolymer and that result in change in pore size of membrane.

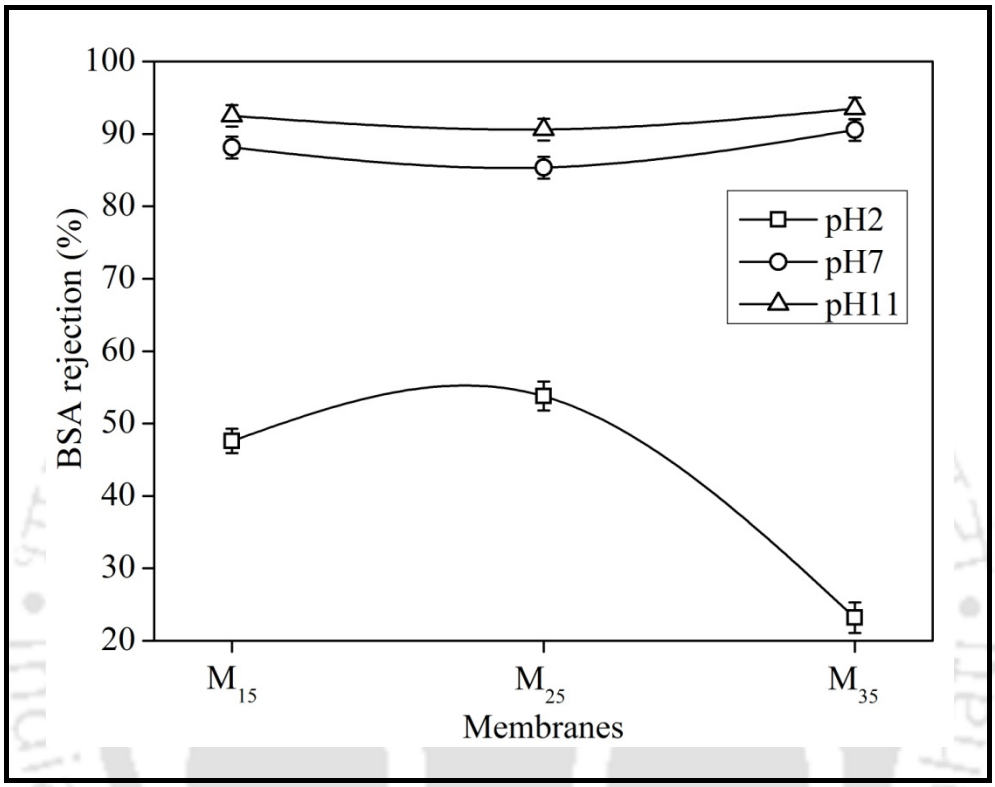


**Figure 6.13b: Effect of pH on BSA rejection behaviour of membranes containing different poly (AA-co-PEGMA) copolymer.**

Thus, due to the swelling of poly (AA-co-PEGMA) in skin layer of modified membranes at pH 11, pores of the modified membranes become smaller, which results in higher BSA rejection. Further, when the pH of BSA solution decreases to 2, membrane pore size become larger due to collapse of poly (AA-co-PEGMA) copolymer and thus results in lower rejection of BSA. It is well known that isoelectric point of BSA molecules is around pH 4.7 and at this pH BSA molecules contain zero charge. BSA molecules have net positive and negative charge below and above pH 4.7, respectively. So, at pH 11 BSA molecules are negatively charged and molecules of poly (AA-co-PEGMA) copolymers are also negatively

charged due to complete deprotonation of –COOH group to $–COO^-$. Thus, electrostatic repulsion between negatively charged BSA molecules and $–COO^-$ present in membrane makes the permeation of BSA molecules very difficult, which results in higher rejection. At pH 11 all the membranes have rejection around 90 %. Same is the case at pH 7, as copolymer molecules and BSA remains negatively charged. So rejection values remain almost same. Whereas, at pH 2 only BSA molecules have positive charge and membranes contain no charge. Apart from that, pores are comparatively much larger due to collapse of PAA component of copolymer. So, combination of these two effects results in low rejection of BSA at pH 2. As the wt % of copolymer was increased rejection was decreased for membrane with different wt % of copolymer. On the other hand, for membranes with different copolymer, rejection was lowest for $M_{35}$ membrane due to higher content of PAA in copolymer. This, phenomena is schematically shown in Figure 6.14.

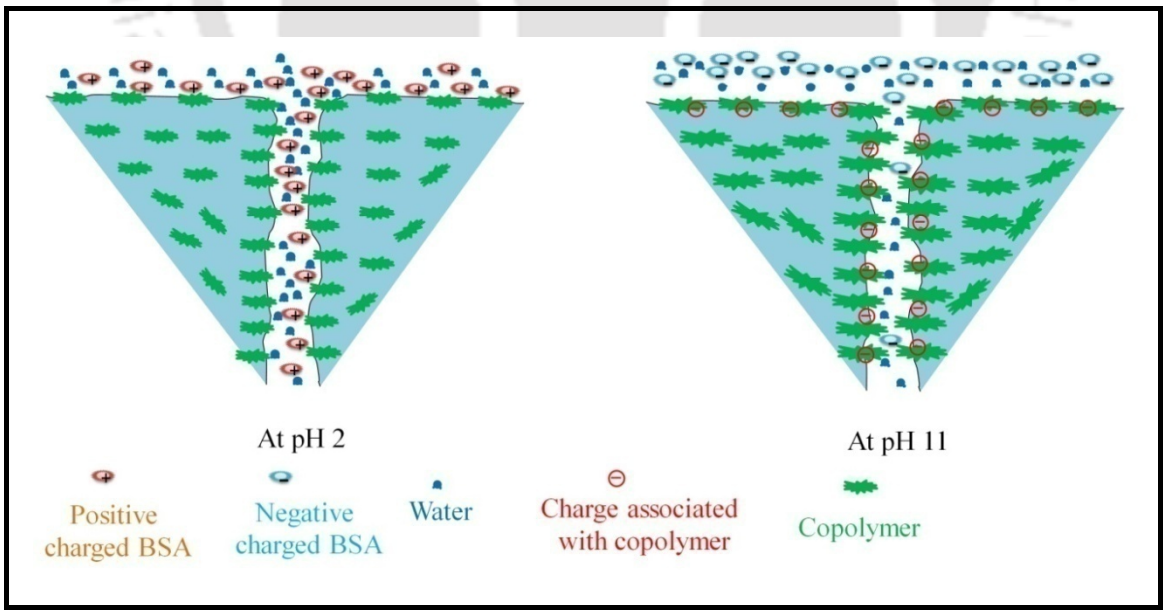


**Figure 6.14: Schematic presentation for the mechanism of pH responsive phenomenon of membranes for BSA rejection.**

# Chapter 7

## Fabrication of fouling resistance PSF flat sheet UF membrane using amphiphilic polyurethane macromolecules

# Chapter 7
# Fabrication of fouling resistance PSF flat sheet UF membrane using amphiphilic polyurethane macromolecules

*In this chapter four different types of amphiphilic PU macromolecules were synthesized with end capping of citric acid, malic acid, lactic acid and 4-hydroxy benzoic acid. Proton NMR and FTIR analysis was done to confirm the chemical structure of synthesized PU macromolecule. Synthesized PU macromolecules were blended directly in membrane casting solution and membranes were fabricated by phase separation method. Morphology and surface chemical features were analyzed with SEM, FESEM, AFM, FTIR-ATR and water contact angle. Blended membranes showed enhanced pore density, pure water flux, hydration capacity and hydrophilicity compared to plain membrane. SEM photographs showed significant change in cross sectional morphology of modified membrane with highest wt % of additive. UF performance and anti fouling property of modified membranes were investigated and analysed.*

## 7.1. Experimental

### 7.1.1. Materials

Polysulfone (PSF), 4-hydroxybenzoic acid (BA), 4,4'- methylenebis(phenyl isocyanet) (MBI), dimethyl sulfoxide-d6 (DMSO-d6), N- methylpyrrolidone (NMP), poltasium bromide (KBr), Azobisisobutyronitrile (AIBN), dimethyl acetamide (DMAc), citric acid (CA), malic acid (MA), lactic acid (LA), stannous octoate, 1, 6-hexanediol (HD) and Bovine

Content of this chapter is published as below:

M K Sinha, M K Purkait, Preparation of fouling resistant PSF flat sheet UF membrane using amphiphilic polyurethane macromolecules**,** Desalination 355 (2015) 155-168.

serum albumin (BSA) were used for this chapter. Additional detail of all the chemicals is given in Table 2.1 of chapter 2.

### 7.1.2. Synthesis and characterization of polyurethane macromolecules

Four kinds of polyurethane macromolecules (PU) were synthesized by two step solution polymerization method. First, MBI and HD were mixed (MBI:HD molar ratio of 3:2) in DMAc with the total monomer concentration of 20 wt % in a three neck round bottom flask with nitrogen supply, subsequently the initiator, stannous octoate, was added into the reaction mixture at 1 wt % of total weight of the monomers under constant stirring. After passing nitrogen for 30 min, polymerization was carried out in sealed flask at 80 $^{o}$C for 2 h. In second step, 4 different compounds (citric acid, malic acid, lactic acid and 4-hydroxybenzoic acid) were end capped onto the polyurethane for 4 different PU macromolecules. After addition of mentioned end capping compounds, reaction was carried out at 85 $^{o}$C for 16 h. In order to get linear polymer, the molar ratio of NCO:OH was kept at 1:1. The molar ratio of the used compounds was as follows: MBI:HD:BA/CA/LA/MA=3:2:2. The reaction pathway is shown in Figure 1. After the completion of reaction, obtained products were added drop wise to the cold DI water under vigorous stirring to precipitate the PUs. These precipitated PUs washed several times with DI water and dried in a hot air oven at 50 $^{o}$C for 5 days. PUs end capped with CA, BA, MA and LA was named as PU-CA, PU-BA, PU-MA and PU-LA, respectively. FTIR and $^{1}$H NMR spectroscopy were performed as described in section 2.4.2 and 2.4.1, respectively of chapter 2.

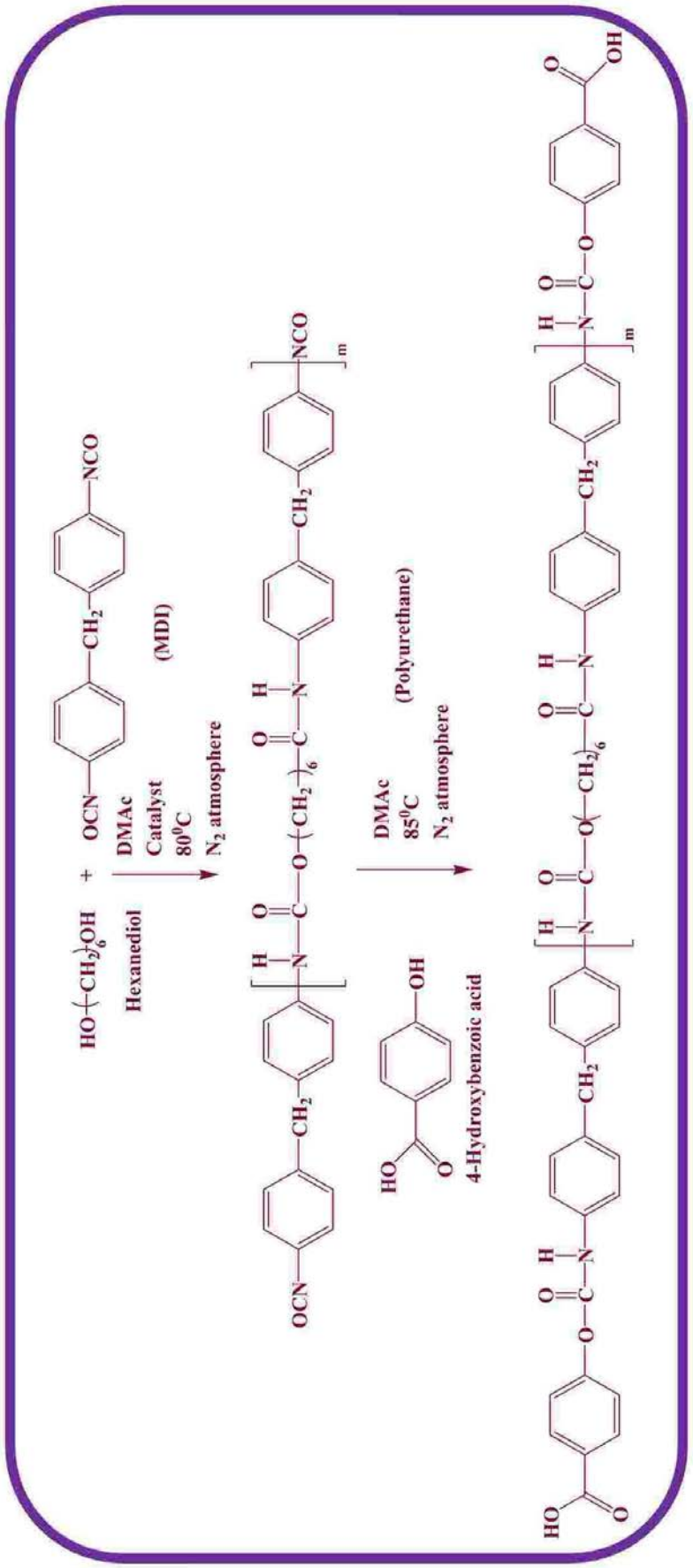


**Figure 7.1: Synthesis route of PU macromolecules.**

### 7.1.3. Fabrication of blended flat sheet membranes by phase inversion method

Flat sheet membranes were prepared by phase inversion method (as shown in Figure 7.2) using different PU macromolecules and different wt % of PU macromolecules (as shown in Table 7.1). Concentration of PSF was kept constant at 12 wt % and maximum concentration of PU macromolecules was 6 wt % of casting blend. Viscosities of membrane casting blends for different wt % of polyurethane (PU) macromolecules were also measured at a constant shear rate of 50 $s^{-1}$. The membrane casting blend was stirred at 50 $^{o}$C and 500 rpm for 18 h, further degassed for 12 h at 50 $^{o}$C temperature. Further, steps of membrane preparations are provided in section 2.2 of chapter 2.

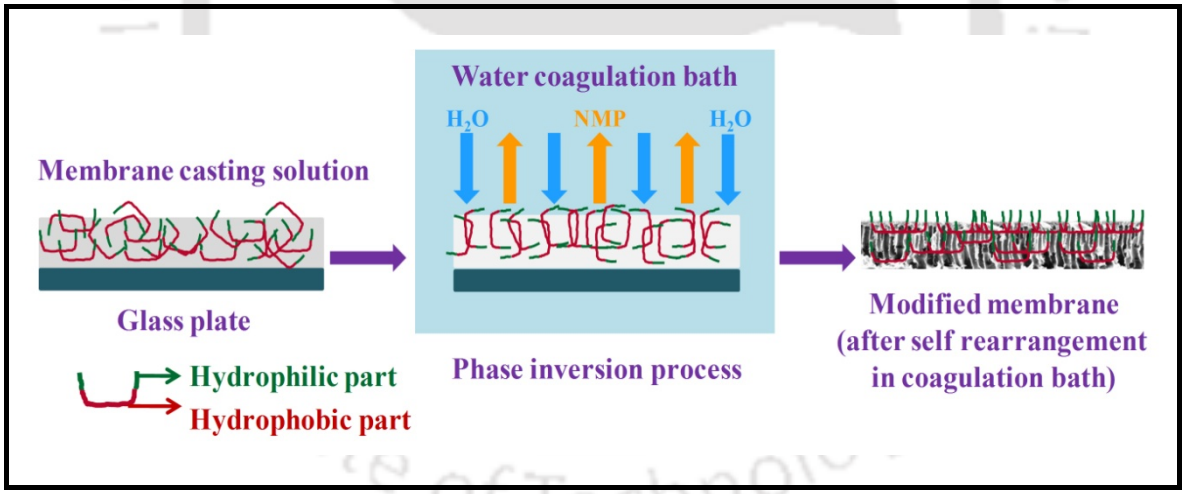


**Figure 7.2: Schematic of membrane preparation by phase inversio process.**

In the casting solution, it is expected that hydrophilic segment of PU macromolecules located at the upper interface will be oriented toward the liquid, which provides a more hydrophilic environment. Hydrophobic segment should be in contact with air. But after the immersion of casting solution in coagulation bath, once phase inversion has been prompted, copolymer molecules are rearranged up-side down. Certainly, the polymer system becomes

more hydrophobic due to the outflow of solvent. At the end, hydrophobic segment interact with PSF while hydrophilic segments should be oriented toward the top surface. Apart from that, PU macromolecules initially present in the bulk solution phase may migrate toward the top surface of membrane during phase inversion [110].

**Table 7.1: Composition of different membrane casting solution containing PU macromolecules.**

| Membranes | PSF (wt%) | PEG4000 (wt%) | Macromolecules (wt%) | | | | NMP (wt%) | Viscosity $\times 10^2$ (Pa s) |
|---|---|---|---|---|---|---|---|---|
| | | | PU-CA | PU-MA | PU-LA | PU-BA | | |
| **Plain** | 12 | 5 | 0 | – | – | – | 83 | 5.88 |
| **$CA_2$** | 12 | 5 | 2 | – | – | – | 81 | 11.26 |
| **$CA_4$** | 12 | 5 | 4 | – | – | – | 79 | 22.3 |
| **$CA_6$** | 12 | 5 | 6 | – | – | – | 77 | 27.1 |
| **$MA_6$** | 12 | 5 | – | 6 | – | – | 77 | 26.8 |
| **$LA_6$** | 12 | 5 | – | – | 6 | – | 77 | 25.3 |
| **$BA_6$** | 12 | 5 | – | – | – | 6 | 77 | 25.6 |

## 7.2. Membrane characterization

### 7.2.1. Surface characterization of polyurethane blended membranes

The presence of functional groups of PU macromolecule in modified membrane was confirmed by comparing IR spectra of plain PSF membrane and modified PSF membrane. Attenuated total reflectance - Fourier transform infrared spectra (ATR-FTIR) for the membranes were measured with FTIR instrument using attachment ATR-8200 HA (Shimadzu, Japan). Morphological study of the membranes was done by scanning electron

microscope (SEM), field emission scanning electron microscope (FESEM) and atomic force microscopy (AFM). Cross section and top surface images were taken by SEM with an EHT voltage of 10 kV and by FESEM with an EHT voltage of 2 kV after the coating of thin gold layer, respectively. Top surface morphology and surface roughness of the membranes were measured by AFM in the size of 5μm × 5μm size.

Change in hydrophilicity or hydrophobicity of the modified membranes compared to plain membrane were observed by measuring the static contact angle between water and membrane surface. Lower the water contact angle (WCA) higher the hydrophilicity of the membranes. For each samples 4 angles were measured at different part of membranes and average was taken. The adsorption of BSA on membrane surface was performed. The absorbed amount of BSA was measured by UV-VIS spectrophotometer at wavelength of 280 nm. Three duplicate tests were performed for each membrane. Hydration capacity of the fabricated membranes was also studied in terms of amount of absorbed water per unit volume of membranes ($mg/cm^3$). For each membrane sample, 4 different tests were performed and the average was considered.

### 7.2.2. Pore size distribution experiment

Pore size distribution of the membranes was determined by liquid-liquid displacement porosimetry (LLDP) method. This method gives the number of pores, average pore size and pore size distribution of the fabricated membranes. For this method, it is assumed that all the pores are cylindrical and thickness of the membrane layer is uniform [1]. Water – isobutanol - methanol (25:15:7, v/v, surface tension of 0.35 mN/m and dynamic viscosity of 3.4 mPa s) was taken in separating funnel and mixed vigorously. Then, this mixture was allowed to settle overnight. In the separating funnel water reach phase was separate in the lower part and taken out to wet the membrane. The remaining alcohol reach phase was used as permeating liquid.

The variation in flow with change in pressure gives the pore size distribution.

### 7.2.3. Pure water permeation experiment

Prepared membranes were compacted with deionized water for 2 h at a transmembrane pressure of 300 kPa and flux was measured at regular interval. The compaction factor (CF) was calculated as the ratio of initial pure water flux to steady state pure water flux. Pure water flux (PWF) was determined by allowing deionized water to pass through the compacted membrane. PWF was measured by the equation 2.9. Flux values of pure water at different transmembrane pressures were measured under steady state condition. Permeability ($P_m$) ($L/m^2h$ kPa) was evaluated from the slope of the plot of $J_w$ vs $P$. Hydraulic permeability was calculated by equation 2.10.

### 7.2.4. Ultrafiltration performance and fouling behaviour experiment

Ultrafiltration experiment was conducted to study the solute separation, permeate flux and fouling behaviour of the prepared membranes. BSA was dissolved in DI water and the concentration and pH were kept constant at 1000 $mgL^{-1}$ and 7 respectively for all the experiments. Each membrane was initially compacted for 30 min at 300 kPa, then the pressure was reduced to 250 kPa and the water flux ($J_{w1}$) was measured for 1 h duration. Afterwards water permeation, cell was refilled with BSA solution and flux was measured ($J_p$). The BSA rejection ratio was calculated by the equation 2.16.

After 2 h of ultrafiltration and later hydraulic cleaning of the membrane, water flux was measured ($J_{w2}$). With the help of $J_{w1}$ and $J_{w2}$, flux recovery ratio ($Flux_{RR}$) was measured. After the first round of BSA rejection and membrane cleaning, water flux was measured, that is used to calculate first flux recovery ratio ($Flux^1_{RR}$). Again, BSA rejection experiment was

done for 2 h and all the operation was repeated to calculate the second flux recovery ratio ($Flux^2_{RR}$). Fouling of membrane causes flux loss $(J_{w1}-J_p)$ and the flux loss caused by total fouling ($F_t$), reversible fouling ($F_r$) and irreversible fouling ($F_{ir}$) are calculated by equations 2.17, 2.18 and 2.19 respectively.

## 7.3. Results and discussion

### 7.3.1. FTIR and NMR spectroscopy analysis of polyurethane macromolecules

As shown in Figure 7.3, peaks at 3409 $cm^{-1}$ and 3478 $cm^{-1}$ are due to polyurethane linkage of NH with CO in the macromolecules, which confirms the formation of polyurethane. The peak at 1726 $cm^{-1}$ is characteristic peak of –COOH group present in end capping of all the PU-macromolecule. This confirms the presence of BA, CA, MA and LA in PU-BA, PU-CA, PU-MA and PU-LA. Another peak at 1508 $cm^{-1}$ is due to secondary amide present in the polyurethane structure.

Four different types of PU macromolecules were synthesized with different end capping agent. Figure 7.4 shows $^1$H NMR of synthesized PUs and their chemical structures. For all the PUs shifts at δ = 9.3 – 9.6, 8.3 – 6.6, 3.7 – 4.1, and 1.2 – 1.9 are due to −COOH (1), −NH− (3), $-CH_2-$ (6), and $-CH_2-$ (6) respectively. For PU-CA, PU-LA and PU-MA, all aromatic shifts were found between δ = 7 and 7.4 but in case of PU-BA the new aromatic shifts observed in addition to previous ones between δ = 6.8 and 7.8. In addition for all the PUs except PU-BA, they have shift at δ = 1.9 – 2.1. This shift is due to $-CH_2-$ group present in CA, LA and MA. Combining the FTIR spectra and NMR shifts, the results signified typical PU structure had been obtained and end capped with compounds containing different number of carboxylic groups.

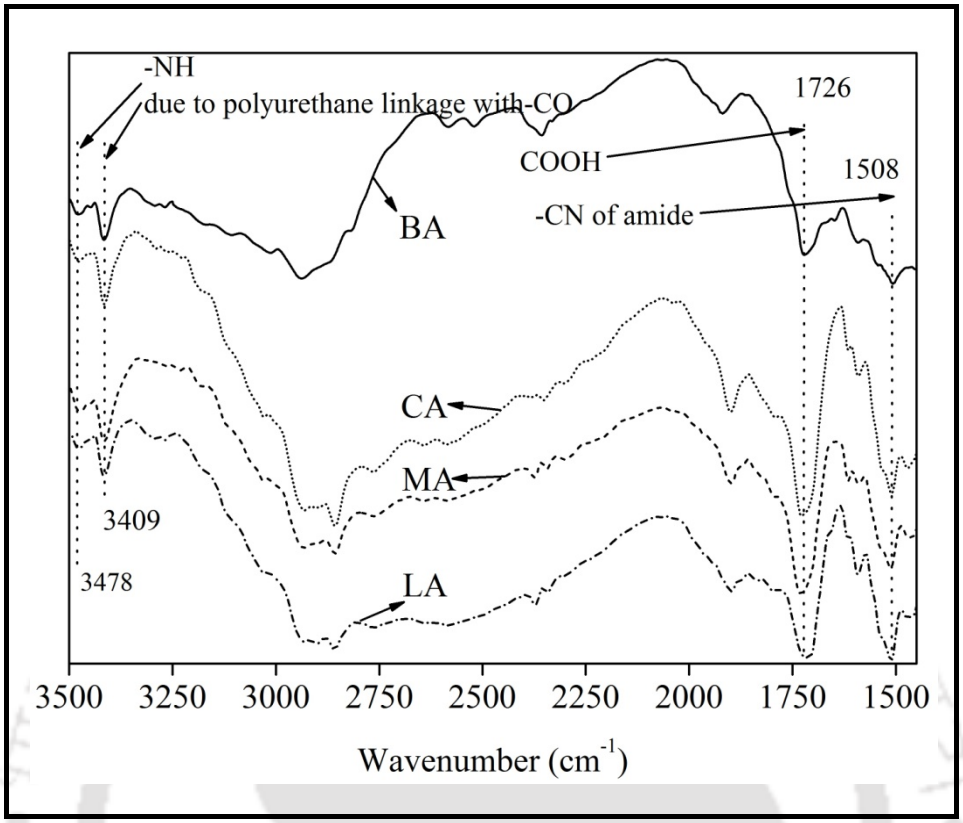


**Figure 7.3: FTIR spectroscopy of different PU macromolecule.**

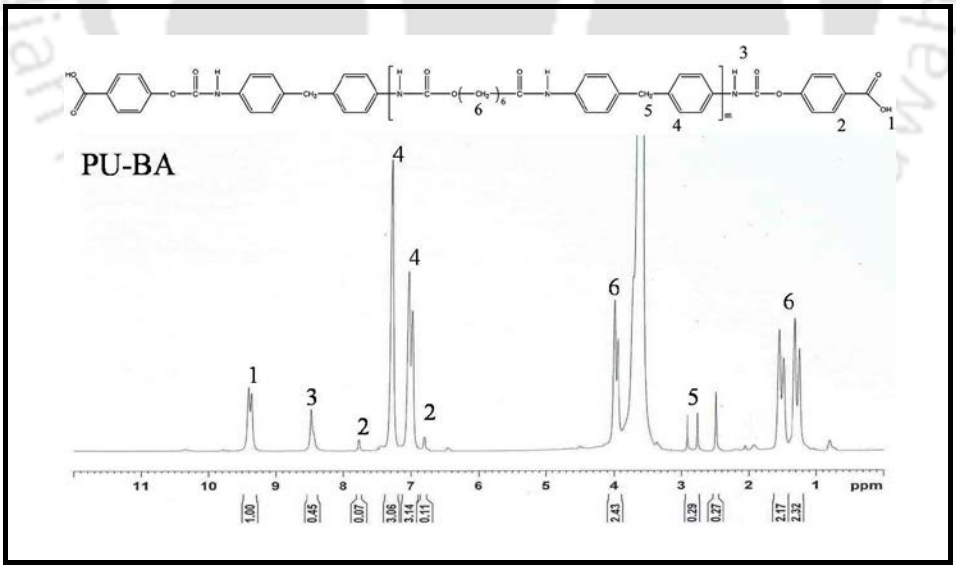


**Figure 7.4: $^{1}H$ NMR specrtoscopy of synthesized PU macromolecule.**

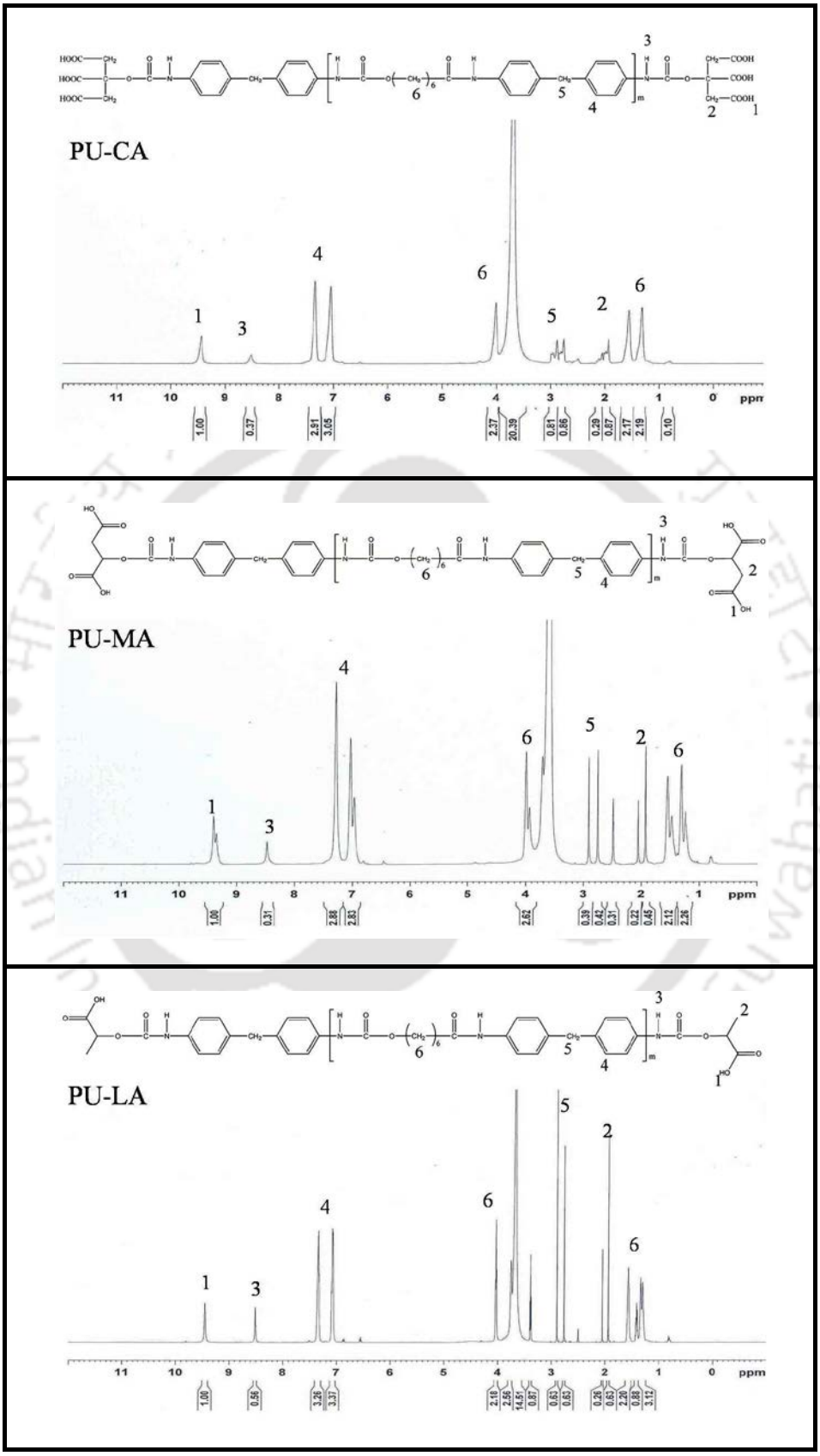


**Figure 7.4: $^{1}H$ NMR specrtoscopy of synthesized PU macromolecule. (continued)**

## 7.3.2. Surface and morphological characterization of modified PSF membranes

### 7.3.2.1. ATR-FTIR analysis of plain and blended membranes

Figure 7.5a shows ATR-FTIR spectra of plain and blended PSF membranes surfaces fabricated with different wt % of PU-CA polyurethane macromolecule. A New peak appears around 1511 $cm^{-1}$, confirms the presence of secondary amide group present in PU macromolecule. The most important change is the emergence of new peak at around 1730 $cm^{-1}$, which confirms the presence of –COOH group, from end capping of citric acid. The intensity of carboxyl group peak is much more for membrane $CA_6$ compared to $CA_2$, it means membrane $CA_6$ has more amount of hydrophilic carboxyl group.

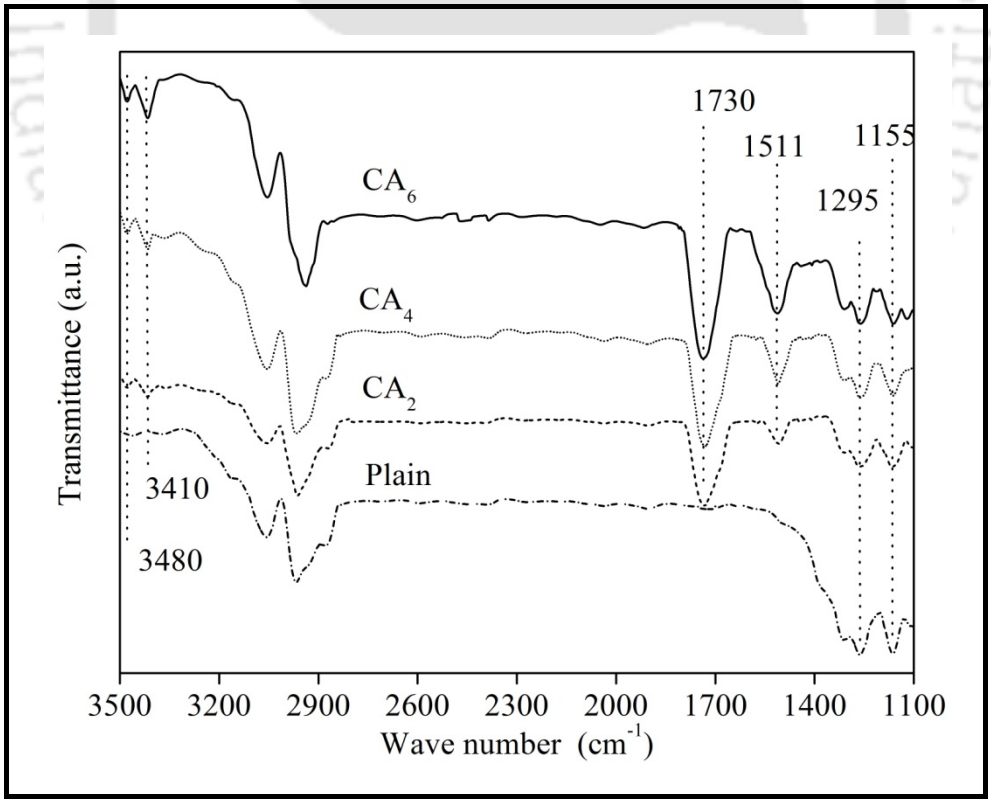


**Figure 7.5a: ATR-FTIR of membrane with different wt % of PU-CA.**

Similarly, in case of different macromolecule intensity of peak around 1730 $cm^{-1}$ is highest for membrane $CA_6$ compared to others (Figure 7.5b). As it contains more number of –COOH group compared to other membranes. It may be seen new peaks at around 3410 $cm^{-1}$ and 3480 $cm^{-1}$, which are due to polyurethane linkage between NH and CO groups. These peaks authenticate the presence of PU-CA in the blended membrane. Also the strength of these peaks varies with the wt % of PU macromolecule in modified membranes. The peaks at 1155 $cm^{-1}$ and 1295 $cm^{-1}$ are due to –C–O–C– and S=O group present in PSF, thus verifying the presence of PSF.

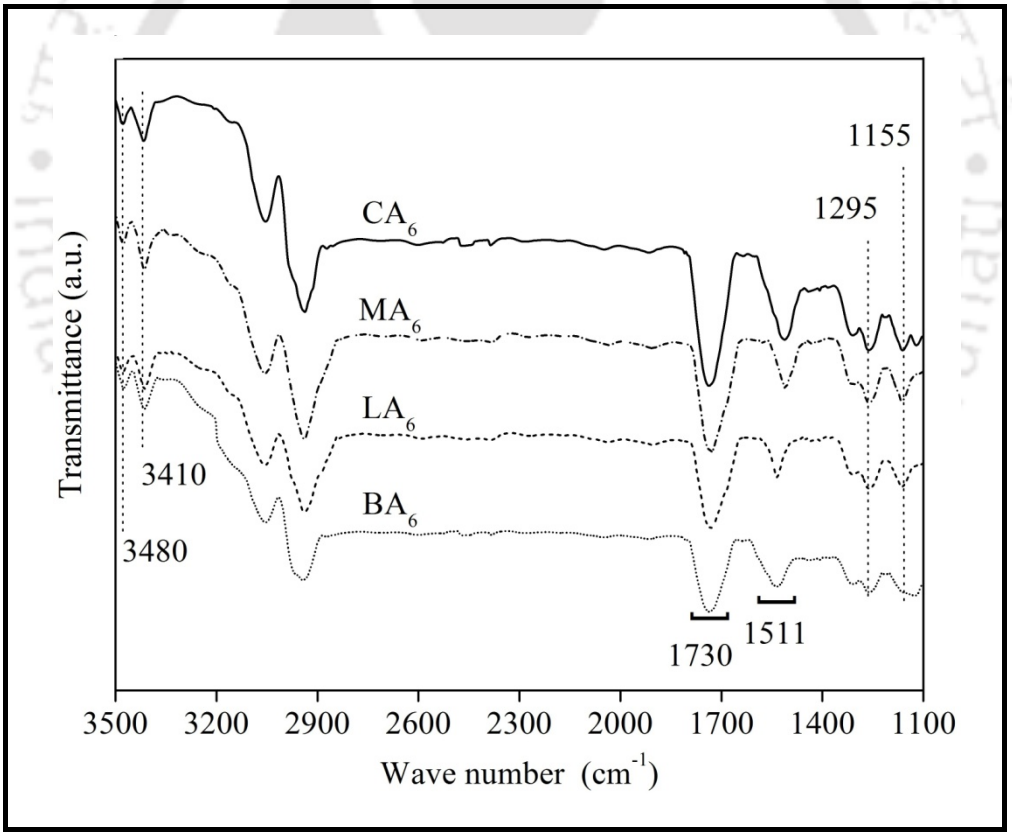


**Figure 7.5b: ATR-FTIR of membrane with different PU macromolecule.**

### 7.3.2.2. Microscopic studies

Figure 7.6 shows the cross sectional SEM images of plain and blended membrane with 6 wt % of PU-CA fabricated in this study. From the Figure it is clear that, fabricated membranes exhibit asymmetric structure in cross section. Addition of the PU macromolecule did not change the characteristic asymmetric structure of the membranes. Both the membranes have porous sub-layer consists of finger like structure. These structures formed due to the high mutual affinity of NMP for water, which results instantaneous demixing [138]. However, it may be observed significant change in the finger like structure of the modified membrane. Finger like structures became more prominent, longer and uniform in modified membrane compared to plain membrane. This result in more porous blended membranes compared to plain membrane. Also, in the plain membrane, smaller finger like structures are present near the top dense skin layer. Whereas in modified membrane that structure changed to porous sponge like structure. It is reported that membrane structure is formed by driving force between nonsolvent and solvent and their relative diffusion rate [140, 141]. If there is strong affinity between solvent and nonsolvent then in such condition out diffusion rate of solvent is much higher than the in diffusion rate of nonsolvent. Thus dense skin layer is formed and reduces the diffusion rate of nonsolvent into the sub layer, this result in small finger like structure. Whereas, if there is weak affinity between solvent and nonsolvent, the skin layer will be porous and sponge like structure can be formed. Since, PU macromolecule has amphiphilic property, the addition of the same influences the relative diffusion rate of solvent and non solvent by reducing the affinity between solvent and nonsolvent. Thus the in diffusion rate of nonsolvent decreases during phase inversion process at higher PU macromolecule content. This results in sponge like sub layer structure just below the dense skin layer. One can see that membranes modified with other PU macromolecules also have similar type of structure.

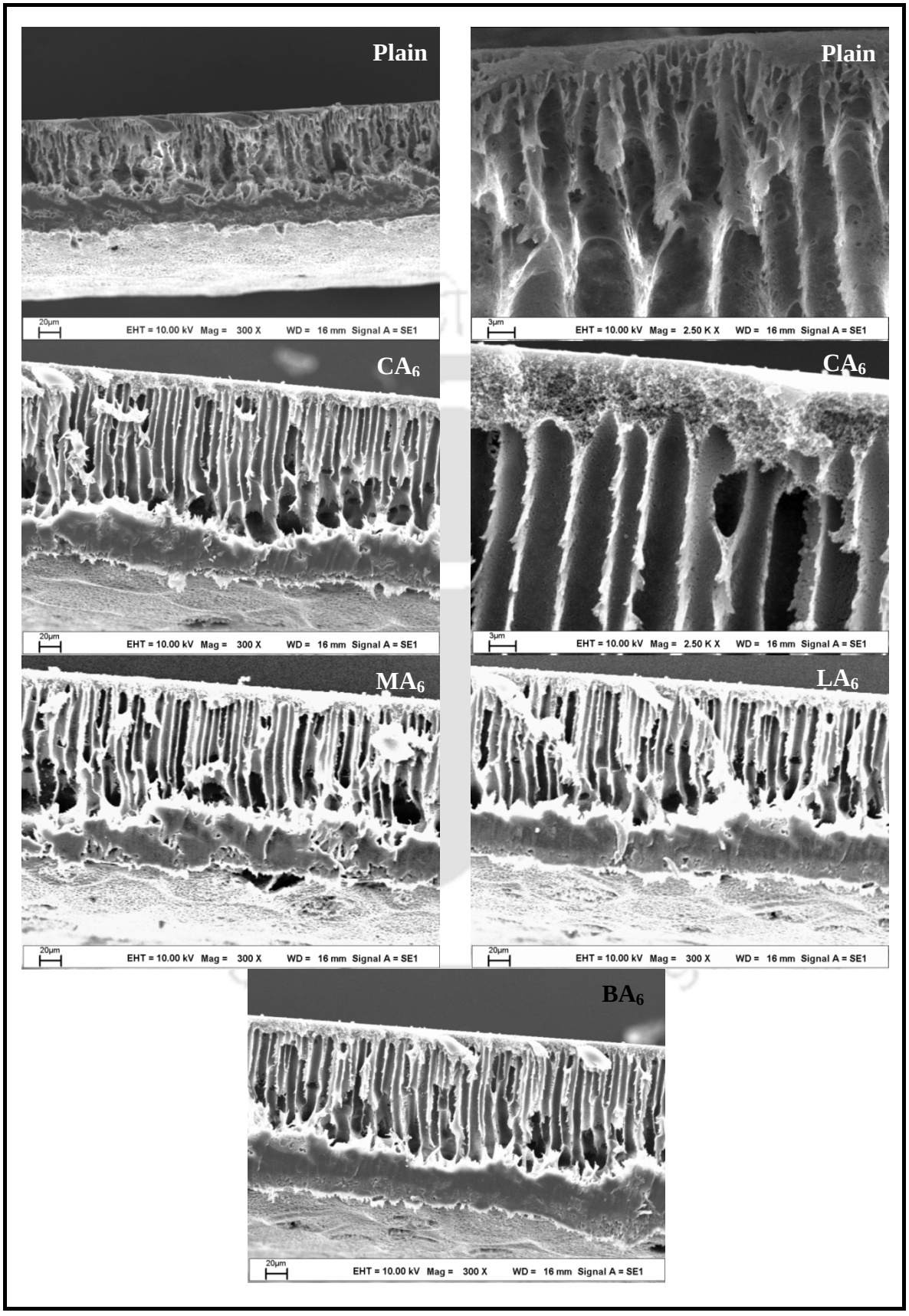


**Figure 7.6: Cross sectional SEM image of plain and modified membrane.**

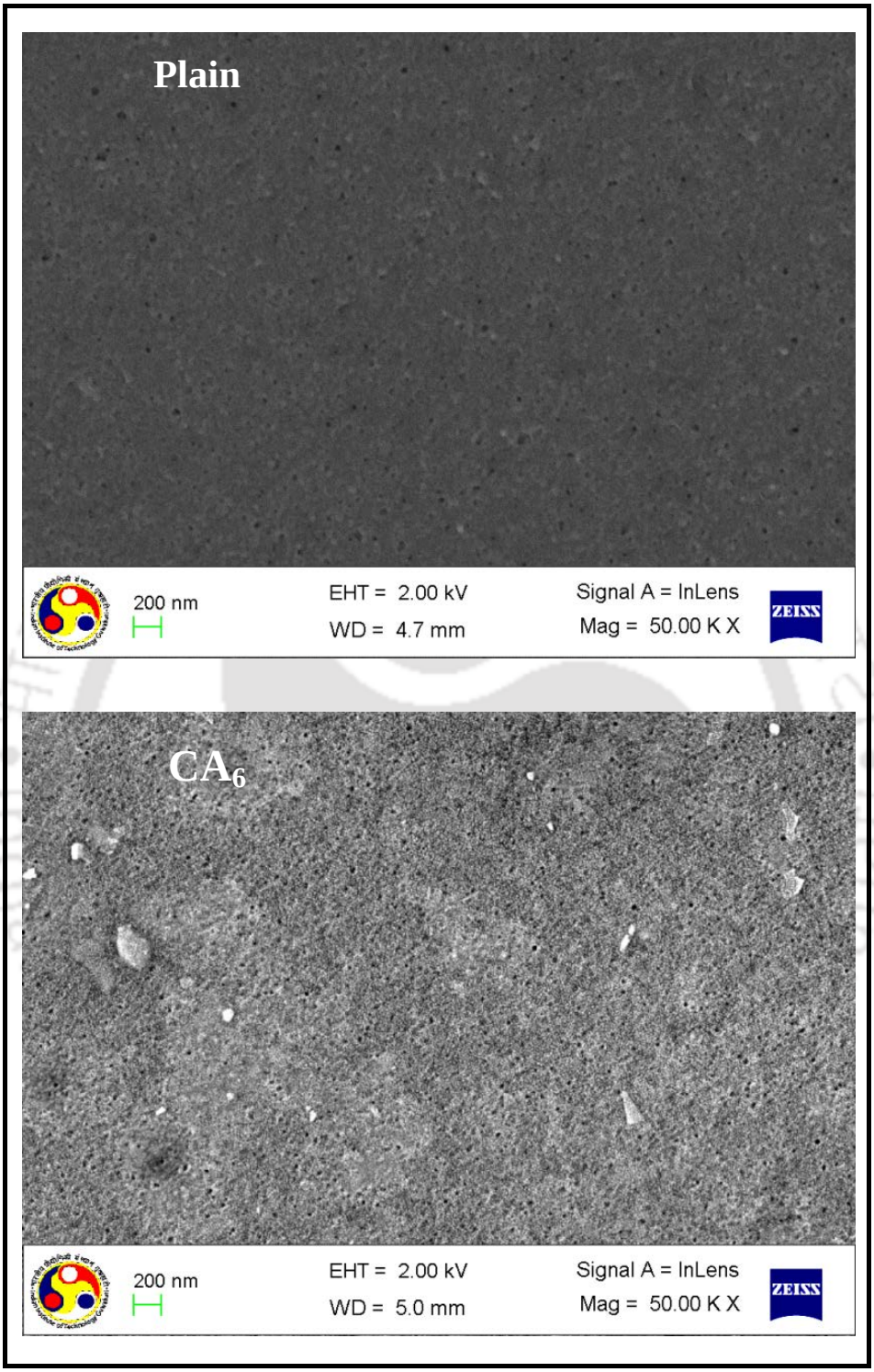


**Figure 7.7: Top surface FESEM image of plain and modified membranes.**

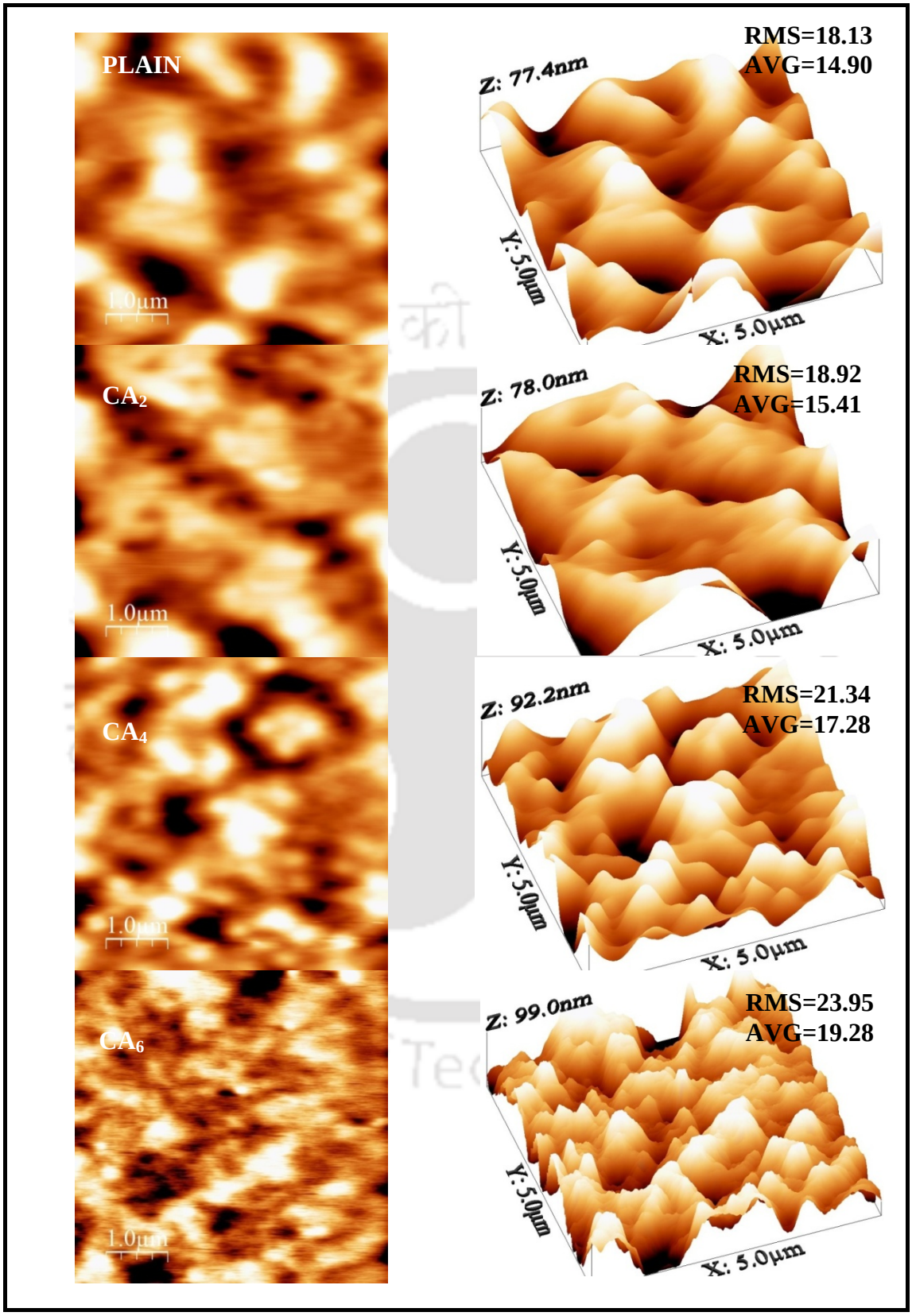


**Figure 7.8: Effect of PU-CA macromolecule wt % on surface roughness of PSF membranes.**

Figure 7.7 shows the top surface high magnification FESEM images of the plain and blended PSF membranes with 6 wt % of PU-CA. It can be seen that blended membrane has significantly lower pore size and higher pore density. According to Young and Chen [128], increase in the viscosity of blended casting solution causes increase in the ratio of nonsolvent inflow to solvent outflow. This in turn, increases the pore density of the modified membrane. It may be seen from Table 7.1 that the addition of PU in the membrane casting solution significantly increases the viscosity of the same. Furthermore, it was found that amphiphilic copolymer improves the permeation performance of membrane by working as pore forming agent. Zhao et al. and Lv et al also found similar type of results [89, 142].

Figure 7.8 shows the AFM images of plain PSF membrane and modified membranes with different wt % of PU-CA. It is observed from AFM topography images and their 3D reproductions that plain PSF membrane has relatively smooth surface and as the wt % of PU macromolecule increases in the membrane their top surface becomes rougher. RMS roughness and average roughness values for plain PSF membrane are 18.13 and 14.90, respectively. Same values for membrane $CA_6$ are 23.95 and 19.28, respectively. The reason for increase in roughness is the addition of amphiphilic PU macromolecules. The long chain of the PU stays with the bulk PSF phase and hydrophilic end group comes to the surface, also bulk phase amphiphilic macromolecules have tendency to migrate towards top surface during phase inversion process. This results in rougher surface as the wt % of amphiphilic macromolecule increases [110, 143].

#### 7.3.2.3. Pore size distribution study

Effect of different wt % of PU-macromolecule on pore size distribution was carried out by LLDP methods. This method estimates the pore size distribution of the membranes in wet state i.e. similar to the condition of UF operation. Pore size, pore density, total number of

pores and average pore size of all the membranes were determined using equations. 2.1, 2.4, 2.7 and 2.8, respectively. Total pore area per unit area of membrane was calculated with the help of equations. 2.5 and 2.6. Right side of the Figure 7.9a shows the LLDP flux profile through plain and modified membranes prepared with different wt % of PU-CA. From the LLDP flux data and by use of equation 2.4, pore number per unit area of different membranes were calculated which is shown in the Figure 7.9b. Nature of LLDP flux profile is almost same for all the membranes. Minimum pressure is required to start the flow, in the case of plain PSF membrane minimum pressure required to start the flow is 32 kPa, but for membrane $CA_6$ this value is 97 kPa. After the start of flow, penetrating liquid (alcohol rich) starts to swap the wetting liquid (water rich) in largest pores. Further, with the increase in pressure penetrating liquid swaps the wetting liquid in the smaller pores and as soon as all the

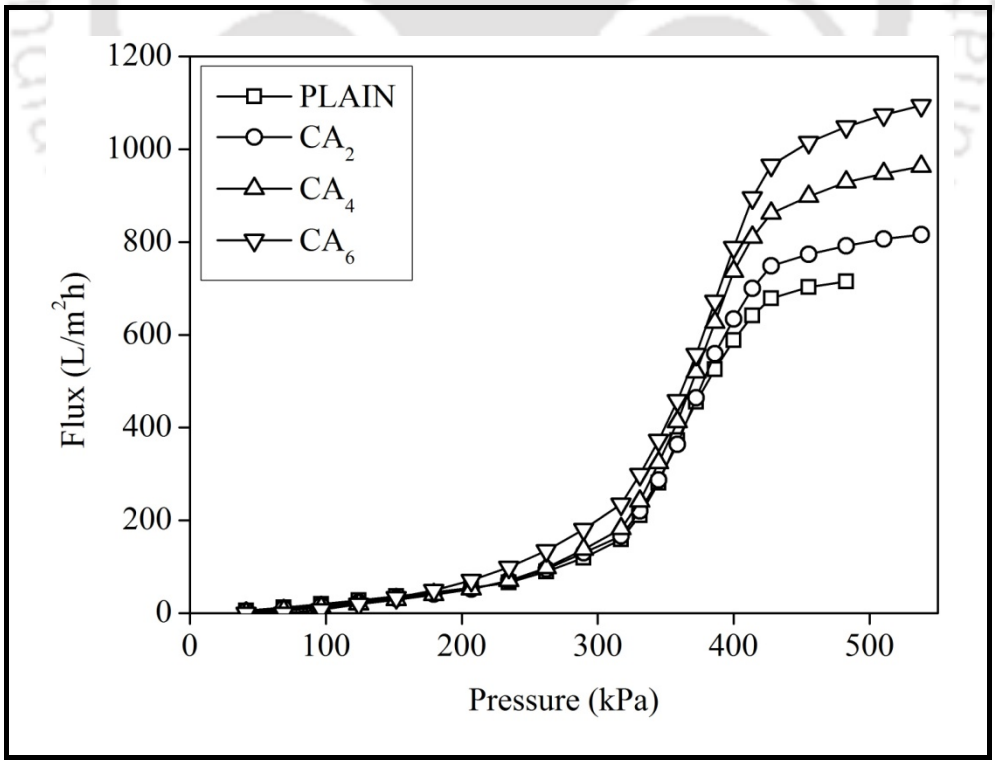


**Figure 7.9a: Effect of wt % of PU macromolecule on LLDP flux profile.**

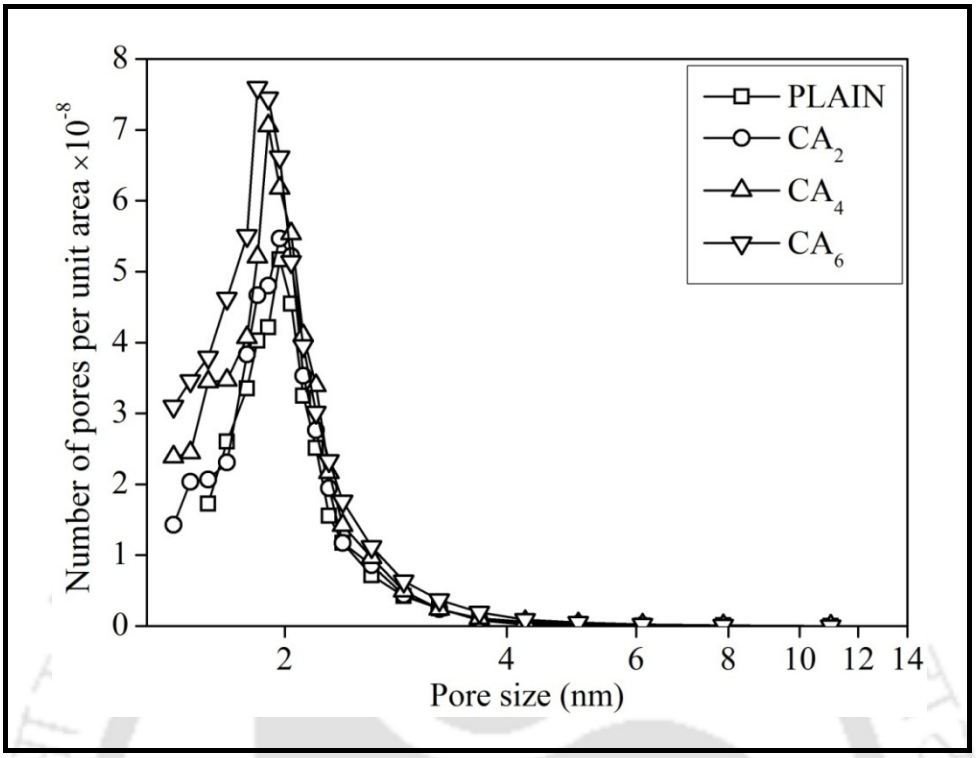


**Figure 7.9b: Effect of wt % of PU macromolecule on number of pores per unit area of membrane.**

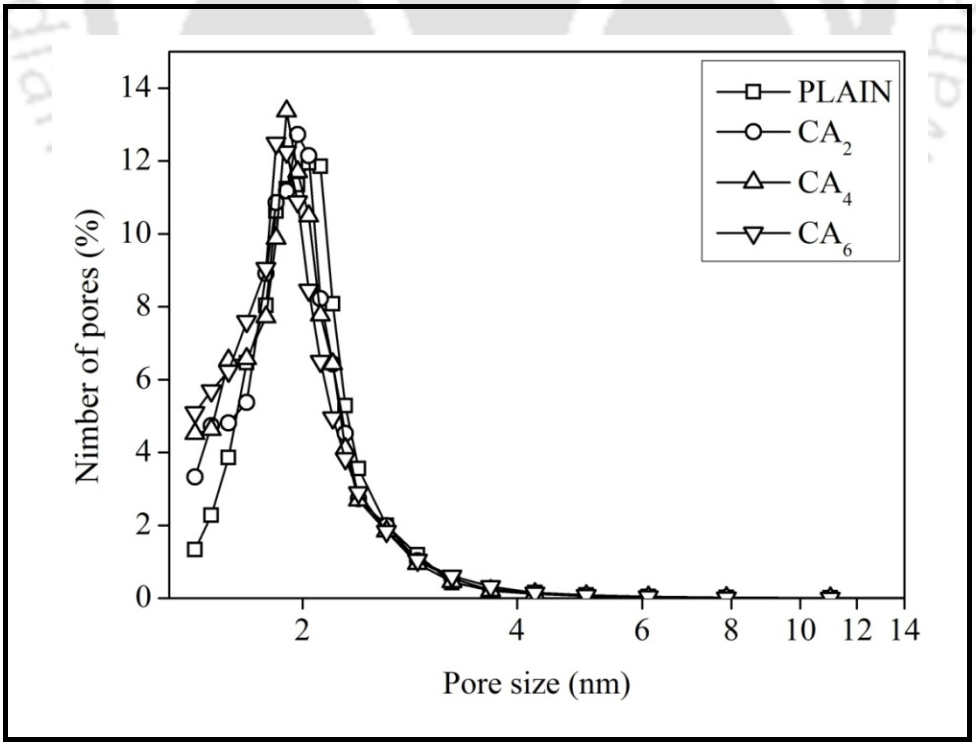


**Figure 7.10a: Effect of wt % of PU macromolecule on pore size distribution in percentage.**

pores of the membrane are opened by swapping the wetting liquid in the pores, the flux starts to remain almost constant (Figure 7.9a). As shown in LLDP flux profile in Figure 9a, in all the plots, from 300 kPa to 400 kPa, flux increases rapidly. This results in increasing number of pores from 4 nm to 2 nm.

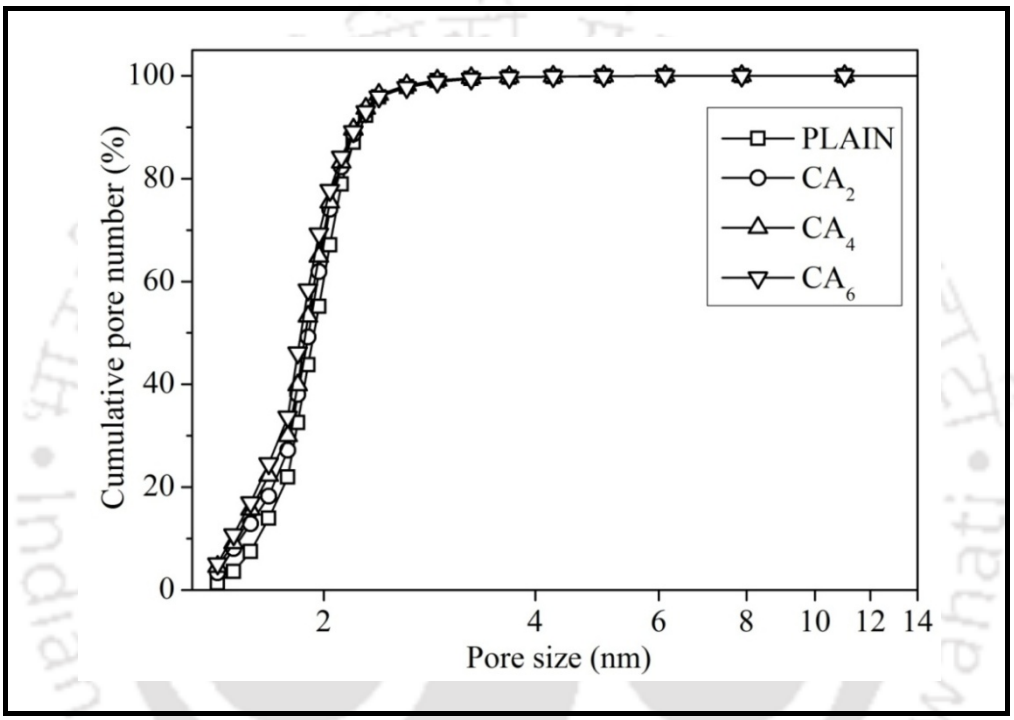


**Figure 7.10b: Effect of wt % of PU macromolecule on cumulative pore size distribution in percentage.**

Figure 7.10a shows the pore size distribution in percentage and figure 7.10b shows the cumulative pore size distribution. For all the membranes, size of more than 90 % of total pores is less than 3 nm, it shows that prepared membranes are appropriate for UF purpose. Results of LLDP study are shown in Table 7.2. It is observed that, with increase in wt % of PU-CA, total pore number per unit area ($N_t$) also increases resulting more porous membranes. It was reported that amphiphilic copolymers enhance the pore forming capacity for membranes by micelle formation and aggregation during phase inversion process [89, 142]. The total number of pores for plain membrane, $CA_2$, $CA_4$ and $CA_6$ are $3.63\times10^9$,

$4.29\times10^9$, $5.28\times10^9$ and $6.08\times10^9$ respectively. These results illustrate that PU-macromolecule content in membrane casting solution enhances the pore forming process, which is discussed in previous section. Also, these results are in line with morphological study of the membranes.

### 7.3.3. Pure water permeation and hydraulic permeability studies

Figure 7.11 shows the effect of wt % of PU macromolecule on the compaction profile during time dependent constant pressure (300 kPa) PWF and compaction factor (CF) is shown in Table 7.2. CF gives an account of the structure of membrane sub layer. Higher the CF, more likely the membrane compacts due to presence of large macrovoids in the sub layer. There is a sharp decline in PWF for all the membranes up to 45 min and after that PWF remains almost constant. Due to compaction the walls of the pores become closer, denser and uniform resulting reduction in pore size as well as the flux [1]. From the inset of the figure 10a it is found that the steady state PWF increases with increase in wt % of PU macromolecule. Steady state flux for plain membrane and membrane $CA_6$ is 102.4 L/m$^2$h and 138.2 L/m$^2$h, respectively. The increase in steady state flux is due to the higher pore density, as shown in Figures 7.7 and 7.9a.

Effect of wt % of PU macromolecule on PWF of the membrane at different transmembrane pressure is shown in Figure 10b. This experiment was done at different transmembrane pressure between 100 - 300 kPa at a difference of 50 kPa. For all the cases, PWF increases almost linearly with increase in pressure. It is seen that at a pressure of 100 kPa, PWF for all the membranes is almost same but at higher pressure PWF for membrane $CA_6$ is much higher compared to plain membrane. This might be because of much superior smaller pore density for membrane $CA_6$ compared to plain membrane, which was reported in Figures 7 and 9a. These results are in agreement with the findings of compaction studies and

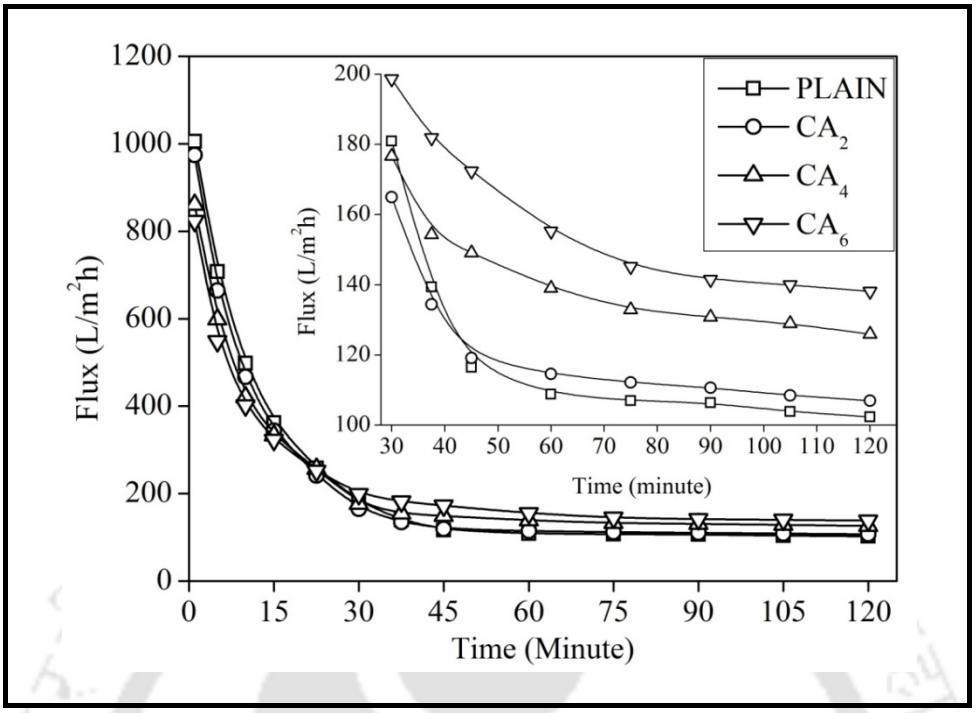


**Figure 7.11: Effect of wt. % of PU macromolecule on constant pressure flux.**

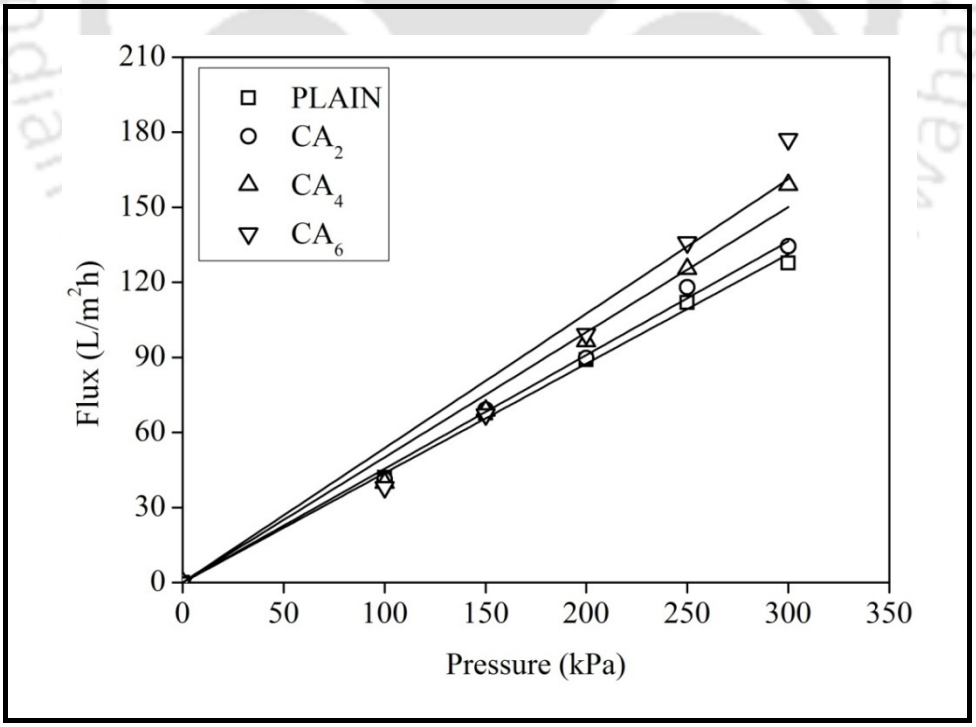


**Figure 7.12: Effect of wt. % of PU macromolecule on hydraulic permeability.**

also with the water contact angle measurements. Pressure dependent flux profiles were usedto calculate the hydraulic permeability ($P_m$) of the membranes. $P_m$ was increased from 0.43 to 0.597 L/m$^2$ h kPa (Table 7.2) for plain membrane to modified membrane with highest PU macromolecule content. Findings of the pure water permeability and hydraulic permeability studies evidently shows that addition of PU macromolecule improves the pore forming activity and also reduces the chance of bigger pore formation in the membranes, which affect the permeability as it is theoretically related to membranes pore for ultrafiltration membranes [9]. These finding are uniform with morphological study, hydrophilicity and pore size distribution study of the membranes reported in the preceding sections.

**Table 7.2: Effect of PU macromolecule on some characterization parameters.**

| Membrane | $N_t$ (m$^{-2}$) × 10$^{-9}$ | $A_t$ (m$^2$) × 10$^8$ | $r_m$ (nm) | CF | $P_m$ (L/m$^2$ h kPa ) |
|---|---|---|---|---|---|
| **Plain** | 3.63 | 4.66 | 1.99 | 9.85 | 0.433 |
| **$CA_2$** | 4.29 | 5.33 | 1.96 | 9.18 | 0.461 |
| **$CA_4$** | 5.28 | 6.4 | 1.94 | 6.88 | 0.532 |
| **$CA_6$** | 6.08 | 7.28 | 1.91 | 5.96 | 0.597 |

## 7.3.4. Membrane hydration and BSA adsorption studies

Bio-foulants like BSA strongly interacts with hydrophobic membrane surfaces and thereby causes significant water flux decline by fouling during the ultrafiltration. In this regard, it is of major concern to fabricate membranes with ability to resist protein adsorption. The physical deposition of foulants can be reduced by controlling the membrane surface hydrophilicity. Therefore, in this chapter membranes are modified by different amphiphilic

PU macromolecule to increase the surface hydrophilicity of the fabricated membranes. Water contact angle (WCA) for different membranes are shown in Figure 7.13. Hydrophilic behaviour of the membrane is explained by water contact angle measurement. Lower the WCA value higher will be the hydrophilicity of the membranes and more hydrophilic membranes are less prone towards fouling. Therefore, WCA is a significant parameter in membrane separation process and very much related to membrane's fouling behaviour. For unmodified membrane CA is 63.5$^{o}$ and for membrane ($CA_6$) with highest PU-CA content it decreased considerably to 49.5$^{o}$. These results are consistent with the finding of AFM roughness parameter results. It was stated that hydrophilic surface had smaller WCA due to higher surface roughness [144]. According to Zhao et al. [89], when an amphiphilic modifier is incorporated for the membrane modification, the improvement in hydrophilicity is an inclusive result which includes the structure changes as well as the constitution evolution. In present case, the increased surface porosity as well as the higher hydrophilic constitution is deliberation to promote the membranes hydrophilicity. In case of membrane with different additive, it was found that hydrophilicity was increased as the number of –COOH group in end capping was increased. It is well known that presence of carboxylic group at the end enhances the hydrophilic behaviour of PU macromolecule. So, hydrophilicity increases with the number of carboxylic group.

It has been discussed that with the increase in wt % of PU macromolecule, surface hydrophilicity had increased for blended membranes. Though, the estimation of protein adsorption on the membrane surfaces should be considered not only with respect to surface hydrophilicity but also with respect to the hydration capacity of the membranes [144]. It is reported that, the formation of the bound water layer on a surface is considered crucial to repel protein and generate anti-bio fouling surface [145]. Figure 7.14 shows the adsorption of BSA and hydration capacity of membranes as a function of PU-CA content in membranes as

well as with different PU macromolecule. The addition of amphiphilic PU macromolecule reduces the adsorption of BSA molecule from 0.14 mg/cm$^2$ for plain membrane to 0.019 mg/cm$^2$ for $CA_6$ membrane. On the other hand, hydration capacity of membrane increases dramatically with the addition of PU macromolecule. For plain membrane hydration capacity value is around 130 mg/cm$^3$, where as for membrane $CA_6$ that value is around 225 mg/cm$^3$. In case of different PU macromolecule, PU-CA has highest hydration capacity and lowest BSA adsorption. These indicated that larger the number of –COOH group, the more hydrophilic, more hydration capacity and lower BSA adsorption amount takes place. The results also confirmed that blending the amphiphilic PU macromolecule could stem the adsorption of protein molecules, since hydrophilic copolymer could restrain the protein adsorption amount by forming bound hydration layer on membrane surface.

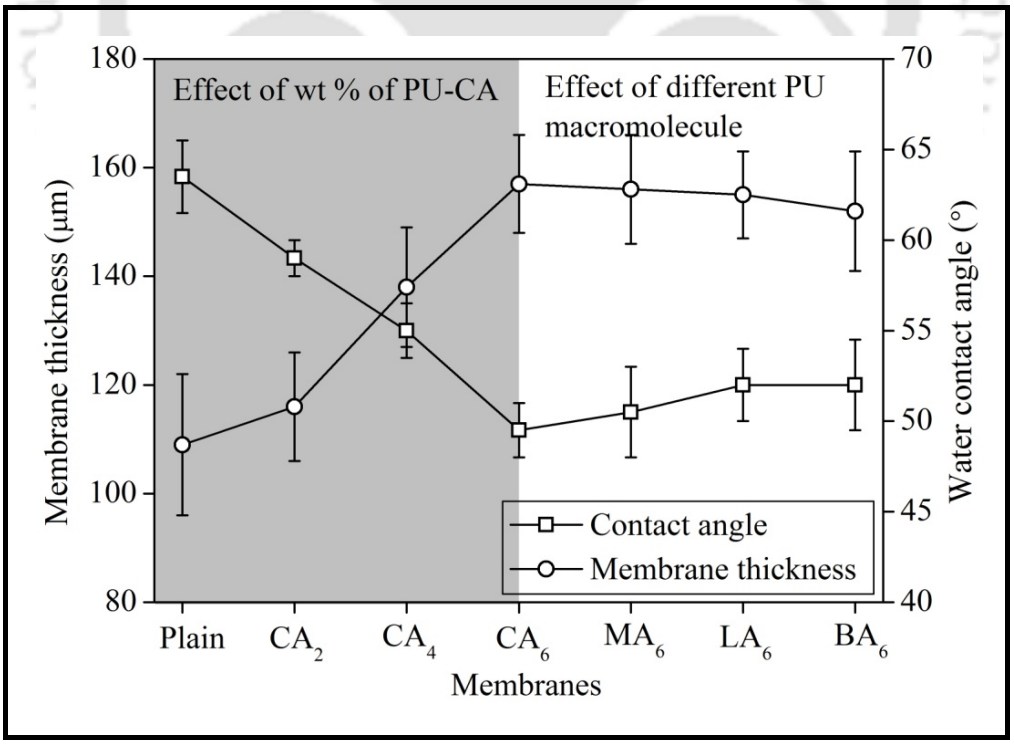


**Figure 7.13: Membrane thickness and water contact angle of fabricated membranes.**

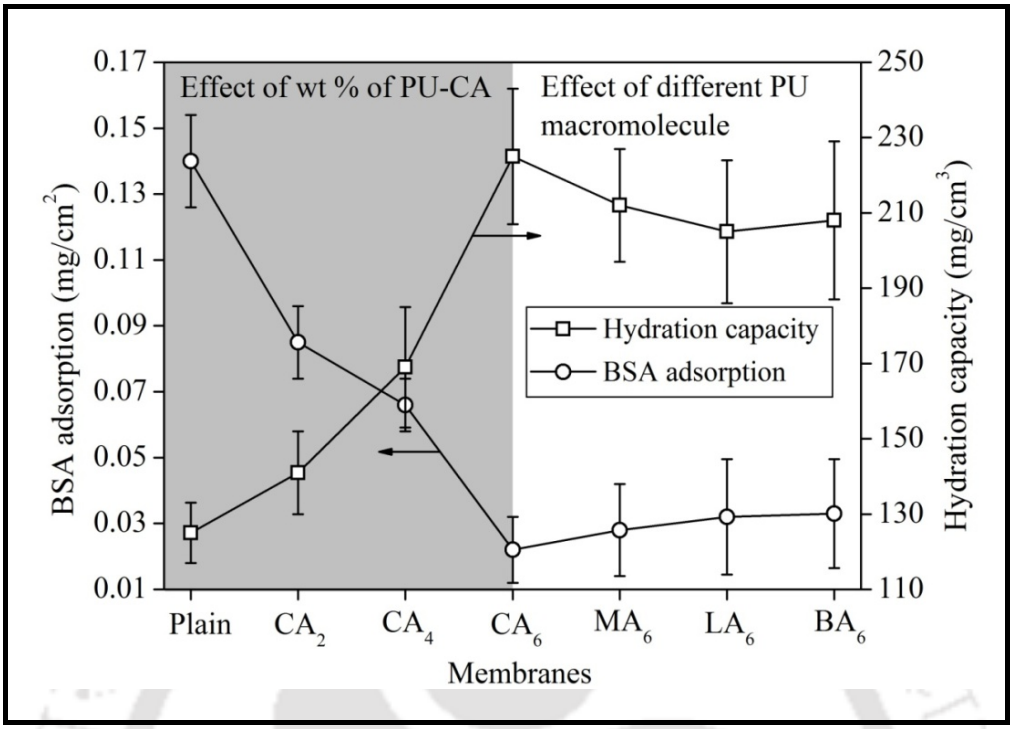


**Figure 7.14: BSA adsorption and hydration capacity of fabricated membranes.**

The measured quantity of the hydration capacity is result of trapping of water in porous structure of membrane, binding of water molecules around the hydrophilic segment of amphiphilic brushes and entrapped water molecules in the confined spaces between amphiphilic chains. So, hydration capacity of plain membrane was attributed to only porous structure compared to blended membranes. In addition Figure 7.14 as well as SEM images in Figure 7.6, reporting the evolution of membrane thickness as function PU macromolecule content. These supported the fact that the membrane shrinkage during its formation must be prevented by amphiphilic PU macromolecule. Thus, the increases in blending amount of PU macromolecule associated with the increase in amount of hydrophilic brush like structure due to the self rearrangement of amphiphilic copolymer on the membrane surface. This in result increased the hydration capacity, which is dependent on the bound and entrapped water

molecules. So, the formation of bound water layer on blended membrane was regarded as vital to repel proteins and generate the bio fouling resistant surface.

### 7.3.5. Ultrafiltration and fouling studies

The time dependent flux of membranes modified with different wt % of PU-CA and with different PU macromolecule is shown in Figures 7.15a and 7.15b. DI water flux was measured from 0 - 60 min, 180 - 240 min, 360 - 420 min and BSA flux was measured from 60 - 180 min and 240 - 360 min. During water permeation, a slight loss of flux is observed through initial time of water permeation and after that it remains constant for all the membranes, but during BSA permeation, a severe flux loss was seen in initial permeation for all the membranes. It is significant to note that blended membranes have lesser flux loss than plain membrane. It may be seen from Figure 7.15a, as time passes, the difference between the flux of plain membrane and modified membranes increases and for membrane modified with higher wt % of PU macromolecule, flux becomes higher compared to other membranes. Similarly, for membranes modified with different PU macromolecule, initially flux is almost same but as the time progresses difference between the flux of different membranes increases. Membrane containing PU-CA had the highest flux at the end of experiment. The main reason is end cap of PU-CA macromolecule contains most number of hydrophilic –COOH group. The more hydrophilic the membrane was, the less decrease in the flux. Deposition or adsorption of BSA molecules inside the pores or on the surface of membranes is the reason of initial loss of flux during BSA UF. So, the fouling resistance membrane should effectively resist the adsorption or deposition of foulants to their surface or pore as reported in literatures [118, 139].

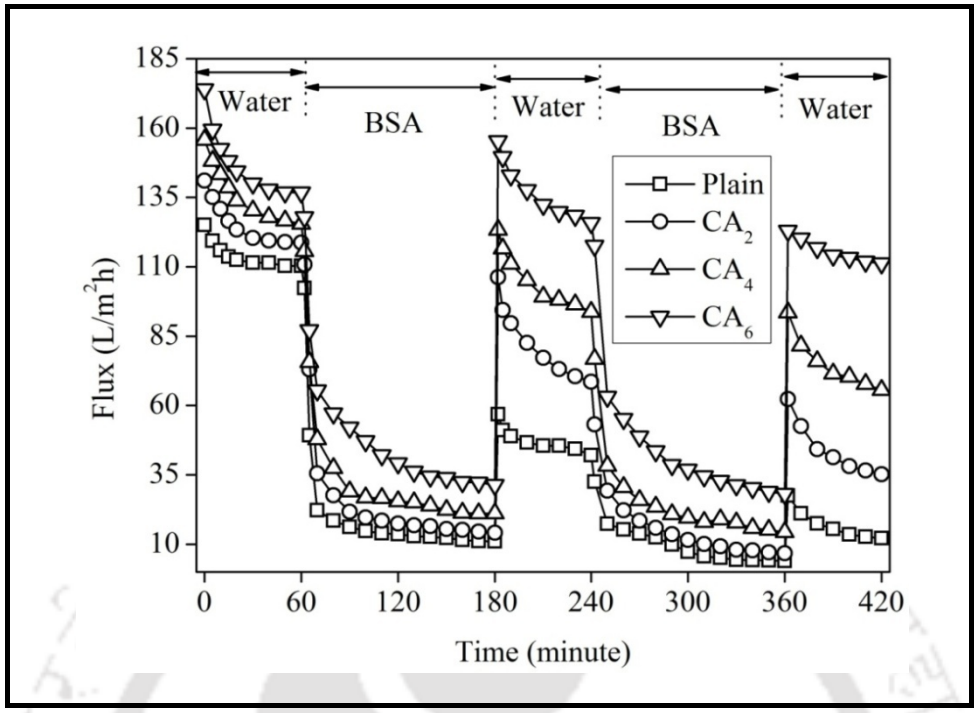


**Figure 7.15a: Effect of wt. % of PU macromolecule on time dependent flux; millipore water: 0-60 min, 180-240 min and 360-420 min; BSA solution: 60-180 min and 240-360 min.**

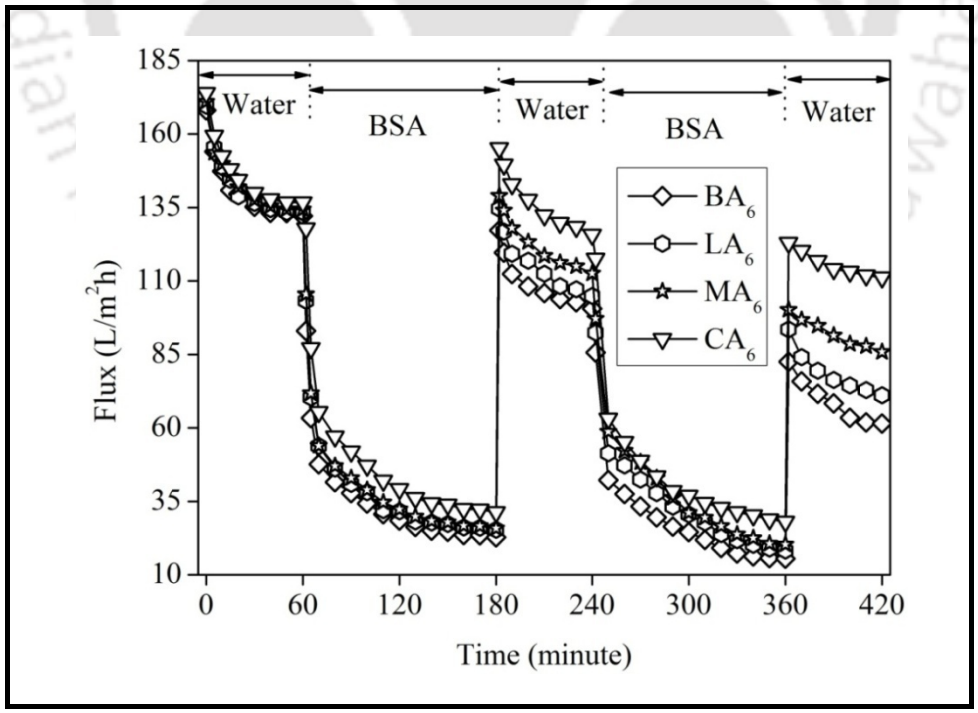


**Figure 7.15b: Effect of different PU macromolecule on time dependent flux; millipore water: 0-60 min, 180-240 min and 360-420 min; BSA solution: 60-180 min and 240-360 min.**

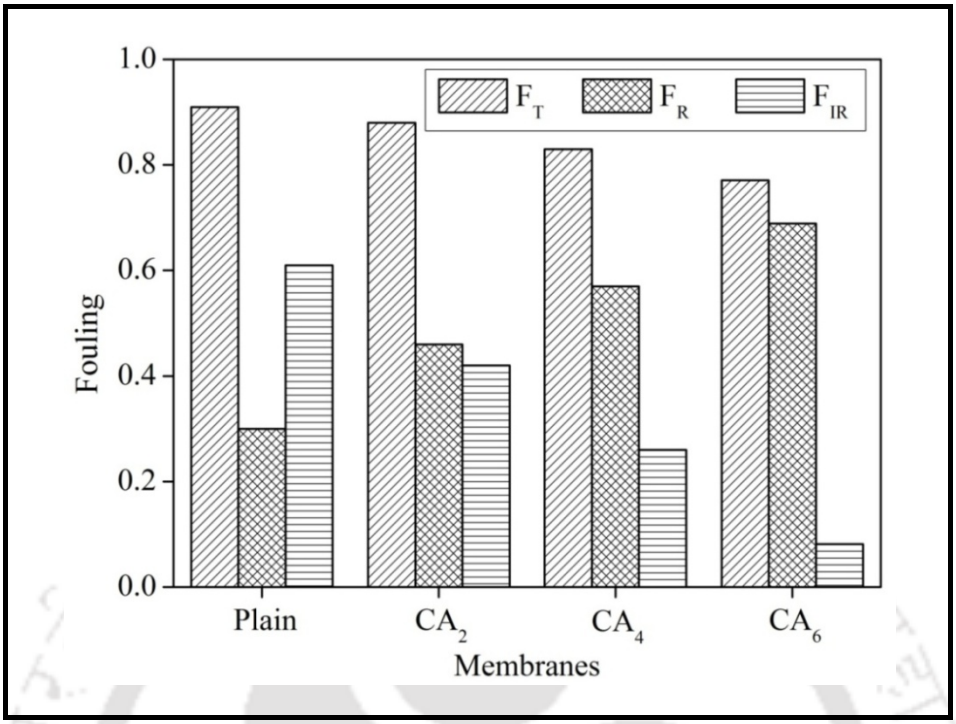


**Figure 7.16a: Effect of wt. % of PU macromolecule on fouling parameters.**

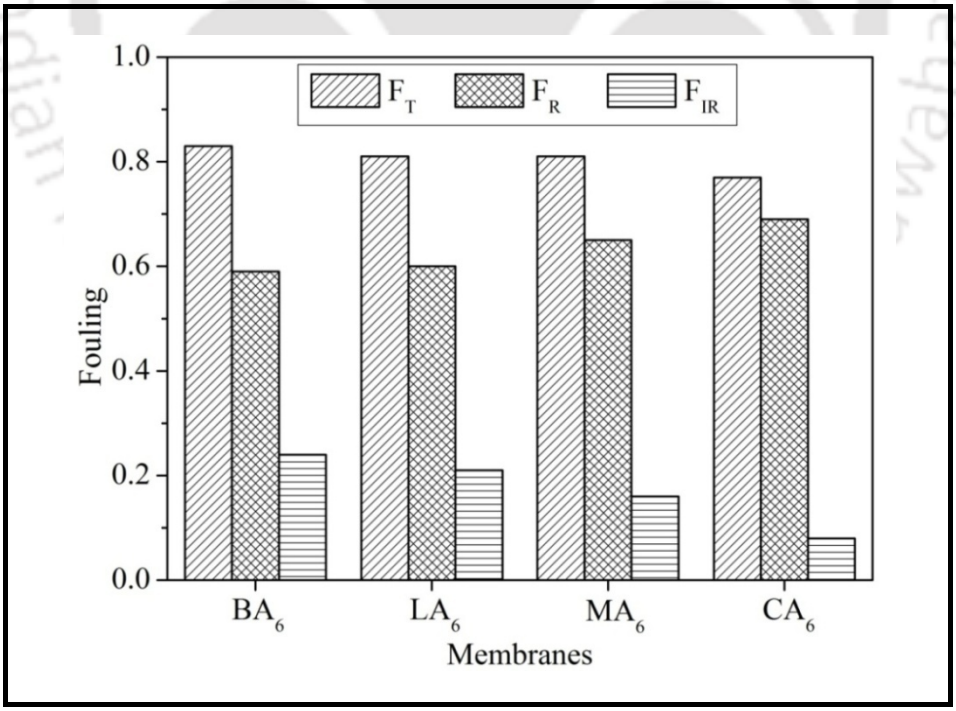


**Figure 7.16b: Effect of different PU macromolecule on fouling parameters.**

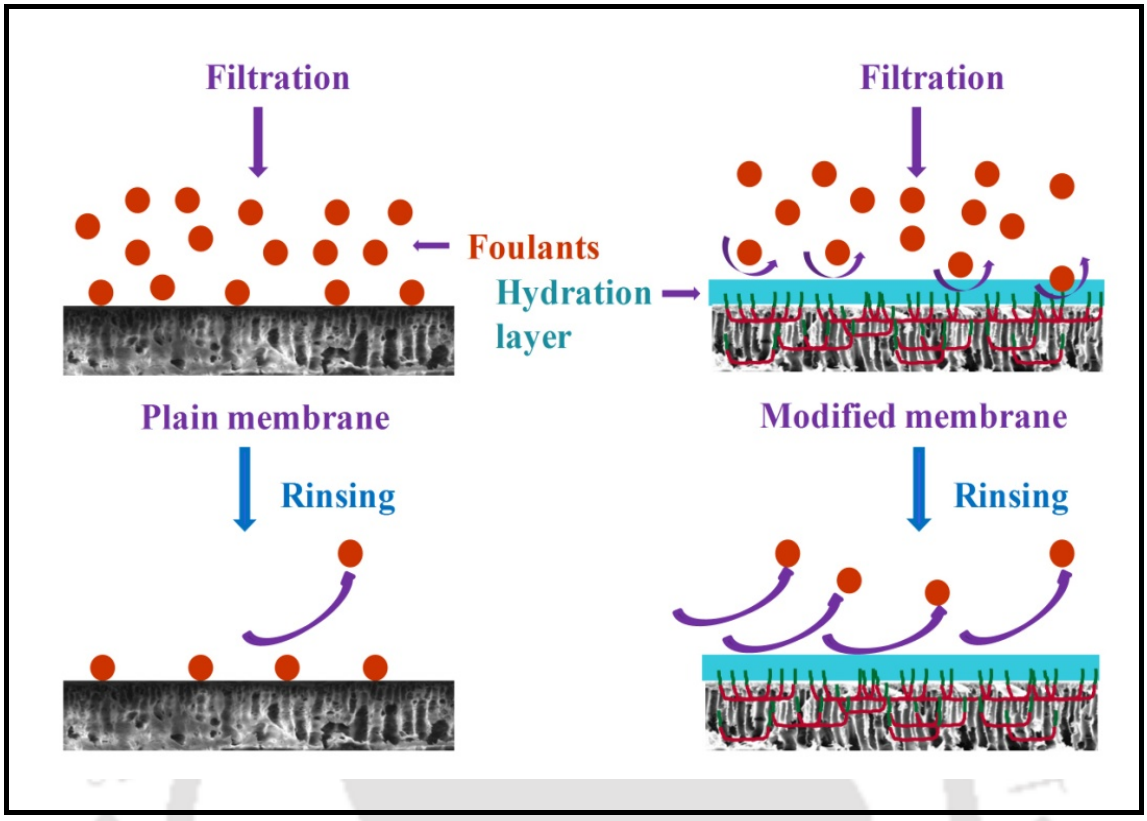


**Figure 7.17: Schematic representation of fouling resistant behaviour.**

Total membrane fouling composed of reversible and irreversible fouling. Reversible deposition or adsorption of foulants, which can be removed by simple hydraulic cleaning, is termed as reversible fouling ($F_r$). Irreversible adsorption of membrane, which can only be removed by chemical cleaning, is termed as irreversible fouling ($F_{ir}$). Sum of $F_{ir}$ and $F_r$ is total fouling. To further investigate the fouling resistant behaviour of the membrane, $F_{ir}$ and $F_r$ values were calculated from Figure 7.15 by using equations 2.17-2.19 and are shown in Figures 7.16a and 7.16b. It can be seen (Figure 7.16a) that as the PU-CA content is increased in modified membranes, $F_{ir}$ values are reduced remarkably with compared to plain membrane and so, the $F_r$ values are increased. Furthermore the sequence of flux recovery ratio and fouling values are consistent with hydrophilicity, hydration capacity and BSA adsorption trend of membranes. Figure 7.17 shows the fouling resistant behaviour of membrane. It was

stated that under static fouling condition, the interfacial energy between a surface and water was expected to play a vital role in inducing antifouling property to membrane surface [146]. In this case also, the hydrophilic segment of the PU macromolecule could form hydration layer through hydrogen bonding, exhibiting anti fouling property and efficiently thwart adsorption deposition of foulants. However, one can observe that $F_r$ values increased after addition of amphiphilic PU macromolecule. The possible reason could be accumulation of more BSA on membrane surface due to comparatively increased BSA rejection. Even though increased $F_r$ value, the $F_t$ value showed a reducing trend due to remarkable decrease in $F_{ir}$ value. So, these trends suggest that anti fouling property, especially irreversible fouling of modified PSF membrane was enhanced appreciably via blending of amphiphilic PU macromolecule.

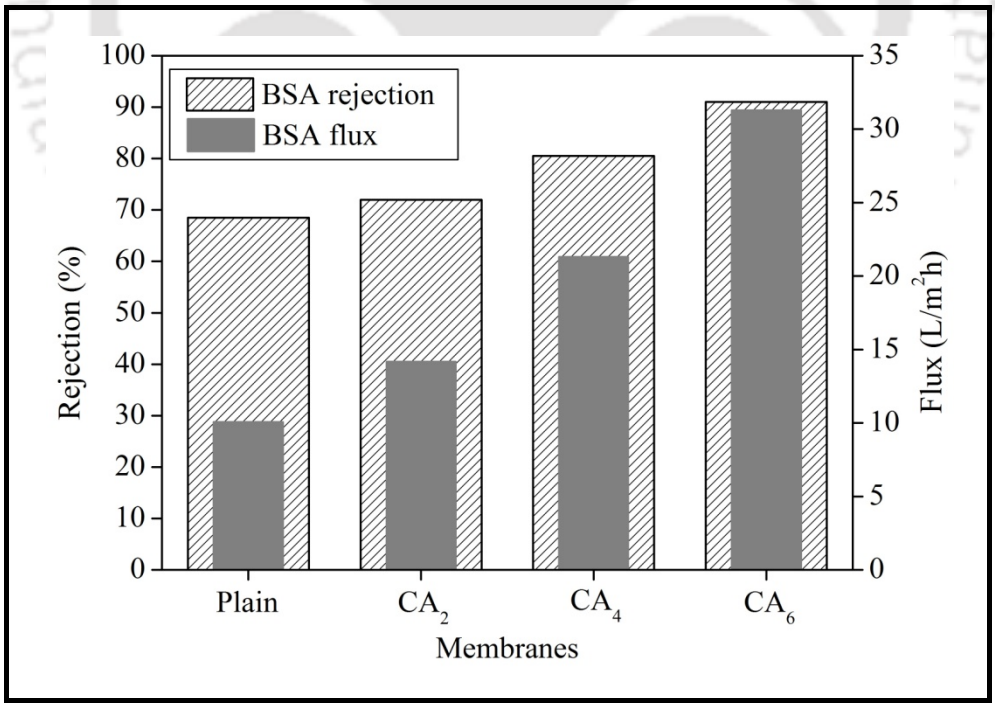


**Figure 7.18a: Effect of wt % PU macromolecules on BSA flux and rejection.**

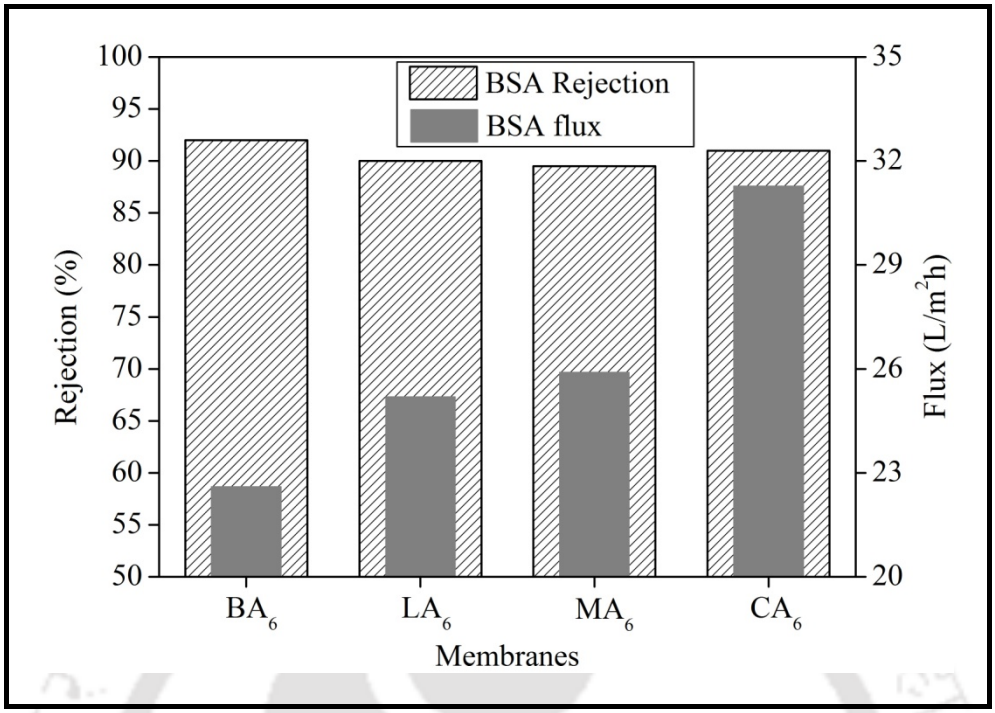


**Figure 7.18b: Effect of different PU macromolecules on BSA flux and rejection.**

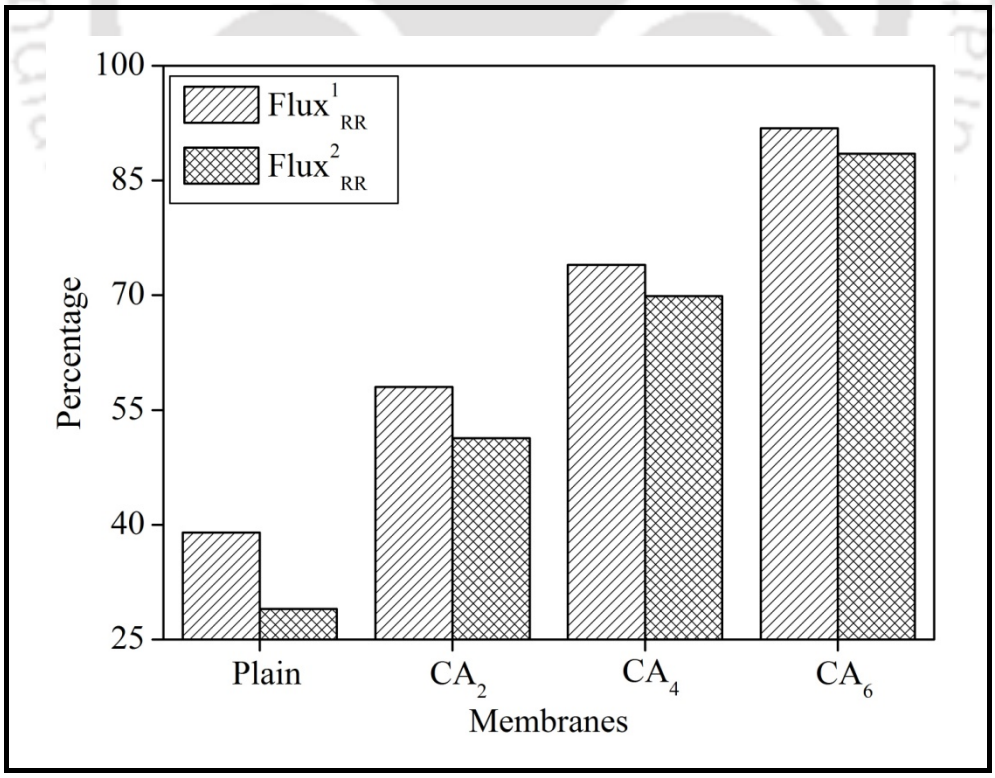


**Figure 7.19a: Effect of wt % PU macromolecules on flux recovery ratio.**

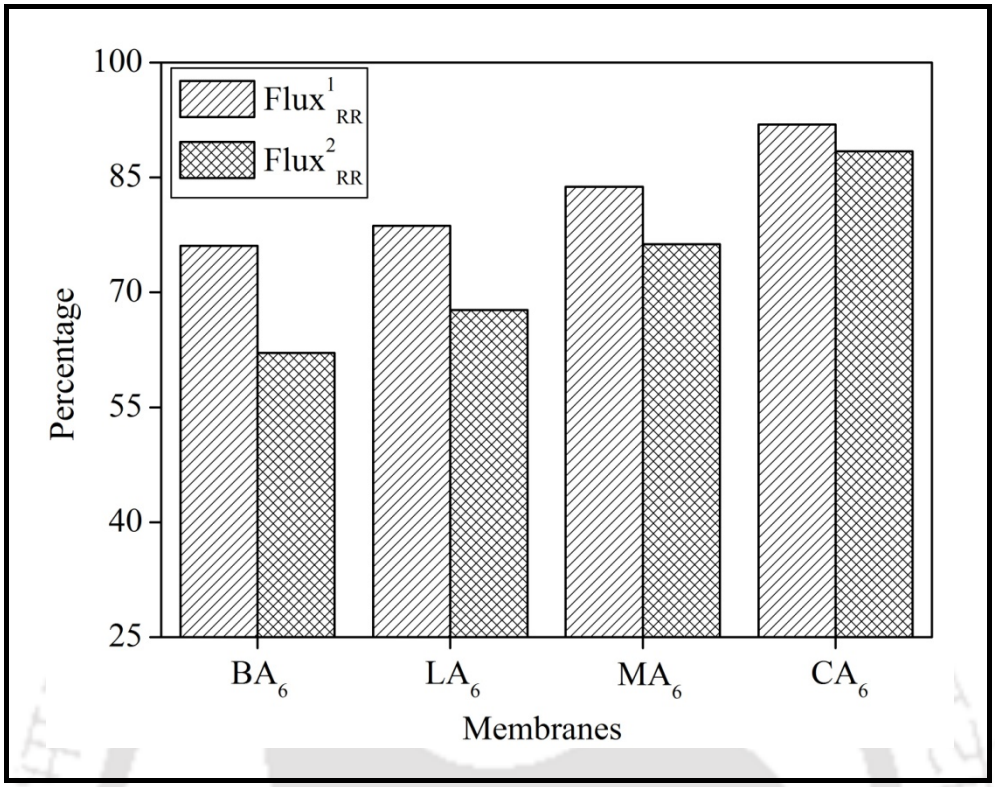


**Figure 7.19b: Effect of different PU macromolecules on flux recovery ratio.**

Figure 7.18 shows the BSA rejection and flux for different membranes. It is already reported in the preceding section that amphiphilic PU macromolecule not only enhances the hydrophilicity but also pore forming capacity. So, the flux as well as BSA rejection was higher for modified membranes. In case of different PU macromolecule, PU-CA has most number of carboxylic groups, hence membrane $CA_6$ had highest flux as well as flux recovery ratio. Second time flux recovery ratio ($Flux^2_{RR}$) for plain membrane is much lower than $Flux^1_{RR}$, in case of membrane $CA_6$, it is almost same (Figure 7.19). The main reason is, plain membrane had already some amount of deposited or adsorbed BSA on their surface, which again increased after second round of BSA ultra filtration. $Flux^2_{RR}$ value came close to $Flux^1_{RR}$ value, with the increase in wt % of PU macromolecule. Similarly for different additive, results are in line with hydrophilicity study of membranes.

# Chapter 8

## Fabrication of novel thermo responsive PSF membrane, with cross linked PVCL–co–PSF copolymer for protein separation and easy cleaning

# Chapter 8
# Fabrication of novel thermo responsive PSF membrane, with cross linked PVCL-co-PSF copolymer for protein separation and easy cleaning

*In this chapter an amphiphilic thermo responsive cross linked polyvinylcaprolactam-co-polysulfone (PVCL-co-PSF) copolymer was synthesized via solution polymerization of vinylcaprolactam (VCL) in PSF solution by use of three different initial ratio of PSF to VCL monomer. After the synthesis of copolymer, required amount of PSF was dissolved in PVCL-co-PSF copolymer solution. Presence of copolymer in blended membrane was confirmed by Fourier transform infrared-attenuated total reflectance (FTIR-ATR) spectroscopy. Blended membranes showed enhanced pure water flux, hydrophilicity and evident of thermo sensitivity. Hydration capacity of prepared membranes was measured at two different temperatures i.e. at 25 to 40 ˚C. Reversible volume phase transition of PVCL around the lower critical solution temperature (LCST) was used as an environmentally-friendly approach for membrane cleaning. Temperature change water elution hydraulic cleaning for modified membranes around the LCST of the PVCL-co-PSF copolymer brushes was proposed.*

## 8.1. Experimental

### 8.1.1. Materials

Polysulfone (PSF), N,N'-methylenebisacrylamide (MBAA), N–vinylcaprolactam (VCL), N-methylpyrrolidone (NMP), bovine serum albumin (BSA) and azobisisobutyronitrile (AIBN)

Content of this chapter has been submitted for publication as below:

M K Sinha, M K Purkait, Preparation of novel thermo responsive PSF membrane, with cross linked PVCL-co-PSF copolymer for protein separation and easy cleaning, RSC Adv. (Submitted on 25/09/2014)

were used in this chapter, further details related to these chemicals are given in Table 2.1 of chapter 2.

### 8.1.2. Synthesis of PVCL-co-PSF copolymer and fabrication of modified PSF membranes

The cross-linking of VCL in PSF solution was carried out by free radical polymerization of VCL in NMP solvent. Azoisobutyronitrile (AIBN) was used as the initiator and N, N'-methylene bisacrylamide (MBAA) was used as the cross-linking reagent. All the reactants i.e. VCL, PSF, MBAA, AIBN and NMP were taken in a three neck round bottom flask; thereafter the reaction mixture was purged with pure nitrogen gas to remove oxygen which could act as a scavenger in the radical polymerization. After the purging with nitrogen gas, polymerization reaction was carried at 70 ˚C for 24 h. After the completion of reaction required amount of PSF and PEG4000 was directly dissolved in PVCL-co-PSF copolymer solution, so that the total concentration of PSF was 15 % and that of PEG4000 was 7 %. This mixture was vigorously mixed at 50 ˚C for 12 h and further degassed for 6 h at 50 ˚C. The solution was then casted on a clean glass plate with a casting knife maintaining a uniform thickness of 200 µm, in the ambient atmosphere. Afterwards the casted membrane was immersed into the coagulation bath at room temperature. The prepared membranes were kept in fresh deionized water for overnight to eliminate any residual solvent. Finally, membrane sheets were air dried at room temperature. Steps for the fabrication of modified membranes are shown in Figure 8.1 and composition of different membrane casting solutions are shown in Table 8.1.

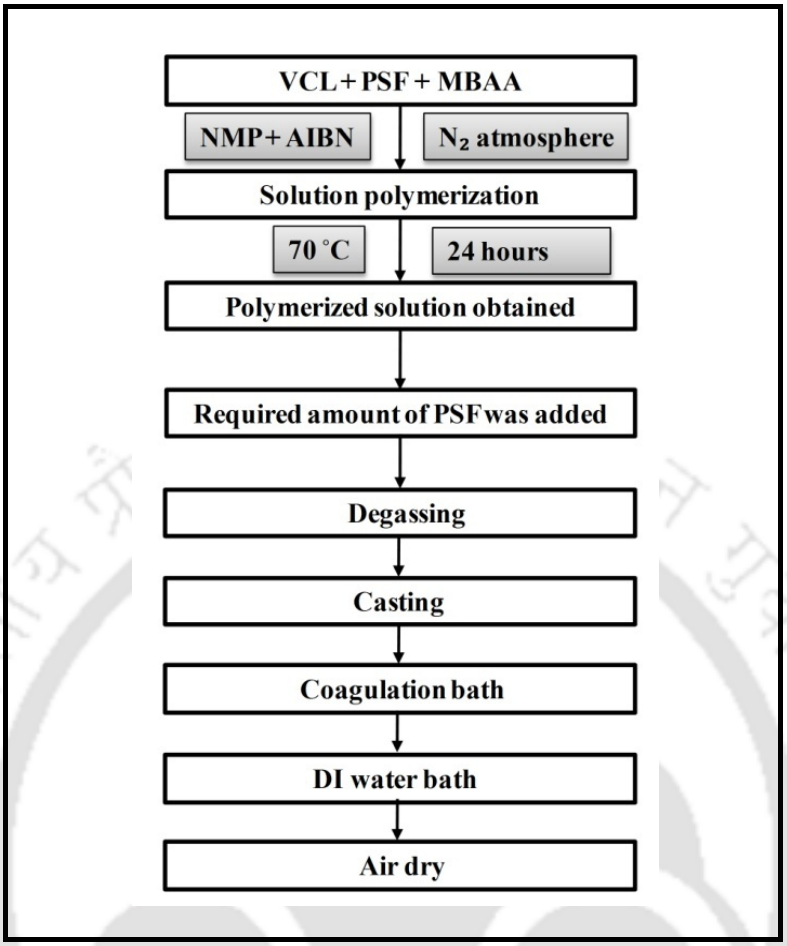


**Figure 8.1: Steps for fabrication of PVCL-co-PSF modified membranes.**

**Table 8.1: Composition of membrane casting solution containing PVCL-co-PSF copolymer.**

| Membrane Solution | Ratio of PSF:VCL | PSF I | VCL | MBAA | PEG 4000 | PSF II | NMP |
|---|---|---|---|---|---|---|---|
| **Plain** | – | – | – | – | 7 | 15 | 78 |
| **$M_{05}$** | 2:05 | 1 | 2.5 | 035 | 7 | 14 | 75.15 |
| **$M_{10}$** | 2:10 | 1 | 5.0 | 0.60 | 7 | 14 | 72.4 |
| **$M_{15}$** | 2:15 | 1 | 7.5 | 0.85 | 7 | 14 | 69.65 |

## 8.2. Membrane characterization

### 8.2.1. Surface characterization

The presence of cross linked PVCL-co-PSF copolymer in blended membrane was confirmed by ATR-FTIR. Morphological study of the plain and modified membranes was done by FESEM and SEM. Water contact angle (CA) between membrane surface and water droplet is the measure of the hydrophilicity of the membrane surface, smaller the contact angle, higher the hydrophilicity of the surface. Average of 8 contact angle measurements was considered for all the prepared membranes. Hydration capacity of the fabricated membranes was also studied in terms of amount of absorbed water per unit volume of membranes ($mg/cm^3$). Thicknesses of the membranes for calculation of volume of membranes were measured by a digimatic measuring unit at 10 different places and average was taken. The adsorption of BSA on membrane surface is an important parameter for the estimation of fouling behaviour of membranes. Three duplicate tests were performed for each membrane. Details of these membrane characterization techniques and instrumentation details are provided in section 2.3 of chapter 2.

### 8.2.2. Pure water permeation and filtration experiments

All the membranes were compacted for 2 h at transmembrane pressure of 400 kPa and flux was measured at regular interval. After the compaction water permeation through all the membranes at different pressure was measured and hydraulic permeability ($L_m$) was measured using that data. The flux was measured by using the equation 2.9. Hydraulic permeability ($L_m$) ($L/m^2h$ kPa) is calculated from the slope of the plot of $J_w$ vs $P$ from the equation 2.11.

For evaluation of fouling due BSA ultrafiltration, all the membranes were first compacted at 300 kPa for 30 minute. Then pressure was reduced to 250 kPa and pure water flux was measured at regular interval for 60 minutes. Flux at the end of 60 minute was termed as $J_{w1}$. Subsequently feed was changed with 1000 PPM BSA solution and BSA flux was measured for next 120 minutes. BSA flux at the end of this 120 minute was called as $J_{BSA}$. BSA rejection was measured UV-VIS spectroscopy by using equation 2.16.

## 8.3. Results and discussions

### 8.3.1. FTIR analysis

Figure 8.2 shows ATR-FTIR spectra of plain and blended PSF membranes surfaces fabricated with different initial ratio of PSF and VCL monomer. The peaks at 1158 $cm^{-1}$ and 1287 $cm^{-1}$ are due to –C–O–C– and S=O group present in PSF, thus verifying the presence of PSF. A new peak become visible around 1529 $cm^{-1}$, confirms the presence of secondary amide group present in N,N'-methylenebisacrylamide (used as cross linker for PVCL-co-PSF copolymer). The most important change is the emergence of new peaks at around 1658 $cm^{-1}$ 1476 $cm^{-1}$ which confirms the presence of PVCL in membrane matrix. The peak at 1476 $cm^{-1}$ is due to –CH- group attached to nitrogen atom on PVCL structure and the peak at 1658 $cm^{-1}$ is due to the tertiary amide group present in PVCL segment of copolymer. The intensity of these peaks is much higher for membrane $M_{15}$ compared to $M_{05}$, it means membrane $M_{15}$ has more amount of PVCL segment present in copolymer, as VCL monomer was present in higher ratio for initial cross linking polymerization reaction for membrane $M_{15}$ compared to membrane $M_{05}$.

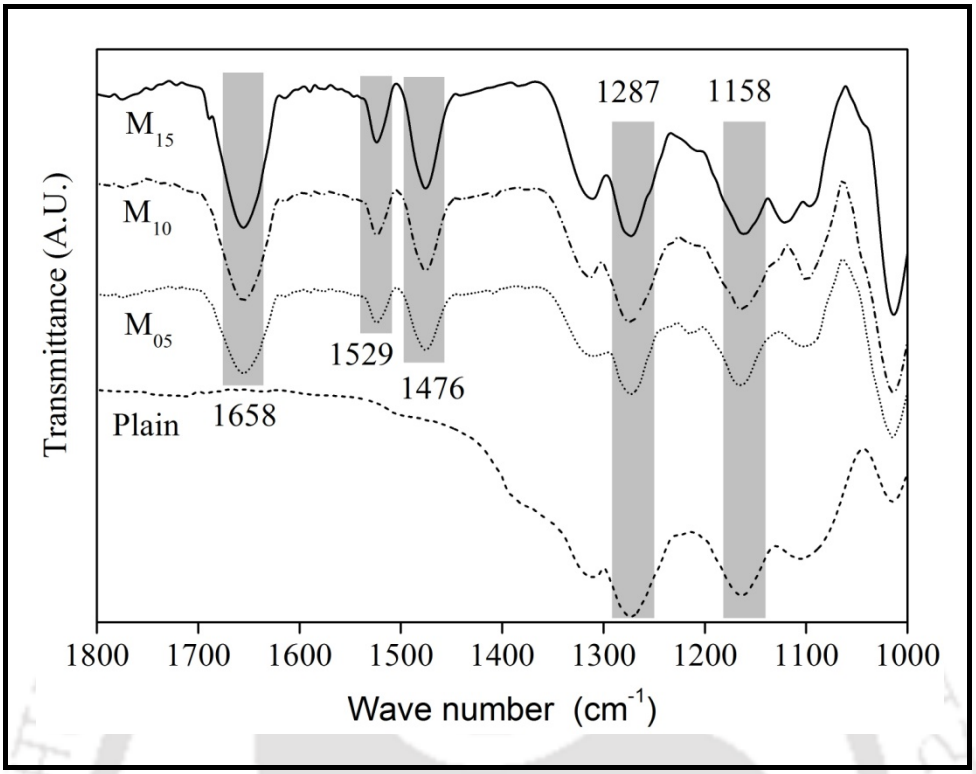


**Figure 8.2: ATR-FTIR spectra of plain and PVCL-co-PSF copolymer blended membranes.**

## 8.3.2. Membrane hydration, hydrophilicity and BSA adsorption studies

Figure 8.3 shows the effect of initial ratio of PSF and VCL monomer on hydration capacity of membranes. The measured quantity of the hydration capacity is result of trapping of water in porous structure of membrane, binding of water molecules around the hydrophilic segment of amphiphilic brushes and entrapped water molecules in the confined spaces between amphiphilic chains. So, hydration capacity of the plain membrane was attributed to only porous structure compared to the blended membranes. In addition Table 8.2 is reporting the growth of membrane thickness as function PVCL content. It supported that PVCL-PSF copolymer prevent the shrinkage of the membrane during membrane formation. Thus, the increases in initial ratio of VCL monomer associated with the increase in amount of hydrophilic brush like structure due to the self rearrangement of amphiphilic PVCL-co-PSF copolymer on the membrane surface. This in result increased the hydration capacity, which is

dependent on the bound and entrapped water molecules. So, the formation of bound water layer on blended membrane was regarded as vital to repel proteins and generate the bio fouling resistant surface.

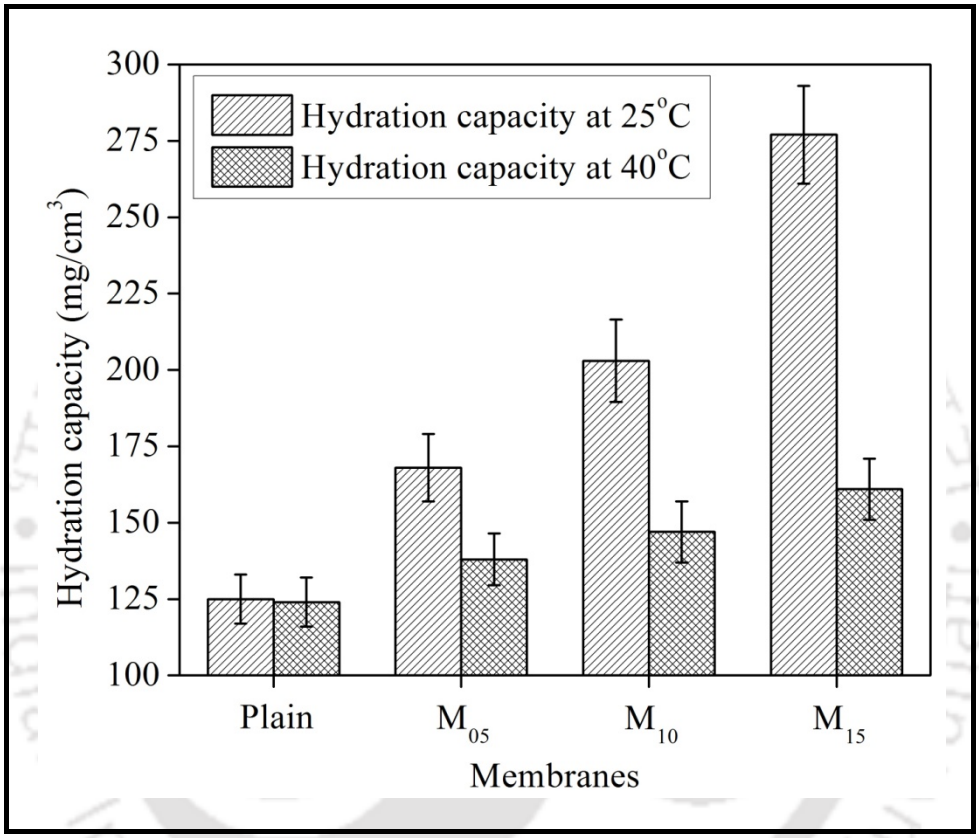


**Figure 8.3: Temperature dependent hydration capacity of prepared membranes.**

Figure 8.3 also shows the hydration capacity of the prepared membranes at 25˚ C and 40˚ C. It is well known that PVCL has lower critical solution temperature (LCST) of ~ 35˚C, which gives thermo responsive property to the copolymer, which in result provides thermo responsive behaviour to the modified membrane. This thermo responsive property of the PVCL is present due to the configurational changes in PVCL chain. Below the LCST, the PVCL polymer chains adopted an extended random coils configuration and absorb more amount of water within its coil type configuration. Whereas at temperature above LCST, the

PVCL polymer chains shrinked to form a compact structure and dehydrated the absorbed water [70, 71]. Due to this swell and shrink function of PVCL, hydration capacity of modified membrane changes below and above LCST.

Bio-foulants like BSA strongly interacts with hydrophobic membrane surfaces and thereby causes significant water flux decline by fouling during the ultrafiltration. In this regard, it is of major concern to fabricate membranes with ability to resist protein adsorption. The physical deposition of foulants can be reduced by increasing the membrane surface hydrophilicity. Water contact angle (WCA) and adsorb BSA quantity for different membranes are shown in Figure 8.4. Hydrophilic behaviour of the membrane is explained by water contact angle measurement. Lower the WCA value higher will be the hydrophilicity of the membranes and more hydrophilic membranes are less prone towards fouling. Therefore, WCA is a significant parameter in membrane separation process and very much related to membrane's fouling behaviour. For unmodified membrane WCA is 67.5˚ and for membrane $M_{15}$ it decreased considerably to 49.5˚. It is well known that in the presence of hydrophilic functional group like amide group enhances the hydrophilic behaviour of membranes. So, as the quantity of PVCL increases, hydrophilicity of the modified membranes also increases.

It has been discussed that with the increase in initial ratio of VCL monomer, surface hydrophilicity had increased for blended membranes. Though, the estimation of protein adsorption on the membrane surfaces should be considered not only with respect to surface hydrophilicity but also with respect to the hydration capacity of the membranes [144]. It is reported that, the formation of the bound water layer on a surface is considered crucial to repel protein and generate anti-bio fouling surface [145, 146]. Figure 8.4 shows the adsorption of BSA on membranes as a function of PVCL content in membranes. The addition of amphiphilic PVCL-co-PSF macromolecule reduces the adsorption of BSA molecule from 0.145 mg/cm$^2$ for plain membrane to 0.02 mg/cm$^2$ for $M_{15}$ membrane. On the other hand

hydration capacity of membrane increases dramatically with the addition of PVCL-PSF, for plain membrane hydration capacity value is around 125 mg/cm$^3$, where as for the membrane $M_{15}$ that value is around 280 mg/cm$^3$ at 25°C. These indicated that higher the initial quantity of VCL monomer, the more hydrophilic, the more hydration capacity and lower BSA adsorption amount. The results also confirmed that blending the amphiphilic PVCL-co-PSF copolymer could stem the adsorption of protein molecules, since hydrophilic copolymer could restrain the protein adsorption amount by forming bound hydration layer on membrane surface.

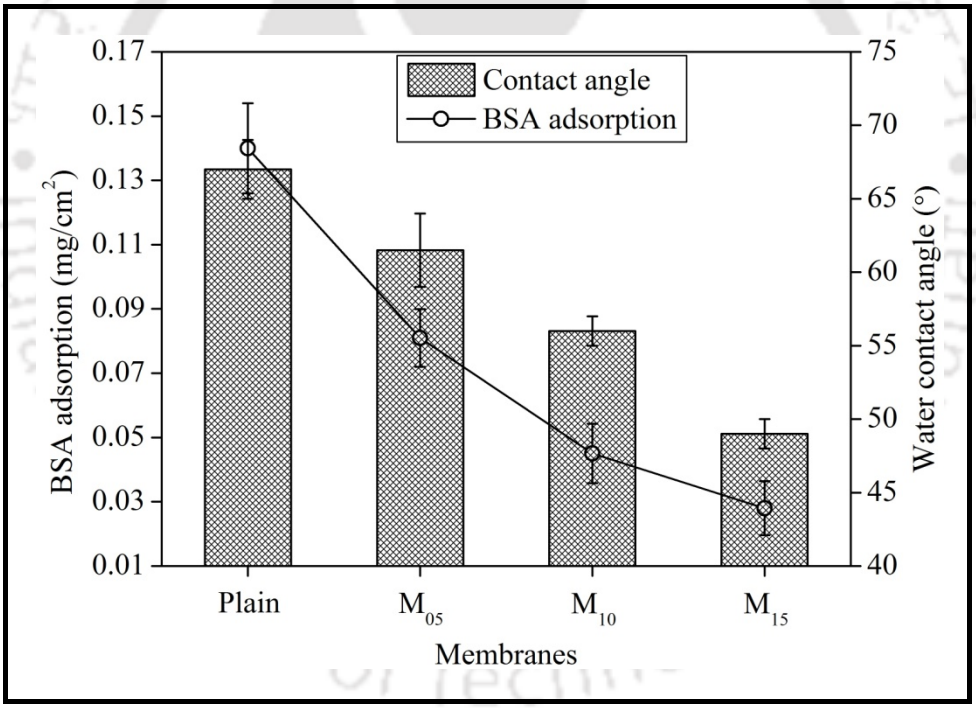


**Figure 8.4: Effect of initial quantity of VCL monomer on BSA adsorption and hydrophilicity of prepared membranes**.

## 8.3.3. Microscopic studies

Figure 8.5 and 8.6 show the top surface FESEM images and cross sectional images of the plain and blended PSF membranes with different initial ratio of PSF to VCL monomer. All

the membranes have observable pores on the top surface and pore size is around 25-30 nm or less than that. One can observe that the membrane $M_{15}$ has higher pore density compared to plain membrane and also compared to other modified membranes. It has been stated that amphiphilic or hydrophilic additives would helps in pore formation and also segregate at the membrane surface [147, 148]. And in case of the membrane $M_{15}$ the ratio of hydrophilic part in amphiphilic copolymer is higher, so it further induces the pore formation in the membrane $M_{15}$. In case of cross sectional morphology, all the membranes exhibit asymmetric structure. All the fabricated membranes have top dense layer or skin layer supported by porous sub-layer consists of finger like structure and bottom layer. These structures formed due to the high mutual affinity of NMP for water, which results instantaneous demixing [69].

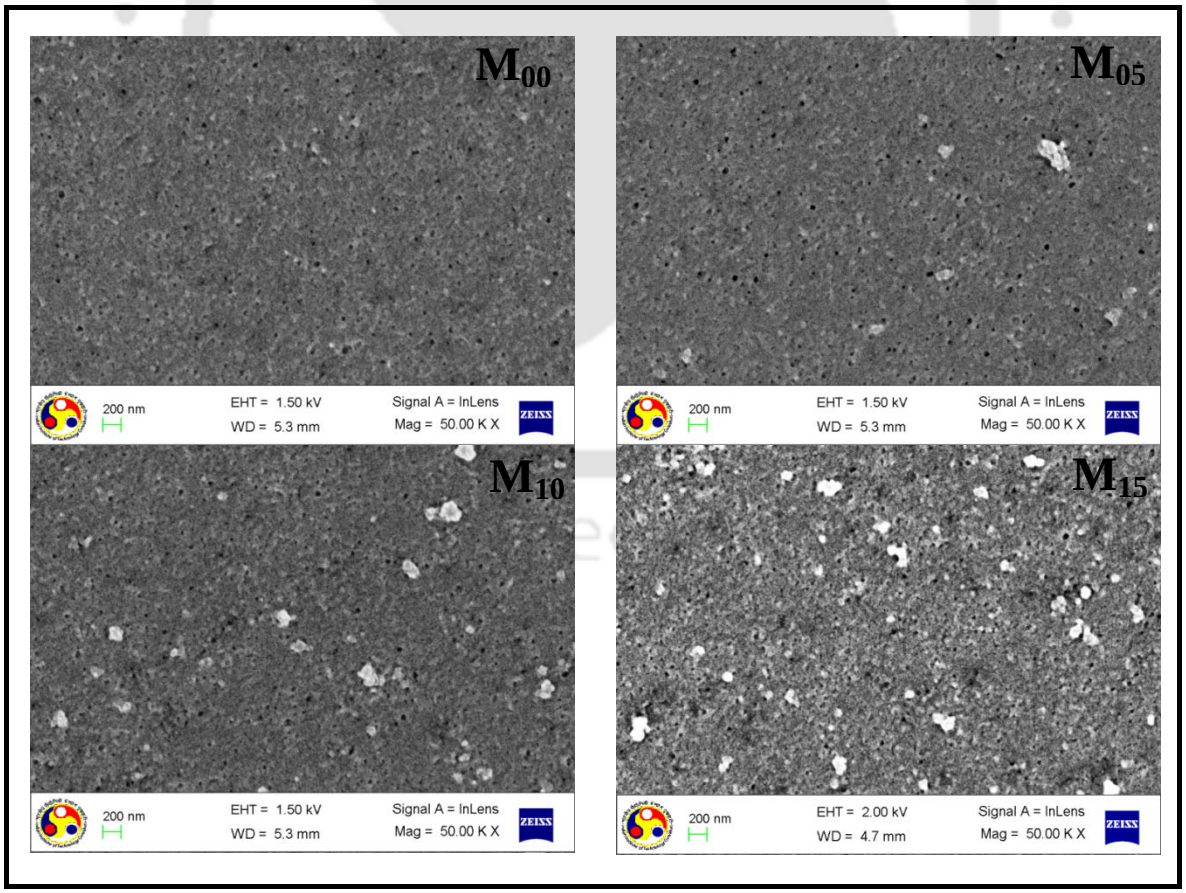


**Figure 8.5: Effect of initial quantity of VCL monomer on top surface of plain and modified membranes.**

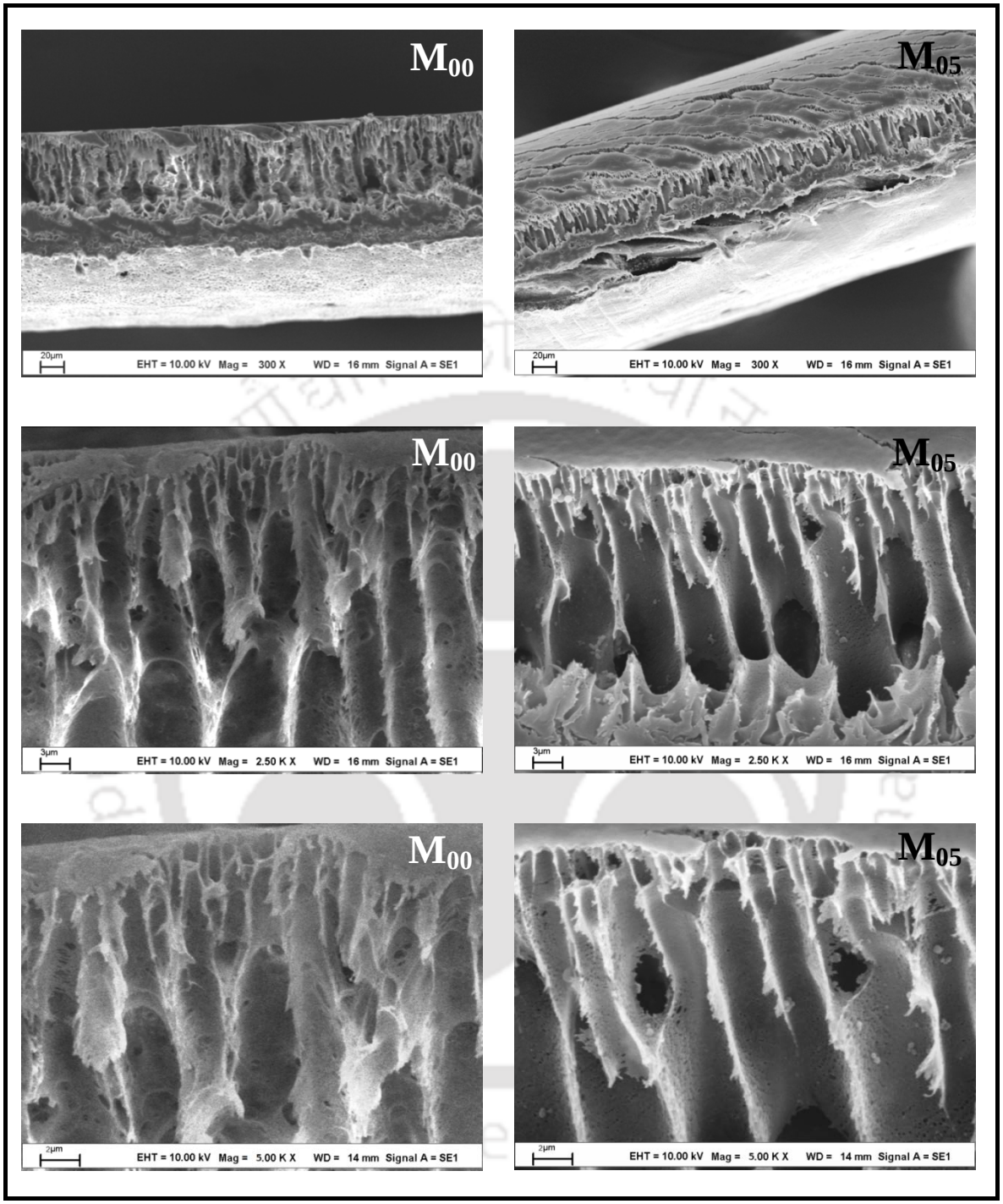


**Figure 8.6: Effect of initial quantity of VCL monomer on cross section of plain and modified membranes.**

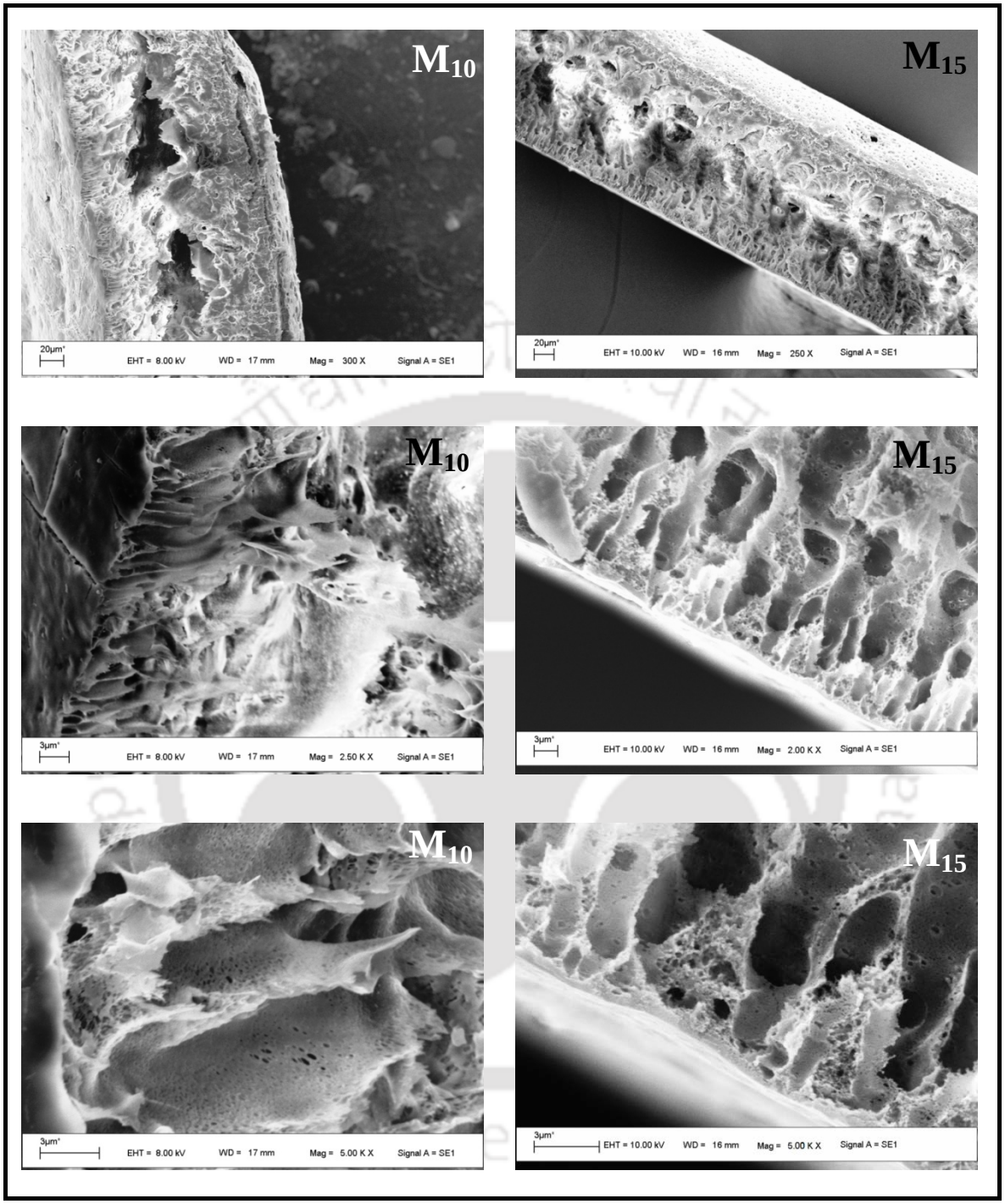


**Figure 8.6: Effect of initial quantity of VCL monomer on cross section of plain and modified membranes. (continued)**

However, significant change in the finger like structure of the modified membrane can be observed. In case of plain membrane, there are different layers of finger like structure

and over all thickness of porous sub layer is more compared to bottom layer. Whereas, in case of membrane $M_{05}$ (less quantity of PVCL), finger like structure coalesced together and form bigger finger like structure, but thickness of the porous sub layer in membrane $M_{05}$ is still less than plain membrane. Further, in case of the membranes $M_{10}$ and $M_{15}$, those fingers like structure became shorter and converted to porous sponge like structure (membrane $M_{15}$). It is reported that membrane structure is formed by driving force between nonsolvent and solvent and their relative diffusion rate [140, 141]. If there is strong affinity between solvent and nonsolvent then in such condition out diffusion rate of solvent is much higher than the in diffusion rate of nonsolvent. Thus dense skin layer is formed and reduces the diffusion rate of nonsolvent into the sub layer, this result in bigger porous sub layer with finger like structure. Whereas, if there is weak affinity between solvent and nonsolvent, the skin layer will be porous and sponge like structure can be formed. Since, PVCL-co-PSF copolymer has amphiphilic property, the addition of the same influences the relative diffusion rate of solvent and non solvent by reducing the affinity between solvent and nonsolvent. Thus, the in diffusion rate of the nonsolvent decreases during phase inversion process at higher PVCL content. This results in porous sponge like sub layer structure just below the dense skin layer.

### 8.3.4. Pure water permeation and hydraulic permeability studies

Figure 8.7 the shows effect of initial ratio of PSF and VCL monomer on the compaction profile during time dependent constant pressure (300 kPa) PWF and calculated compaction factor (CF) is shown in Table 8.2. CF recounts to the structure of membrane sub layer. Higher the CF, more likely the membrane compacts due to presence of large macro voids in the sub layer. It was already seen that modified membranes have smaller voids in sub layer, which reduces the CF of modified membranes compared to plain membranes. PWF declined sharply for all the membranes for up to 45 minutes and after that PWF remains almost

constant. Due to compaction the walls of the pores become closer, denser and uniform resulting reduction in pore size as well as the flux during compaction [1]. From the inset of the Figure 8.7 it is found that the steady state PWF increases with increase in ratio of VCL monomer. Steady state flux for plain membrane and membrane $M_{15}$ are 103.5L/$m^2$h and 127.2 L/$m^2$h, respectively. The increase in steady state flux is due to the higher pore density, as shown in Figures 8.5. However, increase in flux is not that much; the possible reason is thermo responsive behaviour of modified membranes. Due to the fact that, PVCL segment of copolymer has LCST around 35 °C. So, below this temperature, PVCL remains in swell state, which reduces the effective pore diameter of modified membranes.

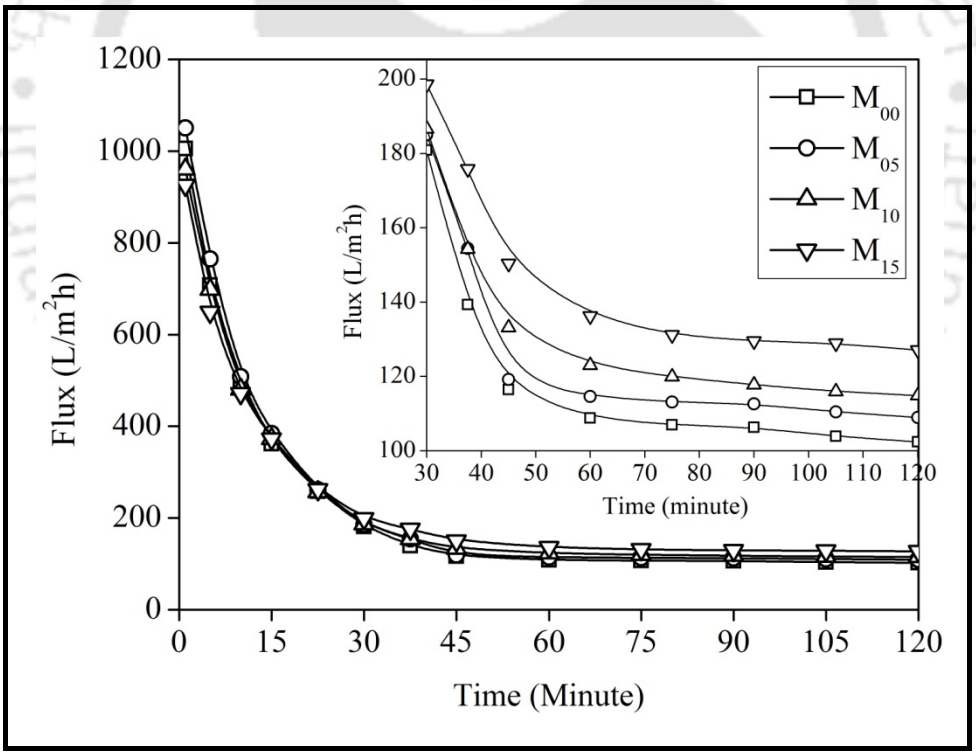


**Figure 8.7: Effect of initial quantity of VCL monomer on flux profile during compaction (at 300 kPa).**

Effect of initial ratio of PSF and VCL monmer on PWF of the membrane at different transmembrane pressure is shown in Figure 8.8. This experiment was done at different transmembrane pressure between 0 - 300 kPa at a difference of 50 kPa. For all the cases, PWF increases almost linearly with increase in pressure. Pressure dependent flux profiles were used to calculate the hydraulic permeability ($P_m$) of the membranes. $P_m$ was increased from 0.44 to 0.50 L/m$^2$ h kPa (Table 8.2) for plain membrane to modified membrane $M_{15}$. Despite the increase in pore density the hydraulic permeability increased marginally due to thermo responsive property of membrane as discussed earlier. These results are in agreement with the findings of compaction studies and temperature dependent hydration capacity of modified membranes.

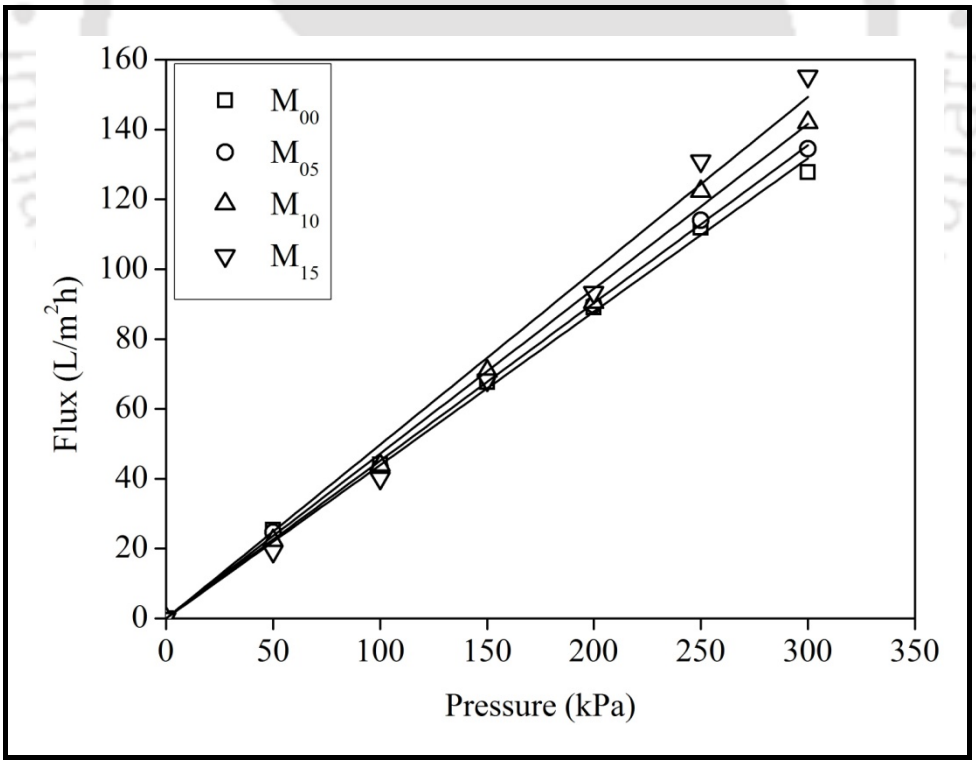


**Figure 8.8: Effect of initial quantity of VCL monomer on pressure dependent flux through different membranes.**

**Table 8.2: Value of some characterization parameters of membranes modified with PVCL-co-PSF copolymer.**

| Membrane | Contact angle (°) | CF | $P_m$ | Thickness |
|---|---|---|---|---|
| **Plain** | 67±2 | 9.85 | 0.44 | 109±13 |
| **$M_{05}$** | 61.5±2.5 | 9.64 | 0.45 | 122±15 |
| **$M_{10}$** | 56±1 | 8.36 | 0.47 | 143±12 |
| **$M_{15}$** | 53±1 | 7.28 | 0.50 | 157±10 |

## 8.3.5. Ultrafiltration performance and fouling studies

The ultrafiltration performance, antifouling behaviour and easy cleaning properties of PVCL-co-PSF modified membranes were examines by filtering 1000 PPM BSA solution at constant transmembrane pressure of 250 kPa. Figure 8.9 shows the BSA flux and rejection through plain and modified membranes. PVCL-PSF modified membranes have comparatively much higher flux than plain membranes, indeed membrane $M_{15}$ has almost 3 times higher flux than plain membrane. Despite the increase in flux, the rejections through modified membranes are on the higher side than plain membrane $M_{00}$. As we have already discussed that amphiphilic PVCL-co-PSF copolymer not only enhances the hydrophilicity but also pore forming capacity. Also, due to the thermo responsive property of the membranes the pore size of the modified membranes were smaller due to expansion of copolymer molecules at the working temperature (≈ 25°C), which was lower than LCST of PVCL as discussed earlier. The PVCL-co-PSF copolymer also helps to form pure water layer on top surface of membranes, which in returns reduces the deposition of BSA molecules on the membrane surfaces and enhances the flux through modified membranes.

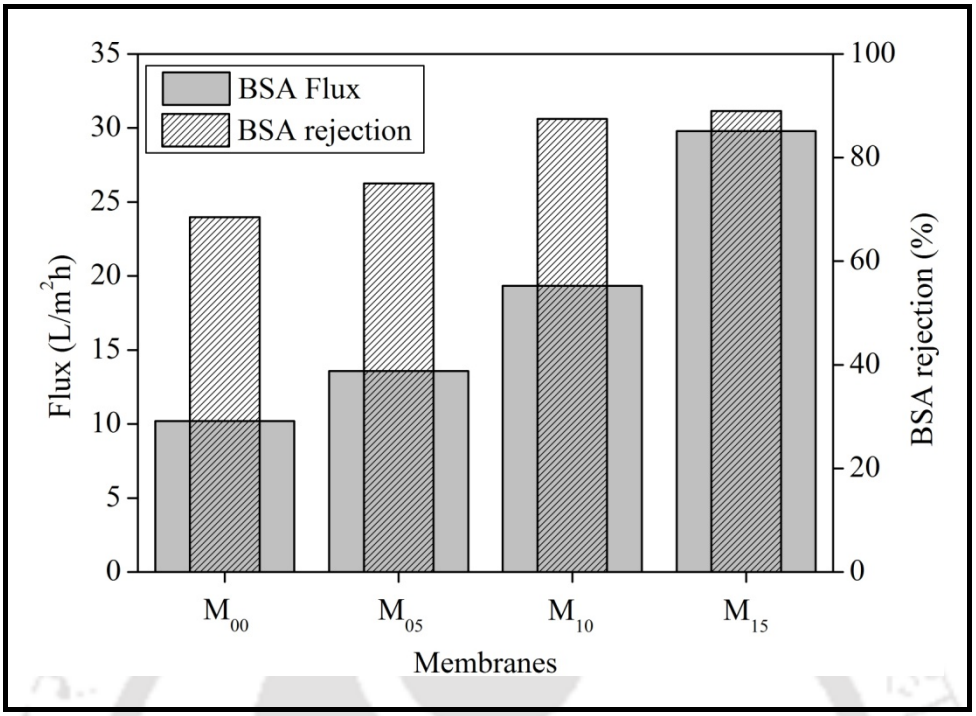


**Figure 8.9: Effect of initial quantity of VCL monomer on BSA flux and rejection values through different membranes.**

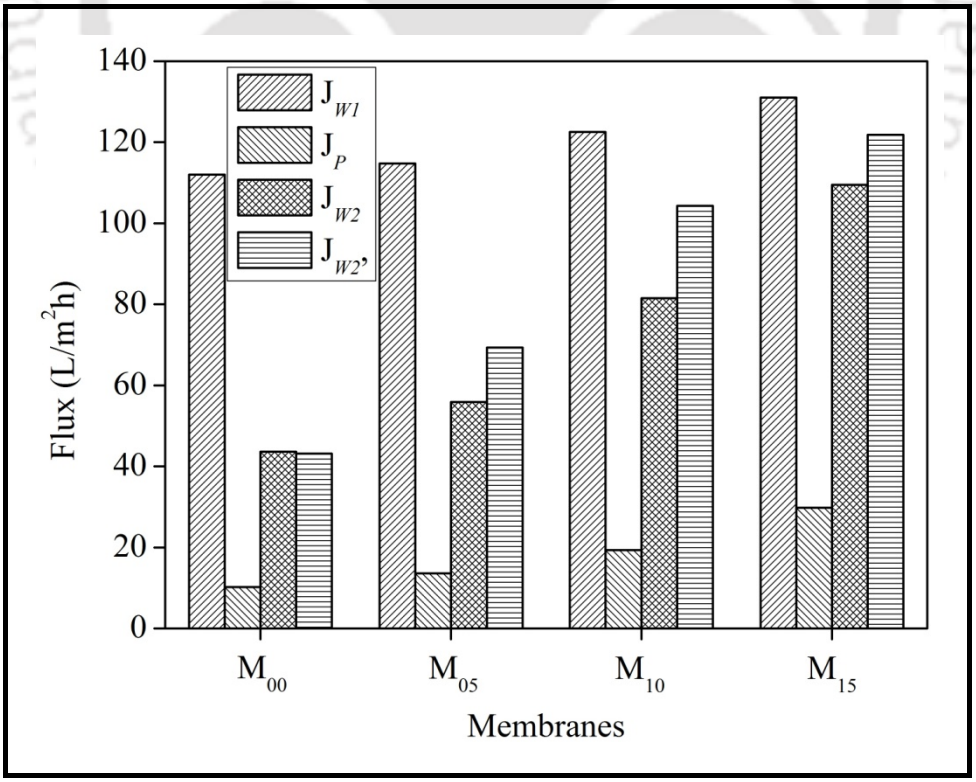


**Figure 8.10: Different flux values through prepared membranes during fouling study.**

The dynamic fouling resistance experiment was done to study the antifouling property of prepared membranes, and process was recorded at constant TMP of 250 kPa and shown in Figure 8.10. In first step DI water flux was measured and called as $J_{w1}$, after that in 2nd step 1000 PPM BSA solution was used to permeate through membranes and measured flux was named as $J_{BSA}$. Again in 3rd step after simple hydraulic cleaning, DI water flux was measured and recorded as $J_{w2}$. In another case, 3rd step was changed with modified hydraulic cleaning (as shown in Figure 8.11), first membrane was hydraulically washed at 40˚C and after that again hydraulically washed at 25˚C. Finally, DI water flux was measured and named as $J_{w2}'$. Data of Figure 8.10 was used for the calculation of total fouling ($F_t$), reversible fouling ($F_r$), irreversible fouling ($F_{ir}$) and flux recovery ratio ($Flux_{RR}$) by equations 2.17, 2.18, 2.19 and 2.21 respectively.

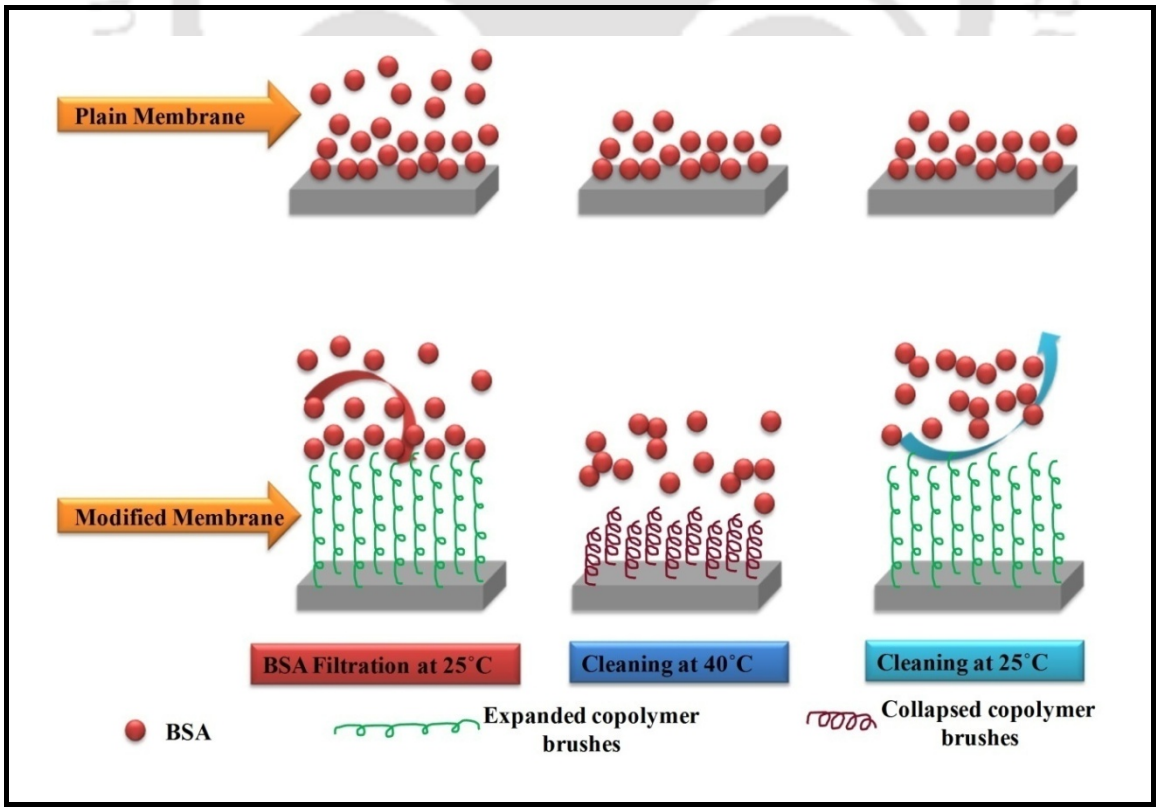


**Figure 8.11: Schematic representation of mechanism modified hydraulic cleaning.**

As it is already discussed that modified membranes have higher BSA flux than plain membranes, apart from that it can be observed, flux in first step is almost similar for all the membranes. But, as the experiment was progressing the difference between the flux values through different membranes were tend to increasing. Flux value $J_{w2}^{'}$ for membrane $M_{15}$ is much higher than membrane $M_{00}$. Effect of these changing values can be seen in Figure 8.12, it shows the value of different fouling parameters for the prepared membranes. The plain membrane has the highest value of total fouling and irreversible fouling and also lowest value of reversible fouling. Addition of PVCL-co-PSF copolymer resisted the adsorption of BSA molecule inside the membrane pores by increasing the hydrophilicity. Due to this reason, as the initial ratio of VCL monomer to PSF was increased in the modified membrane, the irreversible fouling was started to reduce in modified membranes. Further when modified hydraulic cleaning was applied for membrane cleaning after fouling with BSA, the value of $F_{ir}$ was further decreased for modified membranes, but for plain membrane $F_{ir}$ value was same. In modified hydraulic cleaning BSA fouled membrane was first washed with water at 40˚C. Due to LCST of PVCL around 35˚C, the molecules of PVCL-co-PSF copolymer shrinked to form a compact structure and water molecules expelled from the PVCL-co-PSF structure and subsequently deposited BSA layer was damaged . Changing the cleaning temperature again to 25˚C, tended the expansion of PVCL-co-PSF copolymer chain and stretching the chain come out of the membrane surface. This resulted in the further damaging or loosening of BSA layer, thus increasing the efficiency hydraulic cleaning. So, incorporation PVCL-co-PSF copolymer in membrane matrix reduces the use of traditional chemical cleaning for polymeric membrane, which reduces the efficiency and life time of the membranes.

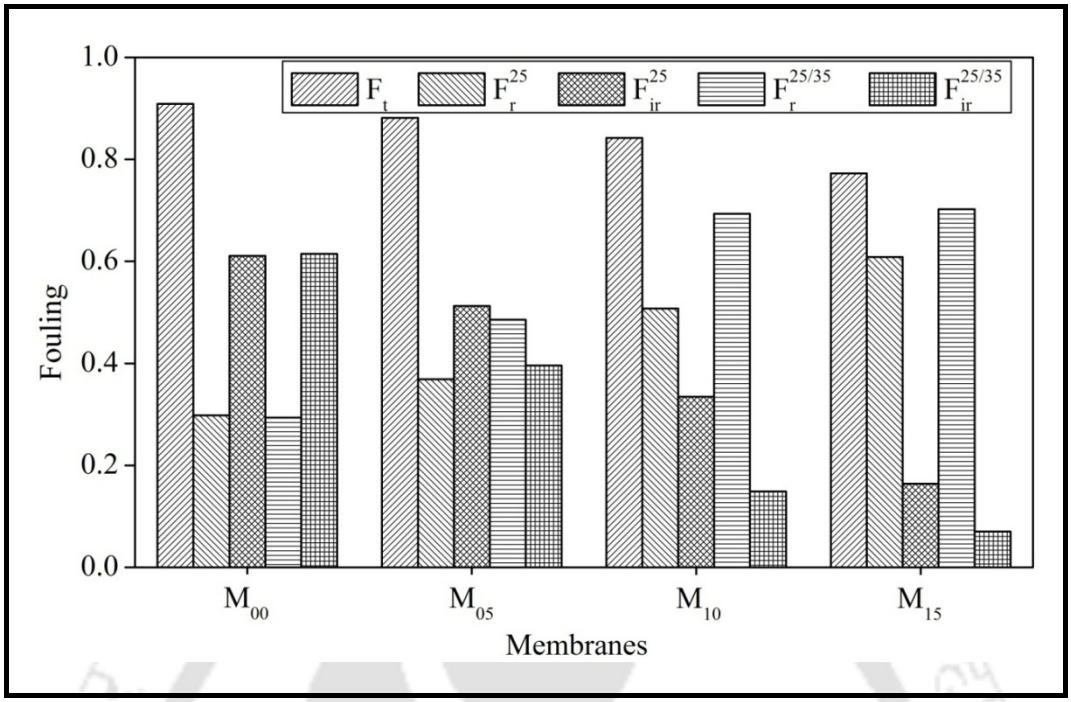


**Figure 8.12: Effect of initial quantity of VCL monomer on different fouling values for prepared membranes.**

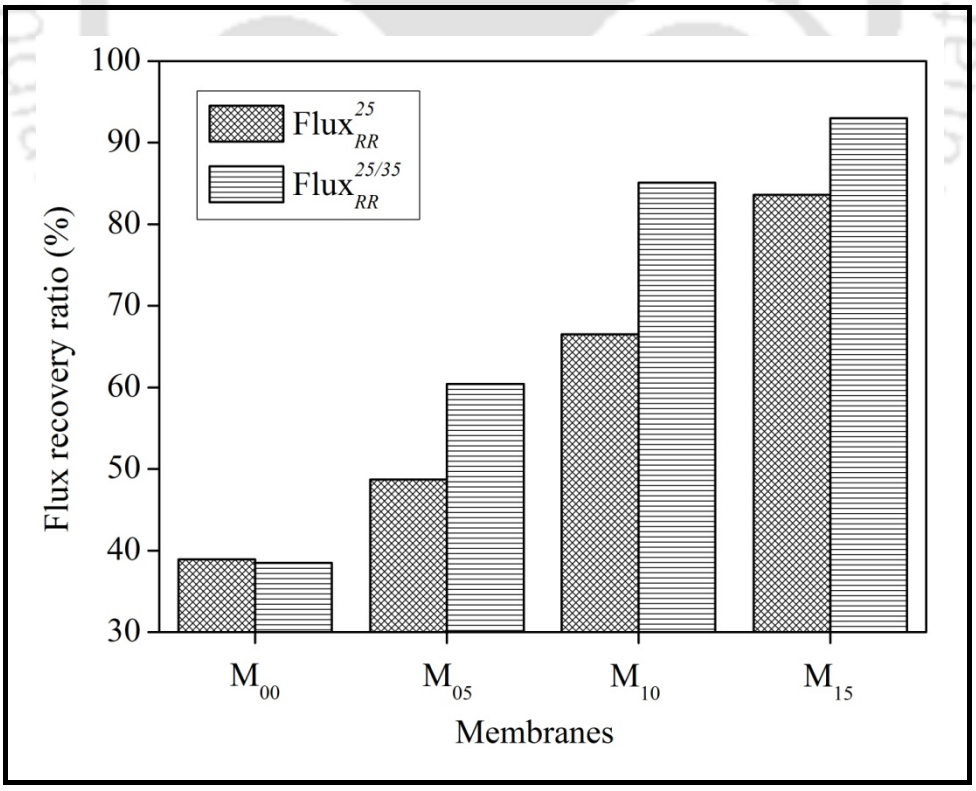


**Figure 8.13: Flux recovery ratio after normal and modified hydraulic cleaning.**

Figure 8.13 shows the flux recovery ratio of prepared membrane after normal hydraulic cleaning and also after modified hydraulic cleaning. Reduction in irreversible fouling causes increase in flux recovery ratio for the modified membranes. As flux recovery ratio is directly related to irreversible fouling. The flux recovery ratio for the plain membrane is only around 39 %, while it is 84 % for membrane $M_{15}$. The good antifouling performance of the PVCL-PSF blended membrane possibly credited to the presence of large number of amide groups in the surface of modified membranes resulted from rearrangement of the amphiphilic copolymer towards the top surface of the modified membranes. This results in reduction in water contact angle, increase in hydration capacity and reduction in BSA adsorption (Figure 8.3 and 8.4). The more hydrophilic surface cause formation of a water layer and repel the hydrophobic foulants. In case of cleaning by modified method, it further enhances the flux recovery ratio of modified membranes by reducing the value of $F_{ir}$, as discussed earlier. The flux recovery ratio of membrane $M_{15}$ is 92.5 % compared to 39 % of plain membrane, after cleaning with modified method.

# Chapter 9

## Modification of PSF membrane by CS–PAA complex nanoparticles

# Chapter 9
# Modification of PSF membrane by CS–PAA complex nanoparticles

*The present chapter focused on the synthesis and characterization of CS-PAA nanoparticle cross-linked with glutaraldehyde. Nanoparticle was characterized by Fourier transform infrared spectroscopy (FTIR) and photon correlation spectroscopy (PCS). PCS shows the size and zeta potential of nanoparticle and it also confirms the stability of CS-PAA nanoparticle in different pH condition. Morphology and composition of the fabricated membranes were analyzed by FESEM and ATR-FTIR. Pure water flux (PWF), hydraulic permeability, BSA adsorption, hydrophilicity and UF performance during BSA separation through prepared membranes were also analyzed. Finally, total fouling, reversible and irreversible fouling caused during BSA ultrafiltration was estimated.*

## 9.1. Experimental

### 9.1.1. Materials

Polysulfone (PSF), chitosan (CS), N-methylpyrrolidone (NMP), FTIR grade potassium bromide (KBr), acrylic acid, potassium persulphate ($K_2S_2O_8$), glutaraldehyde (GA), PEG4000 and bovine serum albumin (BSA) were used in this chapter. Information related to chemicals used in this chapter is provided in Table 2.1 of chapter 2.

### 9.1.2. Synthesis and characterization of CS-PAA nanoparticle

CS-PAA nanoparticles were synthesized according to method given in reference [106] with slight modification. In short, 1 gm of CS was dissolved in 50 ml acrylic acid (AA) solution

Content of this chapter has been submitted for publication as below:

M K Sinha, M K Purkait, Use of CS-PAA polymeric nanoparticle in fouling resistant polysulfone ultrafiltration membrane preparation, J. Membr. Sci.

containing 1 gm of AA. When the solution became clear, temperature of the mixture was raised to 80° C and $K_2S_2O_8$ was added as initiator for polymerization under nitrogen atmosphere. After around 2 h of reaction, the solution turns to milky in colour. After that temperature was lowered to 40° C and GA was added to the system as cross linker and reaction was carried out for further 2 h. Finally, the reaction mixture was centrifuged at 6000 RPM and obtained nanoparticles were kept aside for further characterization and modification of membrane.

The physicochemical properties of synthesized nanoparticles were investigated by using FTIR and photon correlation spectroscopy (PCS). FTIR studies were performed for the verification and to investigate the complex formation between chitosan and poly acrylic acid (PAA). The hydrodynamic size distribution and zeta potential of the CS-PAA nanoparticles was done by PCS. For the zeta potential analysis each sample was adjusted to a concentration of 0.1 % (w/w) in 10 mmol/L sodium chloride solution. Information related to FTIR and PCS instruments are given in section 2.4.

### 9.1.3. Fabrication of polymeric nanoparticle blended membranes

Centrifuged nanoparticles were dispersed in equal amount of water, so that it should appear as a solution. 10 g of dispersed nanoparticles were vigorously mixed with 100 ml of NMP at 60 $^oC$. On the other hand, 30 wt % of PSF was dissolved in NMP with 2 wt % of PEG 4000 as pore forming agent. To this 30 wt % PSF solution, different amount of dispersed nanoparticle solution was mixed and required amount of NMP was added to get 15 wt % of PSF in final casting solution. This mixture was vigorously mixed at 60 $^oC$ for 12 h and further degassed by ultra sonication for 30 minute. Finally the membranes were prepared by phase inversion process with a uniform thickness of 200 µm. Steps for the fabrication of the modified membranes is shown in Figure 9.1 and information related to membrane casting

steps are given in section 2.2 of chapter 2. Composition and viscosity of all the membrane casting solutions are provided in Table 9.1. Viscosities of the membrane casting solutions were measured with a constant shear rate of 50 $s^{-1}$.

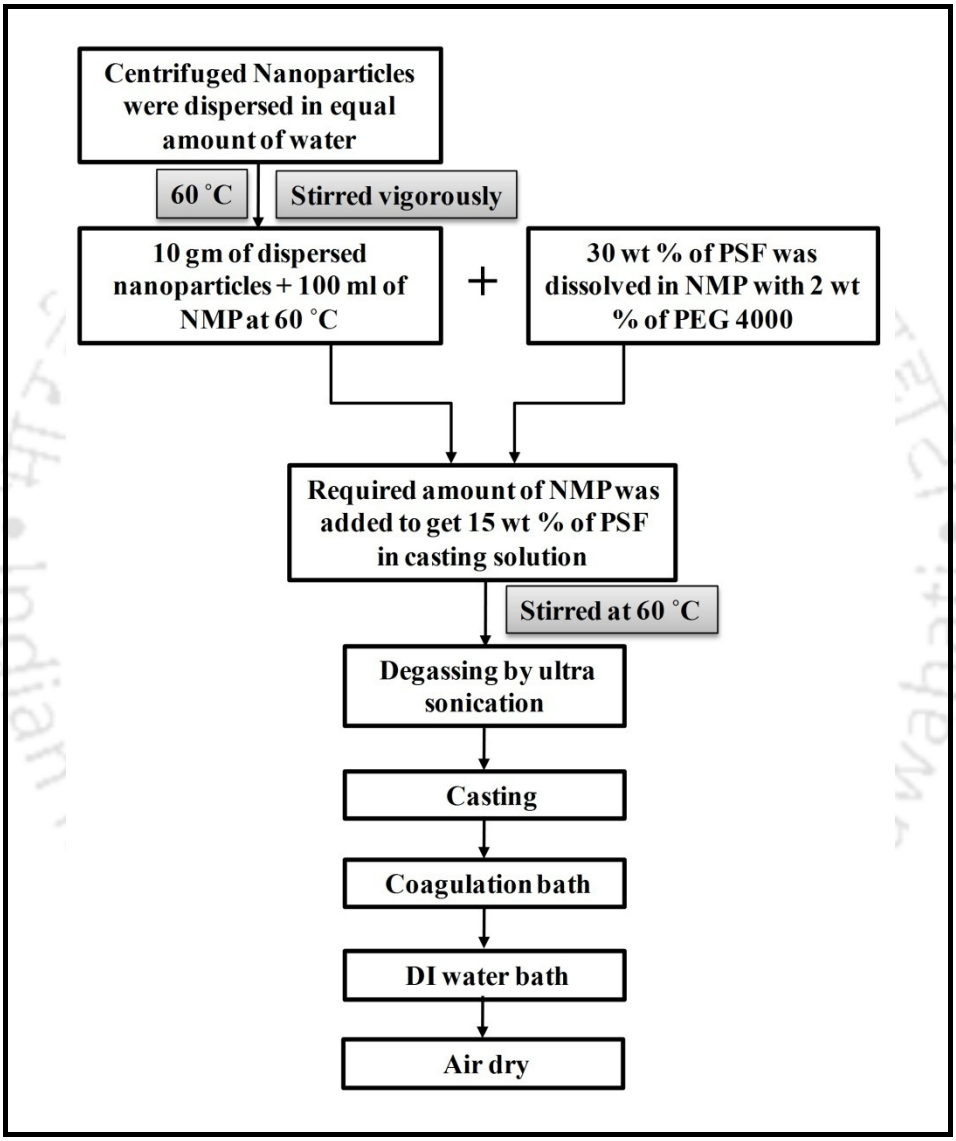


**Figure 9.1: Steps for fabrication of modified membranes.**

**Table 9.1: Composition and viscosity of different membrane casting solution containing CS-PAA nanoparticles.**

| Membranes | 30 % PSF solution in NMP (wt %) | 10 %CS-PAA solution in NMP (wt %) | NMP (wt %) | Viscosity×$10^2$ (Pa s) |
|---|---|---|---|---|
| **M00** | 50 | 0 | 50 | 5.68 |
| **M10** | 50 | 10 | 40 | 6.45 |
| **M20** | 50 | 20 | 30 | 8.05 |
| **M30** | 50 | 30 | 20 | 10.85 |

## 9.2. Membrane characterization

### 9.2.1 Morphological and surface characterization of blended membranes

The presence of CS-PAA nanoparticle in blended membrane was confirmed by ATR-FTIR. Comparison in the cross sectional and top surface morphology of the plain membrane and modified membranes was done by FESEM. It also provided the dispersion of the nanoparticle in blended membrane. Water contact angle (CA) between membrane surface and water droplet is the measure of the hydrophilicity of the membrane surface, smaller the contact angle, higher the hydrophilicity of the surface. For all the prepared membranes, 5 contact angles were measured and average was considered. The adsorption of BSA on membrane surface was performed. At first, membranes were placed in 5 ml vials and were soaked in 4 ml of phosphate buffer for 1 h at 25 $^{o}$C. After that, buffer was removed and membranes were incubated with 4 ml of 1000 ppm BSA solution for 12 h at 25 $^{o}$C. The absorbed amount of BSA was measured by UV-VIS spectrophotometer at wavelength of 280 nm. Three duplicate tests were performed for each membrane. The porosity (ε) of the membranes was determined by gravimetric method, using following equation 2.13 Thickness of the membranes were

measured by a digimatic measuring unit at 10 different places and average was taken. Mean pore radius of the membrane was calculated by Guerout–Elford–Ferry equation (equation 2.14) [97]. Detail methods and instrumentation are provided in section 2.3 of chapter 2.

### 9.2.2. Pure water permeation and filtration experiments

All the membranes were compacted at 400 kPa transmembrane pressure for 2 h and flux was measured at regular interval. After the compaction water permeation through all the membranes at different pressure was measured and hydraulic permeability ($L_m$) was measured using that data. The flux was measured by using the equation 2.9. Hydraulic permeability ($L_m$) (L/m$^2$h kPa) is calculated from the slope of the plot of $J_w$ vs $P$ from the equation 2.10.

For evaluation of fouling due BSA ultrafiltration, all the membranes were first compacted at 400 kPa for 30 minute. Then pressure was reduced to 300 kPa and pure water flux was measured at regular interval for 90 minutes. Flux at the end of 90 minute was termed as $J_{w1}$. Subsequently, feed was changed with 1000 PPM BSA solution and BSA flux was measured for next 90 minutes. BSA flux at the end of this 90 minute was called as $J_{BSA}$. BSA rejection was measured UV-VIS spectroscopy by using equation 2.16. After BSA ultrafiltration, membranes were washed with pure water flushing, and then again pure water was permeated through membranes for 90 minutes. The water flux at the end of this 90 minute was labelled as $J_{w2}$.

## 9.3. Results and discussion

### 9.3.1. FTIR and PCS analysis

For the confirmation and to investigate the complex formation between PAA and CS, FTIR study was performed (Figure 9.2). The main peaks can be assigned as follows: 3421 $cm^{-1}$ (O–H stretching vibration), 2951 $cm^{-1}$ and 2897 $cm^{-1}$ (C–H stretching related to glutaraldehyde, 1736 $cm^{-1}$ (peak of the carboxyl group of PAA), 1624$cm^{-1}$ (peak of $NH_2$ of CS), 1521 $cm^{-1}$ and 1400 $cm^{-1}$ (symmetric and asymmetric stretching vibrations of $COO^-$ anion groups), 1284 $cm^{-1}$ and 1076 $cm^{-1}$ (C–O group).

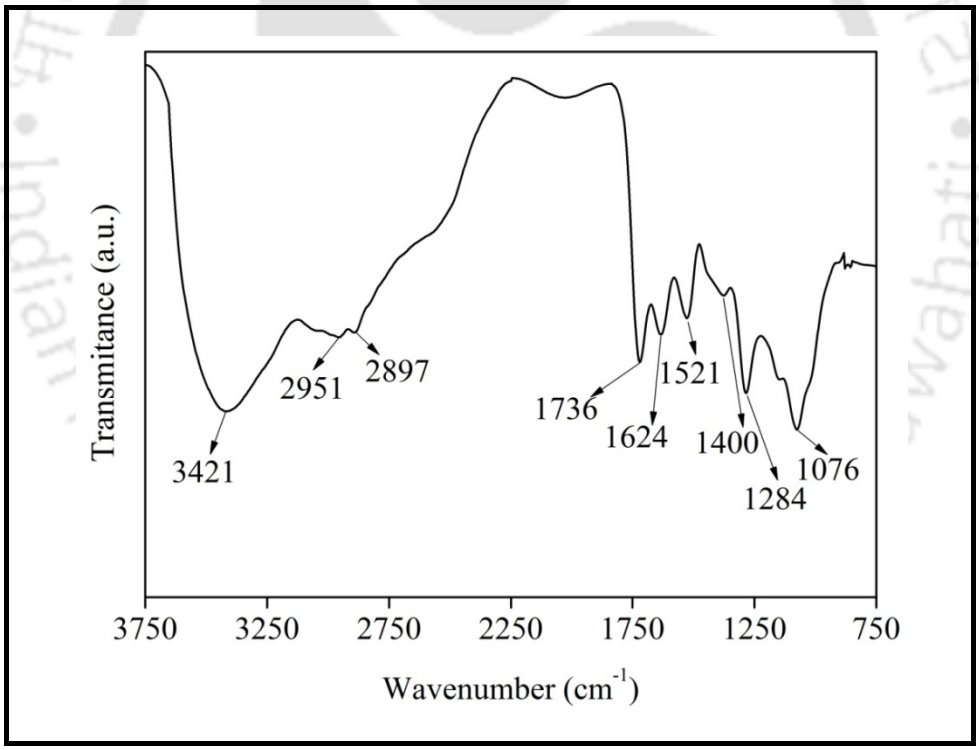


**Figure 9.2: FTIR spectra of CS-PAA nanoparticle.**

The particle size distribution and zeta potential of the CS-PAA nanoparticles in different pH conditions were characterized by PCS (Figures 9.3 and 9.4). The hydrodynamic size of CS-PAA nanoparticle is found to change with change in pH. The size of nanoparticle

attains the minimum value at pH 4, and becomes considerably bigger in size at pH 1 and much bigger at pH 7.5. At low pH of 1, the CS is fully ionized and form $–NH^{+}_{3}$. Thus, the CS-PAA nanoparticles become larger due to electrostatic repulsion between $–NH^{+}_{3}$ groups

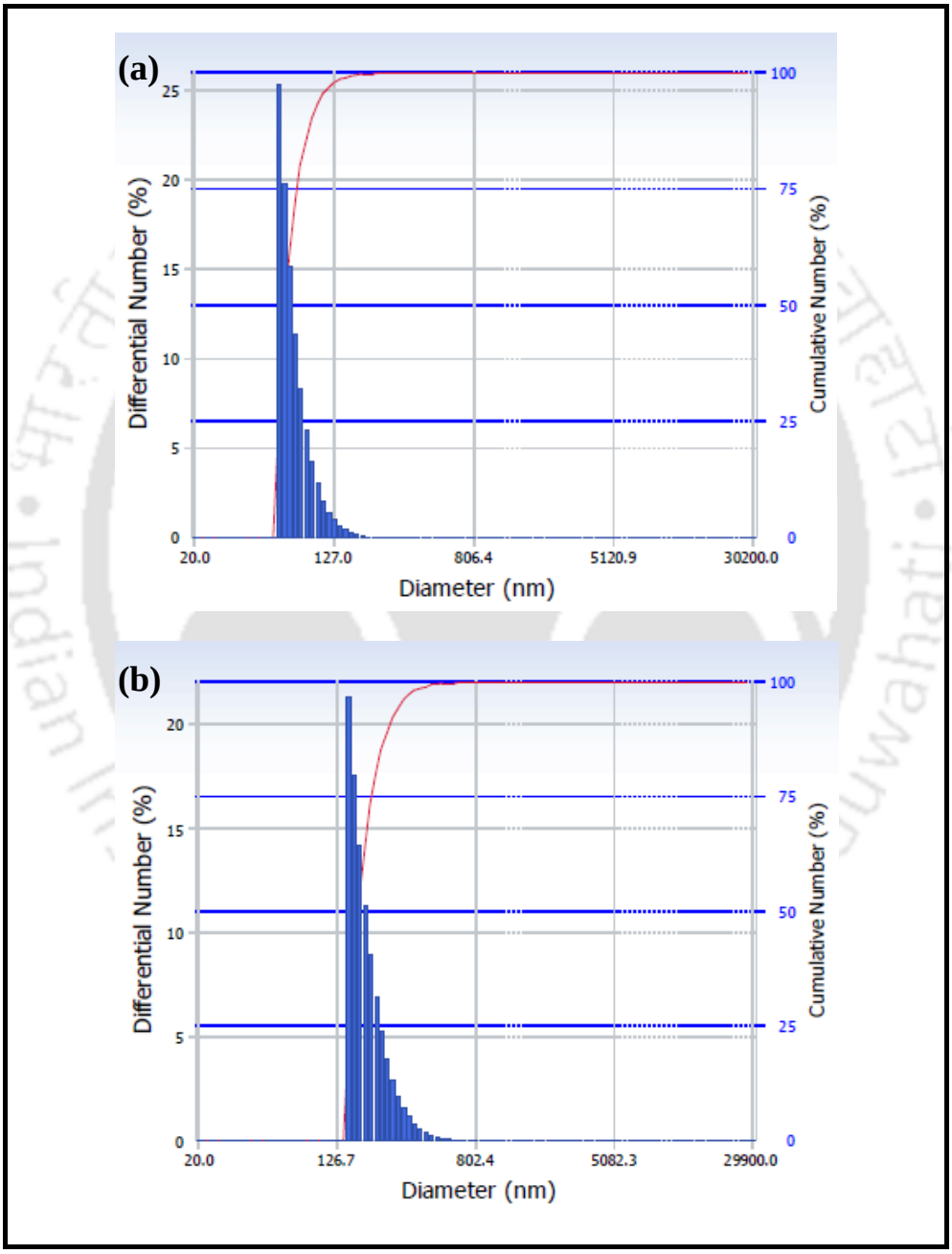


**Figure 9.3: Size distribution of synthesized nanoparticle (a) at pH 4 (b) at pH 7.5.**

and increase in size is observed. At pH 7.5, the situation is opposite; here PAA is fully ionized and form -COO$^-$ groups. Thus, the electrostatic repulsion between -COO$^-$ groups of PAA causes the increase in the size of CS-PAA nanoparticle. Also, this study confirms the stability of nanoparticle in different pH conditions due to the cross linking with GA [106]. On the other hand, zeta potential shows a monotonous trend and keeps decreasing with the increase in pH. Though, when the pH reaches 7.5, a negative zeta potential is observed. The adsorption of anions such as OH$^-$ is the reason of negative zeta potential at pH above 7 [149]. These changes in hydrodynamic size and zeta potential with pH are attributed to the presence of amine and carboxyl group in nanoparticle and could be helpful for antifouling property of membranes.

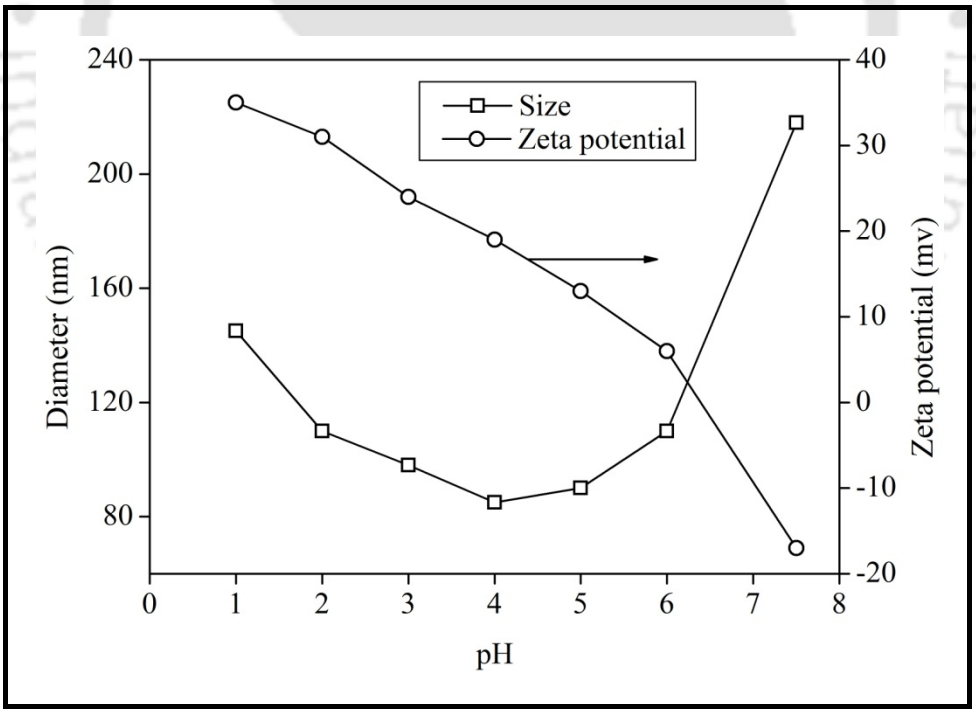


**Figure 9.4: Effect of pH on CS-PAA nanoparticle size and zeta potential.**

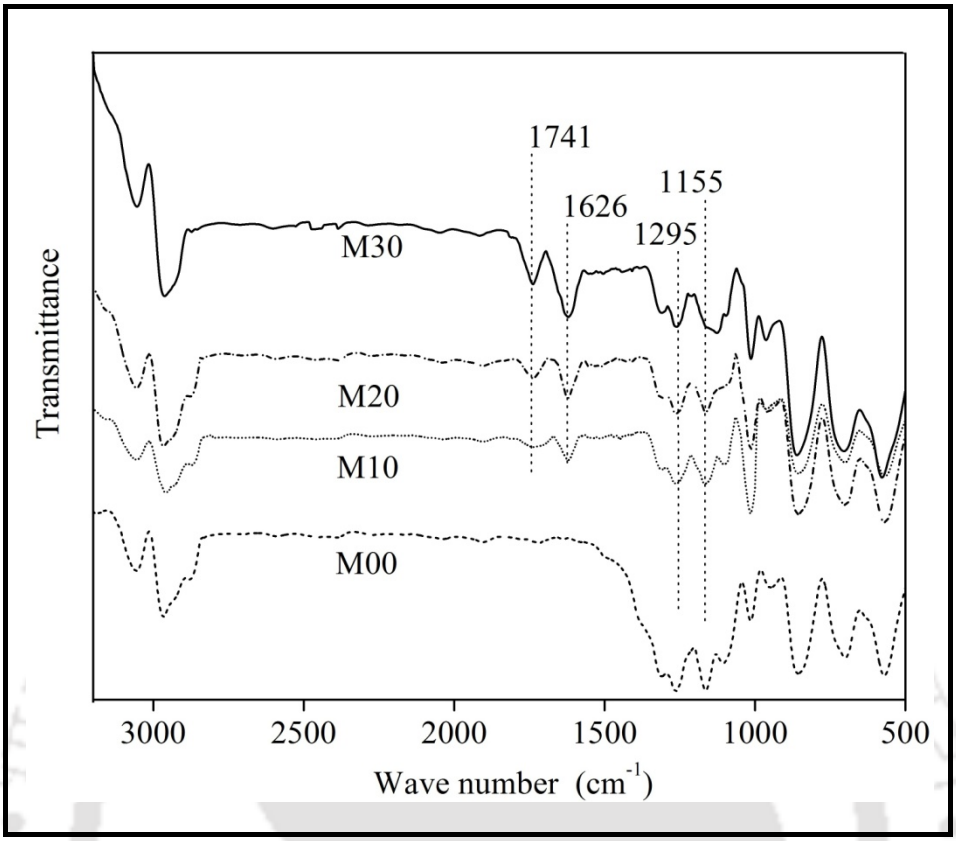


**Figure 9.5: ATR-FTIR spectra of different membranes.**

Figure 9.5 shows ATR-FTIR spectra of plain and modified PSF membranes surfaces fabricated with different wt % of CS-PAA nanoparticles. Peak appears around 1626 $cm^{-1}$, confirms the presence of $NH_2$ group present in chitosan. Another new peak appears at around 1741 $cm^{-1}$, which confirms the presence of –COOH group, polyacrylic acid segment of CS-PAA nanoparticle. The intensity of both these peaks is highest for membrane M30, as it contained highest quantity of CS-PAA nanoparticle. The peaks at 1155 $cm^{-1}$ and 1295 $cm^{-1}$ are due to –C–O–C– and S=O group present in PSF.

## 9.3.2. Hydrophilicity and BSA adsorption study of the membranes

Water contact angle of the top surface of membranes reveal the hydrophilicity of the membrane. It explains the wettability of the membrane, as it could enhance the fouling

resistance as well as flux through membranes [34, 69]. The initial water contact angle measured on the top surface of membrane, just after the DI water dropped on it; reflects the natural wettability of the membrane. As represented in Figure 9.6, water contact angle decreased considerably with the addition of CS-PAA nanoparticle. Plain membrane had the highest contact angle of 72±1.5$^{o}$. With the increase in quantity of CS-PAA nanoparticle in membrane matrix, contact angle reduced from 68±1.5$^{o}$ to 54±1$^{o}$ for membranes M10 and M30, respectively. The reduction in contact angle leads to the enhancement of hydrophilicity of the membrane, which induces from the –$NH_2$ and –COOH group present in the nanoparticle. This is the reason, as the quantity of CS-PAA nanoparticle increases, the contact angle decreases i.e. hydrophilicity of membrane enhances.

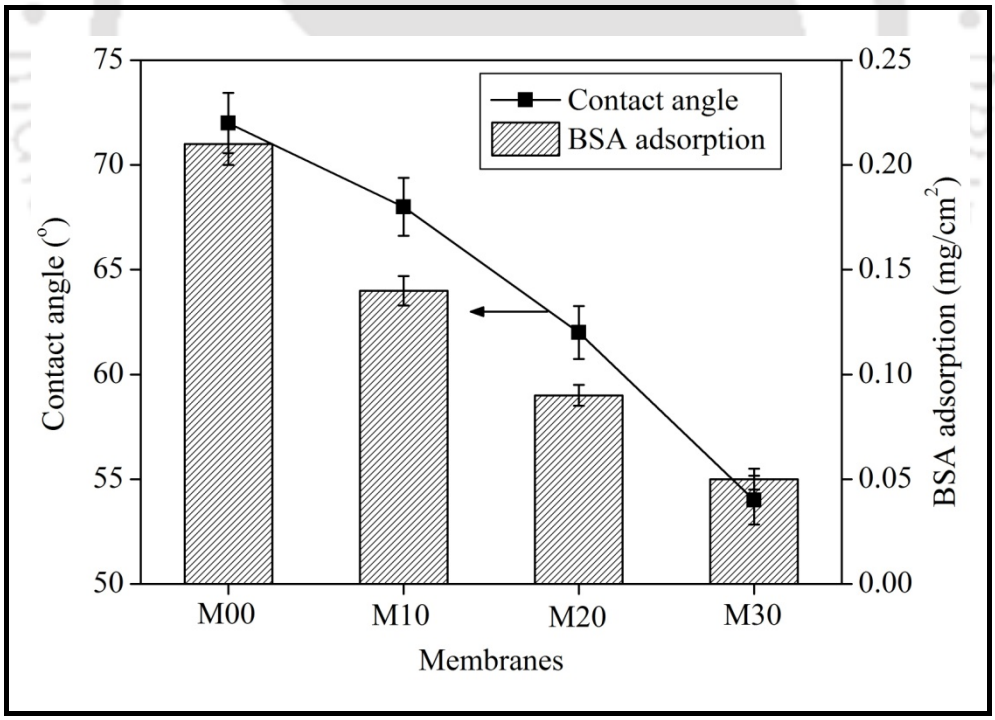


**Figure 9.6: Hydrophilicity and BSA adsorption values of prepared membranes.**

It has been discussed that with the increase in quantity of CS-PAA nanoparticle, surface hydrophilicity had increased for blended membranes. Figure 9.6 shows the amount of

adsorbed BSA on the unit surface area of membranes. It can be seen that modified membranes showed more resistance against the adsorption of BSA. In fact, plain membrane M00 adsorbed almost 4 times higher amount of BSA than modified membrane M30. Reason behind low amount of BSA adsorption is the presence of $-COO^-$ group in CS-PAA nanoparticle. It is well known that isoelectric point of BSA is around pH 4.7; it means that above this pH it remains negatively charged and below this pH it remains positively charged. On the other hand PAA has deprotonation pH of around 4.8, so above pH 5, membrane and BSA both have negative charge. Thus, membrane surface electrostatically repels the BSA molecule.

### 9.3.3. Microscopic study of membranes

Figure 9.7a shows the top surface FESEM images of the plain and blended PSF membranes. Modified membranes have relatively rougher top compared to plain PSF membrane. As can be seen, the amount of CS-PAA nanoparticle on membrane surface has been increased by enlarging the quantity of nanoparticle in membrane casting solution. From the FESEM images, one can see that despite the increasing quantity of nanoparticle in membrane casting solution, their dispersion in membrane is uniform. The dispersion of nanoparticle in membrane top surface is in agreement with the hydrophilicity result of membranes, as it was stated that well dispersed nanoparticles enhances the hydrophilicity with increase in quantity compared to agglomerated nanoparticles [30, 150].

Figure 9.7b shows the cross section image of all the prepared membranes. All the membranes have asymmetric structure, it consist top dense skin layer. Below the skin layer membranes have porous sub layer containing finger like structure. At high magnification one can see the dispersed nanoparticle in modified membranes. But with higher quantity of nanoparticle (membrane M20 and M30), it can be observed that finger like macrovoids became longer and

prominent compared to plain membrane. In case of membrane M10, there is no significant change in cross sectional morphology can be observed, it is all most like membrane M00. This can be correlated to kinetic and thermodynamic effects. The ratio of nonsolvent (water) inflow and solvent (NMP) out flow during the phase change process increases with increase in the hydrophilicity of the membrane casting solution induced with hydrophilic nanoparticle [34, 151]. Also, this change in cross sectional morphology may be attributing to the increase in viscosity of membrane casting solution with the addition of nanoparticle. At higher magnification, one can clearly spot the dispersed nanoparticle in cross section of modified membrane.

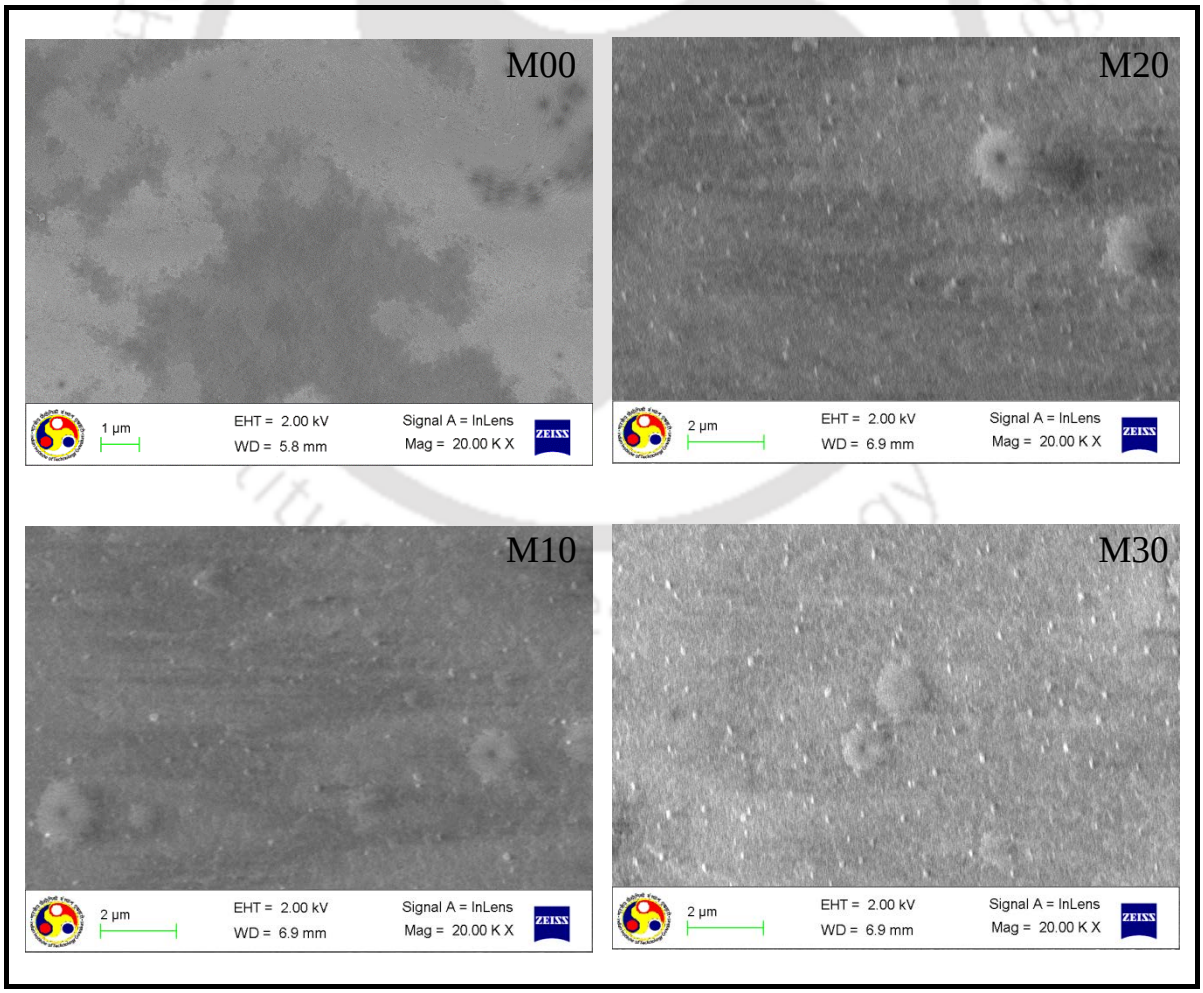


**Figure 9.7a: Top surface FESEM images of prepared membranes.**

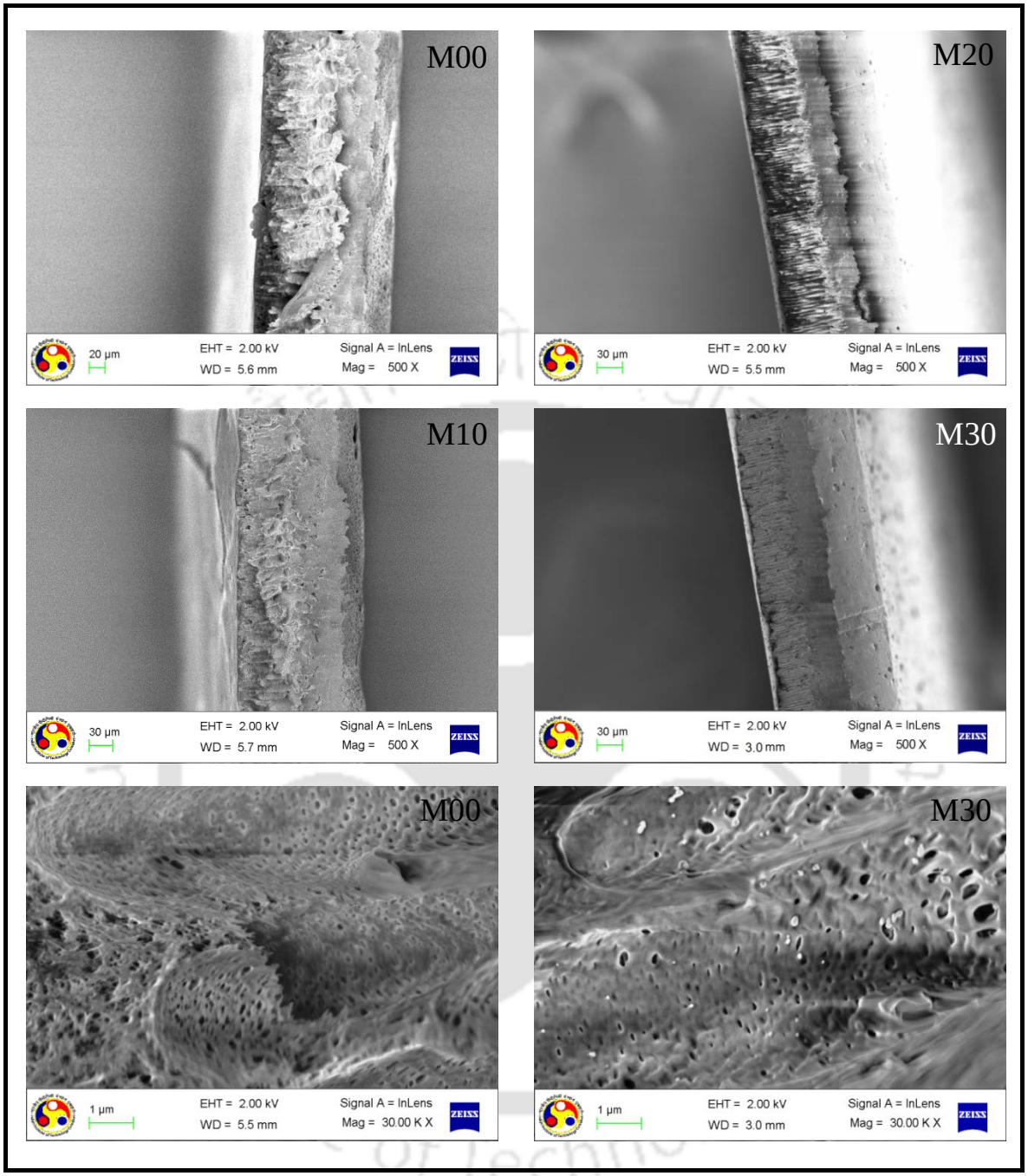


**Figure 9.7b: Cross section FESEM images of plain and modified membranes.**

Table 9.2 shows the overall porosity and average pore size of prepared membranes. Porosity of all the membranes is almost same but average pore size is increased with the incorporation of more quantity of nanoparticles in modified membranes. As it is described earlier that the addition of CS-PAA nanoparticle increases the thermodynamic instability of

casting solution in the coagulation bath, it supports the rapid demixing [152]. This results in large pore formation with the increase in amount of nanoparticle.

**Table 9.2: Some characteristic parameters of membranes modified with CS-PAA nanoparticles.**

| Membranes | CF | $P_m$ ($L/m^2$ h k Pa) | Porosity | $R_m$ (nm) |
|---|---|---|---|---|
| **M00** | 6.23 | 0.146 | 0.785±0.02 | 7.49±0.18 |
| **M10** | 5.76 | 0.183 | 0.77±0.045 | 8.54±044 |
| **M20** | 4.55 | 0.239 | 0.765±0.035 | 9.46±0.44 |
| **M30** | 4.25 | 0.265 | 0.78±0.05 | 10.15±0.5 |

### 9.3.4. Pure water flux and hydraulic permeability

Figure 9.8 shows constant pressure (400 kPa) flux during compaction; it was used to calculate the compaction factor (CF) for prepared membrane (shown in Table 9.2). CF describes the membrane sub layer structure. Presence of large macro voids in membrane sublayer is the reason of compaction. Initially flux declines sharply for all the membranes but after 30 minutes it remains almost steady. Due to compaction the walls of the pores become closer, denser and uniform resulting reduction in pore size as well as the flux during compaction [1]. The steady state PWF increases with increase in quantity of nanoparticle. Steady state flux for plain membrane M00 and membrane M30 was 54 $L/m^2h$ and 112.8 $L/m^2h$, respectively. Permeation flux through the membranes depends upon surface pore size, skin layer thickness, cross sectional morphology of membrane, viscosity of membrane casting solution and hydrophilicity of membrane. It is shown in Figure 9.6 that addition of

CS-PAA nanoparticle led to decrease in water contact angle and enhancement in the hydrophilicity of the prepared membranes. The increase in steady state flux is due to increase in hydrophilicity as well as increase in average pore size.

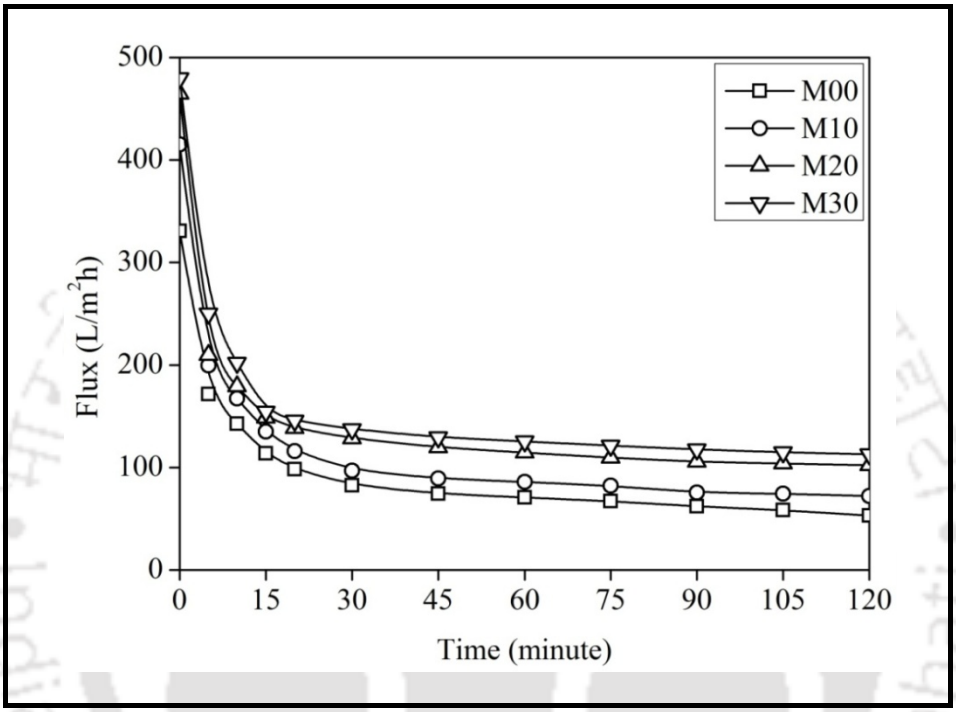


**Figure 9.8: Effect of quantity of CS-PAA nanoparticles on flux profile during compaction (at 400 kPa).**

Figure 9.9 shows the effect of different quantity of CS-PAA nanoparticle on PWF through membrane at different transmembrane pressure (TMP). PWF was measured at 4 different TMP i.e. 100, 200, 300 and 400 kPa. The plot of pressure versus flux was used to calculate the hydraulic permeability of membranes. For all the prepared membranes, PWF was increased linearly with increase in pressure. Increase in transmembrane pressure (effective driving force for permeation) is responsible for this linear variation. Table 3 shows the hydraulic permeability ($P_m$) of the membranes, calculated with the help of Figure 9 and $P_m$ was increased from 0.146 to 0.265 L/m$^2$ h kPa (Table 9.2) for plain membrane to modified membrane with maximum quantity of nanoparticle. Findings of the pure water permeability

and hydraulic permeability studies evidently show that addition of CS-PAA nanoparticles improves the pore size and hydrophilicity, which affect the permeability. These results of PWF and hydraulic permeability are in line with the results of previous studies using metal oxide nanoparticle [31, 33, 88].

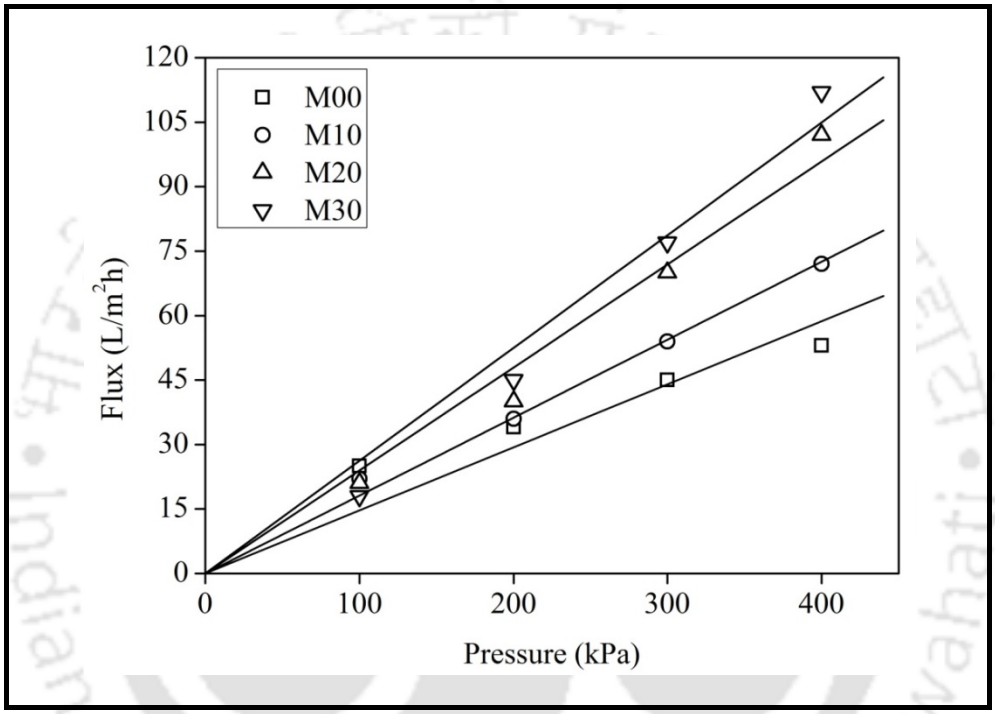


**Figure 9.9: Effect of quantity of CS-PAA nanoparticles on pressure dependent flux through different membranes.**

### 9.3.5. Fouling resistant characteristic of membranes by BSA ultrafiltration experiment

The dynamic fouling resistance experiment was done to study the antifouling property of prepared membranes, and process was record and shown in Figure 9.10. DI water flux was measured from 0 - 90 min and 180 - 270 min, while BSA flux was measured from 90 - 180 min. Flux measured at the end of 90, 180 and 270 minute were called as $J_{w1}$, $J_{BSA}$ and $J_{w2}$

respectively. It was observed that during BSA permeation, a sudden flux loss was seen in initial permeation for all the membranes. Earlier flux loss during BSA ultrafiltration is caused by adsorption or deposition of BSA molecules inside the pores or on the membrane surface. It is significant to note that blended membranes have higher BSA flux than plain membrane. It was stated that the more hydrophilic the membrane was, the less extent of fouling [153]. Also, it was discussed earlier that modified membranes adsorbed less quantity of BSA compared to plain membrane. So, the fouling resistance membrane should effectively resist the adsorption or deposition of foulants to their surface or pore as reported in literatures [118, 139]. Total membrane fouling ($F_t$) can be categorised as reversible and irreversible fouling.

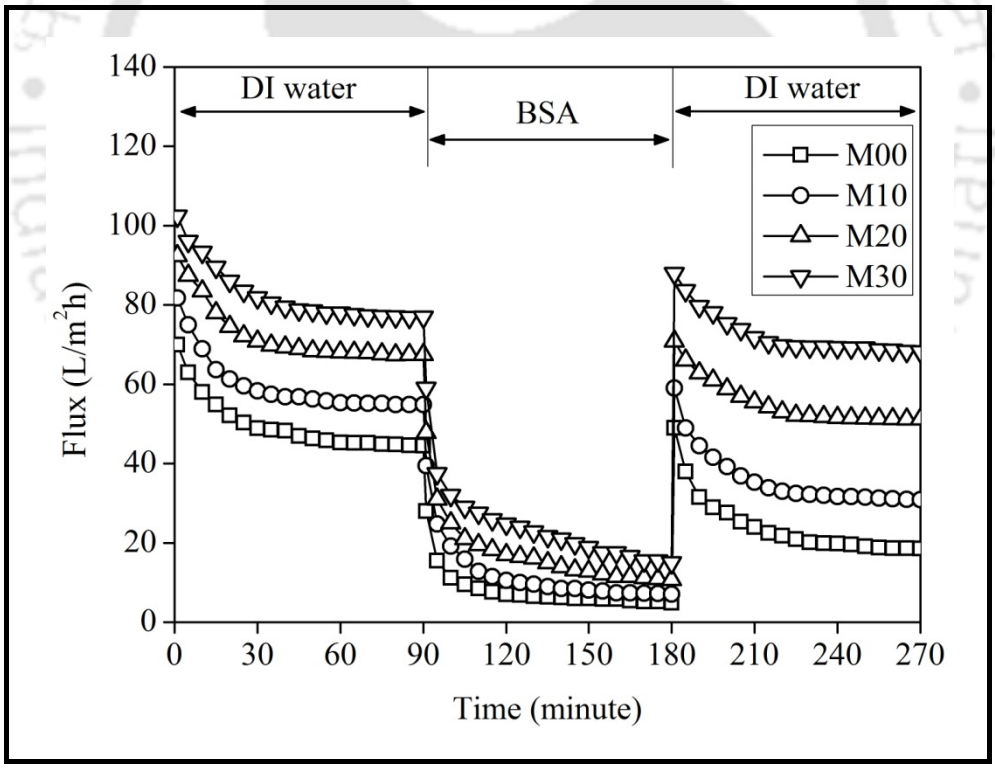


**Figure 9.10: Effect of quantity of CS-PAA nanoparticles on time dependent flux for prepared membranes for fouling study.**

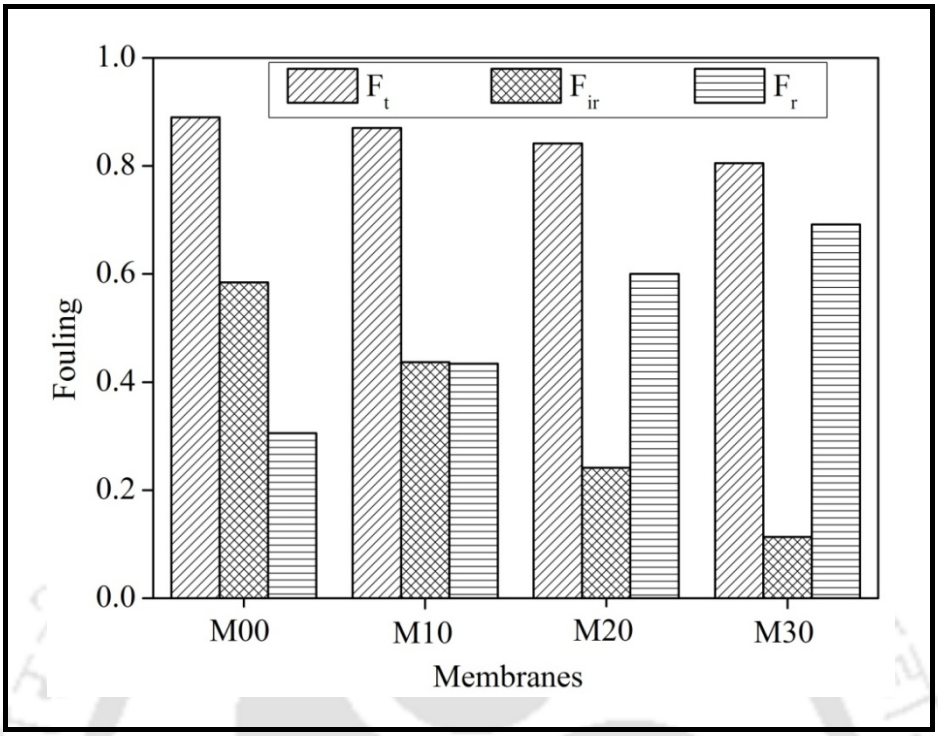


**Figure 9.11a: Effect of quantity of CS-PAA nanoparticles on fouling behaviour of prepared membranes.**

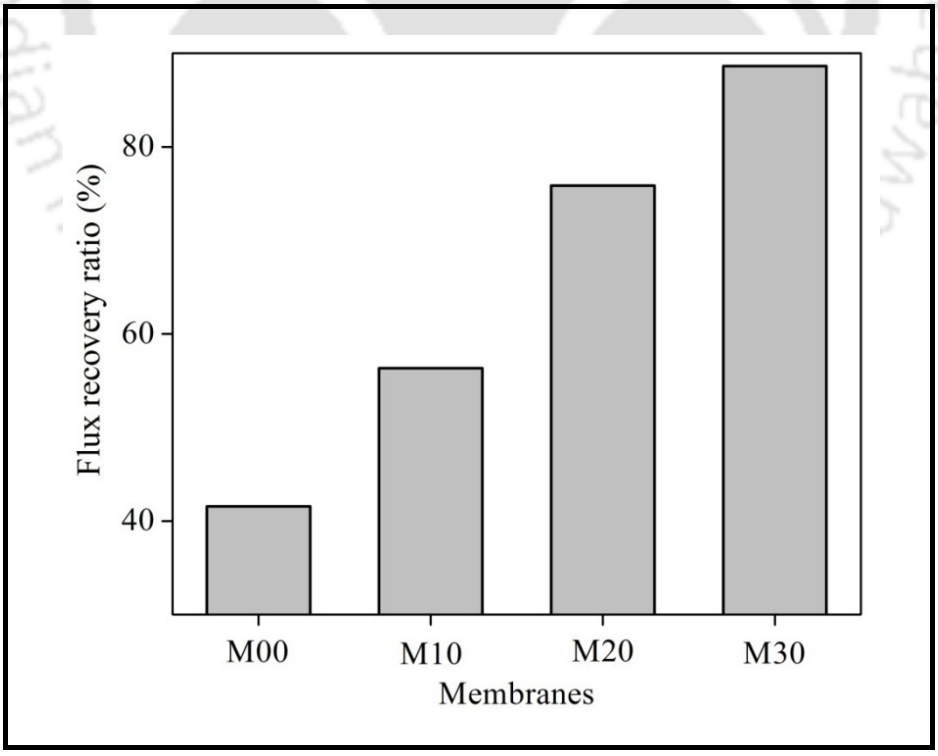


**Figure 9.11b: Effect of quantity of CS-PAA nanoparticles on flux recovery ratio of prepared membranes.**

Reversible deposition or adsorption of foulants, which can be removed by hydraulic flushing, is named as reversible fouling ($F_r$). On the contrary irreversible adsorption of membrane can only be removed by chemical cleaning and it is termed as irreversible fouling ($F_{ir}$). These values were calculated by equations 2.17, 2.18, 2.19 and 2.21.

Figure 9.11a and 9.11b shows the values of different fouling resistance and flux recovery ratio for prepared membranes. The plain membrane has the highest value of total fouling and irreversible fouling and also lowest value of reversible fouling. Addition of CS-PAA nanoparticle resisted the adsorption of BSA molecule inside the membrane pores by increasing the hydrophilicity and by electro static repulsion. Due to this reason, as the quantity of CS-PAA nanoparticle was increased in the membrane, irreversible fouling was reduced in modified membranes. Also, reduction in irreversible fouling causes increase in flux recovery ratio for modified membranes. As flux recovery ratio is directly related to irreversible fouling. The flux recovery ratio for plain membrane was only around 41.5 %, while it was reached to 88.6 % for membrane M30. The good antifouling performance of the CS-PAA blended membrane possibly credited to the presence of large number of carboxyl, amine and hydroxyl groups in the surface of modified membranes resulted from settling of CS-PAA nanoparticles on the top surface of modified membranes (as shown in Figure 9.7a). This results in reduction in water contact angle and BSA adsorption (Figure 9.6). The more hydrophilic surface cause formation of a water layer and repel the hydrophobic foulants.

As shown in Figure 9.12, BSA flux through prepared membranes was increased with the increase in CS-PAA nanoparticle quantity in membrane. BSA flux for membrane M30 was measured around 24.3 L/m$^2$h compared to 8.2 L/m$^2$h for plain membrane. It is almost 3 time higher flux for membrane M30 with respect to plain membrane. It was discussed earlier that CS-PAA nanoparticle enhances the hydrophilicity as well as it also enhances the pore size and its formation. Also, may be due to higher flux and increase in pore size caused a little

drop in BSA rejection with the increasing quantity of nanoparticle. BSA flux reduced from 90.5 % for plain membrane to 86.4 % for modified membrane M30.

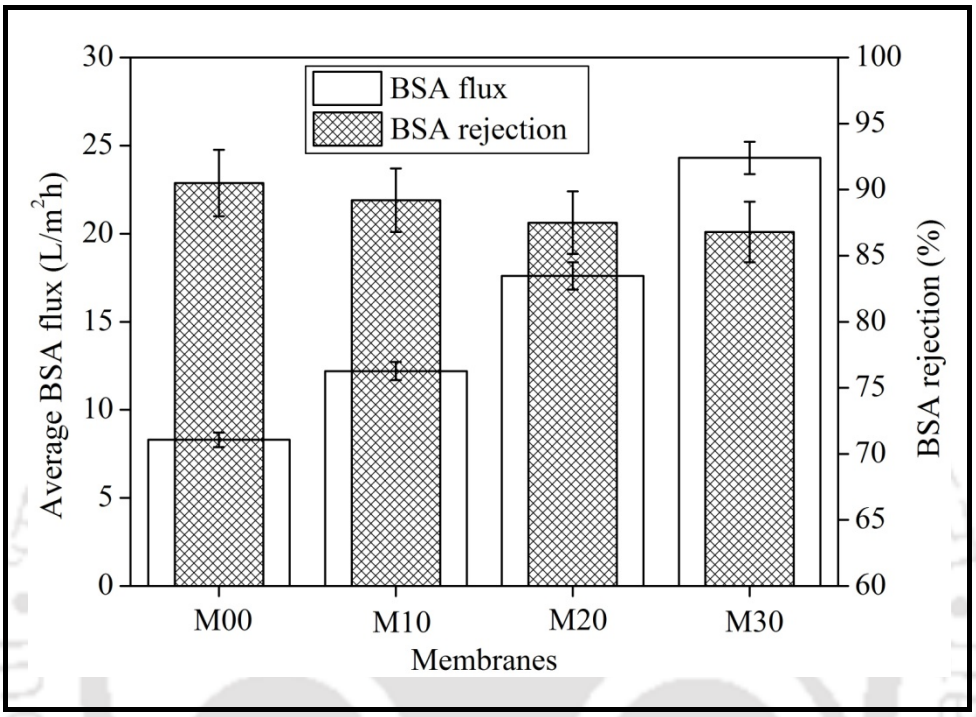


**Figure 9.12: Effect of quantity of CS-PAA nanoparticles on BSA flux and rejection values through prepared membranes.**

# Chapter 10

## Conclusion, summary and scope of future work

# Chapter 10
# Conclusion, summary and scope of future work

*This chapter includes three sections; first section is named as conclusions, which contains the inferences drawn from various works presented in this thesis. Second section restrains the winding up of all the chapters and provides the final verdict on all the works done in the thesis under the section called as summary. Last section is about suggestions towards the future scope.*

## 10.1. Conclusions

This work deals with the preparation and characterization of fouling resistance ultrafiltration polymeric membranes. Different type of membranes were prepared, using seven different type of modifying agent or additives viz. nonsolvent (alcohols), water soluble polymer (PEGME of different molecular weight, pH responsive copolymer, thermo responsive copolymer, dual responsive copolymer, amphiphilic copolymer and polymeric nanoparticles. Among these different additives, most of the additives were synthesized and characterized by FTIR, NMR, DSC, PCS etc. Modified membranes were characterized morphologically by FESEM, SEM, AFM, LLDP, ATR-FTIR as well in term of porosity, equilibrium water content. In some case ion exchange capacity, hydration capacity was also calculated for prepared membranes. Fouling resistant property of the membranes was measured by BSA ultrafiltration through different membranes. The major conclusions from the different studies are presented below.

**Enhancement of hydrophilicity of poly (vinylidene fluoride-co-hexafluoropropylene) (PVDF-HFP) membrane using various alcohols as nonsolvent additives (Refer Chapter 3):**

- The FESEM images indicate that all the membranes have a symmetric structure.
- It was found that various characterization parameters remain almost unchanged for different alcohols but varied with the quantity of same alcohol. It was observed that membrane containing 5 wt. % of methanol had highest value of porosity, EWC, hydraulic permeability, BSA flux and reversible fouling.
- For membrane M_5 change in EWC, porosity, hydrophilicity, CF and permeability of 49.8%, 129.6%, 11.8%, 26.5% and 100.9%, respectively were observed compared to M_0 membrane (Refer Table 3.2).
- For all the modified membranes, up to 10 wt % of non solvent additives, it was found that BSA flux was higher than the plain membranes.
- Up to 5 wt % of methanol addition as non-solvent to the casting solution the pore formation was enhanced but beyond that less porous membrane was formed.

**Increase in hydrophilicity of polysulfone membrane using polyethylene glycol methyl ether (Refer Chapter 4):**

The results of the study showed that with increase in molecular weight of PEGME from 550 to 5000 Da in membrane casting solution,

- The membrane sublayer seems to have dense structure with comparatively less macrovoids and more porous top surface (Refer Figure 4.1).
- The pore number as well as pore area per unit surface area (porosity) of the prepare membrane was found to be increased. Also, the PWF and hydraulic permeability were seen to enhance with increase in molecular weight of PEGME (Refer Table 4.2).

- The EWC increases which might be interpreted as indication of increase in hydrophilicity (which was also confirmed by contact angle measurement) as well as increase in number of pores of the membranes.
- A significant increase in rejection as well as in flux of BSA was observed. The pH of the protein solution also played an important role in this regard. At pH 4.8 (IEP of BSA) rejection of BSA was found more irrespective of the molecular weight of PEGME. Highest rejection was found to be 85% by PSF 3 membrane at pH 4.8 (Refer Figures 4.11 and 4.12).
- Total fouling ($F_t$), reversible fouling ($F_r$) and irreversible fouling ($F_{ir}$) were also calculated and it was observed that value of $F_t$ was decreased with molecular weight of PEGME (Refer Figure 4.10).

**Preparation and characterization of stimuli-responsive hydrophilic polysulfone membrane modified with poly (N-vinylcaprolactam-co-acrylic acid) (Refer Chapter 5):**

The results of the study showed that with increase in wt. % of poly (N-vinylcaprolactam-co-acrylic acid) poly (N-vinylcaprolactam-co-acrylic acid) from 0 to 2.5% in membrane casting solution,

- The PWF and hydraulic permeability were enhanced by 22.26 and 17.9 times respectively for membrane M_5 compared to membrane M_0.
- The hydrophilicity of the modified membranes was also enhanced significantly (Refer Table 5.2).
- Modified membranes showed evidence of pH and thermo sensitivity (Refer Figures 5.7a and 5.7b).
- BSA flux was increased significantly, while the rejection was almost same at normal pH condition (Refer Figure 5.10).

- pH dependent BSA rejection was also studied and the BSA rejection was almost same for all the membranes at pH 11 and pH 7, but at pH 2 rejection values had decreasing trend with the increases in wt % of copolymer (Refer Figure 5.11) .
- Total fouling ($F_t$), reversible fouling ($F_r$) and irreversible fouling ($F_{ir}$) were also calculated and it was observed that value of Ft decreased with increase in wt % of the copolymer (Refer Figure 5.9).

**Preparation and characterization of novel pegylated hydrophilic pH responsive polysulfone ultrafiltration membrane (Refer Chapter 6):**

Effects of wt% of copolymer in membrane morphology and properties were observed and following inferences were made.

- SEM photographs showed that with the increase in copolymer content finger like structure became shorter and large voids were formed in sub layer (Refer Figure 6.2a).
- FESEM images of top surface and LLDP data revealed that copolymer enhances the pore formation and therefore pore density of the modified membranes get increased with increase in copolymer content (Refer Figures 6.2b and 6.3b).
- The hydrophilicity, PWF and hydraulic permeability were seen to enhance with the increase in copolymer wt% and these values increased by 15 %, 63.7 % and 23.8 % respectively for membrane with maximum amount of copolymer compared to plain membrane.
- Presence of PAA in copolymer also induces pH sensitivity in the membrane and modified membranes showed evidence of pH sensitivity and ion exchange capacity (Refer Table 6.3 and Figure 6.7).

- Presence of PEG derivative enhances the fouling resistance of the modified membranes and maximum of ≈ 90% flux recovery ratio was achieved for modified membrane (Refer Figure 6.11).
- Membranes with different copolymer were also prepared. It was found that IEC value and pH sensitivity of membranes was increased with the increase in AA content in copolymer. In summary, modified membranes showed enhanced water permeation, hydrophilicity, BSA flux and antifouling property compared to unmodified membrane.

**Fabrication of fouling resistance PSF UF flat sheet membrane using amphiphilic polyurethane macromolecules (Refer Chapter 7):**

Effects of wt % of PU macromolecule on membrane morphology, hydrophilicity, permeability and BSA fouling were studied and based on that following conclusion were made.

- Cross section SEM image showed that fabricated membrane modified with highest wt % of additive had a more sponge like structure below the dense skin layer and in porous sublayer finger like structure were more bigger and prominent (Refer Figure 7.6).
- Top surface FESEM images depicted that amphiphilic PU macromolecule induces the pore formation and as a result more porous membranes were formed (Refer Figure 7.7).
- AFM and WCA measurement confirmed rougher and hydrophilic top surface for modified membranes compared to plain membranes as RMS roughness value increased from 18.1 to 23.9, whereas WCA decreased from 65˚ to 50˚ for membrane $BA_6$ compared to plain membrane respectively (Refer Figures 7.8 and 7.13).

- Presence of the amphiphilic additive improves the wettability and hydrophilicity of modified membranes and therefore enhances fouling resistance property of the same (Refer Figures 7.8 and 7.13).
- Membrane with different PU macromolecules were also fabricated and their fouling resistance behaviour, wettability, hydrophilicity, permeability were found in following order PU-CA>PU-MA>PU-LA≈PU-BA.

**Fabrication of novel temperature responsive PSF membrane, with cross linked PVCL-co-PSF amphiphilic copolymer for protein separation and easy cleaning (Refer Chapter 8):**

Membranes were prepared with different initial wt ratio PSF to VCL monomer and the results are summarized as follows:

- Membranes modified with PVCL-PSF copolymer showed the visible thermo sensitivity as hydration capacity of membrane $M_{15}$ increased from 160 mg/cm$^3$ to 280 mg/cm$^3$, when temperature was changed from 40˚ C to 25˚ C (Refer Figure 8.3).
- Top surface FESEM images of modified membranes showed the uniform pore size distribution and as well as increase in pore density for modified membrane (Refer Figure 8.5).
- Cross sectional FESEM images showed that all the membranes had asymmetric structure with visible change in finger like structure (Refer Figure 8.6).
- Blending of PVCL-PSF amphiphilic copolymer increases the hydrophilicity and reduces the BSA adsorption on membrane surface (Refer Figure 8.4).
- Modified hydraulic cleaning increased the flux recovery ratio considerably compared to normal hydraulic cleaning for instance the $Flux_{RR}$ for membrane $M_{10}$ by modified

hydraulic cleaning was around 85 % compared to 65 % by normal hydraulic cleaning (Refer Figure 8.13).

**Modification of PSF membrane by chitosan (CS)–poly (acrylic acid) (PAA) complex nanoparticles (Refer Chapter 9):**

The CS-PAA nanoparticles were blended in different quantity for the modification PSF membrane. The results are summarized as follows:

- Prepared CS-PAA nano particles shows change in hydrodynamic size with change in pH due to the presence of amine and carboxyl group (Refer Figures 9.3 and 9.4).
- Top surface FESEM images of modified membranes showed the uniform dispersion of CS-PAA nanoparticle (Refer Figure 9.7a).
- Cross sectional FESEM images sowed that all the membranes had asymmetric structure, but in modified membranes finger like macrovoids became longer and prominent (Refer Figure 9.7b).
- Blending of CS-PAA nanoparticle increased the hydrophilicity and pure water flux through membranes. It also affected the mean pore size of blended membranes.
- Addition of CS-PAA nanoparticle caused decrease in BSA adsorption, which in result decreased the irreversible fouling of the modified membranes (Refer Figures 9.6 and 9.11).

## 10.2. Summary

Fouling resistant behaviour of all the prepared membranes are compared and summarised in Table 10.1. Modified membranes were compared on the basis of total fouling, irreversible

fouling and BSA rejection. In case of membranes from chapter 8, the bracketed data shows the values by normal hydraulic cleaning.

**Table 10.1: Comparative analysis of all the prepared membranes.**

| Membrane composition | Type of additives | Membrane name | Water contact angle (°) | Total fouling (normalized) | Irreversible fouling (normalized) | IEC (mmol/g) | BSA rejection (%) |
|---|---|---|---|---|---|---|---|
| As in Table 3.1 of Chapter 3 | Non solvent additives | Me_0 | 71±1.5 | 0.90 | 0.23 | Nil | 61.8 |
| | | Me_1 | 68.5±1 | 0.91 | 0.27 | Nil | 79.6 |
| | | Me_2 | 66±1 | 0.87 | 0.24 | Nil | 81.2 |
| | | Me_5 | 63.5±1.5 | 0.88 | 0.21 | Nil | 54 |
| | | Me_10 | 72±0.5 | 0.88 | 0.26 | Nil | 78.5 |
| | | Me_15 | 73±0.5 | 0.92 | 0.22 | Nil | 83 |
| As in Table 4.1 of Chapter 4 | Water soluble polymer | PSF1 | 71±1 | 0.89 | 0.5 | Nil | 13 |
| | | PSF2 | 59±2 | 0.84 | 0.22 | Nil | 49 |
| | | PSF3 | 47±1.5 | 0.78 | 0.14 | Nil | 60 |
| As in Table 5.1 of Chapter 5 | Functional copolymer | M_0 | 76±1 | 0.87 | 0.74 | Nil | 89.5 |
| | | M_1 | 70±1 | 0.83 | 0.48 | 0.12 | 87.8 |
| | | M_2 | 68±2 | 0.80 | 0.36 | 0.15 | 86.2 |
| | | M_3 | 65±2 | 0.77 | 0.25 | 0.19 | 82.2 |
| | | M_4 | 62±1 | 0.75 | 0.16 | 0.21 | 79.8 |
| | | M_5 | 58±2 | 0.74 | 0.10 | 0.28 | 76.5 |

| | | | | | | | |
|---|---|---|---|---|---|---|---|
| As in Table 6.1 of Chapter 6 | Cross-linked hydrophilic pH responsive | $M_{10}$ | 63.2±2 | 0.92 | 0.63 | Nil | 87.2 |
| | | $M_{11}$ | 61.5±1.5 | 0.9 | 0.55 | 0.09 | 87.5 |
| | | $M_{13}$ | 55.6±2 | 0.88 | 0.33 | 0.14 | 87.5 |
| | | $M_{15}$ | 50.4±1 | 0.8 | 0.24 | 0.18 | 88.2 |
| | | $M_{17}$ | 48.7±1.5 | 0.74 | 0.10 | 0.22 | 88.9 |
| | | $M_{25}$ | 46.5±2 | 0.71 | 0.19 | 0.15 | 85.4 |
| | | $M_{35}$ | 53±1 | 0.84 | 0.25 | 0.21 | 90.6 |
| As in Table 7.1 of Chapter 7 | Amphiphilic PU macromolecules | Plain | 63.5±2 | 0.91 | 0.61 | Nil | 68.5 |
| | | $CA_2$ | 59±1 | 0.88 | 0.42 | Nil | 72 |
| | | $CA_4$ | 55±1.5 | 0.83 | 0.26 | Nil | 80.5 |
| | | $CA_6$ | 49.5±1.5 | 0.77 | 0.09 | Nil | 91 |
| | | $MA_6$ | 50.5±2.5 | 0.81 | 0.16 | Nil | 92 |
| | | $LA_6$ | 52±2 | 0.81 | 0.21 | Nil | 90 |
| | | $BA_6$ | 52±2.5 | 0.83 | 0.24 | Nil | 89.5 |
| As in Table 8.1 of Chapter 8 | Thermo responsive amphiphilic copolymer | Plain | 67±2 | 0.91 | 0.61 (0.61) | Nil | 68.5 |
| | | $M_{05}$ | 61.5±2.5 | 0.88 | 0.40 (0.51) | Nil | 75 |
| | | $M_{10}$ | 56±1 | 0.84 | 0.15 (0.33) | Nil | 87.5 |
| | | $M_{15}$ | 49±1 | 0.78 | 0.07 (0.16) | Nil | 89 |
| As in Table 9.1 of Chapter 9 | Polymeric nanoparticle | M00 | 72±1.5 | 0.89 | 0.58 | Nil | 90.5 |
| | | M10 | 68±1.5 | 0.87 | 0.44 | Nil | 89 |
| | | M20 | 62±1 | 0.84 | 0.24 | Nil | 87.5 |
| | | M30 | 54±1 | 0.80 | 0.11 | Nil | 87 |

It is clear from Table 10.1 that all the membranes have one common fouling resistant property i.e. hydrophilicity or water contact angle (WCA) and some membranes have another fouling resistant property i.e. ion exchange capacity (IEC). It can be seen that membranes PSF3, M_5, $M_{17}$, $CA_6$, $M_{15}$ and M30 have the best fouling resistant behaviour among all the prepared membranes. These membranes have total fouling in the range of 0.74 to 0.80 and irreversible fouling in the range of 0.09 to 0.11. The possible reason is hydrophilicity, all these membranes have almost same WCA value of ≈48˚, except membrane M_5, it has WCA value of 58˚ ; but then also it has same fouling resistant due to IEC. So, it can be said that IEC is also a main parameter in fouling resistant behaviour, as it can reduce the fouling by inducing electrostatic repulsion. Among above mentioned membranes $M_{17}$, $CA_6$, $M_{15}$ and M30 have BSA rejection around 90 %. Membrane PSF3 has very low rejection of 60 % and Membrane M_5 has also low rejection of 76.5 % compared to other four mentioned membranes. Overall, it can be concluded that the membrane $CA_6$ and $M_{16}$ are the best performing membranes, as they have highest BSA rejection, then also they have least value of total and irreversible fouling after normal hydraulic cleaning. Also hydrophilicity of the membrane these membranes are on the higher side. In case of membranes $CA_6$, the additive used was amphiphilic PU macromolecule end capped with citric acid containing 6 wt % of additive concentration in membrane casting solution. Due to amphiphilic behaviour, these additives migrate towards top surface of membranes during phase inversion process of membrane. So, the amphiphilic PU additives just don't increase the hydrophilicity, but it also restricts the fouling of membranes by steric repulsion. In case of membrane $M_{16}$, 6 wt % of pegylated poly (AA-co-PEGMA) copolymers in the membrane casting solution was used. One of the components of copolymer gives hydrophilicity to the membrane surface, while second component provides IEC capacity to the membrane. So, this additive offers both hydrophilicity as well as IEC to the membranes and can eliminate the fouling of membrane

by forming pure water layer with electrostatic repulsion. Hence dual property of these additives gives better fouling resistant property to the modified membranes.

## 10.3. Recommendations on future directions

This section highlights some of the new areas of research, that can be carried out to further the preparation and applicability of polymeric membranes. Some of the important areas of recommended research are suggested as an extension of the present study:

- PEGME 5000 provided better result than other molecular weight of PEGME, so the effect of different wt. % of PEGME 5000 on PWF, BSA flux and on fouling behaviour can be studied.
- Dual sensitivity of the membranes modified with poly (N-vinylcaprolactam-co-acrylic acid) can be studied i .e. simultaneously at different pH and temperature like at pH 2 and 40˚C, ph 11 and 40˚C, pH 2 and 25˚C, ph 11 and 25˚C.
- Polymeric membrane can be modified by adding metal oxide nanoparticle modified with some pH or temperature responsive polymer. Effect of their addition on fouling resistant behaviour of polymeric membrane can be studied.
- Different type of amphiphilic copolymer containing some hydrophobic part like polystyrene and hydrophilic part like poly vinyl pyrrolidine or polyethylene glycol can be synthesized for the antifouling modification of polymeric membranes.
- Chitosan-PEG based polymeric nanoparticle can be synthesized, as both are hydrophilic in nature and may improve the fouling resistant of the polymeric membranes.

- Extension of the present UF experiments and fouling study in other modes of operations like cross-flow to obtain more realistic idea upon the performance of the prepared membrane in industrial applications.
- Fouling modelling of UF membrane using different pore blocking models and combined blocking models.

# References


[1] M. Mulder, Basic Principles of Membrane Technology, Kluwer Academic Publishers, Dordrecht, 1991.

[2] Munir Cheryan , Ultrafiltration and Microfiltration Handbook, Technomic Publishing Co. Inc. Lancaster, Pennsylvania, U.S.A, 1998.

[3] S. P. Nunes and K.V. Peinemann (Eds.), Membrane Technology in the Chemical Industry, Wiley-VCH Verlag GmbH., 2001.

[4] Application of membrane technologies for liquid radioactive waste processing, International Atomic Energy Agency, Vienna, Technical Reports Series No. 431, 2004.

[5] T. Matsuura, Synthetic Membranes and Membrane Separation Processes, CRC Press. Inc., Corporate Blvd., N.W., Boca Raton, Florida 33431, 2000.

[6] G. Pearce, Introduction to membranes: Membrane selection, Filtration and Separation, April 2007.

[7] A. J. G. Abrahamse, E. Cornelissen, J. A. M. Hofman, Fiber failure frequency and causes of hollow fiber integrity loss, Desalination 194, (2006), 251-258.

[8] Y.L. Su, C. Li, W. Zhao, Q. Shi, H.J. Wang, Z.Y. Jiang, S.P. Zhu, Modification of polyethersulfone ultrafiltration membranes with phosphorylcholine copolymer can remarkably improve the anti-fouling and permeation properties, J. Membr. Sci. 322 (2008) 171–177.

[9] Y. Wang, T. Wang, Y. Su, F. Peng, H. Wu, Z. Jiang, Remarkable reduction of irreversible fouling and improvement of the permeation properties of poly(ether sulfone) ultrafiltration membranes by blending with pluronic F127, Langmuir 21 (2005) 11856–11862.

[10] W. J. Koros, Y. H. Ma, T. Shimidzu, Terminology for membranes and membrane processes; IUPAC recommendations, J. Membr. Sci., 120 (1996), 149–159.

[11] M. R. Wiesner, and P. Aptel. Mass transport and permeate flux and fouling in pressure driven processes (Ch. 4). In: Water Treatment Membrane Processes. Mallevialle, J., Odendaal, P.E. and Wiesner, M.R. (eds.), McGraw-Hill, New York. 1996.

[12] Y. Kim, D. Rana, T. Matsuura, W. Chung, K. C. Khulbe, Sep. Purif. Technol.,72 (2010), 123–132.

[13] P. Wang, K. L. Tan, E. T. Kang, K. G. Neoh, Plasma induced immobilisation of poly (ethylene glycol) onto poly (vinylidene fluoride) microporous membrane, J. Membr. Sci. 195 (2002) 103–114.

[14] J. Wang, C. J. Pan, N. Huang, H. Sun, P. Yang, Y. X. Leng, J. Y. Chen, G. J. Wan, P. K. Chu, Surface characterization and blood compatibility poly(ethylene terephthalate) modified by plasma surface grafting, Surface & Coatings Technol. 196 (2005) 307–311.

[15] B. Chakrabarty, A. K. Ghoshal, M. K. Purkait, Preparation, characterization and performance studies of polysulfone membranes using PVP as an additive, J. Membr. Sci. 315 (2008) 36–47.

[16] S. A. A. Malek, M. N. A. Seman, D. Johnson, N. Hilal, Formation and characterization of polyethersulfone membranes using different concentrations of polyvinylpyrrolidone, Desalination 288 (2012) 31–39.

[17] B. Chakrabarty, A. K. Ghoshal, M. K. Purkait, Effect of molecular weight of PEG on membrane morphology and transport properties, J. Membr. Sci. 309 (2008) 209–221.

[18] A. Idris, N. M. Zain, M. Y. Noordin, Synthesis, characterization and performance of asymmetric polyethersulfone (PES) ultrafiltration membranes with poly- ethylene glycol of different molecular weights as additives, Desalination 207 (2007) 324–339.

[19] W. R. Bowen, T. A. Doneva, H. B. Yin, Polysulfone sulfonated poly (ether ether) ketone blend membranes: systematic synthesis and characterization, J. Membr. Sci. 181 (2001) 253–263.

[20] A. Rahimpour, S. S. Madaeni, Y. Mansourpanah, The effect of anionic, non-ionic and cationic surfactants on morphology and performance of polyethersulfone ultrafiltration membranes for milk concentration, J. Membr. Sci. 296 (2007) 110–121.

[21] N. Ghaemi, S. S. Madaeni, A. Alizadeh, P. Daraei, M.M.S. Badieh, M. Falsafi, V. Vatanpour, Fabrication and modification of polysulfone nanofiltration membrane using organic acids: morphology, characterization and performance in removal of xenobiotics, Sep. Purif. Technol. 96 (2012) 214–228.

[22] J. Sikder, C. Pereira, S. Palchoudhury, K. Vohra, D. Basumatary, P. Pal, Synthesis and characterization of cellulose acetate–polysulfone blend microfiltration membrane for separation of microbial cells from lactic acid fermentation broth, Desalination 249 (2009) 802–808.

[23] M. Sivakumar, D. Raju, R. Rangarajan, Studies on cellulose acetate polysulfone ultrafiltration membranes II. Effect of additive concentration, J. Membr. Sci. 268 (2006) 208–219.

[24] N. Ul-Haq, J.K. Park, Optical resolution of phenylalanine using D-pheimprinted poly (acrylic acid-co-acrylonitrile) membrane-Racemate solution concentra- tion effect, Polym. Compos. 29 (2008) 1006–1013.

[25] L. Li, Z. Yin, F. Li, T. Xiang, Y. Chen, C. Zhao, Preparation and characterization of poly (acrylonitrile-acrylic acid-N-vinyl pyrrolidinone ) terpolymer blended polyethersulfone membranes, 349 (2010) 56–64.

[26] H. Li, J. Liao, T. Xiang, R. Wang, D. Wang, S. Sun, et al., Preparation and characterization of pH and thermo sensitive polyethersulfone hollow fiber membranes modified with P ( NIPAAm-MAA-MMA ) terpolymer, 309 (2013) 1–10.

[27] F. V Adams, E. N. Nxumalo, R. W. M. Krause, E. M. V Hoek, B. B. Mamba, Preparation and characterization of polysulfone / β-cyclodextrin polyurethane composite nanofiltration membranes, J. Memb. Sci. 405-406 (2012) 291–299..

[28] A. Venault, Y. H. Liu, J. R. Wu, H. S. Yang, Y. Chang, J. Y. Lai, Low-bio fouling membranes prepared by liquid-induced phase separation of the PVDF/polystyrene-b-poly (ethylene glycol) methacrylate blend, J. Memb. Sci. 450 (2014) 340–350.

[29] Z. L. Xu, L. Y. Yu, L. F. Han, Polymer nanoinorganic particles composite membranes: a brief overview, Front. Chem. Eng. China 3 (2009) 318–329.

[30] A. Razmjou, J. Mansouri, V. Chen, The effects of mechanical and chemical modification of $TiO_2$ nanoparticles on the surface chemistry , structure and fouling performance of PES ultrafiltration membranes, J. Membr. Sci. 378 (2011) 73–84.

[31] A. L. Ahmad, M. A. Majid, B.S. Ooi, Functionalized PSf/$SiO_2$ nanocomposite membrane for oil-in-water emulsion separation, Desalination 268 (2011) 266–269.

[32] C. Dong, G. He, H. Li, R. Zhao, Y. Han, Y. Deng, Antifouling enhancement of poly(vinylidene fluoride) microfiltration membrane by adding $Mg(OH)_2$ nanoparticles, J. Membr. Sci. 387-388 (2012) 40–47.

[33] S. Balta, A. Sotto, P. Luis, L. Benea, B. Van Der Bruggen, J. Kim, A new outlook on membrane enhancement with nanoparticles : The alternative of ZnO, J. Membr. Sci. 389 (2012) 155–161.

[34] V. Vatanpour, M. Esmaeili, M. H. D. A. Farahani, Fouling reduction and retention increment of polyethersulfone nanofiltration membranes embedded by amine-functionalized multi-walled carbon nanotubes, J. Membr. Sci. 466 (2014) 70–81.

[35] V. Vatanpour, S. Siavash, L. Rajabi, S. Zinadini, A. Ashraf, Boehmite nanoparticles as a new nanofiller for preparation of antifouling mixed matrix membranes, J. Membr. Sci. 401-402 (2012) 132–143.

[36] J. R. Du, S. Peldszus, P. M. Huck, X. Feng, Modification of poly (vinylidene fluoride) ultrafiltration membranes with poly (vinylalcohol) for fouling control in drinking water treatment, Water Res. 43 (2009) 4559–4568.

[37] A. Chanachai, K. Meksup, R. Jiraratananon, Coating of hydrophobic hollow fiber PVDF membrane with chitosan for protection against wetting and flavor loss in osmotic distillation process, Sep. Purif. Technol. 72 (2010) 217–224.

[38] D. W. Gao, T. Zhang, C. Y. Y. Tang, W. M. Wu, C. Y. Wong, Y. H. Lee, D. H. Yeh, C. S. Criddle, Membrane fouling in an anaerobic membrane bioreactor: differences in relative abundance of bacterial species in the membrane foulant layer and insuspension, J. Membr. Sci. 364 (2010) 331–338.

[39] Q. Shi, Y. Su, S. Zhu, C. Li, Y. Zhao, Z. Jiang, A facile method for synthesis of pegylated polyethersulfone and its application in fabrication of antifouling ultrafiltration membrane, 303 (2007) 204–212.

[40] M. J. Han, G. N. B. Baroña, B. Jung, Effect of surface charge on hydrophilically modified poly (vinylidene fluoride) membrane for microfiltration, Desalination 270 (2011)76–83.

[41] G. Arthanareeswaran, P. Thanikaivelan, M. Raajenthiren, Fabrication and Characterization of CA / PSf / SPEEK Ternary Blend Ultrafiltration Membranes, (2008) 1488–1494.

[42] Y. W. Chen, L. Ying, W. H. Yu, E. T. Kang, K. G. Neoh, Poly (vinylidene fluoride) with grafted poly(ethyleneglycol) side chains via the raft mediated process and pore size control of the copolymer membranes, Macromolecules 36 (2003) 9451–9457.

[43] Y. Chang, Y. J. Shih, R. C. Ruaan, A. Higuchi, W. Y. Chen, J. Y. Lai, Preparation of poly (vinylidene fluoride) microfiltration membrane with uniform surface copolymerized poly (ethyleneglycol) methacrylate and improvemen tof blood compatibility, J. Membr. Sci. 309 (2008) 165–174.

[44] F. Liu, B. K. Zhu, Y. Y. Xu, Improving the hydrophilicity of poly (vinylidene fluoride) porous membranes by electron beam initiated surface grafting of AA/SSS binarymonomers, Appl. Surf. Sci. 253 (2006) 2096–2101.

[45] D. Tyszler, R.G. Zytner, A. Batsch, A. Brügger, Reduced fouling tendencies of ultrafiltration membranes in wastewater treatment by plasma modification, 189 (2006) 119–129.

[46] M.C. Porter, Hand book of Industrial Membrane Technology, Noyes Publications, New Jersey, 1990.

[47] A. Bottino, G. Camera-Roda, G. Capannelli, S. Munari, The formation of micro-porous polyvinylidene difluoride membranes by phase separation, J. Membr. Sci. 57 (1991) 1–20.

[48] J. Ren, T. S. Chung, D. Li, R. Wang, Y. Liu, Development of asymmetric 6FDA-2,6 DAT hollow fiber membranes for CO2/CH4 separation 1. The influence of dope composition and rheology on membrane morphology and separation performance, J. Membr. Sci. 207 (2002) 227–240.

[49] D.L. Wang, W.K. Teo, K. Li, Preparation and characterization of high-flux polysulfone hollow fibre gas separation membranes, J. Membr. Sci. 204 (2002) 247–256.

[50] D. Wang, K. Li, W.K. Teo, Preparation of annular hollow fibre membranes, J. Membr. Sci. 166 (2000) 31–39.

[51] D.L. Wang, K. Li, T.K. Teo, Highly permeable polyethersulfone hollow fiber gas separation membranes prepared using water as non-solvent additive, J. Membr. Sci. 176 (2000) 147–158.

[52] D.L. Wang, W.K. Teo, Polyethersulfone hollow fiber gas separation membranes prepared from NMP/alcohol solvent systems, J. Membr. Sci. 115 (1996) 85–108.

[53] D.L. Wang, K. Li, W.K. Teo, Relationship between mass ratio of nonsolvent-additive to solvent in membrane casting solution and its coagulation value, J. Membr. Sci. 98 (1995) 233–240.

[54] M.A. Aroon, A.F. Ismai, M.M. Montazer-Rahmati, T. Matsuura, Morphology and permeation properties of polysulfone membranes for gas separation: Effects of non-solvent additives and co-solvent, Sep. Purif. Technol. 72 (2010) 194–202.

[55] M. Iqbal, Z. Man, H. Mukhtar, B.K. Dutta, Solvent effect on morphology and $CO_2/CH_4$ separation performance of asymmetric polycarbonate membranes, J. Membr. Sci. 318 (2008) 167–175.

[56] L. Shi, R. Wang, Y. Cao, D.T. Liang, J.HwaTay, Effect of additives on the fabrication of poly(vinylidene fluoride-*co*-hexafluropropylene) (PVDF-HFP) asymmetric microporous hollow fiber membranes, J. Membr. Sci. 315 (2008) 195–204.

[57] S.H. Chen, R.M. Liou, J.Y. Lai, C.L. Lai, Effect of the polarity of additional solvent on membrane formation in polysulfone/*N*-methyl-2-pyrrolidone/water ternary system, Eur. Polym. J. 43 (2007) 3997–4007.

[58] J. J. Qin, T.S. Chung, Development of high-performance polysulfone/poly(4-vinylpyridine) composite hollow fibers for $CO_2/CH_4$ separation, Desalination 192 (2006) 112–116.

[59] A.F. Ismail, N. Yaacob, Performance of treated and untreated asymmetric polysulfone hollow fiber membrane in series and cascade module configurations for $CO_2/CH_4$ gas separation system, J. Membr. Sci. 275 (2006) 151–165.

[60] S. Kazama, M. Sakashita, Gas separation properties and morphology of asymmetric hollow fiber membranes made from cardo polyamide, J. Membr. Sci. 243 (2004) 59–68.

[61] A.F. Ismail, P.Y. Lai, Effects of phase inversion and rheological factors on formation of defect-free and ultrathin-skinned asymmetric polysulfone membranes for gas separation, Sep. Purif. Technol., 33 (2003) 127–143.

[62] A.F. Ismail, I.R. Dunkin, S.L. Gallivan, S.J. Shilton, Production of super selective polysulfone hollow fiber membranes for gas separation, Polymer 40 (1999) 6499–6506.

[63] J.M.A. Tan, T. Matsuura, Effect of nonsolvent additive on the surface morphology and the gas separation performance of poly(2,6-dimethyl-1,4-phenylene)oxide membranes, J. Membr. Sci. 160 (1999) 7–16.

[64] P.L. Clech, V. Chen, A.G. Fane, Fouling in membrane bioreactors used in wastewater treatment, J. Membr. Sci. 284 (2006) 17–53.

[65] R. Ghosh, Z. F. Cui, Protein purification by ultrafiltration with pre-treated membrane. J. Membr. Sci. 167 (2000) 47–53.

[66] A. Barbetta, M. Dentini, E.M. Zannoni, M.E. De Stefano, Tailoring the porosity and morphology of gelatin-methacrylate polyHIPE scaffolds for tissue engineering applications, Langmuir 21 (26) (2005) 12333–12341.

[67] D. Wu, M.R. Bird, The fouling and cleaning of ultrafiltration membranes during the filtration of model tea component solutions, J. Food Process Eng. 30 (2007) 293–323.

[68] Y. Zhang, Z. Jin, X. Shan, J. Sunarso, P. Cui, Preparation and characterization of phosphorylated Zr-doped hybrid silica/PSF composite membrane, J. Hazard. Mater. 186 (2011) 390–395.

[69] M. K. Sinha, M. K. Purkait, Increase in hydrophilicity of polysulfone membrane using polyethylene glycol methyl ether, J. Membr. Sci. 437 (2013) 7–16.

[70] A. Pich, A. Tessier, V. Boyko, Y. Lu, H. P. Adler, Synthesis and Characterization of Poly (N-vinylcaprolactam ) -Based Microgels Exhibiting Temperature and pH-Sensitive Properties, macromolecule 39 (2006) 7701–7707.

[71] X. Jiang, G. Lu, C. Feng, Y. Li, X. Huang, Poly(acrylic acid)-graft-poly(N-vinylcaprolactam): A Novel pH and Thermo Dual-Stimuli Responsive System, Polymer Chemistry 4 (2012) 3876–3884.

[72] B.S. Jiang, J. Li, Preparation and characterization of pH-sensitive polyethersulfone hollow fiber membrane for flux control, J. Membr. Sci. 344 (2009) 297–303.

[73] R. Wang, T. Xiang, W. Yue, H. Li, S. Liang, S. Sun, C. Zhao, Preparation and characterization of pH-sensitive polyethersulfone hollow fiber membranes modified by poly ( methyl methylacrylate-co-4-vinyl pyridine ) copolymer, J. Membr. Sci. 423-424 (2012) 275–283.

[74] C. Cheng, L. Ma, D. Wu, J. Ren, W. Zhao, J. Xue, Remarkable pH sensitivity and anti fouling property of terpolymer blended polyethersulfone hollow fiber membranes, J. Membr. Sci. 378(1-2) (2011) 369–381.

[75] W. Zou, Y. Huang, J. Luo, J. Liu, C. Zhao, Poly ( methyl methacrylate – acrylic acid – vinyl pyrrolidone ) terpolymer modified polyethersulfone hollow fiber membrane with pH sensitivity and protein antifouling property, J. Membr. Sci. 358(1-2) (2010) 76–84.

[76] L. Nebhani, C. Barner-Kowollik, Orthogonal transformations on solid substrates: efficient avenues to surface modification, Adv. Mater. 21 (2009) 3442–3468.

[77] Q. Shi, Y. Su, X. Ning, W. Chen, J. Peng, Z. Jiang, Graft polymerization of methacrylic acid onto polyethersulfone for potential ph-responsive membrane materials, J. Membr. Sci. 347 (2010) 62–68.

[78] Y. C. Chen, R. Xie, L. Y. Chu, Stimuli-responsive gating membranes responding to temperature , ph , salt concentration and anion species, J. Membr. Sci. 442 (2013) 206–215.

[79] H. H. Himstedt, K. M. Marshall, S. R. Wickramasinghe, pH-responsive nanofiltration membranes by surface modification, J. Membr. Sci. 366 (2011) 373–381.

[80] Y.W. Kim, W.S. Ahn, J.J. Kim, Y.H. Kim, In situ fabrication of self- transformable and hydrophilic poly(ethylene glycol) derivative-modified polysulfone membranes, Biomaterials 26 (2005) 2867–2875.

[81] Y. Wu, B. D. Freeman, Structure , water sorption , and transport properties of cross linked N-vinyl-2-pyrrolidone / N , N -methylenebisacrylamide films, J. Membr. Sci. 344 (2009) 182–189.

[82] D. Rana, T. Matsuura, R. M. Narbaitz, Novel hydrophilic surface modifying macromolecules for polymeric membranes : Polyurethane ends capped by hydroxy group, J. Membr. Sci. 282 (2006) 205–216.

[83] N. Pezeshk, D. Rana, R. M. Narbaitz, T. Matsuura, Novel modified PVDF ultrafiltration flat-sheet membranes, J. Membr. Sci. 389 (2012) 280–286.

[84] Q. Wei, J. Li, B. Qian, B. Fang, C. Zhao, Preparation , characterization and application of functional polyethersulfone membranes blended with poly (acrylic acid) gels, J. Membr. Sci. 337 (2009) 266–273.

[85] C.O. M'Bareck, Q.T. Nguyen, S. Alexandre, I. Zimmerlin, Fabrication of ion-exchange ultrafiltration membranes for water treatment. I. Semi- interpenetrating polymer networks of polysulfone and poly (acrylic acid), J. Membr. Sci. 278 (2006) 10–18.

[86] ECC Goh, HDH Stöver, Cross-Linked Poly(methacrylic acid-co-poly(ethylene oxide) methyl ether methacrylate) Microspheres and Microgels Prepared by Precipitation Polymerization: A Morphology Study, Macromolecules 35 (2002) 9983–9989.

[87] C.P. Leo, W.P.C. Lee, A.L. Ahmad, A.W. Mohammad, Polysulfone membranes blended with ZnO nanoparticles for reducing fouling by oleic acid, Sep. Purif. Technol. 89 (2012) 51–56.

[88] N. Maximous, G. Nakhla, W. Wan, K. Wong, Preparation , characterization and performance of $Al_2O_3$ / PES membrane for wastewater filtration, 341 (2009) 67–75.

[89] W. Zhao, Y.L. Su, Ch. Li, Q. Shi, X. Ning, Z.Y. Jiang, Fabrication of antifoul- ing polyethersulfone ultrafiltration membranes using Pluronic F127 as both surface modifier and pore-forming agent, J. Membr. Sci. 318 (2008) 405–412.

[90] C.H. Loh, R. Wang, L. Shi, A.G. Fane, Fabrication of high performance polyethersulfone UF hollow fiber membranes using amphiphilic Pluronic block copolymers as pore-forming additives, J. Memb. Sci. 380 (2011) 114–123.

[91] D.Rana, T. Matsurra, R.M. Narbaitz, C.Feng, Development and characterization of novel hydrophilic surface modifying macromolecules for polymeric membranes, J. Membr. Sci. 24 (2005) 103–112.

[92] M.N.A.M. Norddin, A.F.Ismail, D.Rana, T. Matsurra, S.Tabe, The effect of blending poly(ether ether ketone) with various charged surface modifying macromolecules on proton exchange membrane performance, , J. Membr. Sci., 328, (2009), 148–155.

[93] Y. Kim, D. Rana, T. Matsuura, W. Chung, Influence of surface modifying macromolecules on the surface properties of poly (ether sulfone) ultrafiltration membranes, J. Membr. Sci., 338, (2009), 84–91.

[94] S. Kaur, D. Rana, T. Matsurra, S. Sundarrajan, Preparation and characterization of surface modified electrospun membranes for higher filtration flux, J. Membr. Sci., 390-391, (2012), 235–242.

[95] D. Rana, T. Matsuura, Surface modifications for antifouling membranes, Chem. Rev. 110 (2010) 2448–2471

[96] M. K. Sinha, M. K. Purkait, Preparation and characterization of novel pegylated hydrophilic pH responsive polysulfone ultra fi ltration membrane, J. Memb. Sci. 464 (2014) 20–32.

[97] N. A. A. Hamid, A. F. Ismail, T. Matsuura, A. W. Zularisam, W.J. Lau, E. Yuliwati, M. S. Abdullah, Morphological and separation performance study of polysulfone/titanium dioxide (PSF/TiO2) ultrafiltration membranes for humic acid removal, Desalination 273 (2011) 85–92.

[98] J. H. Li, Y. Y. Xu, L. P. Zhu, J. H. Wang, C. H. Du, Fabrication and characterization of a novel TiO2 nanoparticle self-assembly membrane with improved fouling resistance, J. Membr. Sci. 326 (2009) 659–666.

[99] H.J. Song, Y.J. Jo, S.-Y. Kim, J. Lee, C.K. Kim, Characteristics of ultrafiltration membranes fabricated from polysulfone and polymer-grafted silica nanoparticles: Effects of the particle size and grafted polymer on the membrane performance, J. Membr. Sci. 466 (2014) 173–182.

[100] A.K. Nair, A.M. Isloor, R. Kumar, a. F. Ismail, Antifouling and performance enhancement of polysulfone ultrafiltration membranes using $CaCO_3$ nanoparticles, Desalination 322 (2013) 69–75.

[101] D.Y. K. Imer, B. Kose, M. Altinbas, I. Koyuncu, The production of polysulfone (PS) membrane with silver nanoparticles (AgNP): Physical properties, filtration performances, and biofouling resistances of membranes, J. Membr. Sci. 428 (2013) 620–628.

[102] A. Mollahosseini, A. Rahimpour, M. Jahamshahi, M. Peyravi, M. Khavarpour, The effect of silver nanoparticle size on performance and antibacteriality of polysulfone ultrafiltration membrane, Desalination 306 (2012) 41–50.

[103] J. Garcia-Ivars, M.-I. Alcaina-Miranda, M.-I. Iborra-Clar, J.-A. Mendoza-Roca, L. Pastor-Alcañiz, Enhancement in hydrophilicity of different polymer phase-inversion ultrafiltration membranes by introducing PEG/$Al_2O_3$ nanoparticles, Sep. Purif. Technol. 128 (2014) 45–57.

[104] J. Yin, G. Zhu, B. Deng, Multi-walled carbon nanotubes (MWNTs)/polysulfone (PSU) mixed matrix hollow fiber membranes for enhanced water treatment, J. Membr. Sci. 437 (2013) 237–248.

[105] S. Zinadini, A. A. Zinatizadeh, M. Rahimi, V. Vatanpour, H. Zangeneh, M. Beygzadeh, Novel high flux antifouling nanofiltration membranes for dye removal containing carboxymethyl chitosan coated Fe3O4 nanoparticles, Desalination 349 (2014) 145–154.

[106] Y. Hu, Y. Chen, Q. Chen, L. Zhang, X. Jiang, C. Yang, Synthesis and stimuli-responsive properties of chitosan / poly ( acrylic acid ) hollow nanospheres, Polymer 46 (2005) 12703–12710.

[107] H. Kamusewitz, M. Schossig-Tiedemann, M. Keller, D. Paul, Characterization of polymeric membranes by means of scanning force microscopy (SFM) in comparison to results of scanning electron microscopy (SEM), Surf. Sci. 377–379 (1997) 1076–1081.

[108] K.J. Kim, A.G. Fane, C.J.D. Fell, T. Suzuki, M.R. Dickson, Quantitative microscopic study of surface characterization of ultrafiltration membranes, J. Membr. Sci. 54 (1990) 89–102.

[109] G. Cappanelli, F. Vigo, S. Munari,Ultrafiltration membrane-Characterization technique, J. Membr. Sci.15 (1983) 289–313.

[110] P. Abaticchio, A. Bottino, G. Capannelli, S. Munari, Characterization of ultrafiltration polymeric membranes, Desalination 78 (1990) 235–255.

[111] S. Munari, A. Bottino, G. Capannelli, P. Moretti, Membrane morphology and transport properties, Desalination 53 (1985) 11–23.

[112] B.K. Nandi, R. Uppaluri, M.K. Purkait, Preparation and characterization of low cost ceramic membranes for micro-filtration applications, Appl. Clay Sci. 42 (2008) 102–110.

[113] M. Farbod, S. Rezaian, An investigation of super-hydrophilic properties of TiO2/SnO2 nano composite thin films, Thin Solid Films 520 (2012) 1954–1958.

[114] Z. Jiang, X. Zheng, H. Wu, F. Pan, Proton conducting membranes prepared by incorporation of organophosphorus acids into alcohol barrier polymers for direct methanol fuel cells, J. Power Sources 185 (2008) 85–94.

[115] J. Reuvers, C.A. Smolders, Formation of membranes by means of immersion precipitation. Part II. The mechanism of formation of membranes prepared from the system cellulose acetate-acetone-water, J. Membr. Sci. 34 (1987) 67–86.

[116] K. Kimmerle, H. Strathmann, Analysis of the structure-determining process of phase inversion membranes, Desalination 79 (1990) 283–302.

[117] G. Arthanareeswaran, D. Mohan, M. Raajenthiren, Preparation , characterization and performance studies of ultrafiltration membranes with polymeric additive, 350 (2010) 130–138.

[118] Q. Li, Q. Bi, H. Lin, L. Bian, X. Wang, A novel ultrafiltration (UF) membrane with controllable selectivity for protein separation, J. Membr. Sci. 427 (2013) 155–167.

[119] F. L. Huang, Q. Q. Wang, Q. F. Wei, W. D. Gao, H. Y. Shou, S. D. Jiang, Dynamic wettability and contact angles of poly(vinylidene fluoride) nanofiber membranes grafted with acrylic acid, eXPRESS Polymer Letters 4 (9) (2010) 551–558.

[120] J.F. Hester, P. Banerjee, A.M. Mayes, Preparation of protein-resistant surfaceson poly(vinylidene fluoride) membranes via surface segregation, Macromolecules 32 (1999) 1643–1650.

[121] D.A. Musale, S.S. Kulkarni, Relative rates of protein transmission through poly (acrylonitrile) based ultrafiltration membranes, J. Membr. Sci. 136 (1997) 13–23.

[122] K. Kimmerle, H. Strathmann, Analysis of the structure-determining process of phase inversion membranes, Desalination 79 (1990) 283–302.

[123] A. Higuchi, Y. Ishida, T. Nakagawa, Surface modified polysulfone membranes: Separation of mixed proteins and optical resolution of tryptophan, Desalination 90 (1993) 127–136.

[124] J. Calvo, A. Bottino, G. Capannelli, A. Hernández, Comparison of liquid–liquid displacement porosimetry and scanning electron microscopy image analysis to characterise ultrafiltration track-etched membranes, J. Membr. Sci. 239(2) (2004) 189–197.

[125] A.G. Fane, C.J.D. Fell, A.G. Waters, The relationship between membrane surface pore characteristics and flux for ultrafiltration membranes, J. Membr. Sci. 9 (1981) 245–262.

[126] C. Feng, R. Wang, B. Shi, G. Li, Y. Wu, Factors affecting pore structure and performance of poly(vinylidene fluoride-co-hexafluoro propylene) asymmetric porous membrane, J. Membr. Sci., 277 (2006) 55–64.

[127] H. Strathmann, K. Kock, P. Amar, R.W. Baker, The formation mechanism of asymmetric membranes, Desalination 16 (1975) 179–203.

[128] T.H. Young, L.W. Chen, A diffusion-controlled model for wet casting membrane formation, J. Membr. Sci. 59 (1991) 169–181.

[129] I.M. Wienk, R.M. Boom, M.A.M. Beerlage, A.M.W. Bulte, C.A. Smolders, Recent advances in the formation of phase inversion membranes made from amorphous or semi-crystalline polymers, J. Membr. Sci. 113 (1996) 361–371.

[130] R. Ghosh, Z. F. Cui, Fractionation of BSA and lysozyme using ultrafiltration: effect of pH and membrane pretreatment. . J. Membr. Sci. 139 (1998) 17–28.

[131] Z. Jiang, X. Zheng, H. Wu, F. Pan, Proton conducting membranes prepared by incorporation of organophosphorus acids into alcohol barrier polymers for direct methanol fuel cells, J. Power Sources 185 (2008) 85–94.

[132] J. Brandrup, E.H. Immergut, Polymer Handbook, 3rd ed., John Wiley & Sons, New York, 1989.

[133] R. M. Silverstein, F. X. Webster, Spectrometric identification of organic compounds, 6th Edition, John Wiley & Sons, Inc. Canada, 1998.

[134] R.J. Hunter, Zeta Potential in Colloid Science, Academic Press, London, 1981.

[135] P. Guo, W.Y. Guan, L. Liang, P. Yao, Self-assembly of pH-sensitive random copolymers: poly(styrene-co-4-vinylpyridine), J. Colloid Interface Sci. 323 (2008) 229–234.

[136] M. K. Yoo, Y. K. Sung, C. S. Cho, Y. M. Lee, Effect of polymer complex on the cloud point of pnipaam in the poly (nipaam-co-acrylic acod): polyelectrolyte complex between poly(acrylic acid) and poly (allylamine), Polymer 38(11) (1997) 2759–2765.

[137] O. E. Philippova, D. Hourdet, R. Audebert, A. R. Khokhlov, pH-responsive gels of hydrophobically modified poly(acrylic acid), Macromolecules 30 (1997) 8278–8285.

[138] R. Kumar, A. M. Isloor, A. F. Ismail, T. Matsuura, Synthesis and characterization of novel water soluble derivative of Chitosan as an additive for polysulfone ultrafiltration membrane, J. Membr. Sci. 440 (2013) 140–147.

[139] J.H. Huisman, P. Pradanos, A. Hermandez, The effect of protein–protein and protein-membrane interactions on membrane fouling in ultrafiltration, J. Membr. Sci. 179 (2000) 79–90.

[140] R. M. Boom, I. M. Wienk, T. Boomgaard, C. A. Smolders, Microstructures in phase inversion membranes. Part 2. The role of a polymeric additive, J. Membr. Sci. 73 (1992) 277–292.

[141] J. H. Kim, K. H. Lee, Effect of PEG additive on membrane formation by phase inversion, J. Membr. Sci. 138 (1998) 153–163.

[142] C. Lv, Y. Su, Y. Wang, X. Ma, Q. Sun, Z. Jiang, Enhanced permeation performance of cellulose acetate ultra filtration membrane by incorporation of Pluronic F127, J. Membr. Sci. 294 (2007) 68–74.

[143] M. Taniguchi, J. P. Pieracci, G. Belfort, Effect of undulation on surface energy: a quantitative assessment, Langmuir 17 (2001) 4312–4315.

[144] Y. Chang, Y. J. Shih, C.Y. Ko, J.F. Jhong, Y. L. Liu, T.C. Wei, Hemocompatibility of poly(vinylidene fluoride) membrane grafted with network-like and brush-like antifouling layer controlled via plasma-induced surface PEGylation, Langmuir 27 (2011) 5445–5455.

[145] Y. Chang, W. L. Chu, W. Y. Chen, J. Zheng, L. Liu, R. C. Ruaan, A. Higuchi, A system- atic SPR study of human plasma protein adsorption behavior on the controlled surface packing of self-assembled poly(ethylene oxide) triblock copolymer sur- faces, J. Biomed. Mater. Res. 93A (2010) 400–408.

[146] S. Krishnan, C. J.Weinman, C. K. Ober, Advances in polymers for anti-biofouling surfaces, J. Mater. Chem. 18 (2008) 3405–3413.

[147] J. F. Hester, P. Banerjee, Y. Y. Won, A. Akthakul, M. H. Acar, A.M.Mayes, ATRP of amphiphilic graft copolymers based on PVDF and their use as membrane additives, Macromolecules 35 (2002) 7652–7661.

[148] X. L. Ma, Y. L. Su, Q. Sun, Y. Q. Wang, Z. Y. Jiang, Preparation of protein-adsorption-resistant polyethersulfone ultrafiltration membranes through surface segregation of amphiphilic comb copolymer, J. Membr. Sci. 292 (2007) 116–124.

[149] F. Liu, A. Eisenberg, Preparation and pH Triggered Inversion of Vesicles from Poly(acrylic Acid)-block-Polystyrene-block-Poly(4-vinyl Pyridine), J. Am. Chem. Soc. 125 (2003) 15059–15064.

[150] A. Rahimpour, S. S. Madaeni, A. H. Taheri, Y. Mansourpanah, Coupling TiO2 nano-particles with UV irradiation for modification of polyethersulfone ultrafiltration membranes, J. Membr. Sci. 313 (2008) 158–169.

[151] S. Majeed, D. Fierro, K. Buhr, J. Wind, B. Du, A. Boschetti-de-Fierro, V. Abetz, Multi-walled carbon nanotubes (MWCNTs) mixed polyacrylonitrile (PAN) ultrafiltration membranes, J. Membr. Sci. 403–404 (2012) 101–109.

[152] F. Liu, M. R. M. Abed, K. Li, Preparation and characterization of poly(vinylidene fluoride) (PVDF) based ultrafiltration membranes using nano-$Al_2O_3$, J. Membr. Sci. 366 (2011) 97–103

[153] X. L. Li, L. P. Zhu, B. K. Zhu, Y. Y. Xu, High-flux and anti-fouling cellulose nanofiltration membranes prepared via phase inversion with ionic liquid as solvent, Sep. Purif. Technol. 83 (2011) 66–73.

# Appendix

## A. Error analysis

The errors in experimentally measured quantities and in parameters calculated from those measurements are important in that they determine the accuracy of calculation and predictions using those quantities. There are two types of errors viz. systematic error and random error. Systematic errors are the results of faulty assumptions or improper experimental measuring techniques. In this work, care was taken in eliminating systematic errors by appropriately designing the experiments and adopting qualified methods for analysis of the data. On the other hand, random errors result from variation in the precision of measuring parameters and the slight variations that occur in successive measurements made by the same observer under nearly identical conditions. Random errors cannot be eliminated. The focus of the error analysis presented in this section is on the random errors.

In most of the experiments performed in this work, the quantities that are measured directly are concentrations and permeate flow rates which are used to determine the rejection (%) and permeate flux respectively.

### A.1. Error in measurement of BSA concentration in permeate

BSA concentration in the aqueous phase was determined by measuring the absorbance value at a specific wavelength in the UV-Vis spectrophotometer. A calibration curve was prepared by taking the absorbance values against the corresponding known values of concentrations of BSA as discussed in section 2.3.8 of Chapter 2. From Figure 2.3, which is the calibration curve between absorbance and concentration of BSA, it is seen that the standard deviation of the predicted value from actual value of concentration is 0.9995. Thus, every measurement of BSA concentration in permeation is associated with an error of 0.05 % whose effect on rejection values of BSA can be ignored.

## A.2. Error in the measurement of permeate flux

The errors in the values of permeate flux are related to the errors in the measurements used to calculate those values. In this section, statistical analysis is used for estimation of the uncertainty associated with the values of permeate flux. Determination of standard deviation is generally considered to be one of the best methods to estimate the uncertainty which is based on the following method:

If $u_1$, $u_2$, ....., $u_N$ are the $N$ results of the measurements of a particular quantity $u$, then the mean value of $u$ (i.e. $\bar{u}$), is defined by

$$\bar{u} = \frac{u_1 + u_2 + ..... + u_N}{N} = \frac{1}{N}\sum_{i=1}^{N} u_i \qquad \text{(A.1)}$$

The uncertainty in the result is usually expressed as "root-mean-squared-deviation", which is denoted as $\Delta u$, which is computed using the following Eq. (A.2):

$$\Delta u = \sqrt{\frac{(u_1 - \bar{u})^2 + (u_2 - \bar{u})^2 + ..... + (u_N - \bar{u})^2}{N-1}} \qquad \text{(A.2)}$$

In the present work, all the membranes were cleaned thoroughly following each experiment. Besides, before each experiment, performance of all the membranes were checked through pure water flux (PWF) measurement; hence uncertainties involved in the PWF measurements are reported here.

The uncertainties involved in different experimental measurements for (PWF) for membranes PSF1, PSF2 and PSF3 are estimated and shown in Table A.1.

**Table A.1. Values of uncertainties estimated in PWF measurements for membranes PSF1, PSF2 and PSF3.**

| Membranes | Run 1 | Run 2 | Run 3 | $\bar{u}$ | $\Delta u$ | Uncertainties (%) |
|---|---|---|---|---|---|---|
| **PSF1** | 17.5 | 17 | 18.5 | 17.67 | 0.76 | 4.3 |
| **PSF2** | 172 | 169 | 174.5 | 171.83 | 2.75 | 1.6 |
| **PSF3** | 228 | 225 | 232 | 228.33 | 3.51 | 1.5 |